Department of Pharmacology
University College London
Gower Street
London WC1E 6BT

SODIUM AND POTASSIUM ION CHANNELS AS TARGETS FOR THE CONTROL OF EPILEPSY

by

Lucine Tatulian

2002

A thesis submitted for the Degree of
Doctor of Philosophy
University of London

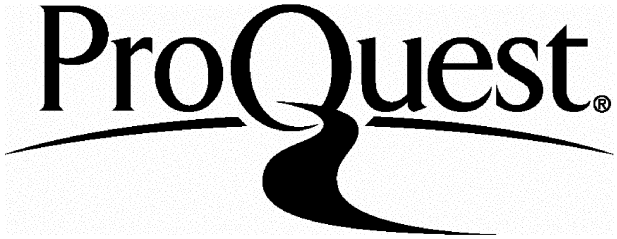

Abstract

Epilepsy is one of the most common neurological disorders and affects roughly 1% of the population. Since the electrical hyperexcitability that causes epilepsy is directly created by currents flowing through ion channels, drugs that selectively block sodium channels, particularly persistent sodium currents, and drugs that open KCNQ potassium channels are a reasonable choice for treating epilepsy.

In the first part of the present study, the whole-cell voltage clamp technique was used to study the biophysical and pharmacological properties of a fully inactivating sodium channel present in rat sympathetic neurones (SCG) and human $Na_v1.3$ brain sodium channel expressed in Chinese hamster ovary (CHO) cells, capable of showing a persistent component. The principal aim of these experiments was to find out whether these currents could be modulated by certain transmitters and intracellular messengers.

Molecular biology and immunocytochemistry were used to show that a combination of $Na_v1.1$, $Na_v1.2$, $Na_v1.3$ and $Na_v1.7$ sodium channels contribute to the fully inactivating sodium current, recorded in SCG neurones. The biophysics of activation were similar for currents recorded in SCG neurones and CHO cells. *Phorbol 12-myristate 13 acetate*, an activator of PKC, decreased the peak amplitude of the sodium current in SCG neurones, but did not induce a persistent component. To see if a more physiological activation of PKC would reproduce this effect, M_1 muscarinic acetylcholine receptors and α_2 adrenoceptors were stimulated by *oxotremorine-M* and *norepinephrine*, respectively. This, however, had no effect on the sodium current. In CHO cells direct PKC stimulation by *phorbol dibutyrate* did not change the peak amplitude of either the transient or persistent components of $Na_v1.3$ current. *Staurosporine*, a non-selective inhibitor of protein kinases, did not change the transient or the persistent current amplitude in CHO cells. Finally, the effects of intracellular application of GTPγS were studied in SCG neurones and CHO cells. This did not have any effect on any of the currents. These results indicate that persistent sodium channels in these cells do not seem to be modulated by G-protein or PKC mediated pathways.

The second part of the thesis concerns the action of *retigabine*. This is a novel anticonvulsant compound now in clinical phase II development. During the course of my studies, retigabine was shown to enhance currents generated by KCNQ2/3 potassium channels, which are considered to be molecular correlates of some mammalian neuronal M channels. In this study, I used the perforated patch clamp technique to compare the actions of retigabine on KCNQ2/3 currents, with those on currents generated by other members of the KCNQ family (homomeric KCNQ1, 2, 3 and 4 channels) expressed in CHO hm1 cells, and on the native M current in rat sympathetic neurones.

Retigabine (10 μM) increased current amplitudes in cells expressing KCNQ2, 3, 4 and 2/3 channels and shifted the voltage-dependence of channel activation. Maximum shifts (mV) were: KCNQ2: -24.2; KCNQ3: -42.8; KCNQ4: -24.6; KCNQ2/3: -30.4. EC_{50} values for half-maximal shifts were (μM; mean ± s.e.m; (*n*)): KCNQ2: 2.5 ± 0.6 (5); KCNQ3: 0.6 ± 0.3 (3); KCNQ4: 5.2 ± 0.9 (3); KCNQ2/3: 1.9 ± 0.2 (5). In contrast, retigabine did not enhance cardiac KCNQ1 currents but instead, at high concentrations (100 μM), reduced currents recorded at strongly positive potentials.

Retigabine also enhanced native M-type currents recorded from dissociated rat SCG neurones. At 10 μM, retigabine produced a 21 mV left-shift in the activation curve for the linopirdine-sensitive component of outward current. In unclamped neurones, retigabine produced a hyperpolarisation and reduced the number of action potentials produced by depolarising current injections, without change in action potential configuration. If replicated in central neurones, this could account for retigabine's anti-epileptic action.

Acknowledgements

I would like to express my gratitude to Professor David A. Brown for providing me with the opportunity to work in his lab, and for his constant support and encouragement throughout my PhD. I would like to extend my gratitude to all members of Prof. Brown's laboratory, particularly to Dr. Steve Marsh, Nicolas Wanaverbecq and Dr. Tim Allen for their help and advice, especially during the initial stages of my PhD. I would like to thank Dr. Alexander Selyanko for his advice and many discussions, who sadly passed away in September.

I am grateful to Dr. Patrick Delmas for his help on recordings in sympathetic neurones, to Dr. Ian Wood, Dr. Fe Abogadie and Dr. Mohini Mistry for helping me with the molecular biology.

I would like to express my appreciation to Dr. Derek Trezise at Glaxo SmithKline for providing me with retigabine and Dr. Xinmin Xie (formerly Glaxo SmithKline) for the opportunity to spend part of my PhD working at Glaxo SmithKline.

Finally, I would like to thank my parents, Rosanna and Stepan, and my sister Susanna for their continuous love and support.

Publications and Communications

Tatulian, L., Delmas, P. Abogadie, F. C. & Brown, D.A. (2001). Activation of expressed KCNQ potassium currents and native neuronal M-type potassium currents by the anti-convulsant drug retigabine. *J.Neurosci.* **21(15)**, 5535-5545.

Selyanko, A. A., Delmas, P., Hadley, J. K., Tatulian, L., Wood, I. C., Mistry, M., London, B. & Brown, D. A. (2002). Dominant negative subunits reveal potassium channel families that contribute to M-like potassium currents. *J. Neurosci.* **22(5)**, RC212.

Sept. 2001: The Physiological Society and British Pharmacological Society joint meeting – Bristol, UK.
Tatulian, L., Delmas, P., Abogadie, F. C. & Brown, D.A. (2001).
The anti-convulsant retigabine enhances both KCNQ potassium currents and native neuronal M-type potassium currents (Oral communication).

Nov. 2000: Society for Neuroscience 30th annual meeting – New Orleans, USA.
Main, M., Tatulian, L., Cryan, J., Selyanko, A. A., Brown, D.A., Clare, J., Trezise, D., Hayes, A. & Burbidge, S.
Modulation of KCNQ potassium channels by retigabine (Poster).

June 2000: European Neuroscience Association meeting – Brighton, UK.
Tatulian, L., Selyanko, A. A., Wood, I., Abogadie, F. C., Buckley, N. J., Delmas, P. & Brown, D.A. (2000).
Dominant negative KCNQ4 blocks M-current in sympathetic neurones (Poster).

Table of Contents

List of Figures

List of Tables

List of Abbreviations

ATP: adenosine 5'-triphosphate

BFNC: benign familial neonatal convulsions

BSA: bovine serum albumin

cAMP: cyclic adenosine monophosphate

CHO: Chinese hamster ovary

CNS: central nervous system

DAG: 1,2 diacylglycerol

DMSO: dimethylsulphoxide

DRG: dorsal root ganglion

DTT: dithiothretol

EC_{50}: half maximal enhancement concentration

ER: endoplasmic reticulum

GDP: guanosine 5'-diphosphate

GTP: guanosine 5'-triphosphate

G protein: guanine nucleotide binding protein

HEK: human embryonic kidney

HEPES: N-[2-hydroxyethyl]piperazine-N-[2-ethanesulfonic]acid

IC_{50}: half maximal inhibitory concentration

IP_3: inositol 1,4,5 triphosphate

LQT: long QT

mAChR: muscarinic acetylcholine receptor

$[Na^+]_i$: intracellular Na^+ concentration

$[Na^+]_o$: extracellular Na^+ concentration

NE: norepinephrine/noradrenaline

NG: neuroblastoma x glioma

Oxo-M: oxotremorine-methiodide

PDBu: phorpbol dibutyrate

PIP_2: phosphatidyl inositol 4,5 bisphosphate

PKA: protein kinase A

PKC: protein kinase C

PLC: phospholipase C

PMA: phorbol myristate acetate

PNS: peripheral nervous system

RTG: retigabine

RT-PCR: reverse-transcriptase polymerase chain reaction

SCG: superior cervical ganglion

SEM: standard error of the mean

TEA: tetraethylammonium

TTX: tetrodotoxin

$V_{1/2}$: half activation/inactivation potential

Amino acid abbreviations:

F: phenylalanine

G: glycine

H: histidine

I: isoleucine

K: lysine

M: methionine

Q: glutamine

R: arginine

S: serine

CHAPTER 1

GENERAL INTRODUCTION

1.1 VOLTAGE – GATED ION CHANNELS

In order to generate, amplify and transmit electric pulses in neuronal cells, three types of voltage sensitive channels operate together in a closely coupled manner, i.e. the sodium (Na^+) channel, the potassium (K^+) channel and the calcium (Ca^{2+}) channel (Hille, 1992a). The sodium channel is essential for the generation of action potentials, while the potassium channel regulates the membrane potential. The calcium channel, however, is involved in many different functions, including muscle contraction and secretory processes (Tsien, 1983; Bean, 1989).

Each channel is regarded as an excitable molecule, as it is specifically responsive to some stimulus, such as a membrane potential change. The channel's response, called *gating*, is apparently a simple opening or closing of the channel pore. All of the three aforementioned voltage-gated channels usually have at least one conducting state and two non-conducting states. At resting membrane potential, the channel open probability is extremely low, meaning that only very few channels open randomly. Upon depolarisation of the membrane, membrane permeability to Na^+, Ca^{2+} or K^+ ions increases dramatically over a period of 0.5 to hundreds of milliseconds. During maintained depolarisation the channel open probability is time-dependently reduced, leading to a closed state, thus decreasing ion permeability to the baseline level over a period of 2 milliseconds to seconds. This biphasic behaviour results from two experimentally separable gating processes that control channel function: *activation*, which controls the rate and voltage dependence of the permeability increase following depolarisation, and *inactivation*, which controls the rate and voltage dependence of the subsequent return of the ion permeability to the resting level during a maintained depolarisation.

Following inactivation, channels cannot be immediately reactivated. Instead, inactivated channels require repolarisation and a certain time for recovery from inactivation. On the other hand, repolarisation of the membrane before the process of inactivation will deactivate the channel, i.e. reverse activation leading to the closed resting state from which the channels can be activated. In this most simple approximate model, transitions from one state to another are possible in both directions. Forward and backward rate constants for the transitions determine the probabilities of the various channel states (*figure 1a*).

Although functions of all ion channels are important, Na^+ and K^+ channels are unique because they are necessary for initiation, propagation and termination of the action potential. Depolarisation of the resting membrane potential stimulates the opening of voltage-sensitive Na^+ channels, which carry Na^+ ions down their electrochemical gradient into the cell. This depolarises the membrane further, thus more Na^+ channels open. However, the inward Na^+ current is short-lived, as these channels are rapidly inactivated. K^+ channels activated by this depolarisation open with a slightly delayed activation and carry K^+ ions out of the cell, down K^+ concentration gradient, which repolarises the membrane to its resting potential. As a result of this *action potential*, voltage-gated Ca^{2+} channels open and Ca^{2+} ions flow into the cell, which triggers the exocytotic mechanism to release neurotransmitters.

Changes in the ionic conductance of the cell membrane can be correctly measured only if the membrane potential of the cell is experimentally controlled. This was first done with the introduction of the voltage clamp technique, which revolutionised the field of electrophysiology (Hodgkin & Huxley, 1952a; 1952b; 1952c). The work of these pioneers enabled a complete analysis of the changes in the elementary processes of ion permeability at the millisecond timescale that are responsible for the generation of the action potential in the squid giant axon. In this approach the voltage across the excitable membranes is controlled by means of a feedback amplifier circuit, and the ionic currents moving across the membrane in response to step changes in the membrane potential imposed by the experimenter is measured. The voltage clamp technique has been used to show that the initial rapid depolarisation during an action potential in nerve axons results from rapid voltage-dependent increases in membrane permeability to sodium ions (Hodgkin & Huxley, 1952c).

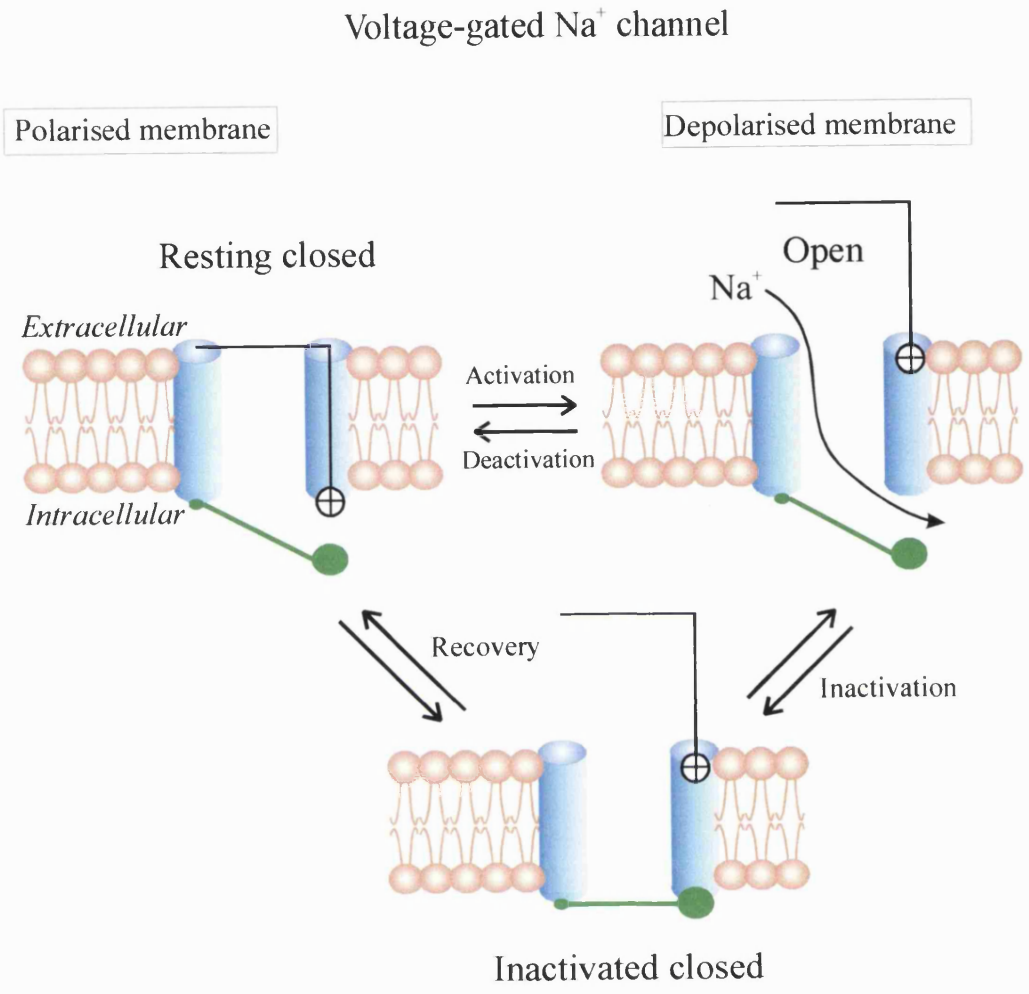

Figure 1a. *Schematic representation of the three states of a sodium channel: resting, open and inactivated. The channel opens rapidly upon depolarisation and then closes to an inactivated state, from which it rarely reopens. Repolarisation of the membrane, initiated by inactivation of the channel, leads to recovery from inactivation, from which activation is again possible. Outward movement of the voltage sensor upon depolarisation results in both opening of the pore and exposure of a docking site for inactivation.* (Adapted from Lehmann-Horn & Jurkat-Rott, 1999).

1.2 VOLTAGE-GATED SODIUM CHANNELS

In their classic experiments of the early 1950s, Hodgkin and Huxley (1952a; 1952b; 1952c) used the newly developed voltage-clamp technique to show that a transient, voltage-activated sodium current was responsible for the initial rapid depolarisation of the action potential. At the time the experimental tools were not available to determine the molecular basis for voltage-dependent sodium currents. Now, some 50 years later, we know that these transient sodium fluxes are mediated by voltage-gated sodium channels - heteromeric membrane proteins that form sodium selective, voltage-gated pores through the plasma membrane (Catterall, 1992; Kallen *et al.*, 1993). At resting membrane potentials, most Na^+ channels are in a closed resting state. In response to membrane depolarisation, sodium channels activate within a few hundred microseconds, resulting in inward Na^+ flux through the open pore. The resulting increase in sodium conductance of the membrane is associated with further depolarisation and activation of further sodium channels. This produces an action potential that rises to a peak close to the sodium equilibrium potential within ~1ms. The hallmark of Na^+ channels is their short open time, and the channel's intrinsic inactivation occurs within a few milliseconds, stopping the Na^+ influx by rapidly converting the Na^+ channels to a non-conducting, inactivated state. Channels almost never open from inactivated states. This leads under unclamped (i.e. natural) conditions to repolarisation of the membrane, which rapidly removes inactivation, converting the channels back to the resting state from which they can open in response to a subsequent depolarisation. After an action potential, the cell membrane is inexcitable for a short period of time, the so-called refractory period. The duration of this period of time is regulated by the kinetics of recovery of the channels from inactivation and is the limiting factor for the firing rate of the cells. Recovery from inactivation allows the cell membrane to regain its resting excitable properties. Therefore, voltage-gated Na^+ channels exist in three functionally distinct states: *resting, active* and *inactive*. Both resting and inactive states are non-conducting. Thus, voltage gated sodium channels undergo cyclic changes in the form of three functionally distinct states, starting with the resting state, over the activated to the inactivated state.

1.2.1 Structure of voltage-gated sodium channels

Sodium channels were the first voltage-gated ion channels to be cloned in 1980s (Noda *et al.*, 1984). Na^+ channel proteins have been purified from several tissues, including eel electroplax (Agnew *et al.*, 1978), mammalian skeletal muscle (Barchi *et al.*, 1980; Kraner *et al.*, 1985), brain (Hartshorne & Catterall, 1981; Hartshorne *et al.*, 1982) and heart (Lombet & Lazdunski, 1984).

Na^+ channels purified from rat brain are composed of α (260kDa), β1 (36kDa) and β2 (33kDa) subunits (Hartshorne & Catterall, 1984). The β2 subunit is covalently attached to the α subunit by disulfide bonds whereas the β1 subunit is attached non-covalently. The subunits are present in a 1:1:1 stoichiometry when all are present.

The α-subunit

The α-subunit is the major subunit of the sodium channel. When expressed in a heterologous system, it possesses all of the channel's major properties, including voltage-dependent gating and selectivity for sodium. Cloning of the α-subunit of the eel electric organ gave the initial insight into the primary structure of a voltage-gated ion channel. The deduced amino-acid sequence by Noda *et al.* (1986) revealed a structure, which is common to all known voltage-gated sodium channels (*figure 2*). It is a large protein with four internally homologous domains (labelled I-IV), each containing six α-helical transmembrane segments (S1-S6) of 19-27 residues. These transmembrane segments are connected by non-conserved, hydrophilic intervening sequences.

The four domains (I-IV) fold together in a ring-shaped structure so as to create a central pore with the ion permeation pathway in the centre, which determines the selectivity and conductance properties of the channel. This pore is thought to resemble an hour-glass in cross-section, and is formed when the fifth and sixth segments (S5-S6), or P segments in each domain dip back into the membrane to form a structure called a *pore loop* (MacKinnon, 1995). X-ray analysis of the potassium channel architecture from *Streptomyces lividans* (KcsA K^+ channel) has revealed that each subunit is inserted into the tetramer such that one transmembrane helix (inner helix) faces the central pore while the other (outer helix) faces the lipd membrane. The inner helices are tilted with respect to the membrane normal by about 25° and are slightly

kinked, so that the subunits open like the petals of a flower facing the outside of the cell. The open petals house the structure formed by the pore region near the extracellular surface of the membrane, containing the ion selectivity filter (Doyle *et al.*, 1998). This architecture also describes the pore of Na^+ and Ca^{2+} channels.

In the fourth transmembrane segment (S4) every third amino acid is a positively charged lysine or arginine, followed by two hydrophobic residues, potentially creating a cylindrical α helix with a spiral ribbon of positive charge around it. The four S4 segments are now widely acknowledged to serve as *activation sensors* and are believed to move in response to depolarisation, thus opening the channel (Stuhmer *et al.*, 1989). The role of the S4 segments in activation of voltage gated ion channels has been an area of intense investigation, combining site-directed mutagenesis, biochemistry and biophysical analysis. The prediction that these positive charges serve as gating charges has been tested by mutagenesis studies. In voltage gated sodium channels, neutralisation of the positively charged residues in the S4 segments causes a reduction in gating charge and alters the voltage dependence of activation (Stuhmer *et al.*, 1989), providing further evidence for the role of S4 as the voltage sensor.

Channel activation:

According to Hodgkin and Huxley's hypothesis, activation of sodium channels would require the movement of positive charges in the S4 segment from the intracellular to the extracellular side of the membrane. The negative internal transmembrane electrical field would exert a strong force on these positive charges arrayed across the plasma membrane, pulling them into the cell. There are multiple ways one can envision voltage sensing. The sliding helix (Catterall, 1986) or helical screw (Guy & Seetharamulu, 1986) models of gating, for example, propose that these positively charged amino acid residues are stabilised in the transmembrane environment by forming ion pairs with negatively charged residues in adjacent transmembrane segments. Depolarisation of the membrane was proposed to release the S4 segments to move outward along a spiral path, initiating a conformational change that opens the pore. During this outward movement of the S4 segment three of the positively charged residues in the S4 of domain IV become accessible outside the cell (Yang & Horn, 1995). This is consistent with separate studies, showing that ~ 12

electronic charges in the whole of the sodium channel protein move across the membrane electric field during activation (Hirschberg *et al.*, 1995). This movement causes conformational changes that result in opening or *'gating'* of the ion-conducting pathway (*figure 1a*).

However, more recently, Bezanilla has proposed a more accurate model for channel activation (Bezanilla, 2000). Taking as a basic building block the crystal structure of the KcsA bacterial potassium channel (Doyle *et al.*, 1998) it was possible to build a model that would account qualitatively for the structural and functional observations on the *Shaker* potassium channel. This model could also be applied to other voltage gated channels, namely Ca^{2+} and Na^{+} channels. Such a model is presented in *figure 1b*. In this arrangement, the conducting pore structure is shown as the S5 and S6 segments for noncontiguous subunits (in this view the subunit on the right shows the back of the subunit on the left). The lining of the internal water-filled crevice is made up by S1 and S5 forming an inverted "V" that communicates to the intracellular medium while the lining of the external crevice is formed by segments S2 and S3 in a "V" fashion. The S4 segment is located between these two crevices. At hyperpolarised potentials, the first four basic residues in the S4 are located in the intracellular crevice, while the next residues are in a region of the extracellular crevice assumed to be hydrophobic and not in continuity wuth the extracelular medium (*figure 1b, top*). Upon depolarisation, the electric field acts on the charges facing the inside and forces the S4 segment to move toward the outside. As this movement is constrained, the segment rotates (180^{o}) and tilts a little, exposing the basic residues to the outside and transporting ~ 13 positive charges in the process (*figure 1b, bottom*). This rotation and tilt of the S4 segment would pull on the intracellular side of the S5 segment by way of the S4-S5 linker, which would rotate and pull apart the intracellular portion of the S6 segment. This would open the channel in a manner similar to the proposed gating of the KcsA channel (Perozo *et al.*, 1998; 1999).

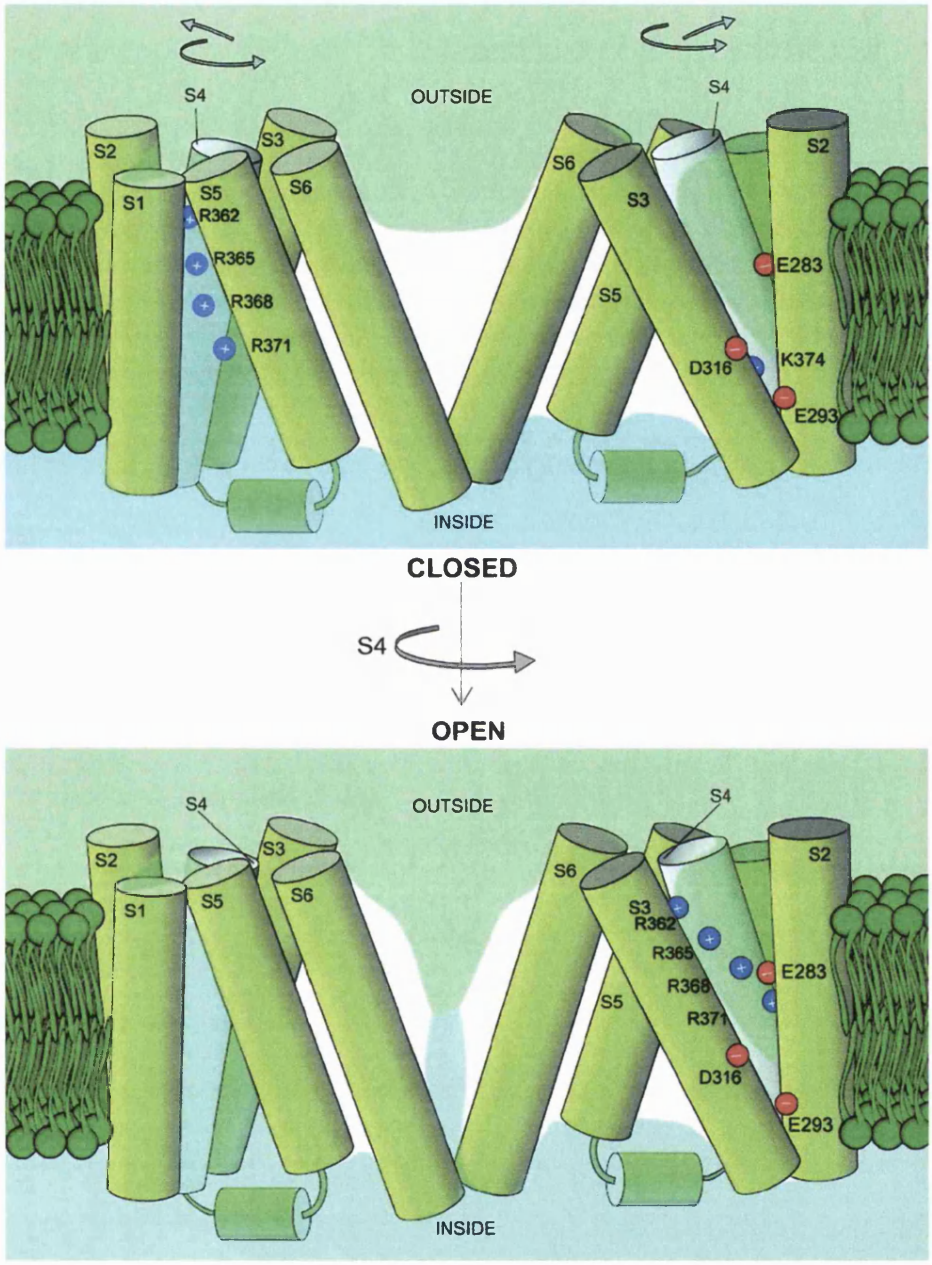

Figure 1b. *Model of the Shaker K^+ channel activation proposed by Bezanilla. Two subunits facing each other across the pore are shown (back face of the subunit on the left is visible as the front face of the subunit on the right). Light green and light blue colours represent the outside and inside bulk solutions. The top figure represents channel structure in the closed state. Depolarisation rotates the S4 segment as described in the text and decreases its tilt, pulling the extracellular regions of the S4 segments further apart from each other* (picture from Bezanilla, 2000).

Channel inactivation:

At present we know about at least two modes of sodium channel inactivation: a *slow inactivation*, which develops over seconds to minutes, and a *fast inactivation*, with a time scale of milliseconds. Fast inactivation describes the rapid and complete decay of currents observed in response to short millisecond depolarisations. Slow inactivation occurs when cells are depolarised for seconds or minutes. Recovery from inactivation takes place on membrane repolarisation at similar time scales as inactivation itself.

Relatively little is known about the slow inactivation. In contrast, the mechanism involved in fast inactivation has been studied intensively. For quite a long time it has been known that a cytoplasmic loop of the channel might be involved in channel inactivation, according to the *"ball and chain"* model (Armstrong & Bezanilla, 1977). [The green line in *figure 1a* represents the *"chain"* and the solid green circle represents the *"ball"*]. The intracellular loop between domains III and IV (*figure 2*) is suspected to be the inactivation gate (Noda *et al.*, 1986). Molecular biology has been used to analyse this inactivation gate (Catterall, 1992). As a result, an '*inactivation loop*' of 45 amino acids on the intracellular loop between domains III and IV has been identified as the inactivation gate. Furthermore, a cluster of hydrophobic amino acids was found to play a crucial role. This cluster, containing *isoleucine 1488*, *phenylalanine 1489* and *methionine 1490* (IFM), labelled *h* in *figure 2*, has been identified as a crucial fragment for inactivation (West *et al.*, 1992). Perhaps the simplest explanation of the inactivation process is that the inactivation loop acts as a physical gate that swings into the pore and blocks the flow of ions, thus inactivating the channel (*figure 1*) (Armstrong & Bezanilla, 1977; Eaholtz *et al.*, 1998). The gate is presumed to be stabilised in the inactivated state by interactions with a receptor site near the inner mouth of the pore. It has been proposed that fast block represents binding of the inactivation gate to the inactivation gate receptor in the short S4-S5 connecting loop of domain IV, while slow block represents binding of the IFM peptide deeper in the pore (Eaholtz *et al.*, 1999).

Sodium channel inactivation derives most or all of its voltage dependence from coupling to the activation process driven by transmembrane movements of the S4 voltage sensors (Armstrong, 1981). Thus, the outward movement of the S4 segment in domain IV (Chen *et al.*, 1996) is believed to be the signal to initiate fast inactivation of

the sodium channel by closure of the intracellular inactivation gate. Furthermore, Hodgkin and Huxley suggest that Na^+ channels transit among various conformational states in the process of activation and another set of conformational states during inactivation. The *m* gates underlie activation and *h* gates underlie inactivation, with *m* representing the proportion of activating molecules on the inside and 1-*m* the proportion on the outside; *h* being the proportion of inactivating molecules on the outside and 1-*h* the proportion on the inside. α_m or β_h and β_m or α_h represent the transfer rate constants in the two directions (Hodgkin & Huxley, 1952c).

In general, the similarity in amino acid sequence of the α-subunit is greatest in the homologous domains from transmembrane segment S1 through S6, while the intracellular connecting loops as well as the intracellular amino- and carboxy- termini are not highly conserved. An exception is the highly conserved interdomain between domains III and IV.

The β-subunits

In addition to the major α-subunit, most voltage gated sodium channels have one or two small auxiliary β-subunits. Both the β1 and β2 subunits consist of a large extracellular domain, a single transmembrane segment and a much shorter cytoplasmic domain (*figure 2)* (Isom *et al.*, 1992, 1995). In addition to β1 and β2 subunits, cDNA clones encoding a β3 subunit have been isolated from rat and human. The β3 subunit RNA is expressed in a complementary fashion to β1 subunit RNA in the CNS, which suggests that α subunits may be associated with either β1 or β3 (Morgan *et al.*, 2000). Despite their similar topologies, β1 and β2 share little sequence similarity and are not closely related proteins. Neither of these subunits can form functional channels when expressed alone and the role of these subunits is probably to regulate the expression and function of the α subunit. The β2 subunit is a 33kDa glycoprotein (Catterall, 1995) and is expressed exclusively in neurones (Isom *et al.*, 1995), whereas β1 (36kDa) is also expressed in muscle tissues (Isom *et al.*, 1992). Thus, sodium channels in the adult CNS are associated with both β1 and β2 subunits, and channels in skeletal muscle are associated with just β1 (Isom *et al.*, 1994).

The β1 and β2 subunits of the sodium channel appear to have dual functions – modulation of channel gating and cell-cell interaction (Vaughn & Bjorkman, 1996). The β1-subunits have multiple and complex effects on sodium channel function: increased peak current, acceleration of activation kinetics and of current decay (Isom *et al.*, 1992, 1995; Makita *et al.*, 1994; Patton *et al.*, 1994; Dietrich *et al.*, 1998;). The β2 subunit has been shown to accelerate the rate of macroscopic current decay (Isom *et al.*, 1995) and significantly increase membrane capacitance, which may indicate that it is involved in insertion of the channels into the cellular membrane (Schmidt *et al.*, 1985, 1986). Thus, β2 subunits increase the functional expression of Na^+ current, alter the voltage dependence and kinetics of channel gating. These findings indicate that β1 and β2 subunits modulate the expression, localisation and function of Na^+ channels (Isom *et al.*, 1994).

It has also been established that there is a small family of β1 subunits and that these may differentially associate with the α subunit contributing to the diversity of the Na^+ channel structure and function. The β1 subunit is also involved in the folding or membrane incorporation of α subunits.

No drugs are known to interact directly with β subunits; therefore the α subunit is the primary target of drug discovery to date.

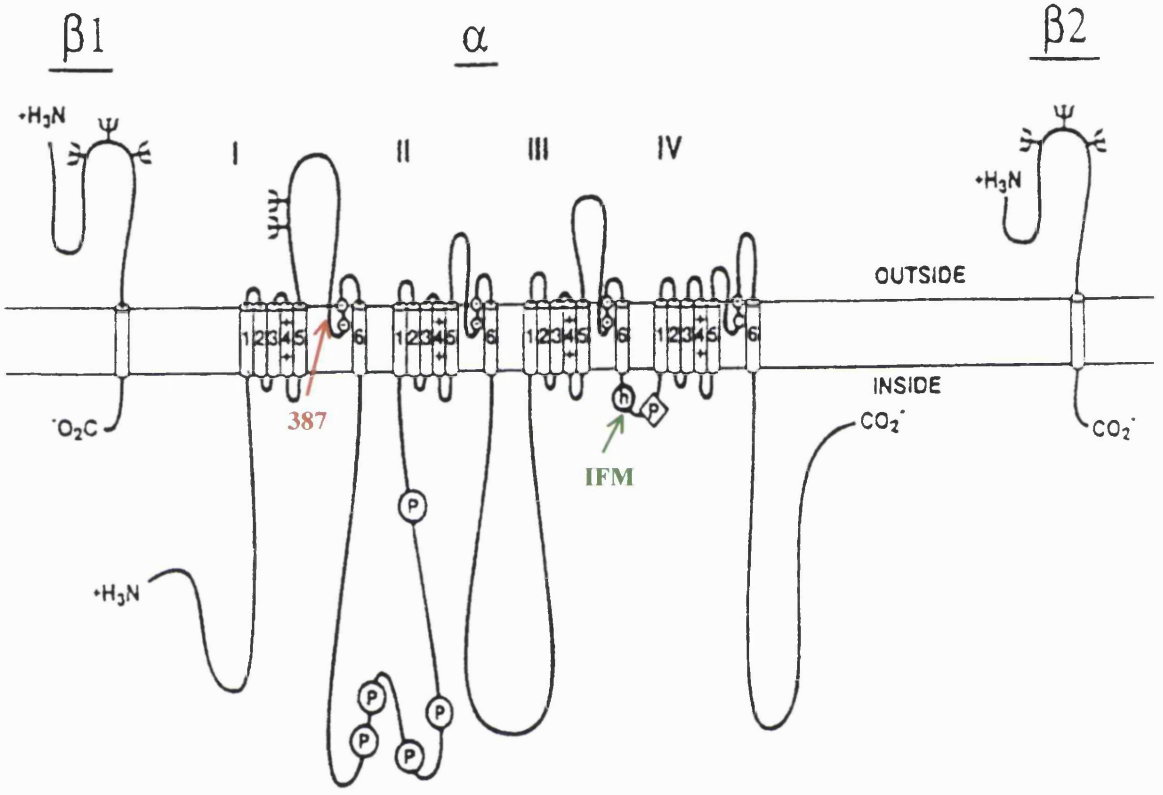

Figure 2. *Proposed structure of the α, β1 and β2 subunits of the Na^+ channel represented as a transmembrane protein. The α-subunit of the Na^+ channel consists of four homologous domains (I-IV), each containing six transmembrane domains (1-6). Cylinders illustrate α helices. ψ show possible glycosylation sites;* P *are the possible phosphorylation sites and* h *are the amino acid residues (IFM) that form the inactivation particle. 387 marks the position of the amino acid residue accounting for TTX sensitivity (see section 1.2.2).* (Catterall, 1995).

1.2.2 Classification of voltage-gated sodium channels

A variety of different sodium channel isoforms have been identified, cloned, functionally expressed and characterised. These isoforms are distinct in terms of developmental and regional expression, and they demonstrate subtle differences in their electrophysiological characteristics. Because voltage gated sodium channels are responsible for the fast component of action potentials, most of these genes are expressed in excitable tissues such as brain, peripheral nerve and skeletal muscle. Despite their similarity of function, the sodium channels have been named in many different ways. To eliminate confusion resulting from the multiplicity of names, Goldin and colleagues proposed a standardised nomenclature for voltage-gated sodium channels (*table 1*) (Goldin *et al.*, 2000).

To date, eleven different genes have been identified, designated *SCN1A* to *SCN11A,* that are known to encode voltage gated sodium channel isoforms, *table 1* (Noda *et al.*, 1984; Auld *et al.*, 1988; Kayano *et al.*, 1988; Malo *et al.*, 1991; Burgess *et al.*, 1995; Schaller *et al.*, 1995). Ten distinctly different sodium channel isoforms have been identified. Three isoforms were cloned from brain - ***$Na_v1.1$***, ***$Na_v1.2$*** and ***$Na_v1.3$*** (Noda *et al.*, 1986; Kayano *et al.*, 1988). One isoform has been cloned from adult skeletal muscle - ***$Na_v1.4$*** (Trimmer *et al.*, 1989); one from heart and embryonic skeletal muscle - ***$Na_v1.5$*** (Rogart *et al.*, 1989; Kallen *et al.*, 1993). And another five isoforms have been cloned from nervous tissue - ***$Na_v1.6$*** (Schaller *et al.*, 1992; Dietrich *et al.*, 1998); ***$Na_v1.8$*** (Akopian *et al.*, 1996; Sangameswaran *et al.*, 1996); ***$Na_v1.7$*** (Sangameswaran *et al.*, 1997; Toledo-Aral *et al.*, 1997); ***$Na_v1.9$*** (Dib-Hajj *et al.*, 1998; Tate *et al.*, 1998) and ***Na_x*** (Gautron *et al.*, 1992; Akopian *et al.*, 1997).

Gene symbol	*Channel isoform*	*Former name*	*Primary tissues*
SCN1A	$Na_v1.1$	Type I, HBSCI, GPBI, SCN1A	CNS, PNS
SCN2A	$Na_v1.2$	Type II, HBSCII, HBA	CNS
SCN3A	$Na_v1.3$	Type III	CNS
SCN4A	$Na_v1.4$	SkM1, μ1	Skeletal muscle
SCN5A	$Na_v1.5$	SkM2, H1	Uninnervated skeletal muscle, heart
SCN8A	$Na_v1.6$	Type VI, NaCh6, PN4, Scn8a, CerIII	CNS, PNS
SCN9A	$Na_v1.7$	NaS, hNE-Na, PN1	PNS, schwann cells
SCN10A	$Na_v1.8$	SNS, PN3, NaNG	DRG
SCN11A	$Na_v1.9$	NaN, SNS2, PN5, NaT, SCN12A	PNS
SCN7 A SCN6A	Na_x	$Na_v2.1$, Na-G, SCL11, $Na_v2.3$	Heart, uterus, skeletal muscle, astrocytes, DRG.

Table 1: Multiplicity of mammalian sodium channel α subunits – *showing the different Na^+ channel isoforms cloned to date, and their primary sites of expression.* (Adapted from Goldin *et al.*, 2000).

In terms of their sensitivity to a guanidinium-containing blocker - *tetrodotoxin* (TTX), Na^+ channels can be broadly divided into two types; *TTX sensitive* and *TTX resistant* (*figure 3*). TTX is a potent poison found in ovaries and liver, with lesser amounts in intestines and skin, of the puffer fish and its relatives from the family *Tetraodontidae.* Externally applied TTX blocks TTX sensitive Na^+ channels (neural and skeletal muscle isoforms) in nanomolar range. TTX resistant channels, such as cardiac Na^+ channels, require much higher concentrations (~ 10^{-5} M). Mutagenesis studies have shown that a single charged amino acid residue located at position 387 in the P region of domain I of the α subunit (*figure 2*) accounts for most of the TTX sensitivity, while its absence renders the channel TTX resistant. Noda and colleagues neutralised a *glutamic acid* residue at position 387 in $Na_v1.2$ brain Na^+ channel in the rat by mutagenesis to *glutamine*, thus decreasing the affinity for TTX by 10000 (Noda *et al.*, 1986). This amino acid is highly conserved in TTX-sensitive Na^+ channels from a number of species but is different in the TTX-resistant cardiac channel (Rogart *et al.*, 1989).

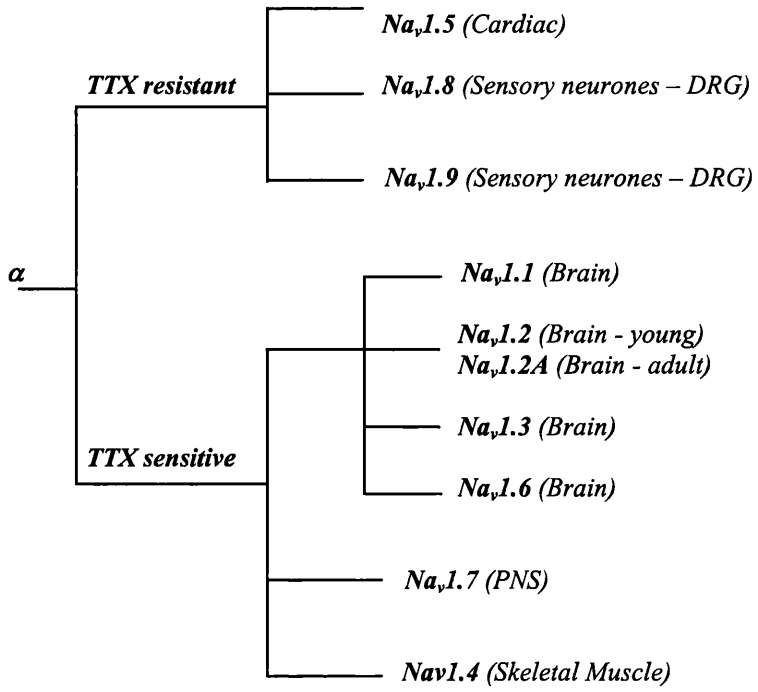

Figure 3. *Diagram showing the classification of the Na^+ channel α-subunits, based on sensitivity to TTX.*

In addition to the nine sodium channels that have been functionally expressed, closely related sodium channel proteins have been cloned from mouse, rat, and human, but have not yet been functionally expressed (Na_x). They are ~ 50% identical to $Na_v1.1$ channels but more than 80% identical to each other (George *et al.*, 1992). They are atypical because the critical IFM residues that form the nucleus of the inactivating particle have been replaced with IFI. However, it is not possible to evaluate the functional significance of these differences because none of these channels have been functionally expressed in an exogenous system despite numerous efforts (Felipe *et al.*, 1994; Akopian *et al.*, 1997).

The nine mammalian sodium channel isoforms that have been identified and functionally expressed are all greater than 50% identical in amino acid sequence in the transmembrane and extracellular domains. $Na_v1.1$, $Na_v1.2$, $Na_v1.3$, $Na_v1.6$ and $Na_v1.7$ are the most closely related group of sodium channels. All five of these sodium channel subtypes are highly TTX sensitive. $Na_v1.1$ $Na_v1.2$, $Na_v1.3$ and $Na_v1.6$

channels are very similar to each other in amino acid sequence and are highly expressed in brain and spinal cord. An alternatively spliced form of $Na_v1.2$ called $Na_v1.2A$ is found predominantly in adult species. The various α subunit subtypes exhibit distinct developmental, regional and subcellular expression patterns (Gordon *et al.*, 1987; Beckh *et al.*, 1989; Westenbroek *et al.*, 1989; Brysch *et al.*, 1991; Black *et al.*, 1994; Felts *et al.*, 1997), *table 1*, suggesting that each subtype may play a specialised role in brain function.

$Na_v1.1$ isoform was originally identified in the rat CNS (Noda *et al.*, 1986), although it has since been shown to be expressed at high levels in the PNS (Beckh, 1990). In contrast, levels of $Na_v1.2$ and $Na_v1.3$ are significantly higher in the CNS than in the PNS (Beckh, 1990). $Na_v1.6$ channels are most abundantly expressed in the CNS and can also be detected in DRG cells (Schaller *et al.*, 1995). Each of these isoforms are present in neurones (Black *et al.*, 1994; Schaller *et al.*, 1995) and glia (Black *et al.*, 1994; Oh *et al.*, 1994; Schaller *et al.*, 1995), although the function of the channels in glial cells is not well understood (Sontheimer *et al.*, 1996). Other neuronal isoforms are predominantly expressed in peripheral tissues, such as the $Na_v1.7$ isoform, found predominantly in dorsal root ganglia (DRG) (Akopian *et al.*, 1996; Felts *et al.*, 1997; Toledo-Aral *et al.*, 1997). In rat brain, the differential distribution of Na^+ channels has been studied using immunohistochemical techniques with site directed antibodies and also by immunoprecipitation (Catterall, 1992). $Na_v1.2$ Na^+ channels comprise more than half of the channels in the neocortex and the forebrain, with $Na_v1.1$ channels making up a large proportion of the remainder. These channels are predominantly located in cell bodies and dendrites ($Na_v1.1$) or in axons ($Na_v1.2$). $Na_v1.3$ channels are expressed only at early stages of development. So far, no major differences in properties or drug sensitivity have been described between $Na_v1.1$ and $Na_v1.2$ channels. However, cloned $Na_v1.3$ Na^+ channels have slower inactivation than $Na_v1.1$ and $Na_v1.2$ channels. For example, heterologous expression of $Na_v1.3$ sodium channel α subunits in cell lines yields currents that do not completely inactivate, i.e. persist (Clare *et al.*, 1999), which may have very important physiological consequences.

1.2.3 Persistent sodium current

Recordings from muscular, cardiac and neuronal tissues have shown that in addition to the fast, rapidly inactivating Na^+ current, several excitable cells show a non inactivating TTX-sensitive sodium current component (Attwell *et al.*, 1979; Llinas & Sugimori, 1980; Patlak & Ortiz, 1985; French *et al.*, 1990). Within the mammalian CNS, a slowly or non-inactivating (*persistent*) Na^+ current has been found in neurones from several brain regions, including neocortex, hippocampus, thalamus and cerebellum. Persistent Na^+ currents have also been observed in glial cells (Barres, 1999) and in several other cells (Alzheimer *et al.*, 1993). These currents typically make up a very small fraction of the peak current and are thought to be generated by the same TTX sensitive Na^+ channels that open transiently during action potentials, but the mechanism by which their activity becomes persistent is unknown. Persistent Na^+ currents probably result from a mode shift in Na^+ channel gating to a state with a reduced likelihood of inactivation, allowing multiple channel openings (Alzheimer *et al.*, 1993). In central neurones persistent Na^+ currents play an important role in summation of synaptic inputs and control of frequency of firing (Taylor, 1993; Crill, 1996). Persistent currents can contribute to important integrative functions such as amplification of excitatory postsynaptic potentials (Schwindt & Crill, 1995; Stuart & Sakmann, 1995; Lipowsky *et al.*, 1996), generation of pacemaker activity (Alonso & Llinas, 1989; Amitai, 1994; Pennartz *et al.*, 1997; Pape & Driesang, 1998) and firing-pattern shaping (Jahnsen & Llinas, 1984; Klink & Alonso, 1993; Parri & Crunelli, 1998). Persistent Na^+ currents can cause long-lasting depolarising plateau potentials that result in bistable membrane voltage. Bistability means that membrane voltage is stable near resting potential, but if neurones become depolarised momentarily, they tend to depolarise almost completely and remain depolarised for a long time. It is likely that the bistability of membrane voltage conferred by persistent Na^+ conductance (French *et al.*, 1990), is involved with the repeated depolarising waves associated with epileptic seizures. With respect to epilepsy, Na^+ channels are particularly relevant since they are a primary target for established anticonvulsant drugs, such as *carbamazepine* and *phenytoin*, which reduce the Na^+ current amplitude in voltage-clamp experiments, shift the voltage dependence of steady-state inactivation in the

hyperpolarising direction, and slow the recovery from inactivation (Upton, 1994; Macdonald & Kelly, 1995).

Since persistent sodium current can generate membrane bistability and plateau potentials, it has also been implicated in the pathogenesis of some forms of epilepsy (Segal, 1994; Ragsdale & Avoli, 1998). Therefore, understanding the mechanisms and modulation of persistent sodium currents could define new targets for drug development.

1.2.4 Modulation of sodium channels

Clearly, sodium channels have a key role in cell physiology. Therefore, alterations in Na^+ channel behaviour that modify Na^+ current amplitude or channel gating can lead to the generation of life-threatening diseases in humans. Hence factors that regulate Na^+ channel function are of considerable interest. Compared to other ion channels, the modulation of voltage-gated Na^+ channels by membrane receptors is poorly documented. However, it has been shown that protein kinase activation and G proteins can modify the gating (opening-inactivation-closing) kinetics of some sodium channels. The study of Na^+ channel modulation offers an excellent opportunity to gain biophysical insights to how Na^+ channels work.

Phosphorylation:

Protein phosphorylation has long been recognised as a key regulatory mechanism to alter the structure and function of cellular proteins. This is achieved by the action of protein kinases and protein phosphatases. Protein kinases have been classified mainly into two groups, the serine/threonine kinases and the protein tyrosine kinases, depending on the target amino acid. Among the serine/threonine kinases are *protein kinase C* (PKC) (Kikkawa *et al.*, 1989) and *protein kinase A* (PKA) (Taylor, 1989).

In the brain, several PKC and PKA consensus phosphorylation sites have been found on the intracellular linkers between domains I and II and domains III and IV on the α subunits. The existence of these sites implies that these channels are capable of being phosphorylated (Costa *et al.*, 1982) by cAMP-dependent protein kinase (PKA)

or Ca^{2+} dependent protein kinase C (PKC) (Sigel & Baur, 1988; Dascal & Lotan, 1991; Chen *et al.*, 1995). In contrast, no phosphorylation of the β1 or β2 subunits was detected.

PKA:

Activation of PKA has been shown to modulate neuronal sodium channels (Costa *et al.*, 1982; Murphy *et al.*, 1993), skeletal muscle (Ukomadu *et al.*, 1992) and cardiac (Cohen & Levitt, 1993) sodium channels. The loop between domains I and II contains four *serines*, which are phosphorylated in vitro and in vivo by PKA (Murphy *et al.*, 1993). Functional effects of PKA activation have been studied on α subunits of rat brain $Na_v1.2A$ Na^+ channels expressed either in CHO cells (Li *et al.*, 1992, 1993), or in *Xenopus* oocytes (Gershon *et al.*, 1992; Smith & Goldin, 1992, 1996). In both cell types, peak sodium current was reduced by 25 - 40% without change in the kinetics or voltage dependence of activation or inactivation (Li *et al.*, 1992). Similar PKA dependent inhibition of $Na_v1.2$ channels was observed in the tsA-201 subclone of human embryonic kidney 293 (HEK-293) cells transiently transfected with $Na_v1.2$ α subunit (Cantrell *et al.*, 1997). PKA dependent inhibition was also reported for $Na_v1.1$ sodium channels expressed in *Xenopus* oocytes (Smith & Goldin, 1998). However, Smith and Goldin (1992) have reported that activation of PKA via stimulation of β2 adrenergic receptors coexpressed in *Xenopus* oocytes enhanced $Na_v1.2A$ Na^+ currents by approximately 80% (Smith & Goldin, 1992). The essential conclusion is that PKA activation can either enhance or attenuate macroscopic rat brain $Na_v1.2A$ currents depending on the physiological (or biophysical) status of the Na^+ channels. What causes PKA to enhance currents is not known. It is possible that Na^+ current enhancement by PKA may be caused by phosphorylation of channel at a different site and/or interaction with a phosphorylated protein that could modulate the channel. Channel phosphorylation results from a complex balance between activities of protein kinases, different kinase isoforms and phosphatases. Different cells express different protein kinases and phosphatases. The same Na^+ channel may have different phosphorylation patterns in different cells, or even in the same cell at different times.

While the activity of neuronal sodium channels clearly changes upon PKA stimulation (Gershon *et al.*, 1992; Li *et al.*, 1993; Smith & Goldin, 1996), the cardiac isoform ($Na_v1.5$) and skeletal muscle ($Na_v1.4$) sodium currents remain unchanged

(Schreibmayer *et al.*, 1994; Frohnwieser *et al.*, 1997). The *serine* residue occurring in the highly conserved interdomain between III and IV (S1506) is required for PKA effect on the rat brain isoform $Na_v1.2$ (West *et al.*, 1991; Li *et al.*, 1993), while it is not necessary for the cardiac isoform (Frohnwieser *et al.*, 1995). Phosphorylation of this site is required for slowing of Na^+ channel inactivation and reduction of the peak current.

PKC:

Na^+ channels in excised, inside out membrane patches have been shown to be directly phosphorylated with purified PKC (Numann *et al.*, 1991), indicating that PKC can modulate Na^+ channel function by phosphorylation of the α subunit of the Na^+ channel (Costa & Catterall, 1984). The effect of PKC modulation on Na^+ channels is quite complex and varies in different neuronal populations. However, direct exposure to phorbol-esters, which are known to activate PKC, has consistently been found to lead to different degrees of reduction in sodium current amplitude in cultured neurones as well as cell lines expressing brain Na^+ channels (Dascal & Lotan, 1991; Numann *et al.*, 1991; Godoy & Cukierman, 1994a, 1994b). For example, activation of PKC in *Xenopus* oocytes, injected with messenger RNA (mRNA) from chick brain, was shown to decrease peak Na^+ current (Sigel & Baur, 1988). Similar results were observed for PKC-dependent regulation of $Na_v1.2$ sodium channels expressed in *Xenopus* oocytes (Dascal & Lotan, 1991; Schreibmayer *et al.*, 1991). It has also been reported that activation of PKC in rat brain neurones or in transfected CHO cells expressing $Na_v1.2A$ Na^+ channels causes rapid and reversible slowing of Na^+ channel inactivation kinetics and reduction of peak Na^+ current amplitude (Numann *et al.*, 1991). This effect is blocked by mutation of a single serine residue in the intracellular loop between homologous domains III and IV (West *et al.*, 1991). The slowing of sodium channel inactivation results from phosphorylation of a site in the inactivation gate (West *et al.*, 1991), while the reduction in peak sodium current requires phosphorylation of sites in the intracellular loop between domains I and II, as observed for PKA modulation.

Reduction of Na^+ current by PKC is expected to cause a significant decrease in cell excitability. Furthermore, in CA1 pyramidal cells activation of PKC has been shown to suppress the persistent sodium current (Alroy *et al.*, 1999). Since Na^+

current is responsible for initiation and propagation of the action potential in neurones, and is an important regulator of neuronal excitability, blocking these channels is an effective way of controlling cell excitability. It is known that PKC activating substances induce uneven changes in Na^+ currents (Godoy & Cukierman, 1994a), which perhaps depend on their effects on different PKC isoforms. Therefore, it is very important to try and understand the detailed mechanism that controls gating of persistent sodium currents and cell excitability.

As in brain, sodium current in skeletal muscle and heart can be attenuated by PKC (Murray *et al.*, 1997; Schreibmayer, 1999; Shin & Murray, 2001). Thus, PKA and PKC have similar effects on neuronal channels: so called *convergent modulation* as described by Li *et al.*, (1993) while PKA and PKC effects on cardiac sodium channels are not similar: so called *divergent modulation.*

Under physiological conditions, protein kinase activation is one of the last steps of a sequence of events starting with activation of a membrane receptor. Therefore, it is important to study the modulation of Na^+ channels by extracellular activation of membrane receptors. Many different neurotransmitters regulate PKA and PKC activity through distinct G protein-coupled receptors. So far, only acetylcholine and dopamine have been shown to alter the functional properties of voltage-gated Na^+ channels in neurones via activation of PKC and PKA, respectively (Cantrell *et al.*, 1996, 1997). However, it can be anticipated that other neurotransmitters will also be found to have similar effects.

Activation of PKC by diacylglycerols or by acetylcholine acting through muscarinic acetylcholine receptors has been shown to slow sodium channel inactivation and reduce peak sodium current amplitude (Sigel & Baur, 1988; Lotan *et al.*, 1990; Numann *et al.*, 1991; Cantrell *et al.*, 1996). As in hippocampal neurones, muscarinic receptor activation in rat neocortical neurones has been shown to inhibit persistent Na^+ currents (Mittmann & Alzheimer, 1998). In cortical neurones, persistent Na^+ currents are active near critical subthreshold voltages (Mittmann & Alzheimer, 1998). Modulation of its functional properties is thought to contribute to the regulation of firing patterns. Reduction of peak Na^+ current would be expected to shift the voltage threshold for action potential generation towards more depolarised potentials. Therefore, a stronger depolarisation would be required to elicit a response.

Thus, the functional role of modulation of sodium channel function by neurotransmitters acting through intracellular signal transduction pathways, including PKC, is an important direction for advances in development of new drugs. In particular, modulation of persistent sodium current would represent a powerful tool in controlling membrane excitability.

G-proteins:

Another likely mechanism for regulation of sodium channels is through *guanine nucleotide binding proteins* (G proteins). The G protein mediated signal transduction pathways are important mechanisms of cellular and physiological regulation (Hille, 1992b). Hundreds of structurally homologous transmembrane receptors (e.g. muscarinic and adrenergic) regulate the activity of heterotrimeric G proteins. Upon binding ligand, these receptors promote the exchange of GDP for GTP in the G-protein α subunit (Gα), an event that presumably dissociates Gα from the strongly associated βγ dimer (Gβγ). Once dissociated, both Gα and Gβγ are capable of interacting with multiple effector and regulatory proteins until the intrinsic GTPase activity of Gα converts the bound GTP to GDP, and the inactive heterotrimer reforms.

It is known that ion channels can be regulated by two different pathways involving G proteins (Breitwieser, 1991; Hille, 1992b; Wickman & Clapham, 1995). One involves diffusible second messengers, including intracellular Ca^{2+}, cyclic nucleotides and diacylglycerol (DAG). In this case, the G protein α subunits (Gα) and βγ subunits (Gβγ) modulate specific effectors through regulation of intracellular second messenger pathways (Codina *et al.*, 1987; Schwiebert *et al.*, 1995; Ikeda, 1996; Ismailov *et al.*, 1996; Neer & Smith, 1996). The other pathway is referred to as *membrane-delimited* G protein regulation, which is independent of second messengers. This type of regulation has been shown to modulate not only Na^+ channels, but K^+, Ca^{2+} and Cl^- channels (Scott & Dolphin, 1987; Tilly *et al.*, 1991; Matsuda *et al.*, 1992; Kurachi *et al.*, 1995; Manavalan *et al.*, 1995; Schreibmayer *et al.*, 1996). Direct binding of Gβγ to ion channels has been reported for brain Na^+ channels by Ma and colleagues, who have shown that co-expression of $G\beta_2\gamma_3$, $G\beta_1\gamma_3$ or $G\beta_5\gamma_3$ subunits with rat brain $Na_v1.2A$ channel α subunit in HEK293 cell line greatly enhances the persistent component of the current (Ma *et al.*, 1997). Furthermore, the same group has shown that Na^+ currents in acutely dissociated rat hippocampal neurones and in CHO

cells transfected with cDNA encoding the α subunit of rat brain $Na_v1.2A$ channel are enhanced following activation of G proteins by GTPγS (Ma *et al.*, 1994). These interesting findings bring out the possibility that the gating of persistent channels can be controlled by certain regulatory mechanisms.

1.2.5 Sodium channels as molecular targets for antiepileptic drugs

With the exception of migraine, the epilepsies are the most common episodic neurological disorders. Until recently, the cellular and molecular basis of this disorder have not been clearly understood. However, it is now widely accepted that alterations in ion channel structure, expression or regulation might play a role in susceptibility to some epilepsies.

Voltage-gated Na^+ channels are prime candidates for a role in mediating cellular excitability because they set the threshold for action potential generation. Neuromodulation of sodium channel function is likely to have an important influence on generation of the high frequency action potentials that are an essential element of epilepsy. Brain sodium channels are already molecular targets for a number of chemically diverse antiepileptic agents such as phenytoin, carbamazepine and lamotrigine (Rogawski & Porter, 1990; Ragsdale *et al.*, 1991; Meldrum, 1996; Taylor & Narasimhan, 1997). These clinically important antiepileptic drugs exert their therapeutic effects principally by blocking brain sodium channels.

The persistent sodium current may be an important component of the sodium current involved in seizures. Segal and Douglas (1997) demonstrated an effect of phenytoin on the late sodium channel openings in hippocampal neurones *in vitro*. These effects were demonstrated at the concentration where fast, transient sodium current remains intact. Because persistent currents usually occur at more negative potentials than transient sodium currents, their inhibition may prevent membrane depolarisation before a neurone starts to fire.

There is a need for the development of new antiepileptic drugs because seizures in one out of three patients with epilepsy are resistant to treatment with currently available anticonvulsant drugs (Loscher, 1998). Development of subtype specific sodium channel blockers may be a promising tool. A better understanding of sodium

channel modulation and mechanism for the gating responsible for persistent currents may improve the development of selective antiepileptic drugs with decreased adverse effects.

1.3 VOLTAGE-GATED POTASSIUM CHANNELS

Potassium channels are the most diverse family of membrane proteins present in both excitable and nonexcitable cells. They were first recognised and defined by Hodgkin and Huxley in 1952 in their description of nerve impulse generation and propagation in the giant axon of squid, as the molecular entities mediating flows of potassium ions across nerve membranes in action potential generation (Hodgkin & Huxley, 1952c).

Members of this channel family play critical roles in cellular signalling processes regulating neurotransmitter release, heart rate, insulin secretion, neuronal excitability, smooth muscle contraction and cell volume regulation. Over 50 human genes encoding various K^+ channels have been cloned during the past decade and precise biophysical properties, subunit stoichiometry, channel assembly and modulation by second messenger and ligands have been addressed to a large extent.

Although K^+ channels are found in many different types of cells carrying out many different biological tasks, the single basic function of all K^+ channels is the formation of a transmembrane 'leak' specific to K^+ ions. In living cells, the intracellular concentration of K^+ is much greater than that found in the extracellular space. Opening of K^+ channels causes an outward flow of positively charged K^+ ions, generating a negative potential across the membrane. This membrane 'hyperpolarisation' occurs in different physiological contexts for varied purposes. Obvious examples involve termination of the action potential in electrically excitable cells.

In general, K^+ channel activities are elaborately and tightly regulated, both by tissue-specific control of transcription and by biochemical actions on the channel proteins. Some K^+ channels are constitutively active, but most act transiently, being 'gated' by physiological signals, such as voltage, Ca^{2+} or G proteins, to name a few. With the recent progress in understanding of the molecular diversity, structure and function of K^+ channels, came discoveries that mutations in some K^+ channel genes and/or altered regulation of K^+ channel function are linked with various diseases, including several human genetic diseases, such as cardiac arrhythmias, deafness and epilepsy. This highlights the importance of further studies into the structure, function

and regulation of these channels with the aim of identifying novel and more effective drugs to combat the deficiencies associated with these disease states.

1.3.1 Potassium channel diversity and classification

In the nervous system, K^+ channels serve a variety of important functions. They set the resting membrane potential, control cell excitability, membrane repolarisation and regulate action potential duration and frequency (Hille, 1992a). The variety of functions displayed by K^+ channels can be explained by the fact that there is a multiplicity of K^+ channels in nervous tissue (Aronson, 1992). Unlike voltage-gated Na^+ channels, functional K^+ channels are made up of four separate α subunits, which come together in the membrane to surround a water-filled K^+ selective pore (MacKinnon, 1991; Papazian, 1999). Among diverse voltage-gated K^+ channels, only closely related subfamilies of α-subunits are capable of coassembling to form heteromultimers. This by itself has allowed considerable diversity of K^+ channels as a wide range of homomultimers and heteromultimers are possible from the same subfamily. The diversity of potassium channels is enhanced by spliced variants of the K^+ channel genes, which are further forms of protein derived from alternative processing of its mRNA.

Since the first gene encoding a K^+ channel was cloned from *Drosophila Shaker* mutant (Papazian *et al.*, 1987), more than 200 genes encoding a variety of K^+ channels have been identified. K^+ channel families can be divided into three groups defined by the transmembrane topology of the α subunits, with six, four or two putative transmembrane segments.

Structural features of six transmembrane domain one-pore potassium channels

These are the earliest discovered and the best characterised K^+ channels. Members of this voltage-gated family of potassium channels (Kv) include *Shaker*-related K^+ channels, *ether-a-go-go*- related K^+ channels (EAG) and KCNQ channels.

As the name suggests, these potassium channel proteins are composed of four α subunits (Jan & Jan, 1997), each containing six transmembrane helices (S1-S6). The "six-transmembrane" structure bears homology to each of the four domains of voltage-gated sodium channels. Helices S5 and S6 along with the intervening P loop form the central, K^+ selective pore, with a voltage sensor located at S4 (*figure 4*). As with the sodium channels, the S4 segment has a *lysine* or *arginine* residue appearing in every third or fourth position in an otherwise hydrophobic stretch that makes up the fourth transmembrane segment (Papazian *et al.*, 1987; Pongs *et al.*, 1988).

Several variations of these common features are known, such as the large conductance Ca^{2+}-activated K^+ channels (BK_{Ca}), which are architecturally similar to the Kv subtype, with an extra transmembrane segment near the amino terminus. These channels thus have 7 transmembrane domains (S0-S6).

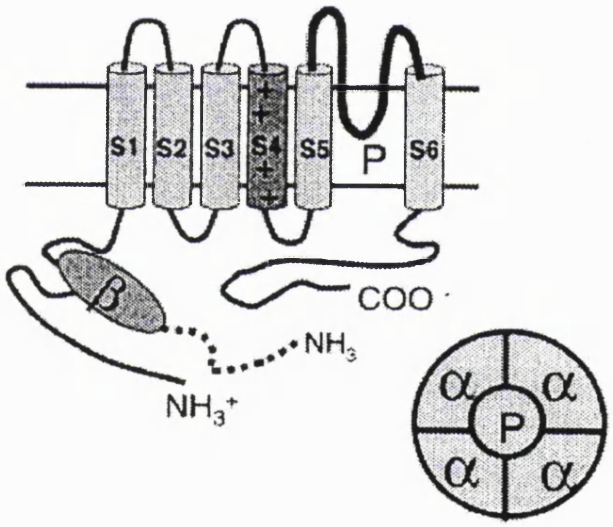

Clones	*Native current*
Kv1-Kv9	IK_{DR},IK_{TO}, IK_{UR}
EAG	IKr
KCNQ	IKs, I_M
HSlo	BK_{Ca}*
SK	SK_{Ca}
IK	IK_{Ca}

Figure 4: *Schematic representation of six transmembrane domain one-pore K^+ channels, composed of four subunits each containing six transmembrane segments (S1-S6) and a conducting pore (P) between S5 and S6 with the voltage sensor at S4. Some K^+ channels include an auxiliary β subunit, which is a cytoplasmic protein with binding site located at the N-terminus of the α subunit. The inset shows the assembly of K^+ channels. Homomeric K^+ channels consist of four identical α subunits while different α subunits form heteromeric K^+ channels. IK_{DR} (delayed rectifying K^+ current), IK_{TO} (transient outward delayed rectifying current), IK_{UR} (ultrarapid delayed rectifying current), IKr (cardiac rapid delayed rectifier, IK_S (cardiac slow delayed rectifier), I_M (M current), BK_{Ca}, SK_{Ca} IK_{Ca} (Ca^{2+} activated currents).* (Picture from Shieh *et al.*, 2000).

** BK_{Ca} has an extra transmembrane domain (S0) and an extracellular N terminus*

Channel activation

In 1998, the fist crystal structure of an ion-selective channel was poublished (Doyle *et al.,* 1998), revealing the structure of a K^+ channel (KcsA) from the bacterium *Streptomyces lividans* at 3.2Å resolution. KcsA has only two transmembrane domains (M1 and M2, see page 45), connected by a pore loop. Nevertheless its structure has the closest kinship to the S5-P-S6 region of the Kv channel family. Crystallographic analysis reveals that the KcsA channel is a tetramer, with four identical subunits arranged symmetrically around a central pore. The subunits are arranged in such a way that they form a structure similar to an inverted teepee. The poles of the teepee are formed by the four M2 (corresponding to S6 in Kv channels) helices. These lie close together at the inner side of the membrane but widen out towards the extrracellular side, forming a funnel-shaped tent that is lined by the M2 helices at its stem and the pore helices at its outer mouth. The pore helix is connected to the M2 helix by a stretch of amino acids that contain the K-signature sequence (TVGYG) and forms a narrow selectivity filter close to the extracellular side of the membrane.

In voltage-dependent ion channels, membrane depolarisation is required to cause conformational changes leading to channel opening, which allows permeant ions to flow. As mentioned previously, the S4 segment in six transmembrane domain potassium channels represents the major component of the voltage sensor (Papazian *et al.*, 1991; Perozo *et al.*, 1994). The S4 segment that contains positively charged residues (*lysine* or *arginine*) at approximately every third position, resulting in a regularly spaced array of 5 to 7 positive charges, is conserved within the voltage-gated K^+ channel family. The central event initiating channel opening is an outward movement of the S4 transmembrane segment. Since this segment carries numerous positively charged residues, this conformational movement is energetically favoured by a depolarising voltage (Larsson *et al.*, 1996; Starace *et al.*, 1997). How this movement is actually coupled to the opening of the pore is still not certain. It is known however, that opening of Kv channels is a direct result of movements of S6 near the intracellular end of the pore (Yellen, 1998). Furthermore, Cha and colleagues have used lanthanide-based resonance energy transfer to measure distances between *Shaker* potassium channel subunits at specific residues during this gating process (Cha *et al.*, 1999). Measured distance changes suggest that the region associated with the S4

segment undergoes a rotation and possible tilt, rather than a large transmembrane movement in response to voltage, as demonstrated in *figure 1b*.

Channel inactivation

Many voltage-dependent K^+ channels activate and inactivate rapidly. Inactivation is a non-conducting state during maintained depolarisation. Three types of inactivation have been characterised and associated with distinct molecular domains of the channel: N-, P- and C-type. For example, fast N-type inactivation of Kv channels, like that of voltage-gated Na^+ channels, results from occlusion of the inner mouth of the pore by the N-terminal residues of the *Shaker* K^+ channel. These residues move into the internal vestibule (in S4-S5 linker) to occlude the pore when the channel opens (Hoshi *et al.*, 1990; Isacoff *et al.*, 1991). The most distal part of the inactivating residues serves as an inactivation 'ball', which can swing into the channel pore and block ion fluxes, while the more proximal region acts as a 'chain' which tethers the 'ball' to the channel. In contrast to the fast process of N-type inactivation, C- and P-type inactivations involve a slower rearrangement of the outer mouth and specific residues in the pore, respectively (Hoshi *et al.*, 1991; De Biasi *et al.*, 1993; Yellen *et al.*, 1994; Liu *et al.*, 1996). For example, TEA has been shown to slow C-type inactivation when applied to the outside, but not inside, of the membrane (the reverse being true for N-type inactivation).

Auxiliary β subunits

As previously mentioned, some K^+ channels can associate with auxiliary β subunits, which themselves are not involved in the voltage sensing or pore formation (reviewed in Isom *et al.*, 1994). These subunits have diverse roles, such as modulation of gating properties like inactivation, cell surface expression, trafficking of the ion channel complex and serving as binding sites for ligands.

Structural features of two transmembrane domain one-pore potassium channels

The two transmembrane one-pore K^+ channels are made up of four α subunits, each containing two-transmembrane segments (M1 and M2) and a pore loop in between, *figure 5* (Papazian *et al.*, 1987; Pongs *et al.*, 1988; Ho *et al.*, 1993; Kubo *et al.*, 1993). The inward rectifier K^+ channels (Kirs) belong to this family of channels. These channels conduct K^+ currents more in the inward direction than outward, and they are important in setting the resting membrane potential. Gating mechanism is controlled by internal Mg^{2+} ions and polyamines that occlude access of K^+ to the internal vestibule of the conducting pore, by binding to a charged amino acid in the second transmembrane domain (Lu & MacKinnon, 1994).

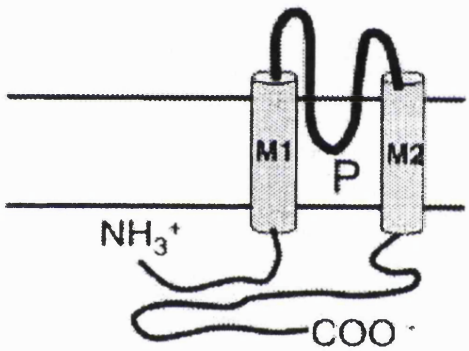

Clones	*Native current*
Kir1.1	RomK
Kir2.1	IK_1
Kir3.1/Kir3.4	I_{Ach}
Kir6.2/SUR	K_{ATP}

Figure 5: *Schematic representation of two transmembrane domain one-pore K^+ channels, composed of four subunits, each containing two transmembrane segments (M1 and M2) and a P loop in between. I_{Ach} (muscarine-activated K^+ current), IK_1 (inward rectifier), K_{ATP} (ATP sensitive current).* (Picture from Shieh *et al.*, 2000).

Four transmembrane domain two-pore potassium channels

The more recently discovered members of the four transmembrane domain two pore channel family have an unusual structure, with two P loops per subunit *(figure 6)*, with two such subunits forming a functional channel to retain the tetrameric arrangement (Ketchum *et al.*, 1995; Lesage *et al.*, 1996). Many of the currents generated by these channels display no voltage dependence and weak rectification. Members of this family include two-pore weak inward rectifier (TWIK), TWIK related acid sensitive K^+ channel (TASK), TWIK-related arachidonic acid stimulated K^+ channel (TRAAK).

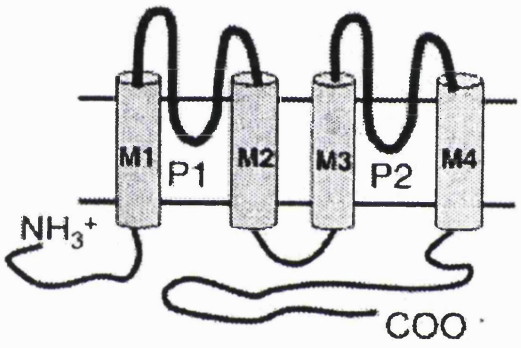

Clones

TWIK
TREK
TASK
TRAAK

Figure 6: *Schematic representation of four transmembrane two-pore K^+ channels, that have four transmembrane segments (M1-M4) with two P-loops.* (Picture from Shieh *et al.*, 2000).

1.3.2 M-type potassium channels

The M channels (I_M) are important members of the six transmembrane domain K^+ channel family. They were first identified and described in 1980 in bullfrog sympathetic ganglion neurones by Brown and Adams (1980) as a voltage- and time-dependent, low-threshold, slowly activating, non-inactivating and slowly deactivating K^+ current. It was termed *"M current"* because of its suppression by muscarinic receptor activation. The mammalian equivalent was soon described in rat sympathetic superior cervical ganglion (SCG) cells (Constanti & Brown, 1981). I_M has since been found in a variety of other cell types, including amphibian dorsal root ganglion (DRG) neurones (Tokimasa *et al.*, 1993), mammalian central neurones (Halliwell & Adams, 1982; Constanti & Sim 1987; Moore *et al.*, 1988), neurone-like NG108-15 neuroblastoma x glioma cells (Brown & Higashida, 1988) and rat pheochromocytoma PC12 cells (Villarroel *et al.*, 1989). The M-current plays a dominant role in regulating excitability because of its unique activity in the voltage range of action potential generation (Brown & Adams, 1980; Marrion, 1997). The M current slowly activates when an excitatory stimulus depolarises the neurone towards spike threshold, repolarising the membrane back toward resting potential and suppresses firing. In this way the M current limits repetitive spike firing in response to a persistent depolarising stimulus and is therefore a key mechanism for *'spike-frequency adaptation'*.

Pharmacology of I_M

M-type potassium currents appear to be insensitive to blockade by other K^+ channel blockers, such as apamin, tubocurarine, and hexamethonium (Brown, 1988). So far, there are seven agents that have been reported to inhibit native I_M through a non-G-protein-coupled-receptor mediated mechanism. These include *barium* (Adams & Brown, 1982); TEA (Adams & Brown, 1982), *methylxanthines* (Marrion & Adams, 1992), *ethanol* (Moore *et al.*, 1990), *wortmannin* (Tokimasa *et al.*, 1995), *calcium* (Selyanko & Brown, 1996) and a cognitive enhancer *linopirdine* [DuP 996; 3,3-bis(4-pyridinylmethyl0-1-phenylindolin-2-one] (Aiken *et al.*, 1995; Lamas *et al.*, 1997), along with its more potent analogue *XE991* (Wang *et al.*, 1998). The first four of the aforementioned M channel blockers are active in only the millimolar concentration range and are quite non-selective. Wortmannin is not a direct M channel blocker,

however, Ca^{2+} and linopirdine/XE991 appear to be direct and relatively specific M-channel blockers. Furthermore, an extracellular site of action was suggested for linopirdine/XE991 since linopirdine blocked single M channels only when administered to outside-out, but not inside-out patches (Lamas *et al.*, 1997). This suggestion was supported by the observation in whole-cell recordings that intracellular application of linopirdine to rat cultured superior cervical ganglia had no effect on I_M amplitude (Costa & Brown, 1997).

Regulation of I_M

I_M is regulated by an array of G-protein linked receptors (Brown, 1988; Hille, 1994), including suppression of the current by acetylcholine acting on muscarinic receptors.

The muscarinic receptor subtype mediating I_M inhibition appears to depend on cell-type. In rat superior cervical ganglia (SCG), muscarine-induced inhibition of I_M was blocked by *pirenzepine* - a selective M_1 antagonist, and not by *gallamine* or *himbacine* - selective M_2 and M_2/M_4 antagonists, respectively (Marrion *et al.*, 1989; Bernheim *et al.*, 1992). This implies involvement of the M_1 muscarinic receptor as the receptor responsible for modulating I_M in sympathetic ganglion neurones (Marrion *et al.*, 1989; Bernheim *et al.*, 1992). Consistent with these finding, Robbins *et al* (1991) have shown that muscarine inhibited M-like current in NG108-15 cells transfected with M_1 or M_3 muscarinic receptors, but not M_2 or M_4 DNA, and that M_1 and M_3 receptors both couple through common pertussis toxin-resistant G protein, $G_{\alpha q/11}$, whereas M_2 and M_4 couple through G_i (Pfaffinger, 1988; Brown *et al.*, 1989; Robbins *et al.*, 1993). Furthermore, Hamilton *et al* have demonstrated that in mutant mice lacking the M_1 receptor, the robust suppression of M current activity evoked by muscarininc agonists, is completely lost (Hamilton *et al.*, 1997).

Suppression of the M-current results in membrane depolarisation and an increase in neuronal input resistance, making the cell more likely to fire action potentials (Adams & Brown, 1982; Aiken *et al.*, 1995; Marrion, 1997). Under physiological conditions, in the absence of acetylcholine, M-channel activity hyperpolarises the cell membrane potential, leading to dampening of neuronal responsiveness to synaptic inputs. However, in the presence of released acetylcholine,

M- channels are inhibited. Thus, centrally acting muscarinic cholinergic agonists and cholinesterase inhibitors that increase the synaptic availability of acetylcholine are powerful convulsants, which is caused partly by M-current suppression (Turski *et al.*, 1989; Hamilton *et al.*, 1997). The M current thus serves to oppose epileptic activity. Indeed, like the M current, a major pharmacological action of many currently available anticonvulsant drugs is to enhance spike-frequency adaptation (Rogawski & Porter, 1990). Taken together, it can be concluded that M-channels play a key role in controlling seizure activity. Because of this, it is very important to study in detail the genetic and physiological links between the regulation of M channels and neuronal hyperexcitability, which can lead to epileptic seizures. The first question that has to be addressed is the molecular composition of the M channel.

For about 20 years or so since its first description, a number of candidate genes have been proposed as being responsible for generating the M current (Stansfeld *et al.*, 1997), however none fulfilled all of the criteria (Marrion, 1997; Mathie & Watkins, 1997) due to a lack of selective pharmacological agents. However, with the discovery of linopirdine and XE991, it was possible to identify the molecular correlates of the M current. In 1998, David McKinnon and colleagues showed that currents induced by two newly discovered potassium channel subunits, *KCNQ2* and *KCNQ3* heteromultimers resembled the gating kinetics and pharmacology of M currents (Wang *et al.*, 1998). Both KCNQ2 and KCNQ3 K^+ channel subunits have predominant brain localisation and are expressed in sympathetic ganglia, which are known to express the M channel. KCNQ2, KCNQ3 and KCNQ2/3 channels can be modulated by muscarinic stimulation when expressed with M_1 receptors in mammalian cells (Selyanko *et al.*, 2000; Shapiro *et al.*, 2000). Furthermore, linopirdine and XE991, both specific inhibitors of the M current (Lamas *et al.*, 1997) blocked KCNQ2/3 channels with similar affinity to that of the native M-current. The overlapping distribution of KCNQ2 and KCNQ3 proteins in the brain, with high levels in critical areas for seizures, including the hippocampus, neocortex and thalamus (Schroeder *et al.*, 1998; Tinel *et al.*, 1998; Yang *et al.*, 1998; Cooper *et al.*, 2000), and the apparent role of KCNQ2 and KCNQ3 in a form of infant epilepsy called benign familial neonatal convulsions (BFNC) (Charlier *et al.*, 1998; Biervert *et al.*, 1998; Singh *et al.*,

1998), provided additional evidence that these subunits underlie the neuronal M-current.

1.3.3 KCNQ2/KCNQ3 potassium channel subunits are the molecular correlates of the M-current

To determine whether KCNQ2 and/or KCNQ3 represented the molecular correlate of the M-current, Wang *et al.*, (1998) examined their: (1) mRNA distribution in sympathetic ganglia; (2) biophysical properties; and (3) response to pharmacological treatment. Wang and colleagues (1998) showed that the relative expression of KCNQ2 message in superior cervical ganglia, coeliac ganglia and superior mesenteric ganglia was nearly identical to the percentage of these neurones that possessed the M current. However, in contrast to the well-known relative insensitivity of the M current to TEA (Adams & Brown, 1982), KCNQ2 was blocked by TEA with a Kd of 160 $\pm$ 20 nM. The TEA sensitivity of KCNQ2 was likely to be due to its *tyrosine* residue at position in the pore region known to confer TEA sensitivity (Hadley *et al.*, 2000). KCNQ2 message was also highly expressed in cerebellum, a brain region consisting primarily of granule cells that are apparently devoid of M current (Watkins & Mathie, 1996). However, these issues were resolved with the co-expression of KCNQ2 and KCNQ3. The resultant KCNQ2 plus KCNQ3 (KCNQ2/3) channels not only yielded a current density 11-fold greater than the expression of KCNQ2 alone, they were approximately 20-fold less sensitive to TEA. The TEA Kd of 3.5 $\pm$ 0.7mM for KCNQ2/3, which correlated well with block of hippocampal M current (Storm, 1989), was attributed to the *threonine* rather than the *tyrosine* residue in the pore of KCNQ3. The marked increase in current density observed upon co-expression helped to explain the lack of M current in the cerebellum. To further confirm the identity of KCNQ2/3 as the M channel, Wang *et al.*, (1998) characterised its biophysical properties and sensitivity to more selective pharmacologic blockade. Accordingly, in situ hybridisation studies (Schroeder *et al.*, 1998; Tinel *et al.*, 1998) have demonstrated that KCNQ2 and KCNQ3 messages are widely distributed in the brain and are largely overlapping. Like the native M current in superior cervical ganglia, KCNQ2/3 currents expressed in *Xenopus* oocytes slowly activated with a $V_{1/2}$ of approximately –40mV, were non-

inactivating and displayed slow deactivation kinetics. Pharmacologically, KCNQ2/3 was strongly inhibited by muscarine when co-expressed with the M_1 receptor and by 1mM Ba^{2+} ions. Furthermore, the observation that linopirdine (Lamas *et al.*, 1997) and XE991 (Schnee & Brown, 1998; Zaczek *et al.*, 1998) were effective blockers of KCNQ2/3 provided yet another important link between this newly discovered heteromultimeric potassium channel and native M currents. In addition, agents that predominantly affect A-type (*4-aminopyridine*; Thompson, 1977), delayed rectifier (*clofilium*; Arena & Kass, 1988), HERG (*E-4031*; Zhou *et al.*, 1998) or Ca^{2+} activated (*charybdotoxin*; Goh *et al.*, 1992) potassium channels had no effect on KCNQ2/3 channels (Yang *et al.*, 1998). Therefore, all available anatomical, biophysical and pharmacological data supports the proposal that KCNQ2/3 is the molecular correlate of the M current.

However, the proposal that KCNQ2 + KCNQ3 heteromultimers are the only channels underlying the M-current is probably an oversimplification. KCNQ2 and KCNQ3 channels are members of a novel potassium channel gene family found in mammals (KvLQT1) (Wang *et al.*, 1996) and to date, 5 members of this family have been identified: KCNQ1, KCNQ2, KCNQ3, KCNQ4 and KCNQ5. The fact that other members of the KCNQ potassium channel family, namely exogenously expressed KCNQ1-KCNQ5 channels all produce functional currents that display M-like characteristics and pharmacology (Hadley *et al.*, 2000; Selyanko *et al.*, 2000; Schroeder *et al.*, 2000a; Shapiro *et al.*, 2000), suggests that other members of this family may contribute to the diversity of native M-like K^+ currents.

1.3.4 KCNQ potassium channel family

Structural features:

Structurally, KCNQ channels are related to the Kv potassium channels, having six transmembrane segments. Like other Kv channels, KCNQ subunits have a single P loop that forms the selectivity filter of the pore (four copies provided by four subunits), a positively charged fourth transmembrane domain (S4) and intracellular amino and carboxi termini. The S4 segments, as with voltage-gated sodium channels and other voltage-gated K^+ channels have been suggested to form the voltage sensor. All KCNQ subunits have a regular distribution of six positively charged amino acids in the S4 segment, except for KCNQ1, which has four. The proteins share between 30 and 65% amino acid identity, with particular high homology in the transmembrane regions (Schroeder *et al.*, 2000a). Although the length of the C terminus is variable, with KCNQ5 having the longest, followed by KCNQ2, then KCNQ3, then KCNQ4 and with KCNQ1 having the shortest C terminus, all five proteins are highly homologous in the intracellular C terminus, termed the "A domain" (Schwake *et al.*, 2000). The A domain is closely followed by a short stretch of amino acids thought to be involved in subunit assembly (Schmitt *et al.*, 2000). In contrast, the length of the intracellular N terminus is similar between 5 types.

All five known KCNQ channels are inhibited by M_1 muscarinic receptor activation (Schroeder *et al.*, 2000a; Selyanko *et al.*, 2000; Shapiro *et al.*, 2000), and can form functional homomultimers. However, the formation of heteromultimers is restricted to certain combinations (Schroeder *et al.*, 1998; Kubisch *et al.*, 1999; Schroeder *et al.*, 2000a; Lerche *et al.*, 2000).

When expressed in cell lines, KCNQ currents produce non-inactivating outwardly rectifying voltage-dependent K^+ currents that activate positive to –60mV (Selyanko *et al.*, 2000), however, the current characteristics change, depending on expression of homomultimers or heteromultimers. For example, as previously discussed KCNQ2/3 heteromultimers produce currents that are 10 times greater than the amplitude expected from simple summation of currents produced by homomultimeric KCNQ2 and KCNQ3. This suggests that the increase in current is not due to an increased single channel conductance or mean open time, but due to an

increased number of functional channels expressed at the cell membrane (Schwake *et al.*, 2000, Selyanko *et al.*, 2001). KCNQ3 has been shown to interact with all KCNQ subunits, except for KCNQ1 (Schroeder *et al.*, 1998). KCNQ4 appears to interact with KCNQ3, with current amplitudes greater than the homomeric sum (Kubisch *et al.*, 1999), but not with KCNQ1 nor KCNQ2. Likewise, KCNQ5 interacts with KCNQ3 but not KCNQ1 or KCNQ2 (Schroeder *et al.*, 2000a). KCNQ1 channels do not seem to functionally interact with any members of its own KCNQ family (Schroeder *et al.*, 1998; Kubisch *et al.*, 1999; Schroeder 2000a; 2000b; Lerche *et al.*, 2000).

KCNQ1

The first member of this family, KCNQ1 (originally termed KvLQT1) was identified by Mark Keating and colleagues (Wang *et al.*, 1996) in a linkage study looking at some of the genetic causes of sudden death from cardiac arrhythmia – most common form of long QT (Romano-Ward) syndrome and a potentially fatal inherited cardiac arrhythmia. Mutations in the KCNQ1 channel, leading to a decrease in channel activity down to ~ 10%, are sufficient to cause cardiac arrhythmias. Thus, it is not surprising that KCNQ1 channels are expressed predominantly in the heart. Although KCNQ1 subunits are able to form functional homomers, they are also able to form functional heteromers with auxiliary β subunits, *KCNE1* (Kaczmarek & Blumenthal, 1997). The KCNE family of proteins are single transmembrane domain proteins that cannot form a pore when expressed alone. However they play important roles in defining the activation characteristics of KCNQ channels. For example, in the presence of KCNE1, KCNQ1 current increases in amplitude, displays a more positive activation range and becomes very slow to activate (Barhanin *et al.*, 1996; Sanguinetti *et al.*, 1996). KCNQ1/KCNE1 heteromultimers are thought to underlie the slow delayed rectifier current (IKs) in the heart and are responsible for the repolarisation of the cardiac action potential. Evidence is based on the similar kinetics and pharmacology of the IKs current and that seen through KCNQ1/KCNE1 heterologously expressed homomultimeric channels (Yang *et al.*, 1997). KCNQ1 in association with the KCNE1 subunit constitutes the IKs current, responsible for repolarisation in the heart (Barhanin *et al.*, 1996; Sanguinetti *et al.*, 1996). Mutations in KCNQ1 genes cause LQT syndrome. It is likely that mutations in KCNQ1 associated with LQT will decrease the availability of IKs by altering gating properties

or by a dominant-negative loss of channel function, leading to a prolonged ventricular repolarisation. Perturbations in the regulation of the cardiac action potential can lead to life-threatening syndromes, such as the LQT syndrome. The QT refers to the time interval between the occurrence of the Q and T waves of the ECG and an increased duration of this interval is diagnostic of the syndrome. In the most common form of LQT, LQT1, which accounts for 50% of the incidents, mutations in KCNQ1 are responsible for the delay in cardiac repolarisation.

KCNQ1 is also able to interact with another member of the KCNE family, KCNE3 and is found in intestinal crypt cells (Schroeder *et al.*, 2000b). Interestingly, in contrast to the KCNQ1/KCNE1 interaction, the KCNE3 nearly abolishes KCNQ1 gating, leading to constitutively open channels. However the physiological relevance of this is not clear.

KCNQ2 and KCNQ3

KCNQ2 and KCNQ3 were identified by homology to KCNQ1 and positional cloning in families with BFNC (Biervert *et al.*, 1998; Schroeder *et al.*, 1998). Both are expressed mainly in neuronal tissues and their expression in the brain overlaps (Biervert *et al.*, 1998; Schroeder *et al.*, 1998; Tinel *et al.*, 1998; Yang *et al.*, 1998; Cooper *et al.*, 2000). When expressed in *Xenopus* oocytes, KCNQ3 elicits currents that are slightly above background. KCNQ2 produces larger currents. When KCNQ2 and KCNQ3 mRNAs were coinjected in *Xenopus* oocytes, the resultant current was more than 10-fold larger than that observed in cells injected with either KCNQ2 or KCNQ3 alone (Schroeder *et al.*, 1998; Wang *et al.*, 1998). The increase in macroscopic current on coexpression of KCNQ2 and KCNQ3 has been proposed to be caused by increased surface expression (Schwake *et al.*, 2000; Selyanko *et al.*, 2001). As described in *section 1.3.2*, the highly regulated neuronal M current that is generated by KCNQ2/3 channels is important for spike frequency adaptation and the regulation of neuronal excitability. An inhibition of the M current leads to neuronal excitability. Thus, it makes perfect sense that mutations in either KCNQ2 or KCNQ3 can lead to BFNC. It is possible that reductions in KCNQ2 and KCNQ3 channel activity in BFNC may result from reductions in channel protein level, or impaired channel assembly, trafficking, or localisation, as well as alteration in intrinsic functional properties (Schroeder *et al.*, 1998; Cooper *et al.*, 2000).

It is also worth pointing out that KCNQ2 and KCNQ3 mRNAs are not always coexpressed in the same ratio (Schroeder *et al.*, 1998; Tinel *et al.*, 1998; Cooper *et al.*, 2000), indicating that channels with different KCNQ2 or KCNQ3 stoichiometries may be present *in vivo*, probably alongside homomeric KCNQ2 or KCNQ3 channels.

KCNQ4

KCNQ4 was cloned by homology to KCNQ3 (Kubisch *et al.*, 1999). KCNQ4 is expressed mainly in the outer hair cells of the cochlea and brainstem (Kubisch *et al.*, 1999; Kharkovets *et al.*, 2000). The vestibular apparatus, like the cochlea, contains two types of hair cells; type I and type II. The KCNQ4 current has similar kinetics to a large voltage-gated K^+ current in the type I outer hair cells. It has been suggested that the role of KCNQ4 is to recycle K^+ ions after stimulation of the hair cells (Kubisch *et al.*, 1999). Mutations in KCNQ4 gene have been associated with a form of slowly progressive dominant deafness (DFNA2). It is currently unclear how mutations in KCNQ4 cause deafness. It has been suggested that a partial loss of KCNQ4 function leads to the degeneration of sensory outer hair cells, which results from chronic depolarisation or potassium overload.

KCNQ4 can form heteromers with KCNQ3 that activate faster, however it is not clear whether they occur *in vivo*.

KCNQ5

KCNQ5 is the most recently identified member of the KCNQ channel family (Schroeder *et al.*, 2000a; Lerche *et al.*, 2000). KCNQ5 has been shown to be present in the brain, including cortex and hippocampus (Schroeder *et al.*, 2000a), as well as in rat SCG and in NG108-15 cells, in which M current has been recorded. The recent observation that KCNQ5 can form functional heteromers with KCNQ3 in the central nervous system and in peripheral ganglia, indicates that M type channels may be more diverse than previously expected. In addition, the native M-current shows an exponential activation and deactivation (Adams & Brown, 1982). However, KCNQ2 and KCNQ3 homomultimers and heteromultimers show sigmoidal activation (Wang *et al.*, 1998; Selyanko *et al.*, 2000). On the other hand, KCNQ4 (Selyanko *et al.*, 2000) and KCNQ5 homomultimers (Lerche *et al.*, 2000) and KCNQ3/5 heteromultimers (Lerche *et al.*, 2000) show more exponential activation, which may suggest that these

subunits also contribute to the native M current. This may contribute to the variations in kinetics and pharmacology of different M-like K^+ currents (Robbins *et al.*, 1992) seen in different tissues. KCNQ4 can also associate with KCNQ3 and yield M-type currents, but its expression pattern is much more restricted in the brain, thus it is unlikely to constitute the neuronal M current in most neurones.

Unlike other KCNQ genes, a spliced variant of KCNQ5 is also prominently expressed in skeletal muscle (Schroeder *et al.*, 2000a; Lerche *et al.*, 2000), although its function is unclear. Because of an extra exon in this spliced variant, this isoform of KCNQ5 kinetically no longer resembles an M current.

1.3.5 M-type and KCNQ potassium channels as molecular targets for antiepileptic drugs

K^+ channels are critical to neurotransmission in the nervous system. Alterations in the function of these channels lead to perturbations in membrane excitability and neuronal functions. The M-type K^+ channel is one of the most important regulators of neuronal excitability because it plays a critical role in determining the excitability threshold, firing properties and responsiveness of neurones to synaptic inputs. Although other K^+ channels also participate in regulation of membrane excitability, the M channel plays a crucial role because of its unique modulation by neurotransmitters, voltage sensitivity and multiple regulatory pathways (Brown & Adams, 1980; Brown, 1988; Bosma *et al.*, 1990; Smith *et al.*, 1992; Marrion, 1997). And with the recent demonstration that KCNQ2 and KCNQ3 subunits constitute the M current in native neurones, it is not surprising that mutations in KCNQ2 and KCNQ3 genes, resulting in reduced K^+ current, leads to enhanced seizure susceptibility.

Benign Familial Neonatal Convulsions (BFNC) is an idiopathic form of epilepsy beginning within the first six months after birth. BFNC is rare (1 in 100,000 incidence) and is generalised by seizures in early life, which disappear within weeks or months of birth. However, about 16% of the patients display seizures in later life. BFNC has been linked to mutations in KCNQ2 and KCNQ3 genes (Biervert *et al.*, 1998; Singh *et al.*, 1998). When cRNA of truncated KCNQ2 identified from families with BFNC alone were injected, no detectable current was found. When mutant and

wild-type cRNA were coinjected in a 1:1 ratio to mimic the situation in a heterozygous patient, the currents were reduced, compared with those recorded from *Xenopus* oocytes injected with similar amounts of wild-type cRNA. Thus, although there was no obvious dominant negative effect, reduction of the current may be enough to explain the dominant mode of inheritance of this disorder (Biervert *et al.*, 1998). Likewise, when the KCNQ3 mutant associated with BFNC was coexpressed with wild-type KCNQ2, reduction in function rather than a dominant negative effect was seen (Schroeder *et al.*, 1998). Together, Schroeder *et al.*, (1998) suggested that a 25% loss of heteromeric KCNQ2/KCNQ3 function is sufficient to cause the hyperexcitability in BFNC. Reduction of total current by about 25% is critical during postnatal brain development and therefore results in seizures associated with BFNC. In later life it is possible that development of other mechanisms help to compensate for this deficiency.

Mediation of M-currents by KCNQ2/3 fits perfectly with the role of KCNQ2 and KCNQ3 in epilepsy. Therefore, KCNQ2 and KCNQ3 are suitable targets for the development of drugs for the treatment of epilepsy. Compounds that open or enhance the activity of M-currents, causing hyperpolarisation of the cell membrane and decreasing cell excitability may serve as useful antiepileptic agents.

1.3.6 Retigabine

Because of the key role of K^+ channels in dampening neuronal excitability, it has been suggested that K^+ channel openers could have an anticonvulsant activity (Turski *et al.*, 1989).

First synthesised in 1988 as an analogue of flupirtine, a non-opioid, centrally-acting analgesic, N-(2-amino-4-[fluorobenzylamino]-phenyl) carbamic acid ethyl ester (*retigabine*, D-23129) has shown efficacy in a wide range of in vitro and in vivo epilepsy models (Tober *et al.*, 1994; Rostock *et al.*, 1996). The drug is currently in Phase II clinical trials for the treatment of epilepsy. In *vitro* studies have shown that retigabine acts differently to other anticonvulsants, particularly in its ability to suppress epileptiform discharges that are resistant to other anticonvulsant agents (Armand *et al.*, 2000). To explore the mechanism underlying this antiepileptic activity, Rundfeldt and

colleagues have investigated the effects of retigabine on voltage- and ligand-gated ion channels. In NG108-15 cells, 10 μM retigabine reduced sodium current by 20% and shifted the voltage activation of N- and L-type calcium channels in the depolarised direction (Rundfeldt *et al.*, 1995). More potent effects were observed in cultured rat cortical neurones, where 0.1 μM retigabine induced a doubling of GABA-gated chloride currents. At concentrations of 0.1 μM and above, retigabine also induced an outward potassium current in NG108-15 cells that was blocked by barium but not by 4-aminopyrdine or glibenclamide (Rundfeldt, 1997). Although not recognised at the time, the retigabine-induced current was likely to be the M-current. Whilst my work was in progress, Rundfeldt and Netzer (2000), Main *et al.*, (2000) and Wickenden *et al.*, (2000) published the observation that in Chinese hamster ovary (CHO) cells transfected with KCNQ2/3 subunits, retigabine shifted the current-voltage activation curve to the left, increasing the rate of activation and decreasing the rate of deactivation. Keeping in mind the role of KCNQ2/3 channels in epilepsy, KCNQ channels in the brain represent a novel target for antiepileptic drugs.

1.4 AIM OF MY PhD STUDIES

Epilepsy is one of the most common neurological disorders and affects roughly about 1% of the population. It is characterised by synchronised, pathological electrical activity of large groups of neurones, and this electrical hyperexcitability leads to epileptic seizures. Since the electrical hyperactivity that causes epilepsy is directly created by currents flowing through ion channels, the genes encoding such channels constitute promising candidate targets for the cause and treatment of epilepsy. Because Na^+ and K^+ channels play such key roles in the control of cellular excitability, it is important to study the expression and regulation of these channels.

Whilst most Na^+ channels fully inactivate within 10ms of depolarisation, some are capable of switching to a different gating mode, thus showing a persistent component. Since activation of Na^+ channels leads to excitation of neurones and generation of action potentials, these persistent currents may have important implications in cell hyperexcitability and generation of epileptic discharges. Drugs that selectively block voltage-sensitive Na^+ channels and particularly persistent Na^+ currents are a reasonable choice for treating epilepsy. The aim of the first part of this study was to compare the biophysical and pharmacological properties of two distinct sodium channels; one that produces a fully inactivating Na^+ current, and one, which in addition to the transient current, is capable of producing a persistent component.

In the first part, I have carried out voltage-clamp studies on the properties of the native Na^+ channels in rat sympathetic neurones from the superior cervical ganglia (SCG). Unlike the Ca^{2+} and K^+ currents in these cells, which have been separated and kinetically characterized (Freschi, 1983; Belluzzi *et al.*, 1985), detailed biophysical and pharmacological properties of the Na^+ currents in rat SCG neurones (Belluzzi *et al.*, 1986; Schofield & Ikeda, 1988) have not been previously documented. It is clear that SCG neurones exhibit a fully inactivating Na^+ current. In contrast, when human $Na_v1.3$ Na^+ channel is expressed in the CHO cell line, the channel shows a persistent Na^+ current component. The biophysical properties of the Na^+ channels in SCG neurones were studied by using the whole cell voltage clamp technique. Regulation of this current by a G protein coupled pathway via membrane receptors was also investigated. Molecular biology and immunocytochemical techniques were used to find out which of the known sodium channels are present in SCG neurones. This data

was used to compare the properties of the fully inactivating sodium channel with the biophysical properties and regulation of the $Na_v1.3$ Na^+ channel expressed in a CHO cell line, which shows a persistent component, with the objective of finding a modulatory mechanism by which the gating of sodium channels switches from a fully inactivating mode to a persistent mode.

In contrast to the role of Na^+ channels in controlling cellular excitability, K^+ currents, especially the M-current, dampen the excitability of neurones. Loss of M current function leads to membrane hyperexcitability. Accordingly, mutations in either KCNQ2 or KCNQ3 genes believed to underlie the M-current, which result in reduced currents, underlie a form of inherited epilepsy, BFNC. Therefore, opening these channels is an effective way of controlling epilepsy. Retigabine is currently undergoing phase II clinical trials for the treatment of epilepsy and only recently the anticonvulsive activity of retigabine has been linked with its ability to open neuronal K^+ currents. When I started my studies, the molecular target was still unidentified. However, during the course of my studies two groups identified the molecular target of retigabine to be the KCNQ2/3 heteromultimer expressed in cell lines. In the second part of my results section I have studied the effect of retigabine on KCNQ1, KCNQ2, KCNQ3, KCNQ4 homomeric and KCNQ2/3 heteromeric channels expressed in CHO cells stably transfected with the M_1 receptor.

Following my observation that KCNQ1 channels were resistant to the current enhancing effect of retigabine and that KCNQ2-4 currents were all enhanced by retigabine, I attempted to identify the site of interaction of retigabine on the KCNQ channel by creating point mutations between KCNQ1 and KCNQ2 channels, and checking for loss or gain of action of retigabine.

I have also shown for the first time the effect of retigabine on the native neuronal M-current recorded in rat SCG cells, as well as the physiological effect of retigabine on action potential generation in these cells and the enhanced dampening effect of M current on cell excitability in the presence of retigabine.

CHAPTER 2

MATERIALS AND METHODS

2.1 TISSUE CULTURE

2.1.1 Ganglion Cell Culture

Primary cultures of neurones were prepared from superior cervical ganglia (SCG) from 17-day-old Sprague-Dawley rats, using a standard enzymatic dissociation procedure, as fully described elsewhere (Marrion *et al.*, 1989; Delmas *et al.*, 1998). Rats were killed by CO_2 inhalation and decapitated, according to the U.K. Animals (Scientific Procedures) Act 1986. Ganglia were dissected from the carotid bifurcation, the surrounding sheath removed and cut into several pieces with iridectomy scissors. The pieces were incubated at 37°C in collagenase (500 U ml^{-1} and bovine serum albumin 6 $mg.ml^{-1}$) for 15 minutes, washed three times in Hank's Balanced Salt Solution (HBSS; no Ca^{2+}, no Mg^{2+}) containing 10 mM Hepes, then in trypsin (1 $mg.ml^{-1}$ with 6 $mg.ml^{-1}$ BSA) for 30 minutes. Following trypsin incubation, the cells were triturated using a fire-polished glass pipette and centrifuged for 3min at 800 r.p.m. The pellet was re-suspended in culture medium (L 15 medium supplemented with 10% fetal bovine serum, 24mM $NaHCO_3$, 38mM glucose, 50 U ml^{-1} penicillin and streptomycin, 25 $ng.ml^{-1}$ nerve growth factor). After plating the dissociated cells onto laminin coated 35mm plastic petri dishes, the cells were kept overnight in a 37°C incubator with 5% CO_2.

When studying the Na^+ current in SCG neurones, it was sometimes necessary to replate the cells prior to recording in order to disrupt the processes such as axons and dendrites, the presence of which can lead to problems associated with poor space clamping (see *section 2.2.1*). The replating procedure involved triturating the cells in the 35mm petri dish using a fine aperture pasteur pipette until the cells are lifted off from the bottom of the dish, then centrifuging them for 3min at 800 r.p.m. The pellet was then resuspended in SCG growth media and plated out onto laminin coated dishes as before. The cells were left in the incubator for about 4 hours or until they adhere to the bottom of the dish before recording.

2.1.2 Chinese hamster ovary (CHO) Cell Culture

Sodium current recordings, CHO NaIII: CHO cells were stably transfected with cDNA that encoded human brain $Na_v1.3$ sodium channel. The *CHO (NaIII)* cells were cultured in Isocove's medium which was supplemented with 10% dialysed fetal calf serum, 1% non-essential amino-acids, streptomycin ($2mg.ml^{-1}$), penicillin ($4mg.ml^{-1}$), hypoxythane (100M) and thymidine (16μM) – HT supplement. Cells were split when confluent, as described for CHO hm1 cells below, and plated onto poly-L-lysine coated glass coverslips. Cells were grown in an incubator for 1-2 days prior to electrophysiological recordings.

Potassium current recordings, CHO hm1: CHO cells stably transfected with cDNA encoding human M_1 muscarinic receptors (Mullaney *et al.*, 1993) were cultured in α-MEM supplemented with 10% fetal calf serum, 1% L-glutamine and 1% penicillin/streptomycin. Cells were split when confluent and plated onto 35mm dishes. Briefly, splitting cells involved washing the cells with HBSS and incubating with trypsin-EDTA ($0.5g.l^{-1}$ trypsin). Once the cells had rounded up, they were dislodged and fresh medium was added to inactivate the trypsin. The cells were centrifuged for 5 minutes at 1000 r.p.m. and the pellet resuspended in fresh medium. Cells were plated in 35mm plastic dishes and left at 37°C and 5% CO_2 for 1 day before transfection.

CHO hm1 Transfection

CHO hm1 cells were transfected with KCNQ potassium channel cDNAs using "LipofectAmine Plus" (Life Technologies, Gaithersburg, MD) according to the manufacturer's recommendations. A total of 1μg DNA was used per dish, of which 10 parts were channel DNA and 1 part marker (T-cell receptor molecule CD8). Plasmids containing KCNQ and CD8 cDNAs, and driven by the cytomegalovirus (CMV) promoter, were co-transfected in a ratio of 10:1. For expression of heteromultimers, equal amounts of KCNQ2 and KCNQ3; KCNQ1 and KCNE1 cDNAs were used. Successfully transfected cells were identified by adding CD8-binding "Dynabeads" (Dynal, Great Neck, NY) prior to electrophysiological recordings.

2.2 ELECTROPHYSIOLOGICAL RECORDINGS

2.2.1 PRINCIPLES

Patch Clamping

The patch clamp technique (Hamill *et al.*, 1981) was developed by Erwin Neher and Bert Sakmann. It is an extremely powerful and versatile method for studying electrophysiological properties of biological membranes. For electrophysiology, perhaps the most important law of electricity is Ohm's law. The potential difference (ΔV) between two points linked by a current path with a conductance G, resistance R and current I is:

$$\Delta V = IR = I/G \text{ (units: volts)}$$

Voltage clamp/Current clamp

Electrophysiological equipment enables researchers to control and manipulate the membrane voltage (*voltage clamp*), thus allowing the study of the voltage dependence of ion channels. In a voltage clamp experiment the membrane is held constant while the current flowing through the membrane required to maintain that voltage is measured. The currents that flow are directly proportional to the membrane *conductance.* Membrane current is measured because there is no direct way to measure membrane conductance.

Alternatively, one may monitor the changes in membrane potential in response to currents flowing across ion channels *(current clamp).* In a current-clamp experiment, a known constant current is applied and the change in membrane potential caused by the applied current is measured.

Recording Configurations

There are various configurations for carrying out patch clamp recordings. Which configuration is chosen depends on the type of question to be addressed and the kind of ion channel under study.

Whole-cell recording

This configuration is used when ion currents of the entire cell are recorded. To perform whole-cell recordings, patch pipettes are fabricated and filled with an appropriate solution. The pipette is pressed onto the cell membrane and a slight suction is applied to establish a "gigaseal" at the contact area. This is the *cell-attached* configuration, *figure 7A*. A further, sharp suction is applied to rupture the membrane at the tip of the pipette to establish the *whole-cell* configuration, *figure 7B*. The electrolyte in the pipette is thus dialysed with the interior of the cell and the total membrane current is recorded.

Perforated-patch recording

Perforated-patch recording techniques allow the measurement of current less invasively than the standard patch-clamp approaches. The technique uses either nystatin or amphotericin B to gain access to the cell's interior. These polyene antibiotics form pores in cholesterol- or ergosterol-containing membranes. These pores are permeable to monovalent cations and Cl^- but exclude multivalent ions such as Ca^{2+} or Mg^{2+}. Amphotericin and nystatin both interfere with seal formation. Therefore, it is best to fill the tip of the pipette with an antibiotic-free solution and then to back fill with the antibiotic-containing solution. Following seal formation and establishment of the cell-attached configuration, the antibiotic slowly diffuses to the tip where it contacts the membrane and begins to form pores, *figure 7C*.

The perforated patch-clamp technique has several advantages over the whole-cell patch clamp method. (1) The channels formed by the antibiotic are impermeable to large molecules and recordings can be done without dialysing important substances from the cell's cytoplasm. Current run down is significantly slower; physiologically relevant second-messenger cascades and mechanisms important to cell signalling and channel regulation remain operative. (2) The perforated-patch technique is less damaging to the cell than the whole-cell method. The suction applied during whole cell recordings to disrupt the membrane patch can sometimes result in loss of seals. This rarely happens with the perforated-patch approach.

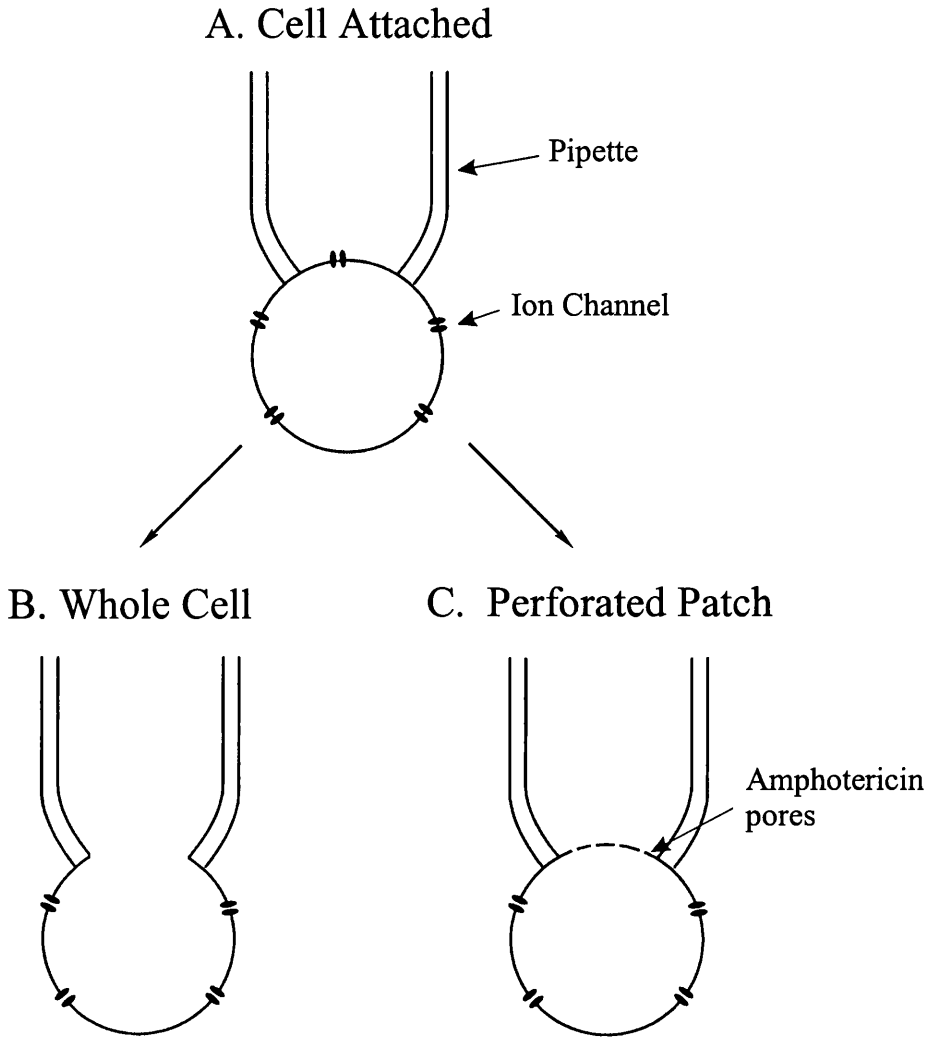

Figure 7. Recording Configurations
A. *A fire polished electrode is induced to form a tight 'gigaohm' seal with the cell membrane by slight suction, giving the 'cell attached' mode.*
B. *Further suction breaks through the membrane of the cell, thus obtaining the 'whole-cell' mode. The cytoplasm is rapidly dialysed out by the contents of the patch electrode.*
C. *Amphotericin B permeabilises the membrane to give a 'perforated-patch' mode, thus preventing the dialysis of the cytoplasm.*

Importance of a good seal

When a heat-polished pipette is pressed against the cell membrane, the interior of the pipette is isolated from the extracellular solution by the seal that is formed. If the resistance of the seal is infinite, no current can leak across this seal. Depending on the size of the seal resistance and the voltage difference between the inside and the outside of the pipette, some fraction of the current through the patch of the membrane will leak out through the seal and will thus not be measured. The lower the seal resistance, the larger the fraction of undetected current. Also, thermal movement of charges in the conducting pathways of the seal constitute the major source of noise in a recording unless the seal resistance is very high (several gigaohms or more). A high seal resistance is a prerequisite of low-noise recording.

Whole-cell capacitance

Biological membranes are typically less than 10nm thick. One of the consequences of the membrane's thinness is that it makes an excellent capacitor. Capacitance (*C*; measured in farads, *F*) is the ability to store charge, *Q* when a voltage change, ΔV occurs across the two sides of the membrane, so that $Q = C \times \Delta V$. The capacitance is proportional to the area and inversely proportional to the distance separating the two conducting sheets, or sides of the membrane. The membrane capacitance increases with cell size. Membrane capacitance is usually expressed as value per unit area; nearly all lipid bilayer membranes of cells have a capacitance of ~ 1 $\mu F/cm^2$ (0.01 $pF/\mu m^2$).

The stored charge on the membrane capacitance accompanies the resting potential, and any change in the voltage across the membrane is accompanied by a change in this stored charge. If a current is applied to the membrane, either by channels elsewhere in the cell or by current from the electrode, this current first satisfies the requirement for charging the membrane capacitance, then it changes the membrane voltage. Thus, when the membrane capacitance is in the circuit, the voltage is not reached immediately, but is approached with the *time constant* τ, given by:

$$\tau = RC$$

Thus, the charging time constant increases when either the membrane capacitance or the resistance increases.

Capacitance compensation

When the command voltage is stepped, a large amount of current flows into the pipette capacitance during transition from one potential to the next. This current transient is required to charge the membrane capacitance. In a patch clamp amplifier it is possible to eliminate this transient. This is done not only to remove transients from records for "cosmetic" reasons, but also to avoid saturation of the amplifiers during the sudden high-amplitude currents generated at the onset of the voltage changes, and to eliminate error signals caused by pipette and pipette holder capacitance.

Series Resistance

When carrying out electrophysiological recordings, many sources of error are possible. In voltage clamp recordings, the membrane potential of the cell is controlled by the potential applied to the pipette electrode. This potential can depend on the size of the *access resistance* between the pipette and the cell interior and on the size of the currents that must flow through this resistance. *Series resistance* constitutes the access resistance plus resistance of the pipette itself, but normally the major part arises from the residual resistance of the broken or perforated patch membrane. When current, I flows across the membrane, the series resistance, Rs leads to a discrepancy between the measured membrane potential, Vm (which is what the clamping amplifier controls) and the true membrane potential. According to Ohm's law, the size of the error is $Rs \times I$, so the problem is most likely to be serious when large membrane currents are recorded. To partly eliminate this error, compensation for Rs may be achieved by subtracting a voltage signal proportional to the membrane current, scaled appropriately to the command voltage of the clamping amplifier. If, for example, a current of 5nA is recorded, in a clamped cell with a series resistance of 10 mΩ, then according to Ohm's law it will yield series resistance error of 50mV. After about 80% compensation the effective value of the series resistance is 2 mΩ. In this case the error due to series resistance for a 5nA current will be reduced to 10mV.

Space clamp considerations

The voltage clamp should be able to change membrane potential sufficiently rapidly for the capacity transient to be over by the time that ionic current is measured. Clearly, this criterion is most severe when fast ionic currents are recorded (e.g. Na^+

current). Therefore it can be technically quite difficult to clamp and record a Na^+ current.

Membrane current should be recorded from an area of uniform potential, so that the current comes from a set of channels that are all experiencing the same voltage. If all portions of the cell membrane are separated from this tip of the electrode by equal access resistance, then the membrane will uniformly be voltage clamped. The voltage clamp is maintained at the tip of the voltage recording electrode and the clamp will be good in round cell bodies. However, many cells such as SCG neurones, may have processes (axons and dendrites) attached to the cell body. The membranes of these processes are separated from the cell body by an axial access resistance whose value depends on the distance to each portion of the membrane in that region of the cell. Thus, there is a voltage drop across the access resistance that becomes substantial for distal components of the membrane, leading to poor space clamp.

There are ways of avoiding the problems of poor space clamping; (1) restrict investigations to spherical cells; (2) replating neurones prior to recording in order to disrupt the processes.

Recording electrodes

At the electrodes, current must be transformed smoothly from a flow of electrons in the copper wire to a flow of ions in solution. The reference electrode in the bath and the test electrode in the pipette holder are usually silver wires coated with AgCl. If electrons flow from the copper wire through the silver wire to the electrode AgCl pellet, they convert the AgCl to Ag atoms and the Cl^- ions become hydrated and enter the solution. If electrons flow in the reverse direction, Ag atoms in the silver wire that is coated with AgCl give up their electrons (one electron per atom) and combine with Cl^- ions that are in the solution and make up insoluble AgCl:

$$Cl^- + Ag \leftrightarrow AgCl + e^-$$

There are several points to remember about Ag/AgCl electrodes: (1) the Ag/AgCl electrode performs well only in solutions containing chloride ions; (2) because current must flow in a complete circuit, two electrodes are needed. If the two electrodes face different Cl^- concentrations, there will be a difference in the half-cell potentials (the potential difference between the solution and the electrode) at the two electrodes, resulting in a large steady potential difference in the two wires attached to

the electrodes. This steady potential difference is termed *liquid junction potential* (see below) and can be subtracted electronically; (3) if the AgCl is exhausted by the current flow, bare silver wire could become in contact with the solution, which may poison many proteins and also cause overvoltage.

Junction potentials

Whenever solutions with two different compositions come into contact, a liquid junction potential is developed between them. They can be understood as a result of some imbalance of charge, which results when the more mobile ion diffuses more rapidly across the concentration gradient at the interface. The problem of liquid junction potentials can be minimised by using concentrated KCl as the electrode filling solution because K^+ and Cl^- have almost equal ionic mobilities, and as a consequence, liquid junction potentials are in the range of 1mV or smaller. The similarity in the mobility of ions results in junction potentials being small. In patch clamping, however, the choice of solutions is dictated by the physiological requirements of the experiment. In patch-clamp measurements solutions containing ions with significantly different mobilities may generate junction potentials of up to about 10mV or even more. In whole cell experiments the presence of junction potentials is generally obscured. When the pipette is immersed into the bath, the electrode potential between the pipette and bath solution is standardised by setting to zero, by applying equal and opposite back-off potential within the patch-clamp amplifier. This can give the impression that any junction potentials have been balanced out. When a seal is formed this junction potential is no longer present. As the patch is ruptured, the former junction potential is replaced by a new one – the junction potential between the internal solution of the cell with respect to the patch electrode, but the problem is that the initial back-off potential is still present within the amplifier. Apart from the situation in which the composition of the pipette and bathing solution are the same, the liquid junction potential contribution to any measured potentials never disappears. The liquid junction potential can be measured as described in Barry & Lynch (1991) and Neher (1992), and a correction made to the command voltages imposed on a cell.

2.2.2 SODIUM CHANNEL ELECTROPHYSIOLOGY

SCG:

Dishes with cultured SCG neurones were placed in the recording chamber on the stage of an inverted microscope (Nikon TMS), supported on an air-table (Wentworth Laboratories) and superfused by gravity with extracellular solution at room temperature. The extracellular solution was designed to isolate Na^+ current from others by using a relatively high concentration of Mg^{2+} to block the Ca^{2+} current and internal Cs^+ to block the K^+ current. A low external Na^+ concentration was used in order to reduce the size of the sodium current and improve the voltage clamp. In SCG neurones, when using normal (140mM) NaCl, currents over 10nA were recorded. The series resistance can be assumed to be about 3 times the original resistance of the electrode when immersed in the bath solution. So when using a 3 mΩ electrode to record a 10nA current you would expect to have errors of about 10 x 9 = 90mV. For this reason, by reducing the extracellular concentration of NaCl to 35mM the size of the Na^+ current recorded was in the range of 1-2nA. In this case the errors would be in the range of 9-18mV. The series resistance compensation on the amplifier was always used and set to 60-80%. The extracellular solution contained the following (mM): NaCl 35, glucosamine 75, Hepes 20, glucose 11, KCl 6, $MgCl_2$ 5, $CaCl_2$ 1, adjusted to pH 7.4 with NaOH, with an osmolarity ranging from 290 to 300 mOsm.

In some cases it was necessary to replate the SCG neurones 4h prior to recording. The replating process was used to disrupt the processes which were produced overnight and significantly reduced the chances of obtaining a good space clamp. Replating the cells reduced the clamp problem (see *section 2.2.1*).

Voltage-clamp experiments were performed using single patch-clamp pipettes in the whole-cell recording configuration (Hamill *et al.*, 1981). Borosilicate glass capillaries (GC 150 TF-10, Clark Electromedical Instruments, 1.5mm outside diameter, 1.17mm inside diameter) were pulled and fire-polished to obtain patch pipettes with a tip resistance of 2-4MΩ when filled with internal solution, containing (in mM): CsCl 22, CsAcetate 110, Hepes 10, EGTA 3, $MgCl_2$ 5, NaCl 10, ATP 3, GTP 0.5. The pH was adjusted to 7.2 with CsOH, with an osmolarity ranging from 290 to 300 mOsm.

The capacitance across the glass wall of the immersed part of the micropipette was reduced by thickening the wall of the micropipette. This was done by coating the micropipette with Sylgard prior to firepolishing. The other obvious way to reduce this capacitance is to reduce the fluid level so that immersion depth is minimal. This is not always as effective as might be expected, because the surface tension causes the bath solution to creep up the surface of the micropipette.

For current recording, patch electrodes were held in a Perspex holder attached to a Narishige mechanical MX1 manipulator. Constant voltage pulses (-10mV, 10ms) were applied through an Axopatch 1-D amplifier (Axon Instruments). This received an input signal from a computer (Dell) running Clampex 6 (software from Axon Instruments), via a TL-1 analogue-to-digital converter. The resulting conductance was detected on the computer screen. The signals were filtered at 5kHz bandwidth and sampled at 20kHz. Before sealing onto the cells, the pipette current was adjusted so that I = 0. The reference ground was a silver wire coated with silver chloride. The pipette was gently lowered into the recording chamber, using the manipulator, until the tip of the pipette was just touching the well-defined membrane of a cell and a small decrease in conductance detected. A small suction was applied to establish a seal between the cell membrane and the tip of the recording electrode with a gigaohm resistance, establishing a "cell-attached" configuration. The fast capacity transients were compensated, and the holding potential was set at –60mV. A further, small, sharp suction was applied to the glass electrode to effectively punch through the cell and obtain access to the interior of the cell, thus generating a "whole-cell" configuration. Series resistance was cancelled and compensation set to 60-80%. Leak subtraction was performed by subtracting the currents recorded after superfusion with 100nM tetrodotoxin (TTX) from currents recorded before. The liquid junction potential was measured as described in Barry & Lynch (1991) and Neher (1992), and a correction made to the command voltages imposed on a cell. Briefly, in these experiments, using a low resistance (1-3 mΩ) patch pipette filled with the internal solution, the pipette potential on the amplifier was zeroed with internal solution in both the bath and the recording electrode. The bath solution was then exchanged for normal extracellular Krebs. The junction potential between the internal and external solution was 11.5 mV (n= 4).

CHO NaIII:

The extracellular solution for recording the sodium current in CHO cells contained the following (in mM): NaCl 140, KCl 4.7, $MgCl_2$ 1.2, $CaCl_2$ 1, glucose 11 and Hepes 5, adjusted to pH 7.4 with NaOH, with an osmolarity ranging from 290 to 310 mOsm. The internal solution had the following composition (in mM): CsCl 120, Cs-EGTA 10, NaCl 10, Hepes 10, ATP 2,and GTP 1, adjusted to pH 7.2 with CsOH, with osmolarity ranging from 290 to 310 mOsm.

CHO cells were clamped at –90mV and after establishing the whole-cell voltage-clamp configuration, time dependent increases in the sodium current amplitude were observed. The increase was usually complete after 15 minutes. Voltage command protocols were generated and the current records stored via Digidata 1200 digital/analogue converter connected to Axopatch 200A amplifier (Axon Instruments). This was controlled by a computer (Viglen Pentium) using Clampex package (pClamp7, Axon Instruments). The signals were filtered at 5kHz and sampled at 20kHz. The capacity transients were cancelled and series resistance compensation set to 70-80%. Linear capacity transients were removed by a P/4 leak subtraction provided with the pClamp7 software.

2.2.3 M/KCNQ POTASSIUM CHANNEL ELECTROPHYSIOLOGY

Potassium currents in CHO hm1 cells and SCG neurones were recorded using the amphotericin-B perforated patch technique (Rae *et al.*, 1991). Because of their limited water solubility, amphotericin stock solutions were prepared in DMSO. These stock solutions lose activity upon prolonged storage and freezing. Therefore it is best to prepare them freshly before use. Solubilisation is enhanced by sonication. Stock solutions were added directly to the pipette filling solution to a final concentration of 0.08 – 0.1 $mg.ml^{-1}$. The solution was sonicated for maximum solubilisation of the antibiotic in the pipette solution. The tip of the patch electrode (2 - 3 MΩ when filled with solution) was dipped into the appropriate filtered antibiotic-free internal solution for about 20-30s, and then back-filled with the internal solution containing amphotericin-B. As perforation occurred, the size of the capacity transient increased and the time constant for the transient decreased. The time constant to charge the cell

capacitance is approximately *Ra x Cm* where *Ra* is the access resistance and *Cm* is the cell capacitance. When Ra is large, a brief voltage pulse change will not charge the capacitance fully before the pulse turns off. Therefore, as perforation continues and *Ra* decreases, the capacity transient gets larger, since an increasing fraction of the cell capacity gets charged during the brief pulse. In most cells, a properly filled pipette will produce minimised *Ra* of about < 15 MΩ by 15min after seal formation. It is important that amphotericin-B free solution does not exceed 500 μm distance from the tip of the electrode, otherwise the time required for the diffusion of amphotericin-B from the back-filled solution to the tip will be excessive.

Recordings from CHO hm1 cells were made at room temperature 1-2 days after transfection. No appreciable current was noticed in untransfected CHO hm1 cells. The extracellular solution consisted of (mM): NaCl 144, KCl 2.5, $CaCl_2$ 2, $MgCl_2$ 0.5, Hepes 5 and glucose 10, pH 7.4 with Tris base. To record tail currents at –120 mV (for the purpose of construction of activation curves), external KCl was raised to 25 mM; the increase in osmolarity was compensated by reducing the concentration of NaCl to 121.5 mM. The internal (pipette) solution contained (mM): K^+ acetate 80, KCl 30, Hepes 40, $MgCl_2$ 3, EGTA 3, $CaCl_2$ 1, pH 7.4 with KOH.

SCG neurones were perfused with an external solution consisting of (mM): NaCl 140, KCl 3, HEPES 5, glucose 11, $MgCl_2$ 1.2, $CaCl_2$ 2.5, tetrodotoxin (TTX) 0.0005 (pH 7.4). Internal solution for M-current recording consisted of (mM): K^+ acetate 90, KCl 40, HEPES 20, $MgCl_2$ 3, (adjusted to pH 7.3 - 7.4 with KOH, and 300 $mOsmol.l^{-1}$ with K^+ acetate). Experiments were performed at room temperature.

Voltage clamp recordings

Data was acquired and analysed using pClamp software (version 6.0.3). Currents in transfected CHO cells were recorded using Axopatch 1D patch-clamp amplifier (Axon Instruments) and filtered at 1kHz. The capacity transients were cancelled using the resistance capacitance circuit within the amplifier. Series resistance compensation was set 60-80%.

SCG neurones were voltage-clamped using an Axopatch 1D amplifier. Current traces were low pass filtered at 2 - 5 KHz using a four-pole Bessel filter and series resistance and membrane capacitance were partially compensated (> 70 %). The

capacity transients were cancelled using the resistance capacitance circuit within the amplifier. Series resistance compensation was also used, and was set to 60-80%.

2.3 DATA ANALYSIS

2.3.1 Biophysical Analysis

The data was analysed using the Clampfit (pClamp6 and 7), ORIGIN 5, Excel and Powerpoint data handling and graphical presentation software packages. All results are presented as mean $\pm$ SEM.

For the construction of the sodium current activation curves, Na^+ conductance (G_{Na}) was calculated from the peak current (I_{Na}), according the following equation: $G_{Na} = I_{Na}/V\text{-}E_{Na}$, where V is the test potential and E_{Na} is the membrane potential at which the peak current is reversed. E_{Na} is calculated from the Nernst equation:

$$E_{Na} = \frac{RT}{F} \ln \frac{[Na^+]_o}{[Na^+]_i} \qquad (1)$$

where $R = 8.314\ JK^{-1}mol^{-1}$, $T = 295K$, $F = 96500Cmol^{-1}$, $[Na^+]_o$ is the extracellular Na^+ concentration, and $[Na^+]_i$ is the intracellular Na^+ concentration. Normalised Na^+ conductance was plotted against test potentials and fitted to a Boltzmann function according to the equation:

$$\frac{G}{G_{max}} = \frac{1}{[1 + \exp((V_{1/2} - V)/k)]} \qquad (2)$$

where G is the measured conductance, G_{max} is the maximal conductance, $V_{1/2}$ is the membrane potential at which half of the channels are open and k is the slope of the curve.

For the construction of sodium current inactivation curves, the peak current (I) was normalised to the maximal value (I_{max}) and plotted against the conditioning pre-pulse potential. Data were fitted by a Boltzmann function according to the equation:

$$\frac{I}{I_{max}} = \frac{1}{[1+\exp((V_{1/2}-V)/k)]} \quad (3)$$

where V is the membrane potential during pre-pulses, $V_{1/2}$ is the potential at which half of the channels are inactivated and k is the slope of the curve.

The methods of recording and analysis of the KCNQ currents were similar to those previously employed for studying KCNQ currents (Selyanko *et al.*, 2000). Results are presented as the mean ± SEM.

Activation curves were fitted by the Boltzmann equation:

$$\frac{I}{I(50)} = \frac{1}{[1+\exp((V_{1/2}-V)/k)]} \quad (4)$$

where I is the tail current recorded at –120 mV following a pre-step to membrane potential V (estimated from the amplitudes of exponentials backfitted to the beginning of the test step), I(50) is the current following a step to +50 mV, $V_{1/2}$ is the membrane potential at which I is equal to $^1/_2$ I(50) and k is the slope of the curve. The concentration response of different KCNQ channels to retigabine was estimated by the shift in the $V_{1/2}$ values caused by 0.1, 0.3, 1, 3, 10, 30, 100 and 300 μM. Dose response curves were fitted to the following equation:

$$y = \frac{1}{1+10^{(\log EC_{50}-x)\mathrm{k}}} \quad (5)$$

where EC_{50} is the concentration corresponding to half maximal activity, x is the agonist concentration and k is the slope of the curve.

The dose response of KCNQ2/3 currents to linopirdine was estimated by evaluating the decrease in current amplitude following a step from –20mV to –50mV upon addition of 1, 3, 10 and 30 μM linopirdine. Inhibition was plotted against concentration and fitted with equation (5).

The inhibition of the KCNQ1 current was evaluated by a decrease in current amplitude following step depolarisations to +50mV from –70mV upon addition of 3,

10, 30, 100, 300 and 1000μM of retigabine. The inhibition curve was fitted with equation (5), with IC_{50} concentration corresponding to half maximal block.

2.3.2 Kinetic Analysis

According to the Hodgkin-Huxley formulation (Hodgkin & Huxley, 1952c), the sodium current can be fitted with the following mathematical description, assuming three activation gates:

$$G_{Na} = G_{Na}^{max} * m^3 * h \tag{6}$$

where G_{Na}^{max} is the maximum Na^+ conductance and stays constant, m and h are the kinetic parameters for activation and inactivation, respectively. The parameters m and h change exponentially with time following a step change of the membrane potential:

$$m = 1 - \exp(-t/\tau_m), \quad h = \exp(-t/\tau_h) \tag{7,8}$$

where τ_m and τ_h are the time constants of m and h, respectively.

The steady state activation parameter, m_∞ was fitted to the following expression:

$$\frac{G_{Na}}{G_{Na}^{max}} = m_\infty^3, \; m_\infty = \frac{1}{1 + \exp\frac{(V_{1/2} - x)}{slope}} \tag{9}$$

The voltage sensitivity of the activation time constant may be expressed as:

$$\tau_m^{-1} = \alpha_m + \beta_m \tag{10}$$

where α_m and β_m are the activation and deactivation rate constants. The following equations were used to calculate the mathematical expressions for α_m and β_m:

$$\alpha_m = \alpha_m(0)\exp+\frac{ze}{2kT}(V - V_{1/2}); \; \beta_m = \beta_m(0)\exp-\frac{ze}{2kT}(V - V_{1/2}) \tag{11,12}$$

where $\alpha_m(0) = \beta_m(0)$ are the rate constants at $V_{1/2}$ (since τ_m is maximal at half activation) (see *results* section).

2.4 MOLECULAR BIOLOGY

2.4.1 Reverse Transcriptase - Polymerase Chain Reaction (RT-PCR) - to identify sodium channel isoforms present in SCG cells

Whole SCG

The procedure for RT-PCR was described previously in detail (Steel & Buckley, 1993). Briefly, total RNA was extracted from 5 17-day-old Sprague-Dawley rat SCG with a single-step guanidine thiocyanate acid-phenol-chloroform method (Chomczynski & Sacchi, 1987); also see TRI REAGENT product information for detail). 11µl of the isolated RNA was mixed with 0.5µl of hexamer random primers and 0.5µl Oligo(dt) primer. The mixture was heated to 65°C for 5min and then immediately put on ice for at least 5min. After this denaturation step the cDNA was synthesised by incubating the RNA mixture with 2µl of 0.1M dithiothretol (DTT), 5µl of first strand buffer, 1µl of RNAse inhibitor, 1µl of 20mM deoxyribonucleotides (dNTPs) and 1µl of Superscript reverse transcriptase enzyme for 1h at 37°C. PCR was performed in PCR buffer (2µl Taq extend buffer, 2µl dNTPs, 0.2µl Taq polymerase enzyme, 12.8µl of nuclease free water, 2µl of the cDNA, 1µl of the sense primer and 1µl of the antisense primer). The PCR procedure involved initial denaturation of 3min at 94°C, 30 cycles of (30s at 94°C - denaturation, 1m at 57°C - annealing, 1m at 72°C - elongation) followed by a final elongation of 10m at 72°C. The PCR products were analysed by electrophoresis through a 2% metaphore gel, containing ethidium bromide (EtBr) and visualised under UV light.

Primers for amplification of sodium channels

Five different subtypes of rat brain Na^+ channel α subunits were simultaneously amplified along with a *cyclophilin* primer as a positive control. The Na^+ channel primers were designed to fall into regions that are highly conserved between subtypes. Primers used for amplification were:

$Na_v1.1$ - NaChI.6433s: CGGCAAACTCTGTGACTCTTAGG
NaChI.6606a: CACTAAAGTGTTTCACGTTAAACCC

$Na_v1.2$ - NaChII.7092s: ATGCACACACAGACCATCACATGC
NaChII7311a: GCAGAAGATGGCTAAACAATACTG

$Na_v1.3$ - NaChIII.6397s: GCCTATACCAGACAGTGACCTCTG
NaChIII.6645a: AACAGACTATGAAGTGGGGACCAGG

$Na_v1.6$ - NaChVI.5247s: GTTCCTGATTGTGGTGAACATGTG
NaChVI.5564a: CTGTCTCCCAGGACTGCCTTGG

$Na_v1.7$ - PN1.1s: ATGGCGATGCTGCCTCCTCCA
PN1.708a: CCCCACGATGGTCTTTAGTCC

Cyc - cyc.4s: GTCAACCCCACCGTGTTCTTCGAC
cyc.217s: TAGATGGACTTGCCACCAGTGCCA

Numbers refer to the first base of the sequence to which the primer corresponds, *s* refers to sense and *a* refers to antisense primers. The expected PCR products for each channel subtype were as follows: $Na_v1.1$ (150 bp), $Na_v1.2$ (200bp), $Na_v1.3$ (250bp), $Na_v1.6$ (317bp), $Na_v1.7$ (707bp) and cyc (213bp).

Single Cell RT-PCR

Single-cell RT-PCR was performed as described by Lambolez *et al* (1992). Recording electrodes with tip resistances as low as possible were filled with 8µl of standard filtered recording solution. Whole SCG neurones were harvested into the electrodes under visual control by applying negative pressure. To expel the contents of the electrode, a positive pressure was applied with a syringe attached to the back of the electrode while the tip of the electrode was broken onto the inner wall of the PCR test tube, containing the following: 0.3µl RNAse inhibitor, 0.5µl Oligo(dt), 1µl first strand buffer and 3.2 µl of nuclease free water. The mixture was incubated at 65°C for 5min and immediately put on ice for 5min. cDNA was synthesised as for whole ganglia, but the RT mix had the following composition: 0.5µl DTT, 1µl first strand buffer, 0.5µl dNTPs, 0.3µl RNAse inhibitor, 1µl Superscript enzyme. All of the synthesised cDNA was added to the PCR mix. The same PCR programme was used as for whole ganglia but the PCR mix had a slightly different composition: 5µl Taq extend buffer, 5µl dNTPs, 7.5µl sense primer, 7.5µl antisense primer, 1µl Taq enzyme, 14.5µl nuclease free water. G protein α_{oA} subunit primers were used as a positive control, as SCGs are an abundant source of this protein (Buckley *et al.*, 1995; Haley *et al.*, 1998). Primers for $G\alpha_{oA}$ amplification were (Buckley *et al.*, 1995);

$G\alpha_{oA}$.266s: ACTTTGGGCGTGGAGTATGGTGAC
$G\alpha_{oA}$.849a: TATTCAGGAAAGCAGATGGTCAAGG

PCR products were run through a 1.5 % metaphor gel with EtBr for the G protein and 2% gel for the sodium channel PCR products. Bands were visualised under UV light.

2.4.2 Construction of KCNQ2/KCNQ1 point mutants

KCNQ2 and KCNQ1 point mutations were constructed to replace residues conserved between KCNQ2-5 but not KCNQ1 in order to determine the site of action of retigabine. Gene fragments containing point mutations were constructed using recombinant PCR and cloned using homologous recombination in yeast (Spencer *et al.*, 1993). By taking advantage of the ability to efficiently perform homologous recombination in yeast we were able to produce several mutations relatively quickly.

KCNQ2 Point Mutants

The human KCNQ2 gene (Genbank accession number AF110020) was carried by a pRS314 expression vector containing CMV promoter, myc tags and a tryptophan (Trp) marker. The size of the plasmid was 8006bp.

The primer sequences for each of the KCNQ2 mutations were as follows, with the mutated base in lower case and bold:

Q188K - 552s: GCCGCCGGCTCC**a**AGGGCAACGTCTTTG
579a: CAAAGACGTTGCCCT**t**GGAGCCGGCGGC

S199G - 585s: TCTGCGCTCCGG**g**GCCTGCGCTTCCTGC
612a: GCAGGAAGCGCAGGC**c**CCGGAGCGCAGA

R210H - 618s: CTGCGGATGATCC**a**CATGGACC
642a: GGTCCATG**t**GGATCATCCGCAG

R214Q - 630s: CGCATGGACC**a**GCGGGGAGGCACCT
654a: AGGTGCCTCCCCGC**t**GGTCCATGCG

KCNQ2 - 292s: GCCTACGTGTTCCTCCTGG
1623a:CTGCTCGATGACGTCCATCTC

In the first step, first round separate PCR reactions were performed with the 292s and an antisense mutant primer, and 1623a and a sense mutant primer to amplify mutant 5' and 3' KCNQ2 fragments. The PCR buffer contained the following: 2 µl Taq buffer (10 x), 1 µl dNTPs (20mM), 1 µl sense primer (10 µM), 1 µl antisense primer (10 µM), 0.2 µl Taq Polymerase (Promega), 0.2 µl Taq extender (Stratagene), 1

µl KCNQ2 plasmid (1ng) and 13.6 µl water to make up the total volume to 20 µl. The PCR conditions were: 2min at 94°C, 30 cycles of (30sec at 94°C - denaturation, 1min at 60°C - annealing, 4min at 72°C - elongation) followed by a final elongation of 10min at 72°C. The PCR products were analysed by electrophoresis through a 1% agarose gel, containing ethidium bromide and visualised under UV light. Appropriate sized bands were cut from the gel and purified using Qiagen's QIAquick gel extraction kit (50).

Mutant 5' and 3' KCNQ2 fragments were then combined and used in a second PCR reaction containing 292s and 1623a. Fusion PCR was run in the following PCR buffer: 5 µl Taq buffer (10 x), 2.5 µl dNTPs (20mM), 2 µl gel purified sense primer PCR product, 2 µl gel purified antisense primer PCR product, 2.5 µl KCNQ2 292 s (wildtype KCNQ2 sense primer), 2.5 µl KCNQ2 1623a (wildtype KCNQ2 antisense primer), 0.5 µl Taq enzyme, 0.5 µl Taq extender, 32.5 µl water to make up the total volume to 50 µl. The PCR procedure involved initial denaturation of 2min at 94°C, 30 cycles of (30sec at 94°C - denaturation, 1min at 60°C - annealing, 4min at 72°C - elongation) followed by a final elongation of 10min at 72°C. The PCR products were analysed by electrophoresis through a 1% agarose gel, containing ethidium bromide and visualised under UV light. The bands were cut, gel purified and transformed into yeast.

For yeast transformations, the wildtype KCNQ2 plasmid was cut with Sac/Xho restriction enzymes by incubating 20 µl of the plasmid with 1µl of Xho I, 1 µl Sac I, 3 µl BSA (buffer), 3µl 10xT (buffer) and 2 µl water at 37°C for 1 hour, followed by a heat inactivation step of 20min at 65°C. Cutting the plasmid at a unique site to one side of the mutation and transformation of the linear plasmid (fusion PCR product) into yeast selecting Trp should result in targeted integration of the plasmid. The yeast strain FM242 was grown to an OD (600) of 0.6 and 50ml of culture was pelleted, washed twice with water and resuspended in 300 µl of 100mM lithium acetate. Yeast transformations were performed by layering on to 50 µl of competent yeast 240 µl PEG (50%), 30 µl lithium acetate (1M), 25 µl boiled salmon sperm DNA (2 µg/µl), 8 µl cut KCNQ2 plasmid and 20 µl of the mutated inset (gel purified fusion PCR product). All reagents were mixed by vortexing for 1 minute, then incubated for 30 min at 30°C, followed by 30 min at 42°C. The pellet was then resuspended in 100 µl

of water and yeast was plated onto growth plates lacking tryptophan (Trp). The plates were incubated at 30°C for 2-3 days.

Single yeast colonies were picked into 50 mls of growth media lacking Trp and grown overnight at 30°C. After pelleting, DNA was extracted from yeast by vigorous vortexing in 300 µl of lysis buffer, 300 µl phenol and 0.5 ml glass beads. DNA was precipitated and resuspended in 20 µl of water. 2 µl was electroporated into competent JS5 E.Coli bacteria and plated onto LB Amp plates. Plasmid DNA was isolated from single colonies and sequenced to identify mutants. This method yielded a mutation rate of greater than 90%.

KCNQ1 Point Mutants

KCNQ1 point mutations were constructed using the same method described for the KCNQ2 point mutants. The human KCNQ1 (Genbank accession number AF000571) gene was carried by a pRS expression vector containing CMV promoter and a Trp marker. The KCNQ1 primers used for each mutation are shown below (point mutant in lower case);

K218Q - 755s: GGGCTCC**c**AGGGGCAGG
755a: CCTGCCCCT**g**GGAGCCC

G229S - 786s: GCCATCAGG**a**GCATCCGC
786a: GCGGATGC**t**CCTGATGGC

H240R - 820s: GGATGCTAC**g**CGTCG
820a: CGACG**c**GTAGCATCC

Q244R - 836s: CCGCC**a**GGGAGGCACC
836a: GGTGCCTCCC**c**GGCGG

KCNQ1 - 1s Bam 5`: GAGAGGATCCATGGCCGCGGCCTCCTCCC
2122a Xba 5`: TCTCTCTAGATCAGGACCCCTCATCGGGGC

2.5 IMMUNOCYTOCHEMISTRY

The principle of immunocytochemistry is to localise antigens using labelled antibodies. Antigen localisation is visualised via fluorescence. Immunocytochemistry involves the use of a primary antibody, which specifically binds the antigen, and a secondary antibody conjugated to a fluorescent marker, such as FITC or TRITC, which must recognise and bind to the primary antibody.

2.5.1 Sodium channel immunolocalisation

Immunocytochemistry was performed on SCG neurones using primary sodium channel antibodies, raised against various peptides of the $Na_v1.1$, $Na_v1.2$, $Na_v1.3$, $Na_v1.6$ and $Na_v1.7$ channels in rabbit and were obtained from Glaxo SmithKline, Stevenage, UK. Antibodies were produced by Glaxo SmithKline, as detailed elsewhere (Whitaker *et al.*, 2001; Coward *et al.*, 2000). Briefly, antibodies were raised against peptide sequences, chosen from divergent regions of the different sodium channels using multiple alignments of the corresponding sequences. Lack of significant homology to other known proteins was confirmed by BLAST searches of SWISSPROT and GenBank. The peptide sequences were in the C-terminus for $Na_v1.1$, $Na_v1.2$, $Na_v1.3$; in the N-terminus for $Na_v1.6$ and in the 1st intracellular loop for $Na_v1.7$. To confirm the specificity of the antibodies Western blots were performed on whole-cell lysates isolated from human embryonic kidney (HEK) 293 cells stably expressing the cloned human α subunits. Each antibody gave broad bands of approximately expected size (~260 kDa) exclusively in the lanes loaded with the corresponding whole-cell lysate. No equivalent bands were seen in control lysates isolated from wild-type HEK293 cells or when the antibody was pre-absorbed with an excess (100 μM) of the corresponding synthetic peptide. Furthermore, solid-phase enzyme linked imunosorbent assays (ELISA) were carried out to show that each antibody did not cross-react with other peptides (Whitaker *et al.*, 2001).

Plated SCG neurones were washed for 5min in PBS 3 times. They were then fixed with acetone for 15min. After fixation the acetone was washed off by two 5min washes in PBS. In order to minimise background staining the non-specific sites were

blocked by incubating the cells in 10% BSA/PBS for 10-20min at room temperature. The cells were washed in PBS as before and incubated with the primary antibody for 3 hours at room temperature. The optimal antibody dilutions were determined through experimentation. Following incubation with primary antibodies, the cells were thoroughly washed in PBS in order to minimise background staining. The cells were then incubated in TRITC (1:40 dilution in PBS) conjugated secondary antibody for $Na_v1.7$ and $Na_v1.3$ antibodies and FITC (1:50) conjugated secondary antibody for $Na_v1.1$, $Na_v1.2$ and $Na_v1.6$ for 30min in the dark. The cells were thoroughly rinsed as before in PBS in the dark to minimise photobleaching of the fluorochromes, mounted on a coverslip and visualised under a fluorescent microscope.

2.5.2 Mutant KCNQ2 channel immunolocalisation

The KCNQ2 point mutants were labelled with an anti Myc tag antibody in order to check expression levels of the protein. CHO cells were plated onto glass coverslips and transfected with either KCNQ2 (R120H), KCNQ2 (Q188K), KCNQ2 (S199G) or KCNQ2 (R214Q) cDNA as described previously. A myc tagged KCNQ2 (G298S) cDNA was transfected and used as a positive control (Tatulian *et al.*, 2000).

For the immunostaining, the cells were washed for 5 min in PBS three times, then fixed with 4% paraformaldehyde for 25 min at room temperature. After fixation the paraformaldehyde was washed off by three 5 min washes in PBS and cell membrane was permeabilised by incubating with 0.1% Triton for 5 min. Cells were washed in PBS as before. In order to minimise background staining non-specific sites were blocked by incubating the cells in 10% BSA/PBS for 15min at room temperature. The cells were washed in PBS as before and incubated with the anti-myc primary antibody (mouse) for 1 hour at room temperature (15 µl antibody/500 µl PBS per dish). Following incubation with the primary antibody, the cells were thoroughly washed in PBS in order to minimise background staining. The cells were then incubated in TRITC conjugated anti-mouse secondary antibody (1:100 dilution in PBS) for 30min in the dark at room temperature. The cells were thoroughly rinsed as before in PBS in the dark to minimise photobleaching of the fluorochromes, mounted on a coverslip and visualised under a confocal microscope.

2.6 COMPOUNDS

The stable CHO cell line expressing the human $Na_v1.3$ sodium channel was obtained from *Glaxo SmithKline (Stevenage, UK).* Collagenase, trypsin, bovine serum albumin, L-15, laminin, poly-L-lysine, non-essential amino acids, HEPES (N-[2-hydroxyethyl]piperazine-N-[2-ethanesulfonic]acid), dimethyl sulfoxide (DMSO), glucosamine, CsCl, EGTA, ATP, GTP, staurosporine, GTPγS, phorbol dibutyrate, norepinephrine, oxotremorine-M, tetrodotoxin (TTX) - *Sigma.* The stock solutions of staurosporine, oxotremorine-M, norepinephrine, GTPγS, TTX and retigabine were prepared with distilled water to the desired concentrations. The stock solution of PDBu was dissolved in DMSO to a concentration of 0.1mM. Fetal bovine serum, glucose, penicillin, streptomycin, nerve growth factor, hypoxythane, thymidine, Isocove's medium - *Gibco.* NaCl, KCl, $MgCl_2$, $CaCl_2$, NaOH - *BDH.* CsOH - *Aldrich.*

cDNAs for human KCNQ2 and rat KCNQ3 were obtained from Dr. D. McKinnon (*Department of Neurobiology and Behavior, SUNY, Stony Brook, NY, USA*), for human KCNQ1 from Dr. M. T. Keating (*HHMI, University of Utah, Utah, USA*), and for human KCNQ4 from Dr. T. J. Jentsch (*ZMNH, University of Hamburg, Hamburg, Germany*). Retigabine was obtained from *Glaxo SmithKline, Stevenage, UK.* All other drugs and chemicals were obtained from *Sigma* or *BDH* (Poole, UK).

Sodium channel primary antibodies were obtained from *Glaxo SmithKline*, anti-myc primary antibody was obtained from *Calbiochem.* All secondary antibodies were purchased from *Dako.*

Molecular Biology

TRI REAGENT - *Sigma*; RNAse inhibitor (50U/μl) - *Boehringer Mannheim*; Superscript II reverse transcriptase (200U/μl), 0.1m dithiothretol (DTT), first strand buffer - *Gibco BRL*; dNTPs - ATP, GTP, CTP, TTP (100mM each), nuclease free water, oligodinucleotides - *Promega*; Taq DNA polymerase, Taq extend buffer - *Stratagene*; primer sequences were ordered from *Genosys.*

CHAPTERS 3 & 4

RESULTS

CHAPTER 3

CHARACTERISATION OF NATIVE, FULLY INACTIVATING SODIUM CHANNELS IN RAT SYMPATHETIC NEURONES AND REGULATION OF PERSISTENT $Na_v1.3$ BRAIN SODIUM CHANNELS EXPRESSED IN CHO CELL LINE.

3.1 INTRODUCTION

The quantitative description of the Na^+ conductance of the squid giant axon membrane by Hodgkin and Huxley (1952c) was shown to be remarkably general. Extending these voltage-clamp experiments to the small-sized and poorly accessible neurones of the mammalian nervous system, however, has been so difficult that in the absence of direct measurements, the kinetic data of the squid axon have frequently been adapted. Recent voltage-clamp studies carried out on isolated superior cervical ganglion have provided a detailed description of the ionic currents produced by membrane depolarisation in a mammalian sympathetic neurone. While the individual components of Ca^{2+} and K^+ currents have been separated and kinetically characterised (Belluzzi *et al.*, 1985; Freschi, 1983), much less is known about the Na^+ current (Belluzzi *et al.*, 1986; Schofield & Ikeda, 1988).

One interesting feature of some sodium channels is their ability to switch to a different gating mode, which results in a persistent component. Persistent Na^+ currents are thought to be generated by the same Na^+ channels that open transiently during action potentials. This persistent current is due to the channel remaining in the open state for a longer time than normally seen, and is believed to be responsible for pathological states such as epilepsy. Due to the fact that Na^+ channels may play such crucial roles in physiological processes and in disease states such as epilepsy, it is very important to study the properties and regulation of Na^+ currents, and particularly of persistent Na^+ currents, as potential future targets for antiepileptic drugs. In order to understand why some channels show a persistent component it is important to compare the biophysical and pharmacological properties of fully inactivating channels and those that show a persistent component.

SCG neurones exhibit a fully inactivating Na^+ current. In contrast, when human brain $Na_v1.3$ Na^+ channel is expressed in the Chinese hamster ovary (CHO) cell line the channel shows a persistent Na^+ current component. The aim of this study was to compare the biophysical and pharmacological properties of two distinct sodium channels: one that produces a fully inactivating Na^+ current, and one that in addition to the transient current is capable of producing a persistent component.

The biophysical properties of Na^+ channels in SCG neurones were studied by using the whole cell voltage clamp technique. Alterations in Na^+ channel behaviour

that modify Na^+ current amplitude or channel gating can lead to the generation of life-threatening diseases in humans. Hence factors that regulate Na^+ channel function are of considerable interest. Protein phosphorylation has long been recognised as a key regulatory mechanism to alter the structure and function of cellular proteins. This is achieved by the action of protein kinases and protein phosphatases. Protein kinases have been classified mainly into two groups, the serine/threonine kinases and the protein tyrosine kinases, depending on the target amino acid. Among the serine/threonine kinases is *protein kinase C* (PKC), the role of which in mediating cellular responses is well established.

It has been widely speculated that Na^+ channels are modulated via phosphorylation of one or more of the cluster of five sites in the intracellular loop between domains I and II of the α subunit. For example, it was shown that PKC is a modulator of brain $Na_v1.2A$ Na^+ current in cell lines and brain slices (Costa *et al.*, 1982; Dascal & Lotan, 1991; Numann *et al.*, 1991). Since these consensus phosphorylation sites are conserved among rat brain Na^+ channels, it is thought that all brain subtypes may be regulated in a similar way. In order to investigate this hypothesis, the effect of protein kinase C on the Na^+ channel in SCG and CHO cells was studied.

Regulation of this current by a more physiological G protein coupled pathway via membrane receptors was also investigated. Evidence for such modulation does indeed exist. Na^+ channels in acutely dissociated rat hippocampal neurones and in CHO cells transfected with cDNA encoding the α subunit of the $Na_v1.2A$ Na^+ channel have been shown to be modulated by a G-protein coupled pathway (Ma *et al.*, 1994). Hundreds of structurally homologous transmembrane receptors regulate the activity of heterotrimeric G proteins. In this study the effect of stimulating the M_1 muscarinic acetylcholine receptor by oxotremorine-M and of the α adrenoceptor by norepinephrine (noradrenaline) were investigated in SCG neurones. Several isoforms of $G\alpha$, $G\beta$ and $G\gamma$ have been characterised. Activation of the M_1 muscarinic receptor by oxo-M causes the dissociation of $G\alpha_q$ from $G\beta\gamma$, which activates PKC via DAG. Norepinephrine strongly stimulates α adrenoceptors, which are coupled to G-proteins. In this case the dissociated $G\beta\gamma$ subunit activates PKC via PLC pathway.

Molecular biology and immunocytochemical techniques were used to find out which of the known sodium channels are present in SCG neurones. This data was used

to compare the properties of this fully inactivating sodium channel with the biophysical properties and regulation of the $Na_v1.3$ Na^+ channel, expressed in a CHO cell line, which shows a persistent component.

The effect of protein kinase activation was studied on $Na_v1.3$ sodium channels with the objective of identifying a pharmacological mechanism for modulation of the persistent sodium channel gating. Evidence for such mechanism was provided by Ma *et al* (1997), who have shown that co-expression of individual G-protein βγ subunits in cell lines expressing $Na_v1.2A$ Na^+ channels can induce persistent currents. When these cells were treated with peptides known to bind with high affinity to G-protein βγ subunits, this effect was inhibited (Ma *et al.*, 1997). It is therefore possible to speculate that Gβγ subunits may act on voltage-gated Na^+ channels to generate persistent currents in neurones. To test this idea on $Na_v1.3$ sodium channels expressed in CHO cells, G-proteins were stimulated by an analogue of GTP, GTPγS, which cannot be hydrolysed by the intrinsic GTPase activity. Thus, treatment of G-proteins with GTPγS results in constitutively active G protein subunits (both α and βγ) and constitutive regulation of corresponding effectors.

3.2 *BIOPHYSICAL PROPERTIES OF SODIUM CHANNELS IN RAT SCG NEURONES*

3.2.1 Activation of voltage-gated sodium currents

In order to isolate the Na^+ current in SCG neurones from other ionic currents activated by depolarisation; namely the Ca^{2+} current and the fast transient K^+ current, a low extracellular concentration of Ca^{2+} with high [Mg^{2+}] was used to prevent flow of Ca^{2+} currents and a Cs^+ based internal solution was used to suppress the K^+ ion flow. Under these conditions, 100nM TTX blocked all of the ionic current, indicating that the studied current is entirely a Na^+ current (*figure 8B,C*). Under reduced extracellular Na^+ concentration (35mM), SCG neurones displayed fast, transient inward currents that reached a peak, ranging from -2nA to -10nA, within 1ms of depolarisation. The holding membrane potential was -60mV. At this potential the holding current was 0pA when a good seal was obtained. The membrane was held at the pre-pulse potential of -90mV for 100ms in order to remove the fast inactivation. The Na^+ currents shown in *figure 8B,C* were generated by series of 25ms depolarising steps from -45mV to +100mV. These inward currents reversed at approximately +33mV, which under these reduced extracellular sodium concentrations, is close to the calculated Na^+ ion equilibrium potential of +38mV.

The peak current at the end of each depolarising step was normalised against maximum inward current amplitude and plotted against the depolarising voltage potential to obtain a current/voltage (I/V) relationship for the Na^+ current (*figure 8D*). The current-voltage curve suggests that the sodium current in SCG neurones activated at ~ -40mV and peaked at around –10mV.

To study the voltage dependence of channel activation, the activation curve in *Figure 8E* was constructed by plotting normalised conductance against the voltage of the depolarising step. Conductance was calculated as described in *Chapter 2, section 2.3.1.* The solid line is a least-squares fit of the data to the Boltzmann function (*Chapter 2, equation 2*), characterised by half activation potential, $V_{1/2}$, at which half of the channels are activated, and by the steepness of the potential dependence of activation (the slope). Mean values for $V_{1/2}$ and the slope analysed in this fashion from

seven cells were -20.8 $\pm$ 0.2mV and 5.6 $\pm$ 0.2mV, respectively. This value is in close accordance to the $V_{1/2}$ of –21.1mV reported by Belluzzi *et al* in rat sympathetic neurones *in vitro* (Belluzzi *et al.*, 1986).

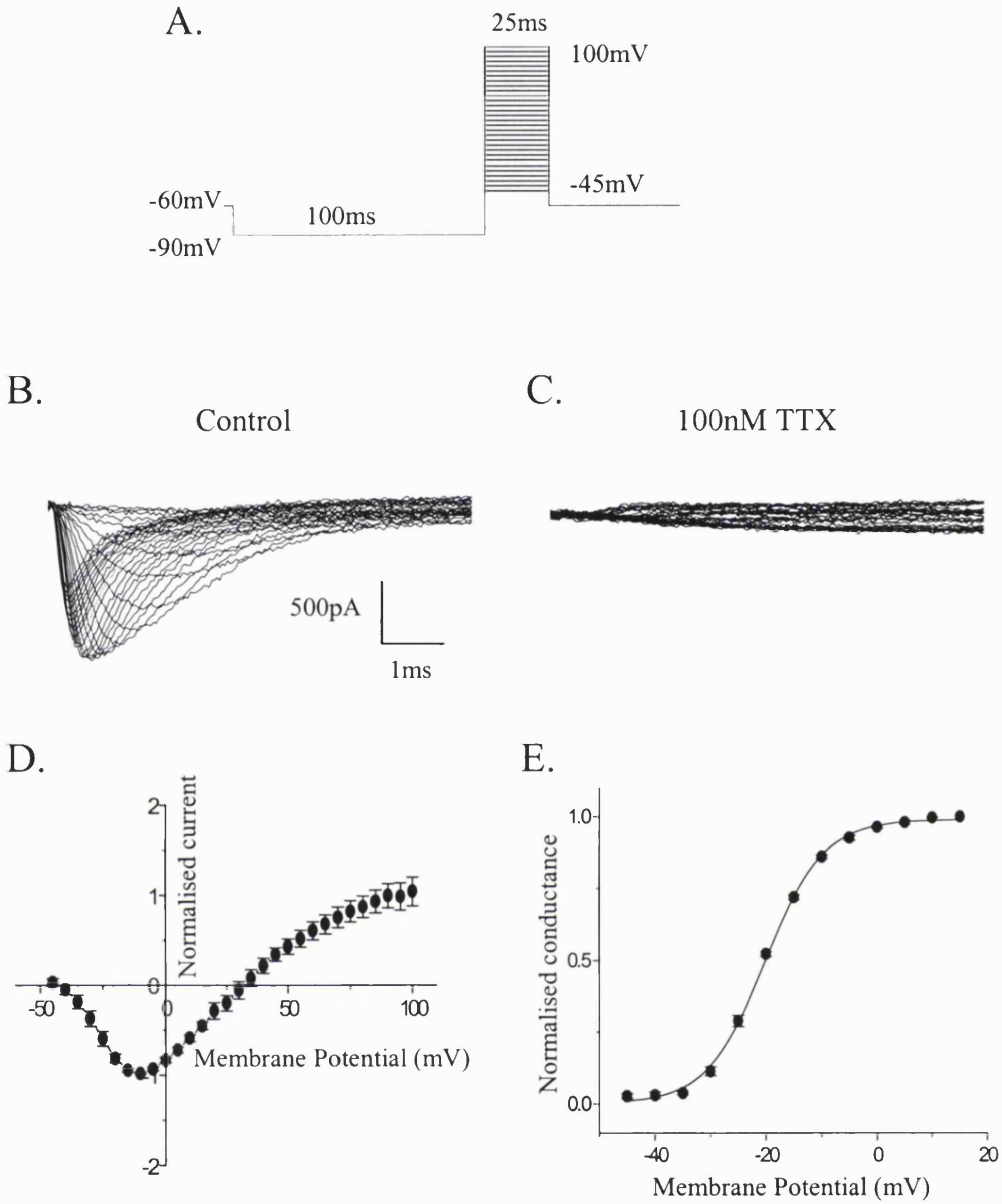

Figure 8. Biophysical parameters of activation of the Na^+ current in SCG neurones.

A. Voltage command protocol: the membrane was held at -90mV for 100ms to remove inactivation, followed by 25ms depolarising steps from -45mV to +100mV to activate the Na^+ current.
B. Na^+ currents recorded following membrane depolarisations under control conditions (traces in response to voltages from -55mV to +10mV are shown).
C. Na^+ currents recorded in the presence of 100nM TTX.
D. Current-voltage relationship of the Na^+ current. Normalised current values were plotted against command potential. Data shown as mean $\pm$ SEM (n=7).
E. Activation curve, showing the voltage dependence of Na^+ current activation. Conductance was calculated as described in *Chapter 2* and normalised values were plotted against the voltage of the depolarising step. Data points were fitted with a Boltzmann function (*equation 2, Chapter 2*), with $V_{1/2}$ of -20.8 $\pm$ 0.2mV and a slope of 5.2 $\pm$ 0.2mV (n=7).

3.2.2 Inactivation of voltage-gated sodium channels

Inactivation of the Na^+ current was studied by using a two-pulse protocol from a holding potential, Vh, of -60mV. The membrane was held at -90mV for 100ms in order to remove any inactivation. To study fast inactivation, conditioning pre-pulses of 25, 50, 100, 150, 250, 500, 750ms and 1s to various potentials between -90 and -25mV were delivered, which induced variable degrees of inactivation, before recording the inward current at -25mV. With pre-pulse potentials more positive than –75mV, the peak sodium current progressively decreased, until it was almost completely inactivated at –25mV *(figure 9A)*.

The inactivation curves in *figure 9B-J* were obtained by normalising the peak inward current after each pre-pulse potential, relative to the maximal current amplitude at the pre-pulse potential of –90mV *(figure 9A, inset)* and plotting against the conditioning pre-pulse potential. Data is shown as mean ± SEM from 6 different neurones. The solid line is a non-linear fit of the points using a Boltzmann function (*Chapter 2, equation 3*). The $V_{1/2}$ and the slope vary with time held at the conditioning pre-pulse and are tabulated in *Table 2* below:

Time at conditioning pre-pulse membrane potential	***$V_{1/2}$ (mV)***	***Slope (mV)***
25 ms	-43.8 ± 0.7	6.3 ± 0.6
50 ms	-43.6 ± 0.6	7.4 ± 0.6
100 ms	-52.3 ± 0.3	6.2 ± 0.3
150 ms	-58.1 ± 0.2	5.1 ± 0.2
250 ms	-58.9 ± 0.3	4.7 ± 0.2
500 ms	-61.1 ± 0.2	4.5 ± 0.2
750 ms	-61.1 ± 0.2	4.5 ± 0.2
1 s	-61.1 ± 0.2	4.6 ± 0.2

Table 2. Time dependence of Na^+ current inactivation in SCG neurones.
Columns show half inactivation potentials ($V_{1/2}$) and slopes of Na^+ current inactivation curves (see figure 9) produced by increasing the time held at the conditioning pre-pulse potentials from 25ms to 1s.

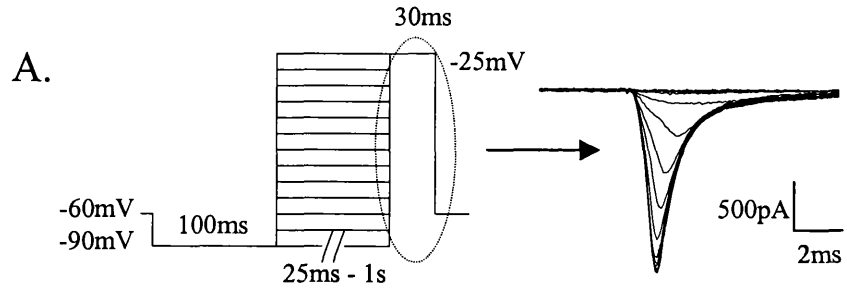
A.
30ms
-25mV
-60mV
-90mV
100ms
25ms - 1s
500pA
2ms

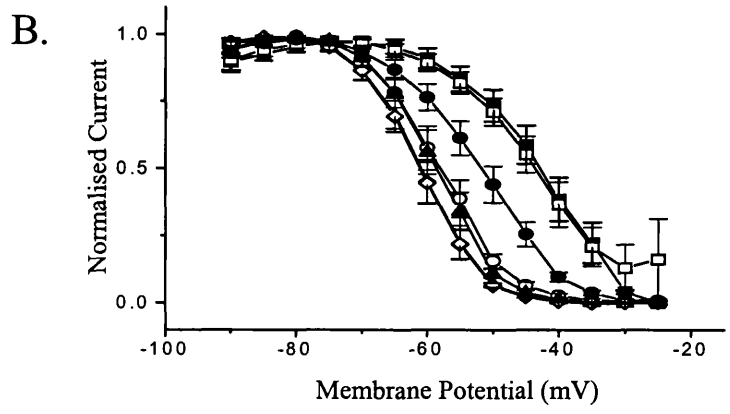
B.
Normalised Current
1.0
0.5
0.0
-100
-80
-60
-40
-20
Membrane Potential (mV)

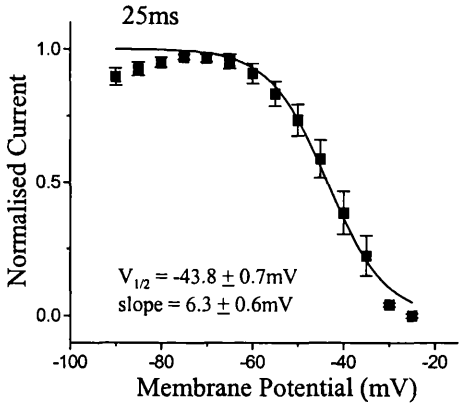
C.
25ms
Normalised Current
1.0
0.5
0.0
V1/2 = -43.8 ± 0.7mV
slope = 6.3 ± 0.6mV
-100
-80
-60
-40
-20
Membrane Potential (mV)

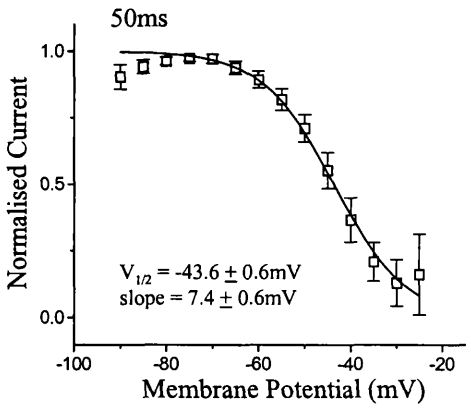
D.
50ms
Normalised Current
1.0
0.5
0.0
V1/2 = -43.6 ± 0.6mV
slope = 7.4 ± 0.6mV
-100
-80
-60
-40
-20
Membrane Potential (mV)

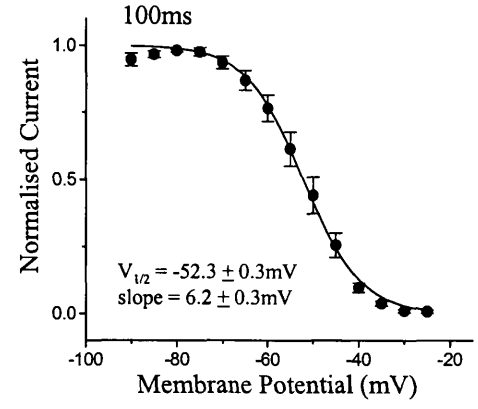
E.
100ms
Normalised Current
1.0
0.5
0.0
V1/2 = -52.3 ± 0.3mV
slope = 6.2 ± 0.3mV
-100
-80
-60
-40
-20
Membrane Potential (mV)

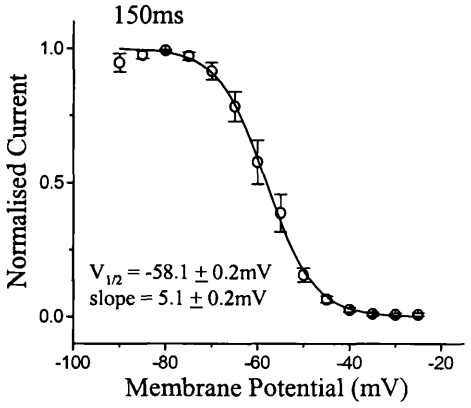
F.
150ms
Normalised Current
1.0
0.5
0.0
V1/2 = -58.1 ± 0.2mV
slope = 5.1 ± 0.2mV
-100
-80
-60
-40
-20
Membrane Potential (mV)

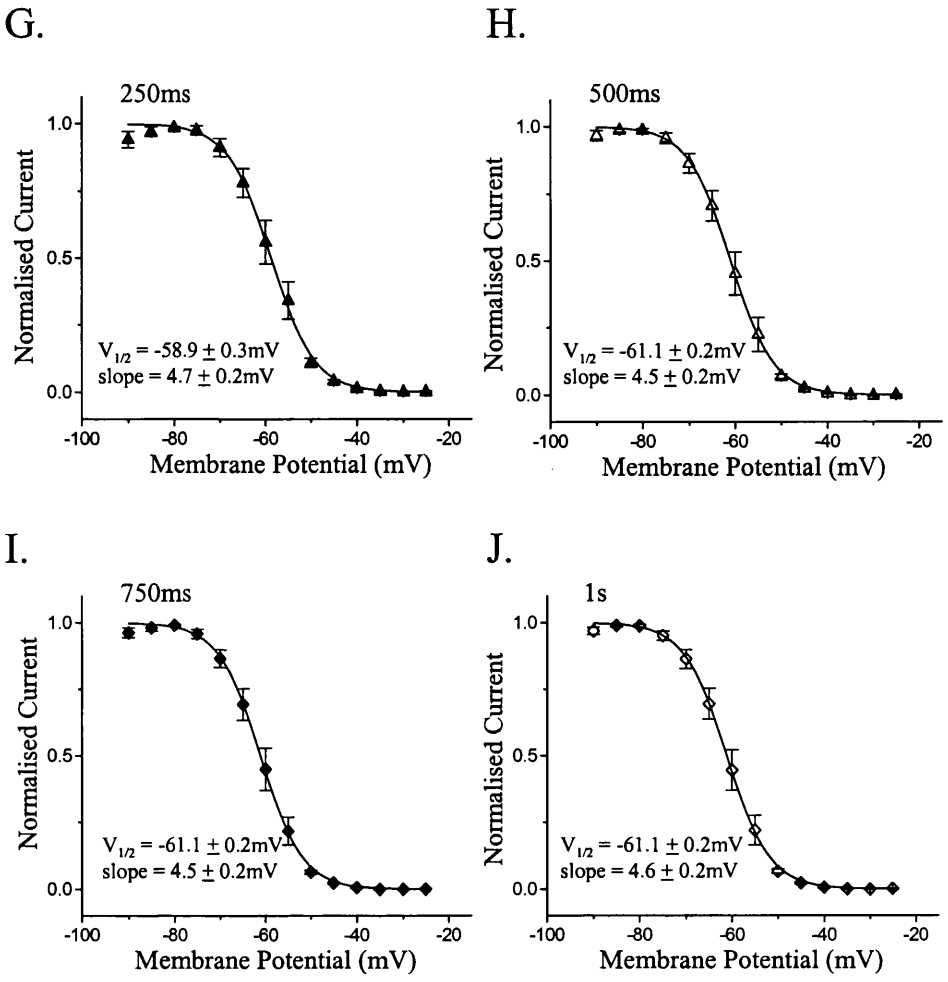

Figure 9. Biophysical parameters of inactivation of the Na^+ current in SCG neurones.

A. Voltage command protocol: from a holding potential of -60mV, the membrane was held at -90mV for 100ms to remove inactivation. The membrane was then held at a range of potentials (from -90mV to -25mV), lasting from 25ms to 1s in order to induce inactivation. The currents were then evoked by depolarisations to -25mV. The inset shows current responses after holding the membrane at a range of pre-pulse potentials for 500ms.

B. Current responses obtained in this manner were normalised and plotted against the conditioning membrane potential for the different time courses: 25ms (■), 50ms (□), 100ms (●), 150ms (○), 250ms (▲), 500ms (△), 750ms (◆) and 1s (◇). Data points were fitted with a Boltzmann function (*equation 3, Chapter 2*).

C - J. Inactivation curves for individual durations at the pre-pulse potentials. The $V_{1/2}$ and slope values are indicated for each curve. The data are shown as mean ± SEM from 6 different neurones.

The sigmoidal inactivation curve was shifted towards more hyperpolarised values as the time held at the various potentials was increased. The explanation for this is straightforward; as the time that the membrane is held at the various membrane potentials increases, more of the Na^+ channels enter the inactivated state. There was very little difference between holding the membrane at a certain membrane potential for 25ms and 50ms; for 150 and 250ms; and for 500, 750 and 1000ms. It can therefore be concluded that steady state for inactivation is reached at 500ms.

3.2.3 Recovery from inactivation

The rate of recovery from the inactivated state can be assayed in voltage-clamp recordings by using a two-pulse protocol. The membrane was hyperpolarised from a holding voltage of -60mV to -120mV for 1s in order to remove any fast inactivation, then depolarised to -25mV for 30ms. This first pulse produces inactivation and the interpulse interval at -120mV from 0.8 to 200ms sets conditions for recovery from inactivation. The second depolarising step assays the extent of recovery, by comparing the current amplitude after the second depolarising pulse with the original response at the same potential during the first pulse. The percentage of recovered current during the second depolarisation step was plotted against the time held at the recovery potential, *figure 10.* The curve plateaus off at around 5ms, suggesting that 5ms at -120mV is sufficient for the current to recover completely from fast inactivation caused by the first depolarisation step.

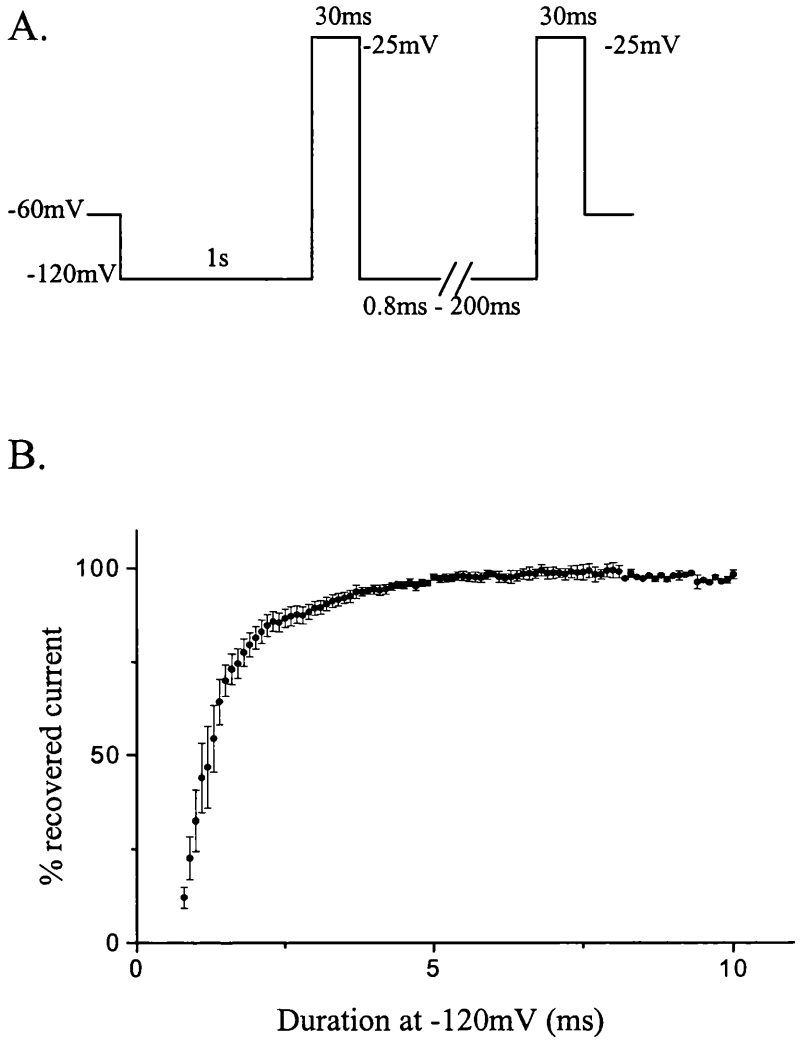

Figure 10. Recovery of the Na^+ current from inactivation.

A. Voltage command protocol: the membrane was hyperpolarised from a holding voltage of -60mV to -120mV for 1s in order to remove inactivation, before the first depolarising step. The membrane was held at the recovery voltage of -120mV from 0.8ms to 200ms. From 0.8 to 10ms, the time change was in 0.1ms increments, from 10ms to 50ms in 5ms increments and from 50 to 200ms in 10ms increments. Frequency - 1Hz.

B. The percentage of the recovered current (y-axis) during the second depolarising step was plotted against the time held at the recovery voltage (x-axis). Data are shown as mean $\pm$ SEM (n=12).

3.2.4 Use-dependent inhibition of sodium currents

In addition to the voltage-dependent inactivation observed at low stimulation frequencies (< 0.1 Hz) Na^+ channels also exhibit use dependent inactivation. It is important to study the use dependence of Na^+ channels, as this enhances the action of drugs that inhibit Na^+ current during sustained electrical activity. The use dependence of Na^+ currents was evaluated with trains of 20 repeated depolarising steps to -25mV from holding voltages of -60, -70, -80, -90 and -100mV. Pulse durations were for 30ms and were delivered at 1Hz (every 1s), 5Hz (every 200ms) and 10 Hz (every 100ms). In *figure 11* the ratio of the x^{th} pulse to the 1^{st} pulse was plotted against the episode number (x). At 1Hz there was no inactivation at any of the holding potentials. This suggests that if the membrane is held at any of the voltages for 1s, it is long enough to prevent any use dependent inactivation. However, at 5Hz, there was a degree of use dependent inactivation at -60mV, with the last, 20^{th} pulse being 90% of the 1^{st} one, and at -70mV, with the 20^{th} pulse being ~98% of the 1^{st} pulse. At -80, -90 and -100mV this inactivation is not present. At 10Hz there was an even greater use dependent inactivation at -60mV, with the 20^{th} pulse being 85% of the 1^{st} pulse. At -70mV this percentage increased to 90%, at -80mV the 20^{th} pulse was 95% of the 1^{st} one. At -90 and -100mV the last pulse was ~ 99% of the 1^{st} pulse. This data suggests that at the normal resting potential of -60mV, the channels need to be kept at that voltage for at least 1s in order to prevent any use-dependent inactivation. Therefore all the experiments were conducted with a 1Hz stimulating frequency. However, if the membrane is held at -80mV, stimulating every 200ms (5Hz) is sufficient to remove use dependent inactivation. At -90 and -100mV no use-dependent inactivation occurred.

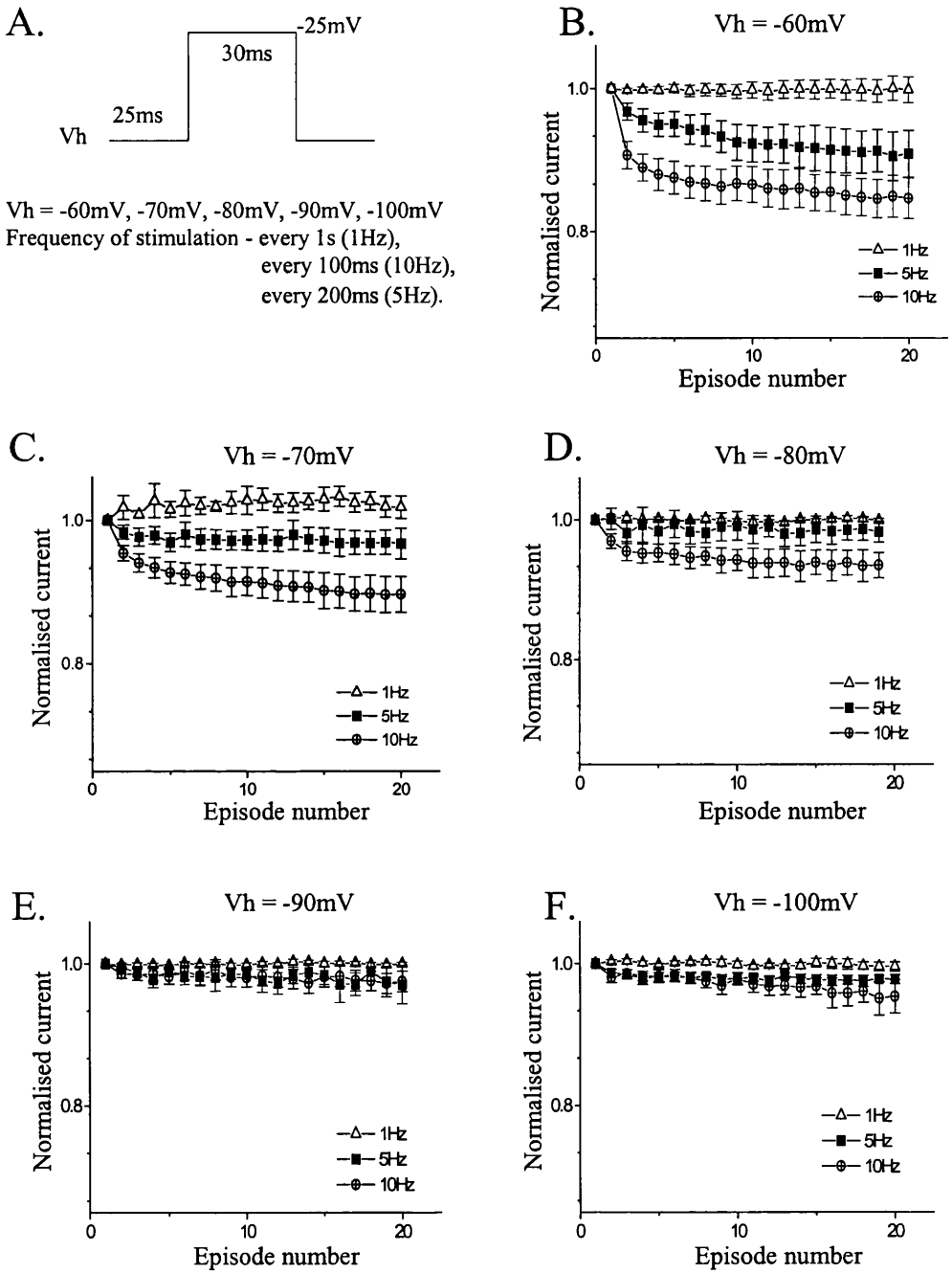

Figure 11. Use dependence of the Na^+ current in SCG neurones.

A. Voltage command protocol: the membrane was challenged with trains of 20 depolarising voltage steps to -25mV from a range of holding potentials, delivered at 1 Hz, 5Hz and 10Hz.
B-F. The ratio of the x^{th} episode with respect to the 1^{st} episode was plotted against the episode number from a holding potential of -60mV **(B)**, -70mV **(C)**, -80mV **(D)**, -90mV **(E)** and -100mV **(F)**, at each of the frequencies tested. Data are shown as mean $\pm$ SEM (n=8).

3.3 *KINETIC ANALYSIS OF SODIUM CURRENT ACTIVATION IN RAT SCG NEURONES*

The Na^+ channel can switch *('gate')* rapidly between open and closed states. When the channel is open, it has constant conductance to Na^+; when it is closed, it is essentially impermeant. In addition, there are several functionally distinct conformations of the closed channel. In the resting state channels can quickly open (< 1ms) on depolarisation. Once the membrane is depolarised, however, channels also quickly (1-2ms) enter an inactivated state from which they rarely reopen. To function again, inactivated channels must be held at hyperpolarised potentials for 5-10ms, permitting recovery to the resting state. The first complete quantitative description of Na^+ channel kinetics was provided by Hodgkin and Huxley based on observations of macroscopic currents at different voltages in the squid giant axon (Hodgkin & Huxley, 1952c). According to Hodgkin & Huxley, activation of the sodium current was a result of movement of hypothetical gating particles from one side of the membrane toward the other, and this reaction was represented as:

$$m_c \underset{\beta_m}{\overset{\alpha_m}{\Leftrightarrow}} m_o$$

where m_c denotes the activation gate in its closed configuration and m_o is the open configuration, and α_m and β_m are the voltage-dependent forward and backward rate constants for this reaction, respectively.

Similarly, inactivation was seen as a parallel reaction of the form

$$h_i \underset{\beta_h}{\overset{\alpha_h}{\Leftrightarrow}} h_a$$

where h_i represents a separate inactivation gate in its inactivated configuration, h_a denotes the gate configuration that would permit ionic conduction, and α_h and β_h are the rates of transition between the two states.

For a channel to conduct, its activation and inactivation gates must simultaneously be in the m_o and h_a configurations. Hodgkin and Huxley observed that Na^+ currents activated with a brief delay, which lead them to postulate that activation requires the movement of three parallel *m* gates, all of which must be in the m_o state

for the channel to open. The parameters m and h change exponentially with time following a step change of the membrane potential:

$$m = 1 - \exp(-t/\tau_m), \quad h = \exp(-t/\tau_h)$$

where τ_m and τ_h are the time constants of m and h, respectively.

Steady state activation kinetics

The steady state activation parameter, m_∞ was plotted as a function of membrane potential, *figure 12A*, characterised by the half-activation potential, $V_{1/2}$, at which the open state probability for each activation gate is one-half and by the steepness of the potential dependence of activation, the slope. m_∞ values were obtained by calculating the cubic root of normalised Na^+ channel conductance values (normalised against the maximum conductance (G_{Na}/G_{Na}^{max})) shown in *figure 8E* (see *Chapter 2, equation 9*). The value of $V_{1/2}$ in this case was around -30mV. The slope of this plot gives an indication of the minimum effective charge transfer required to open the channel. In this case the number is ~ 7. Hodgkin and Huxley initially estimated that a minimum of six charges must cross the membrane to open the Na^+ channel. More recently this number was revised to be no fewer that four charges (Stimers *et al.*, 1985). The gating currents, on the other hand, measure the charge transferred during the individual gating reactions. This elementary charge transfer gives the value of z in the mathematical calculation of the rate constants. In SCG neurones a value of 3.5 was observed (*figure 12C*).

The activation time constant, τ_m was measured by fitting an exponential function to the activation phase of the current and was plotted as a function of voltage, *figure 12B*. The voltage sensitivity of the activation time constant, may be expressed as:

$$\tau^{-1}_m = \alpha_m + \beta_m$$

where α_m and β_m are the activation and deactivation rate constants, measured from:

$$\alpha_m = m_\infty/\tau_m; \ \beta_m = (1-m_\infty)/\tau_m.$$

These values compare favourably with the theoretical values (see legend for *figure 12C* for equations).

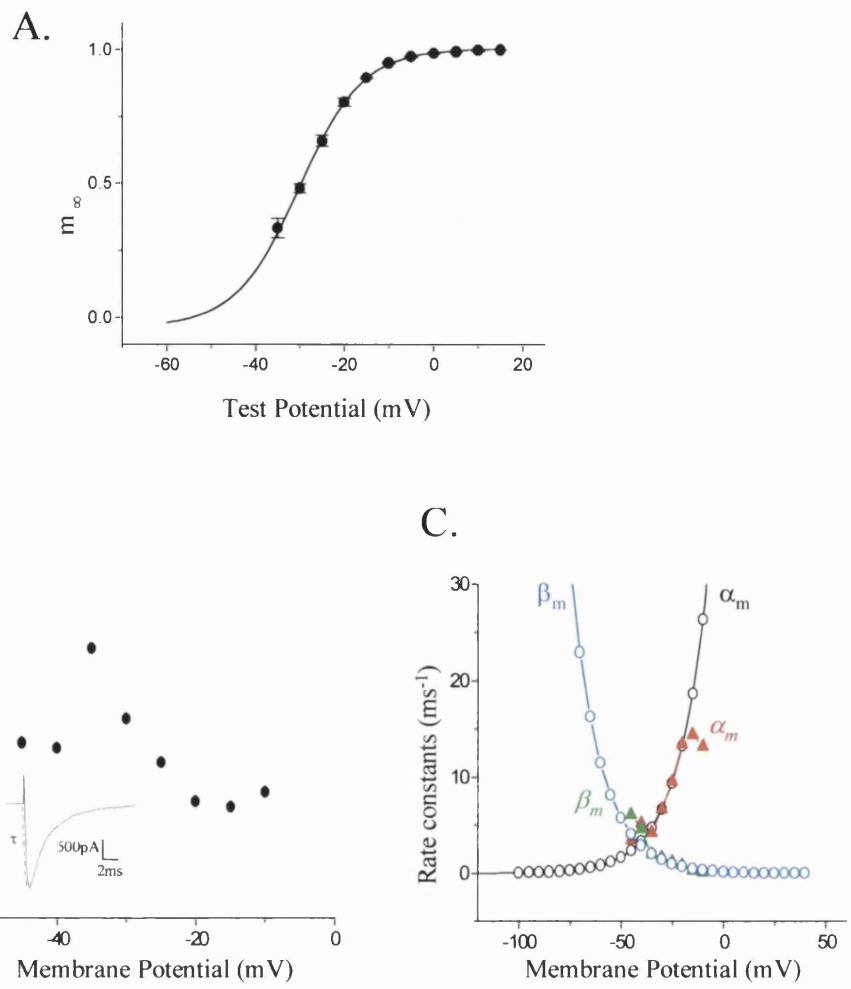

Figure 12. Activation kinetics of the Na^+ current in SCG neurones.

A. Steady state activation, m_∞ values were calculated as the cubic root of the normalised conductance obtained at each test potential (*figure 8E*). m_∞ values were plotted against each test potential. Points were fitted with the following equation: $m_\infty = \frac{1}{1 + \exp\frac{(V_{1/2} - x)}{\text{slope}}}$,

with $V_{1/2}$ = -30.2 ± 0.3mV and slope = 7.1 ± 0.3mV (n=4).

B. The activation time constant, τ_m was measured by fitting a single exponential function to the activation phase of the current in the pClamp 6 programme. The inset shows how the activation time constant was measured for a current activated following a step depolarisation to -10mV.

C. The experimental activation rate constants, α_m and β_m (red and green lines) were calculated from the following equations: $\alpha_m = m/\tau_m$; $\beta_m = (1-m)/\tau_m$. The mathematical curves (black and blue lines) for the rate constants were fitted using the following equations:

$$\alpha_m = \alpha_m(0) \exp\left[+\frac{ze}{2kT}(V-V_{1/2})\right]; \quad \beta_m = \beta_m(0)\exp\left[-\frac{ze}{2kT}(V-V_{1/2})\right],$$

where $\alpha_m(0) = \beta_m(0)$ = 3.1ms are the rate constants at $V_{1/2}$, e is the absolute value of the electronic charge, e/KT (= F/RT) = 0.04, where F = Faraday's constant (96500 coulombs/mol), R = gas constant (8.314 $JK^{-1}mol^{-1}$), T is the absolute temperature (295° K), z charge transferred during individual gating reactions (z = 3.5).

3.4 PHARMACOLOGY OF THE SODIUM CURRENT IN RAT SCG NEURONES:

3.4.1 TTX sensitivity of the sodium current

Na^+ currents in the rat SCG neurone were totally suppressed by 100nM TTX *(figure 8C)*, but completely recovered when TTX was washed off. It has been suggested that SCG neurones do not have a TTX resistant Na^+ current (Schofield & Ikeda, 1988). However, one group has shown a TTX resistant current in rat SCG neurones (Veselovskii *et al.*, 1986). This current was found only in 10% of the cells investigated by Veselovskii *et al* and may not have been detected in the present experiments. To determine the dose-response of TTX in SCG cells, Na^+ currents were evoked by series of step depolarisations to -10mV, following a 100ms pre-conditioning step to -90mV, from a holding potential of –60mV, every 1s. After the current amplitude had equilibrated 1, 2, 3, 10, 30 and 100nM TTX was added through the bath perfusion system. In these cells, the concentration of TTX required to block 50% of the Na^+ current *(IC_{50})* was ~ 4.7nM. This value is in close agreement with IC_{50} values reported in other preparations, e.g. 3.5nM in squid giant axons (Cuervo & Adelman, 1970) and 3.2nM in myelinated nerve fibres (Colquhoun & Ritchie, 1972).

3.4.2 Regulation of the sodium current by protein kinase C, norepinephrine (noradrenaline), oxotremorine-M and GTPγS

The involvement of PKC and G-protein coupled pathways in regulation of the Na^+ current in SCG neurones was studied using *oxotremorine-methiodide* (oxo-M), which is a synthetic tertiary amine that strongly stimulates the M_1 muscarinic acetylcholine receptors; *norepinephrine*, which strongly stimulates α adrenoceptors; and *GTPγS*, which is a non-hydrolysable analogue of the nucleotide *guanosine triphosphate* (GTP). Upon binding ligand, these receptors promote the exchange of *guanosine diphosphate* (GDP) for GTP on the G-protein α subunit, which causes the dissociation of Gα from the strongly associated βγ dimer (Gβγ). Once dissociated, both Gα and Gβγ are capable of interacting with multiple effector and regulatory

proteins, until the intrinsic GTPase activity of Gα converts the bound GTP to GDP, and the inactive heterotrimer reforms. Several isoforms of Gα, Gβ and Gγ have been characterised. The M_1 muscarinic receptors are coupled to $G\alpha_q$, and α-adrenoceptors are coupled to $G\alpha_i/G\alpha_o$. The dissociation of $G\alpha_q$ and the Gβγ subunits coupled to the adrenoceptors are both able to stimulate phospholipase C - β (PLC-β), resulting in the hydrolysis of PIP_2 into two second messengers, DAG and IP_3. The DAG remains in the membrane and can activate protein kinase C (PKC), which can lead to the phosphorylation of proteins (see *figure 13* below) (Nathanson, 1987; Haley *et al.*, 1998).

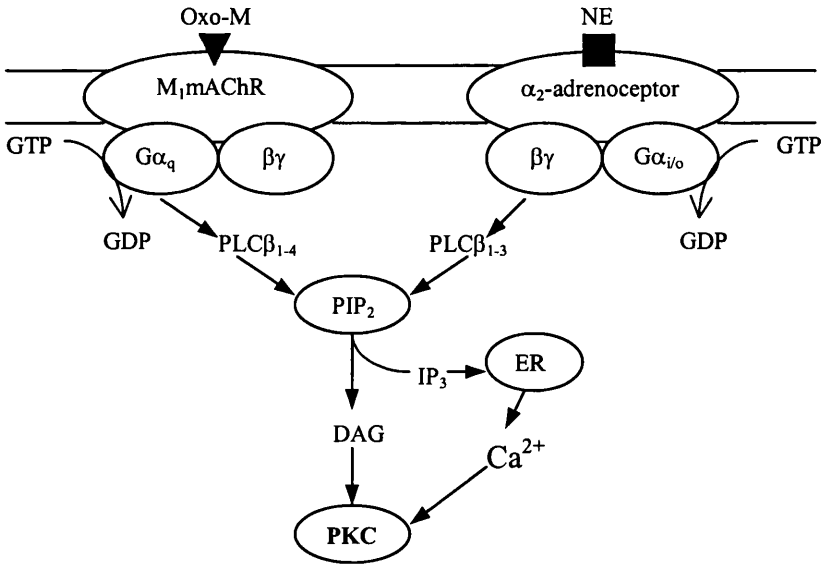

Figure 13. A schematic model of two possible G-protein coupled pathways involved in activation of PKC in SCG neurones.
Oxo-M *(oxotremorine-M);* ***NE*** *(norepinephrine);* ***mAChR*** *(muscarinic acetylcholine receptor);* ***PLC*** *(phosphoinositide specific phospholipase C);* ***PIP_2*** *(phosphatidyl inositol 4,5, bisphosphate);* ***IP_3*** *(inositol 1,4,5 triphosphate);* ***DAG*** *(1,2, diacylglycerol);* ***ER*** *(endoplasmic reticulum);* ***PKC*** *(protein kinase C). In this case, NE and Oxo-M, first messengers, open the pathways by binding to their receptors and stimulating proteins $G\alpha_q$ and βγ to activate PLC. This enzyme, called an effector, converts PIP_2 into second messengers, which then triggers a cascade of enzymatic reactions that stimulate PKC.*

PKC can be directly activated by phorbol esters, such as *phorbol 12-myristate 13 acetate* (PMA). The effect of 1μM PMA was examined on the peak Na^+ current in SCG neurones over 30 minutes, *figure 14A*. From a holding potential of -60mV, Na^+ currents were elicited by 25ms step depolarisations to 0mV from a -90mV pre-pulse

potential, delivered every 1s. The application of PMA dramatically reduced the Na^+ current amplitude. The reduction was time dependent, with 50% current reduction after 30 minutes. This suggests that the effect is not a direct one on the channel, but involves some kind of signal transduction mechanism. This effect was irreversible and suggests that the Na^+ channel in SCG neurones can be modulated by phosphorylation.

In order to test if a more physiological stimulation of PKC will show similar effects, the effects of 10μM oxo-M and 10μM norepinephrine were studied. A similar protocol as the one described for PMA was used. The results of these experiments are shown in *figure 14B* and *14C*. When comparing peak current of norepinephrine and oxo-M treated cells to control peak current, no significant differences were observed.

Similarly when 500μM GTPγS, a non-hydrolysable analogue of GTP, was used in the pipette solution, no significant change in the peak Na^+ current was observed (data not shown).

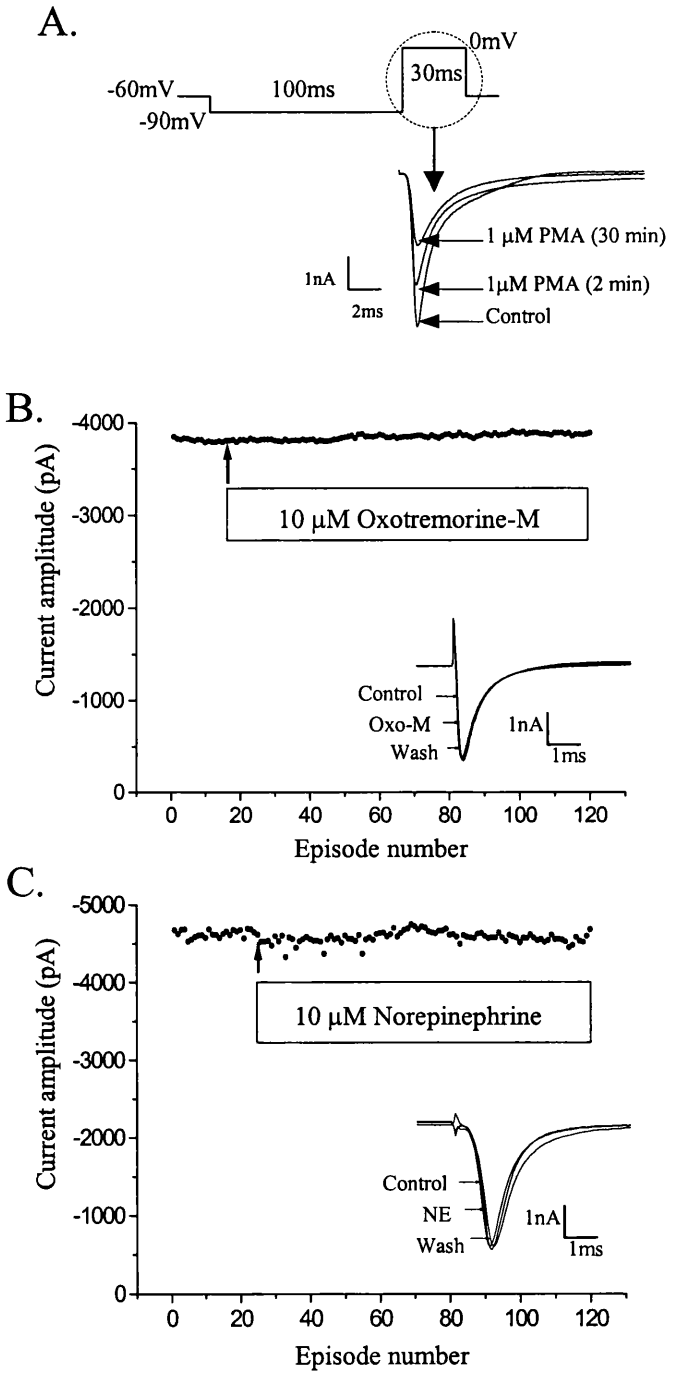

Figure 14. Modulation of the Na^+ current in SCG neurones.

A. Voltage protocol: the currents were evoked by series of 30ms step depolarisations to 0mV from a holding potential of -60mV, delivered every 1s. Prior to depolarisations, the membrane was held at -90mV for 100ms in order to remove inactivation. The inset shows current traces in a representative neurone in response to depolarisation to 0mV (as indicated on the voltage protocol) under control conditions, and 2 min and 30 min after the onset of perfusion with PMA.

B. 10 μM oxo-M did not change the Na^+ current amplitude. The graph shows current amplitude following depolarisations to 0mV, with a 1 s interval between each depolarising pulse. The arrow indicates drug addition. The inset shows current traces following the protocol shown in **(A)**.

C. 10 μM norepinephrine did not change Na^+ current amplitude. The arrow indicates the episode when drug was added. The inset shows current traces before, during and after addition of the drug. The protocol used is described in **(A)**.

3.5 EXPRESSION PATTERNS OF RAT BRAIN $Na_v1.1$, $Na_v1.2$, Nav1.3, $Na_v1.6$ AND $Na_v1.7$ SODIUM CHANNEL α-SUBUNITS IN SCG NEURONES:

3.5.1 Reverse Transcriptase - Polymerase Chain Reaction (RT - PCR).

No previous sodium α-subunit RT-PCR had been done in the rat SCG. Therefore, the composition of Na^+ channel subunits in the rat SCG is not known. The expression of sodium channel α-subunit cDNAs for $Na_v1.1$, $Na_v1.2$, $Na_v1.3$, $Na_v1.6$ and $Na_v1.7$ was examined using RT - PCR of the whole ganglia, followed by single cell RT-PCR of single neurones, in order to distinguish between the expression in glial cell and neurones.

Whole Ganglia

To test whether or not the newly designed primers worked, a rat brain cDNA library was used as a positive control, *figure 15A*. Isoform specific forward (*s* for sense) and reverse (*a* for antisense) primers were designed using rat gene sequences for brain $Na_v1.1$, $Na_v1.2$, $Na_v1.3$, $Na_v1.6$, $Na_v1.7$ Na^+ channels obtained from "Genbank". The selectivity of the primers was controlled using sequence alignment against the gene databank. The PCR reaction (see *Chapter 2, section 2.4.1*) was carried out against a rat brain cDNA library. The rat brain should contain $Na_v1.1$, $Na_v1.2$, $Na_v1.3$ and $Na_v1.6$ sodium channels. $Na_v1.7$ is found in peripheral neurones and therefore should not be present in the brain. As well as the cDNAs, water was also loaded onto the 2% metaphor gel as negative control. *Cyclophilin*, a ubiquitously expressed protein, was used as a positive control. In the presence of cDNA templates, PCR product for cyclophilin was observed, suggesting that the cDNA templates were intact and the amplification reaction was successful. In contrast, no signal was present in the absence of any template (*figure 15A*, lanes 3, 5, 7, 9, 11, 13). For $Na_v1.1$, $Na_v1.2$, $Na_v1.3$ and $Na_v1.6$ α-subunits, products of expected sizes were observed in the rat brain: 150 base pairs (bp) for $Na_v1.1$ (lane 2), 200 bp for $Na_v1.2$ (lane 4), 250bp for $Na_v1.3$ (lane 6) and 317 bp for $Na_v1.6$ (lane 10), however, for $Na_v1.7$ a 150bp band (lane 10) was observed, which is in contrast to the 707bp expected PCR product.

After establishing the optimal conditions for the PCR reactions, the same reaction was repeated on rat SCG. Following reverse transcription of RNA and PCR of the rat SCG cDNA, the expression of all five sodium channel genes, namely $Na_v1.1$, $Na_v1.2$, $Na_v1.3$, $Na_v1.6$ and $Na_v1.7$, were detected in the whole SCG (*figure 15B*, lanes 2, 4, 6, 8, 9, respectively). [For $Na_v1.7$ two bands are seen: ~250bp and ~700bp, with the lighter band (250 bp) being present due to contamination from lane 12]. As with the rat brain, cyclophilin was used as a positive control and was successfully detected in the SCG (*figure 15B,* lane 12). To make sure that the amplified product comes from the mRNA expressed in the cell and not from nuclear DNA, RNA samples were used as negative controls (*figure 15B*, lanes 3, 5, 7, 9, 11, 13).

Single cell RT-PCR

PCR results from the whole SCG revealed the presence of brain $Na_v1.1$, $Na_v1.2$, $Na_v1.3$, $Na_v1.6$ and $Na_v1.7$ sodium channel mRNAs. This takes into account sodium channels present not only in neuronal cells but also in glial cells. In order to identify which sodium channels were present and electrophysiologically recorded in neurones it was necessary to carry out RT-PCR of individual neuronal cells. After SCG were plated onto laminated dishes, individual neurones were harvested using the recording patch electrode and subjected to RT-PCR. In order to test the optimal conditions for the single cell PCR $G\alpha_o$ primer was used as a positive control. G protein α_o subunit is present in great abundance in sympathetic neurones and is therefore an ideal candidate as a positive control. Single cell RT-PCR of SCG neurones revealed products of the expected size (583 bp) corresponding to $G\alpha_o$ (*figure 15C*, lanes 2, 3, 4, 5). Water was used as a negative control and, as expected, no signal was detected (*figure 15C*, lane 7).

When the same conditions for the single cell RT-PCR were used with the sodium channel primers no signals were detected. One possible explanation is that the amount of sodium channel protein is significantly lower that of $G\alpha_o$, which makes their detection using this technique very difficult. I was therefore, unable to detect sodium channel subtypes present specifically in SCG neurones by this technique.

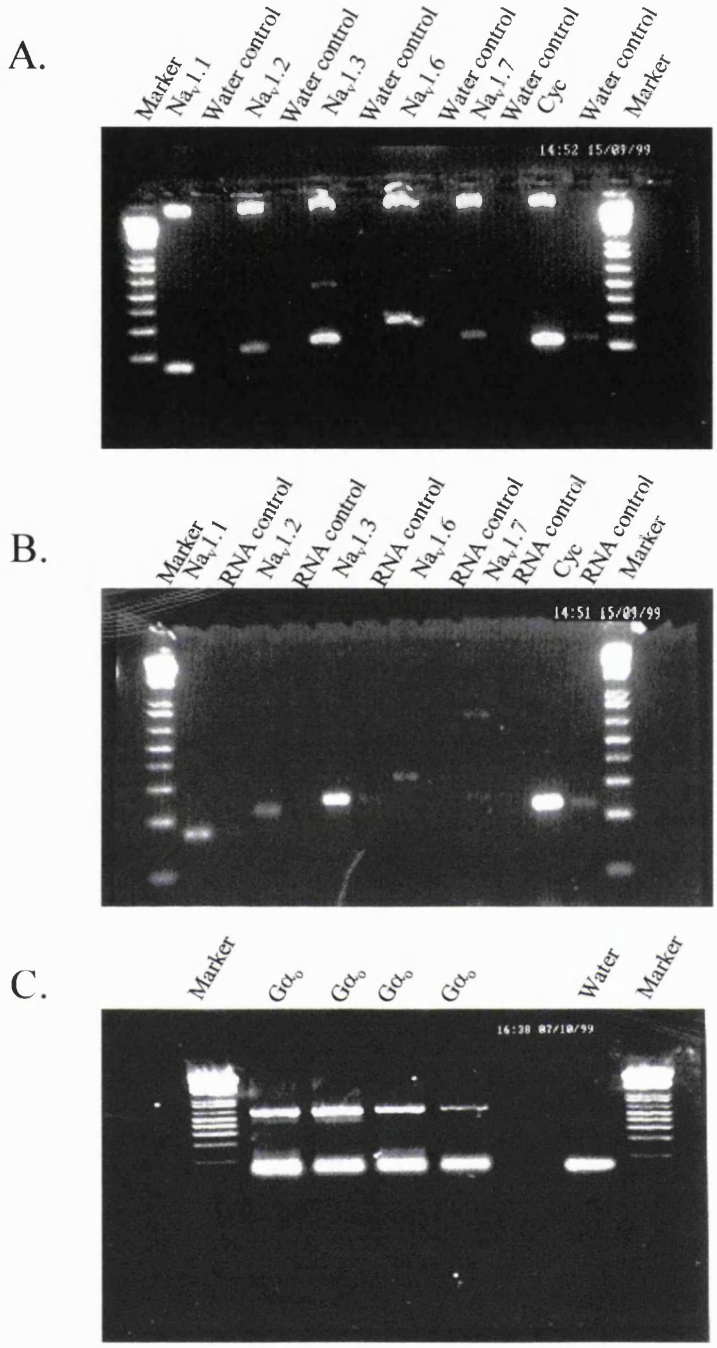

Figure 15. Expression pattern of Na^+ channels in the rat brain and in SCG neurones.

A. RT-PCR of the rat brain cDNA library: cyclophilin primers were used as a positive control and water as a negative control. Results show presence of $Na_v1.1$, $Na_v1.2$, $Na_v1.3$ and $Na_v1.6$ sodium channels in the brain. The band in the $Na_v1.7$ lane does not correspond to the 707 bp expected product and is probably due to non-specific hybridisation.

B. RT-PCR of the rat SCG: cyclophilin primers were used as a positive control and SCG RNA as a negative control. SCG include glial cells and neurones and express all of the sodium channels presently tested, including $Na_v1.7$, which was absent in the rat brain.

C. Single cell RT-PCR of the SCG neurones: each lane shows RT-PCR of a single cell. SCG neurones are an abundant source of the G-protein α_o subunit. $G\alpha_o$ primers were used in order to establish the optimal conditions for this technique. Water was used as a negative control. The bands at the bottom show primer dimer formation.

3.5.2 Immunocytochemistry

Immunocytochemical experiments were carried out to confirm the distribution of Na^+ channel expression in SCG and also to distinguish the subtypes expressed in glial cells from those expressed in neurones. After fixation, neurones were incubated with subtype specific antibodies (see *Chapter 2, section 2.5.1*), and the results of the immunolabelling were examined on a fluorescent microscope. Immunostaining of SCG neurones showed the presence of brain $Na_v1.1$, $Na_v1.2$, $Na_v1.3$, and $Na_v1.7$ sodium channels in both glial cells and neurones, albeit with different intensities, but not brain $Na_v1.6$ sodium channel (although a weak RNA signal was observed – see *figure 15B, lane 8*). Staining with the $Na_v1.1$ sodium channel antibody, *figure 16A,* was not as intense as with the other antibodies. This can either be an indication of the quantity of channel protein present at the cell membrane or the quality of the antibody. $Na_v1.2$ antibody showed abundant staining in neurones, glia and processes, *figure 16B.* The same result was observed with the $Na_v1.3$ antibody, however, the staining was concentrated in neurones and glia, and less in the processes (*figure 16C*). $Na_v1.7$ staining was abundant in both neuronal and glial cell membranes (*figure 16D*).

Immunostaining of rat SCG with the rat brain $Na_v1.6$ sodium channel antibody gave a negative result. However, the signal was detected by PCR (*figure 16B*, lane 8), suggesting that although the mRNA encoding brain $Na_v1.6$ sodium channel is present in SCG cells, it is not being translated into a functional channel protein.

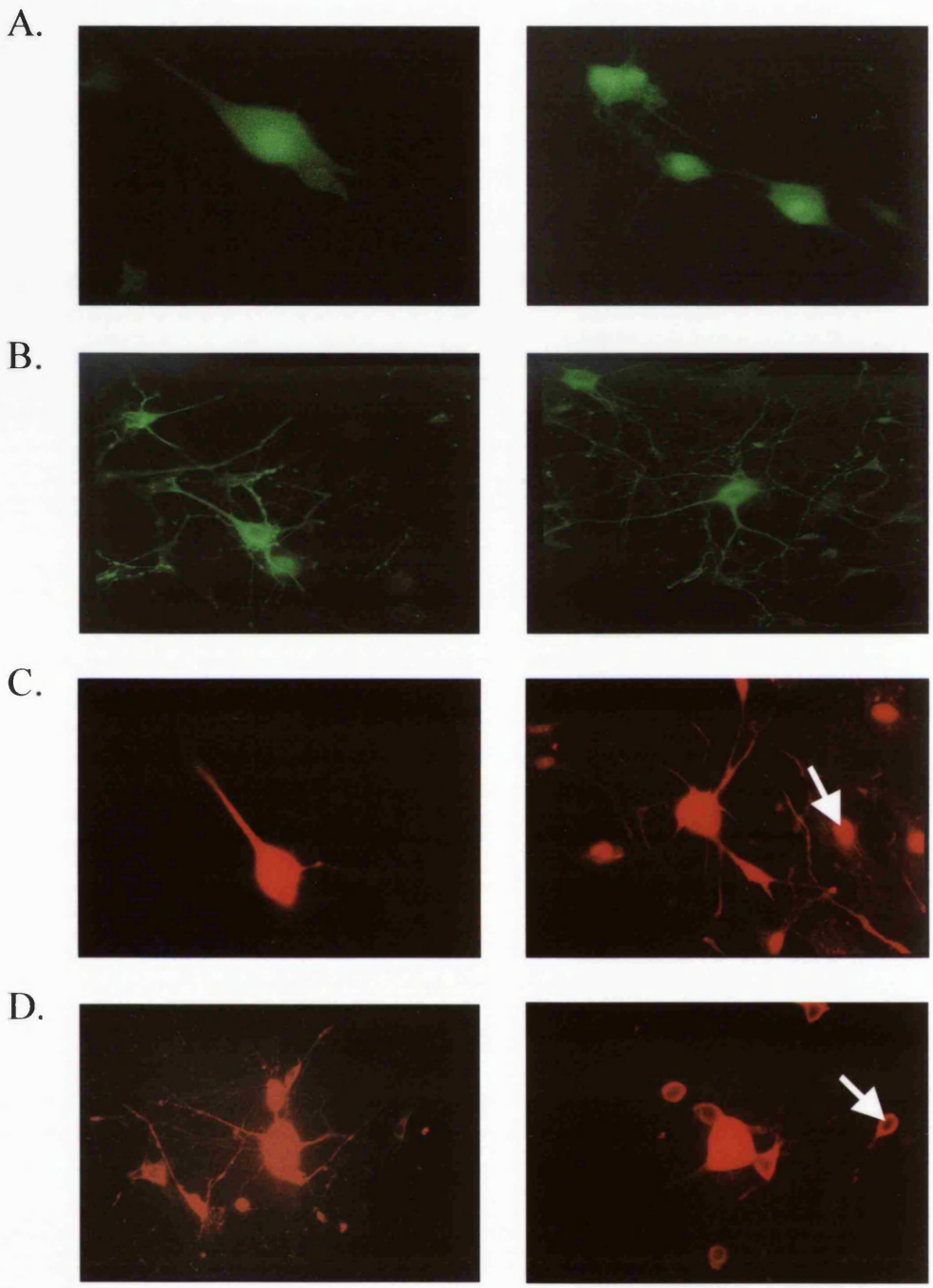

Figure 16. Immunolocalisation of Na^+ channel subtypes in SCG neurones.

The sodium channel isoforms expressed in SCG neurones were determined using isoform specific rabbit polyclonal primary antibodies directed against brain $Na_v1.1$ (1/10) sodium channel **(A)**, $Na_v1.2$ (1/10) **(B)**, $Na_v1.3$ (1/100) **(C)** and $Na_v1.7$(1/100) **(D)**. Primary antibodies were immunolabelled using anti-rabbit secondary antibodies conjugated with either FITC (1/50) for $Na_v1.1$ **(A)** and $Na_v1.2$ **(B)** or TRITC (1/40) for $Na_v1.3$ **(C)** and $Na_v1.7$ **(D)**. White arrows indicate examples of glial cells.

and peak current amplitude could be fitted with a single exponential function. As the ramp speed was slowed, the peak sodium current amplitude decreased, indicating inactivation of the transient current. The relationship between ramp duration and current amplitude reached a plateau phase after 1s. This suggests that any current seen after 1s is purely due to the persistent component. To show the voltage dependence of the persistent current, the membrane was held at -90mV and ramped up to +80mV over a 2s period (*figure 17B*). The ramp speed (85mV/s) was then converted into membrane potential and plotted against corresponding current amplitude to obtain a current-voltage (I/V) relationship for the persistent current in *figure 17D* (open circles).

The I/V relationship for the transient Na^+ current in CHO cells was also determined by plotting the current amplitude at the end of each depolarising step as in *figure 17A*. The I/V plots for both the transient and persistent sodium currents are shown in *figure 17D*. The current-voltage relationship for the persistent component was similar to that of the transient. The activation threshold for both components was found to be approximately -40mV, with a peak current at approximately 0mV and a reversal potential at around +60mV, which was close to the calculated theoretical Na^+ ion equilibrium potential of +61mV.

The voltage dependence of activation was measured by plotting normalised conductance values against membrane potential as described for *figure 8E*, and fitting the points with a Boltzmann equation (*equation 2, Chapter 2*). Activation curves for the transient and persistent $Na_v1.3$ Na^+ currents in CHO cells are shown in *figure 17E*. The activation curve for the persistent component has a slightly more depolarised half activation potential ($V_{1/2} \sim$ -14mV), compared with a $V_{1/2}$ value of around -18mV for the transient component.

The voltage dependence of channel inactivation was studied using a two-pulse protocol. From a holding potential of -90mV, conditioning pulses of 1s to varying potentials between -120 and 0mV were delivered followed by a test pulse to 0mV. The inactivation curve is *figure 17F* was measured by plotting the normalised current during the test pulse against the prepulse potential and fitting the data points with a single-order Boltzmann curve, with a $V_{1/2}$ value of ~ -63mV and a slope of ~ 6.6mV.

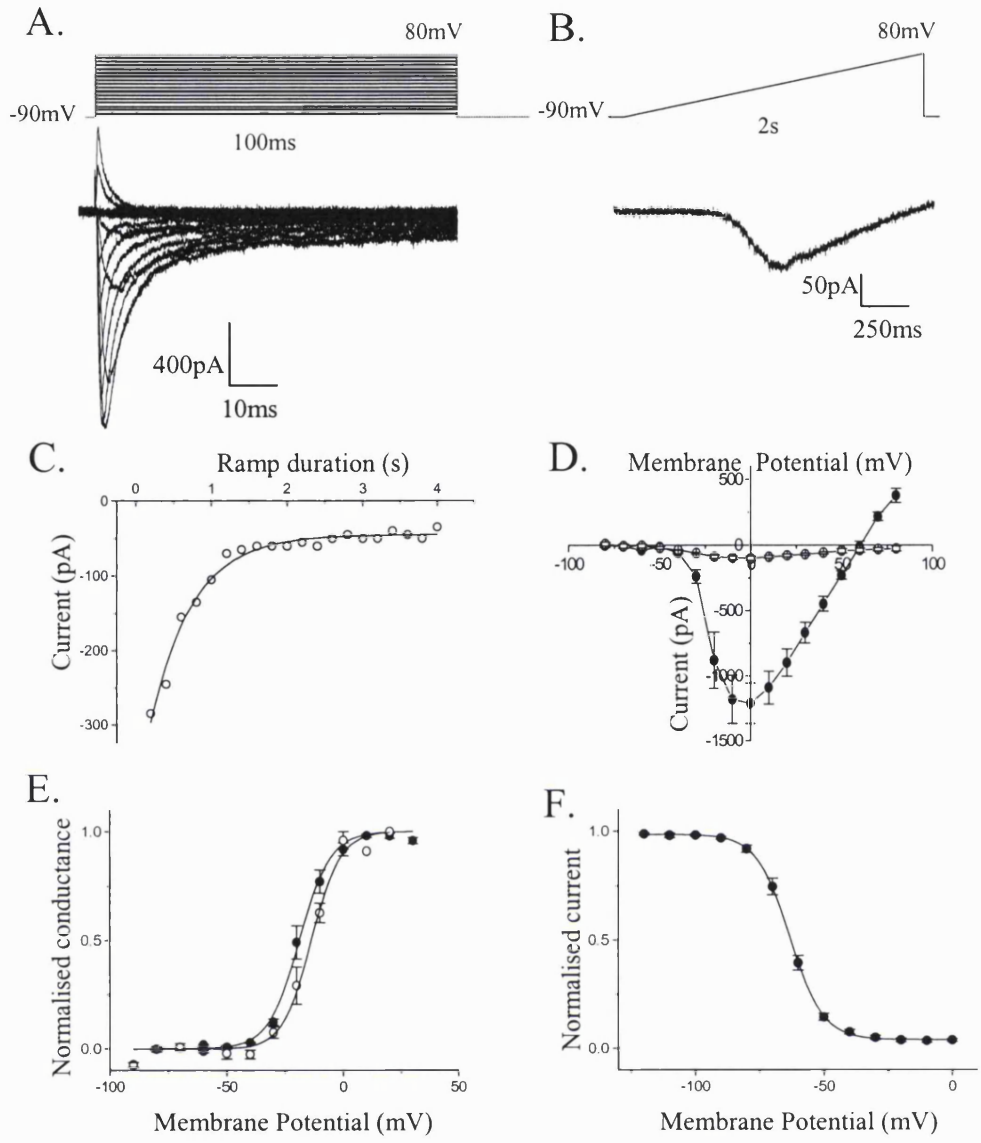

Figure 17. Biophysical parameters of human $Na_v1.3$ Na^+ channels expressed in CHO cells.

A. The membrane was held at -90mV and inward sodium currents were recorded in response to 100 ms step depolarisations from -80mV to +80mV.

B. To show the persistent component of the $Na_v1.3$ Na^+ currents, the membrane was ramped from -90mV to +80mV over a 2s period. The transient component was completely inactivated and only non-inactivating, or persistent current was recorded.

C. The effect of ramp speed on current amplitude: the duration of the ramp protocol shown in **(B)** was varied from 200ms to 4s. The current amplitude with each speed was plotted against ramp duration and points fitted with a single exponential function with $\tau = 0.5$ms.

D. Current-voltage relationship of the transient (closed circles) and persistent (open circles) Na^+ currents. Peak current amplitude for the transient current was evaluated following a voltage protocol shown in (A) and for the persistent component, ramp protocol shown in (B) was used. Data shown as mean $\pm$ SEM (n=7).

E. Voltage dependence of activation of transient (closed circles) and persistent components of the $Na_v1.3$ Na^+ current. Data points were fitted with a Boltzmann function (*equation 2, Chapter 2*), with $V_{1/2}$ of -18.4 $\pm$ 1.9mV and slope of 5.3 $\pm$ 0.6mV for the transient, and $V_{1/2}$ of -13.7 $\pm$ 0.9mV and slope of 6.1 $\pm$ 0.8mV for the persistent current (n=7).

F. Voltage dependence of inactivation of the transient $Na_v1.3$ Na^+ current. The same protocol was used as in *figure 9*, with -90mV as the holding potential and 0mV as the test potential. Fitting was achieved using a Boltzmann function (*equation 3, Chapter 2*), with $V_{1/2}$ of -63.4 $\pm$ 1.1 mV and slope of 6.6 $\pm$ 0.3mV (n=7).

3.7 MODULATION OF THE $Na_v1.3$ SODIUM CHANNEL EXPRESSED IN CHO CELLS

3.7.1 Involvement of Protein Kinases

The effects of drugs known to alter protein kinase activity were investigated on the transient and persistent $Na_v1.3$ Na^+ current components. *Phorbol dibutyrate* (PDBu) is a powerful tumour promoter and can mimic the action of DAG and activate PKC directly. Following PDBu treatment, the enzyme which is mainly cytosolic, translocates to the plasma membrane where it encounters its phospholipid cofactors and undergoes activation.

An alternative method for studying the involvement of PKC and other protein kinases in ion channel regulation is to inhibit them. *Staurosporine* is a non-specific inhibitor of not only PKC, but other protein kinases, and acts at the ATP-binding site of protein kinases, blocking their catalytic activity. Because the ATP-binding sites of PKC share significant homology with the ATP-binding sites of other protein kinases, staurosporine is able to bind and inhibit other kinases.

The effect of PKC activation on the $Na_v1.3$ Na^+ current in CHO cells was studied by applying 500nM PDBu via the bath perfusion system. The effect of PDBu on current amplitude was studied by monitoring the current amplitude following depolarising voltage steps from –90mV to 0mV, every 1s. Application of PDBu did not change the transient current amplitude, nor did it affect the persistent component. *Figure 18* illustrates the effect of PDBu on the current-voltage relationship (*figure 18A*), the activation curve (*figure 18B*) and the inactivation curve (*figure 18C*) of the Na^+ current. The current-voltage relationship was obtained as described for *figure 8D* before addition, after and upon washout of PDBu. PDBu did not have any effect on the current-voltage relationship. PDBu did not affect the voltage dependence of activation of the Na^+ current as seen in *figure 18B*, with $V_{1/2}$ values of ~ -18mV in control recordings, ~ -22mV in the presence of PDBu and ~ -21mV after washout of drug. The inactivation curves shown in *figure 18C* were obtained as described for *figure 9* before, after addition and upon washout of PDBu. The voltage dependence of Na^+ current inactivation was unchanged by PDBu, with $V_{1/2}$ values of ~ -64mV under control conditions, ~ -68mV in the presence of PDBu and ~ -71mV upon washout of

the drug. The lack of effect of PDBu on the Na^+ current expressed in CHO cells may suggest that the $Na_v1.3$ Na^+ current is not regulated by activation of PKC. However, it is likely that the cascade of enzymatic reactions leading to, or after activation of PKC described above, does not occur to completion due to lack of certain receptors/cofactors/enzymes.

To further investigate the involvement of protein kinases in modulating the $Na_v1.3$ Na^+ current, I studied the effect of staurosporine on the current. Bath application of 100nM staurosporine did not change the Na^+ current amplitude. There was also no change in the I-V relationship of the current in the presence of staurosporine (*figure 19A*). Inhibition of protein kinases did not change the voltage dependence of channel activation. *Figure 19B* illustrates activation curves under control conditions, in the presence and after washout of staurosporine. The $V_{1/2}$ values were not significantly different, with values of ~ -18mV under control conditions, ~ -20mV in the presence of staurosporine and ~ -17mV upon washout. There was also no change in the half inactivation potential in the presence of the drug. *Figure 19C* shows the inactivation curves in the absence of staurosporine, with $V_{1/2}$ of ~ -64mV, in the presence of staurosporine $V_{1/2}$ ~ -63mV and upon washout $V_{1/2}$ ~ -68mV.

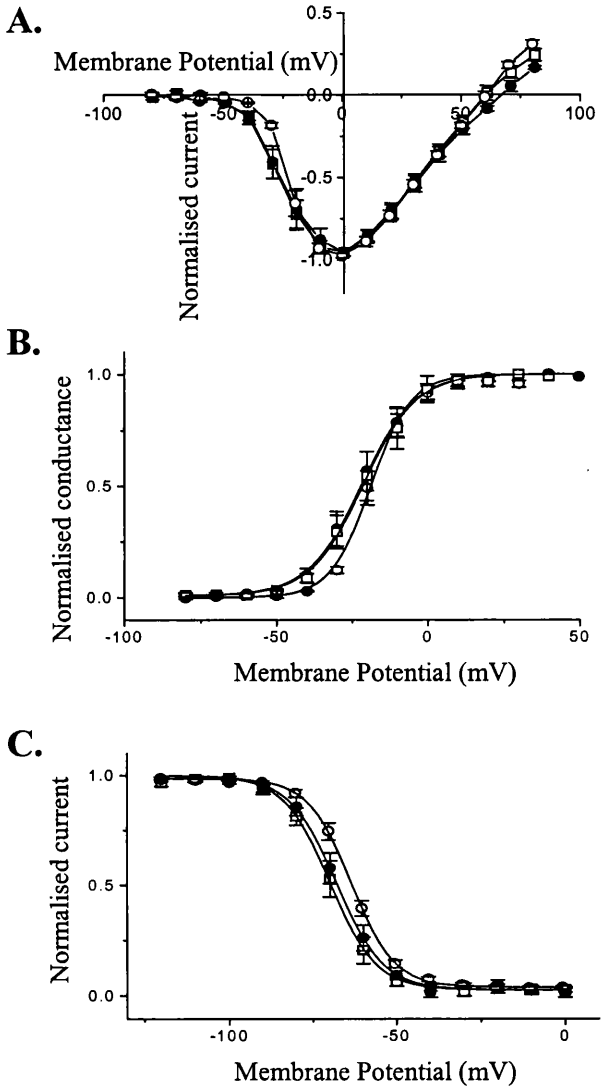

Figure 18: Effects of 500nM Phorbol Dibutyrate (PDBu) on the $Na_v1.3$ Na^+ current.

A. Effect of PDBu on the Na^+ current-voltage relationship. Normalised current values were plotted against command potential before (○), after (●) and upon washout (□) of 500nM PDBu. To obtain normalised values, peak current amplitudes in response to depolarising pulses from a holding voltage of -90mV to +80mV in 10mV increments were normalised against the maximum current amplitude in control recordings. Data shown as mean ± SEM (n = 7).

B. Activation curves in the absence (○), presence (●) and washout (□) of PDBu. Currents were activated by depolarising pulses from -80mV to +80mV from a holding potential of -90mV. Conductance was calculated as described in *Chapter 2*. Normalised conductance values were plotted against the voltage of the depolarising step and fitted with a Boltzmann function (*equation 2, Chapter 2*). The $V_{1/2}$ values were as follows: -18.4 ± 1.8mV (control, n=7), -21.8 ± 0.4mV (PDBu, n=7) and -21.2 ± 0.3mV (recovery, n=7). Slopes were 5.4 ± 0.6mV (control, n=7), 8.8 ± 0.3mV (PDBu, n=6) and 8.7 ± 0.3mV (recovery, n=5).

C. The effect of PDBu on the Na^+ current inactivation curve. Normalised current values were plotted against test potential (as described for *figure 17F*) before (○), after (●) and upon washout (□) of PDBu. In control recordings the $V_{1/2}$ and slope values were -63.5 ± 1.1mV and 6.5 ± 0.3mV (n=7), respectively. In the presence of PDBu $V_{1/2}$ = -68.1 ± 0.4mV and slope = 7.1 ± 0.4mV (n=6), and upon washout $V_{1/2}$ = -71.1 ± 0.2mV and slope = 8.7 ± 0.3mV (n=5).

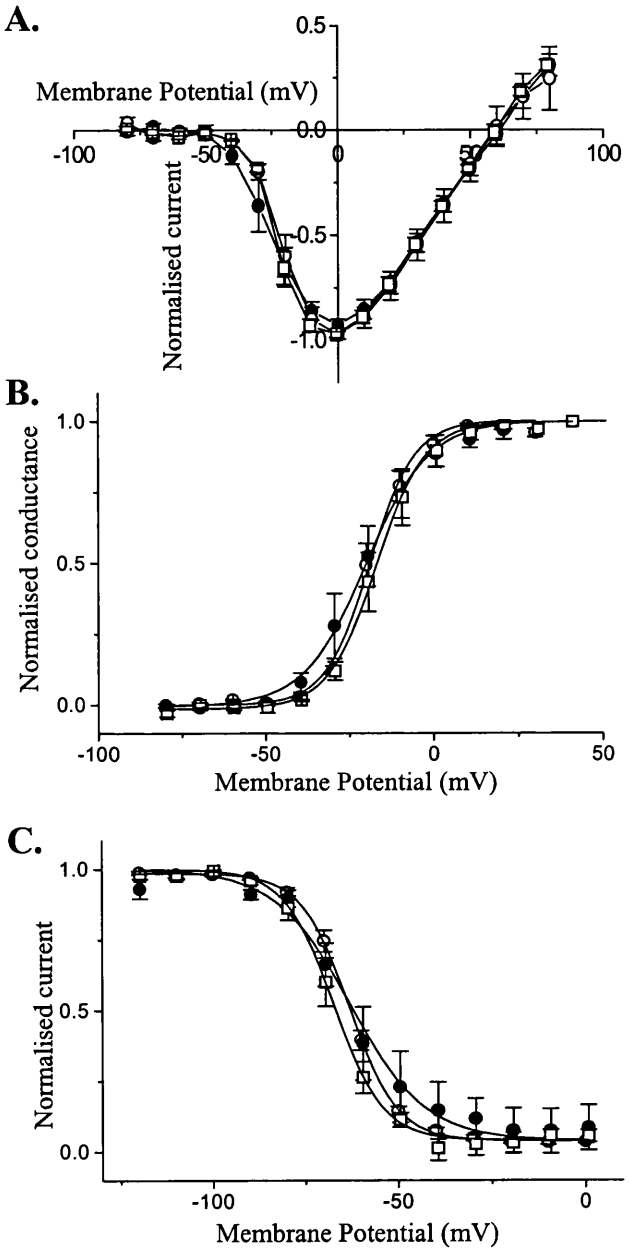

Figure 19: Effects of 100nM staurosporine on $Na_v1.3$ Na^+ current in CHO cells.

A. Effect of PDBu on the Na^+ current-voltage relationship. Normalised current values were plotted against command potential before (○), after (●) and upon washout (□) of 100nM staurosporine. Values were obtained as described in legend for *figure 18A*. Data shown as mean ± SEM (n = 7).

B. Activation curves in the absence (○), presence (●) and washout (□) of Staurosporine. See legend for *figure 18B* for details of how the graph was plotted. Points were fitted with the Boltzmann *equation 2, Chapter 2*. The $V_{1/2}$ and slope values were as follows: -18.4 ± 1.8mV and 5.4 ± 0.6mV, respectively (control, n=7), -20.5 ± 0.5mV and 9.3 ± 0.4mV, respectively (staurosporine, n=9), and -17.6 ± 0.3mV and 7.2 ± 0.3mV (recovery, n=5).

C. The effect of staurosporine on the Na^+ current inactivation curve, as described for *figure 18C* before (○), after (●) and upon washout (□) of the drug. In control recordings the $V_{1/2}$ and slope values were -63.5 ± 1.1mV and 6.5 ± 0.3mV (n=7), respectively. In the presence of staurosporine $V_{1/2}$ = -63.3 ± 1.3mV and slope = 6.5 ± 0.3mV (n=7), and upon washout $V_{1/2}$ = -67.8 ± 0.4mV and slope = 6.5 ± 0.4mV (n=5).

3.7.2 Involvement of a G-protein coupled pathway

Another likely mechanism for modulation of the $Na_v1.3$ Na^+ current in CHO cells is through *guanidine nucleotide binding proteins* (G proteins). Activation of heterotrimeric G proteins by GTP binding causes dissociation of the Gα from the Gβγ subunits to generate active forms that can interact with effectors, which may modulate the Na^+ current. Termination of the signal is brought about by the intrinsic GTPase activity of the α subunit, which hydrolyses GTP to GDP and returns the subunit to its resting state.

In order to study if a G-protein coupled pathway regulated $Na_v1.3$ Na^+ current in CHO cells, 500nM of the nonhydrolysable GTP analogue *GTPγS* was applied intracellularly i.e. included in the pipette solution. The effect of G-protein activation on the $Na_v1.3$ sodium channel was evaluated by looking at the current/voltage relationship, the activation and inactivation curves in the absence and presence of GTPγS. *Figure 20* summarises the results. GTPγS did not change the I/V relationship for the transient current (*figure 20A*), nor did it change the amplitude of the persistent current component (not shown), as expected after findings by Ma *et al* (1997), who have shown that coexpression of βγ subunits with rat brain $Na_v1.2$ Na^+ channel α subunits in tsA-201 cells induces a persistent current. GTPγS did not change the voltage-dependence of activation (*figure 20B*), with $V_{1/2}$ in control recordings ~ -18mV and in the presence of GTPγS ~ -20mV. The voltage dependence of inactivation also remained unchanged (*figure 20C*), with no significant changes in $V_{1/2}$ values (~ -64mV in control and ~ -71mV following G protein activation).

Taken together, these results do not provide any evidence for the involvement of protein kinases and G proteins in modulating the fully inactivating and the persistent currents generated by the $Na_v1.3$ Na^+ channel expressed in CHO cells.

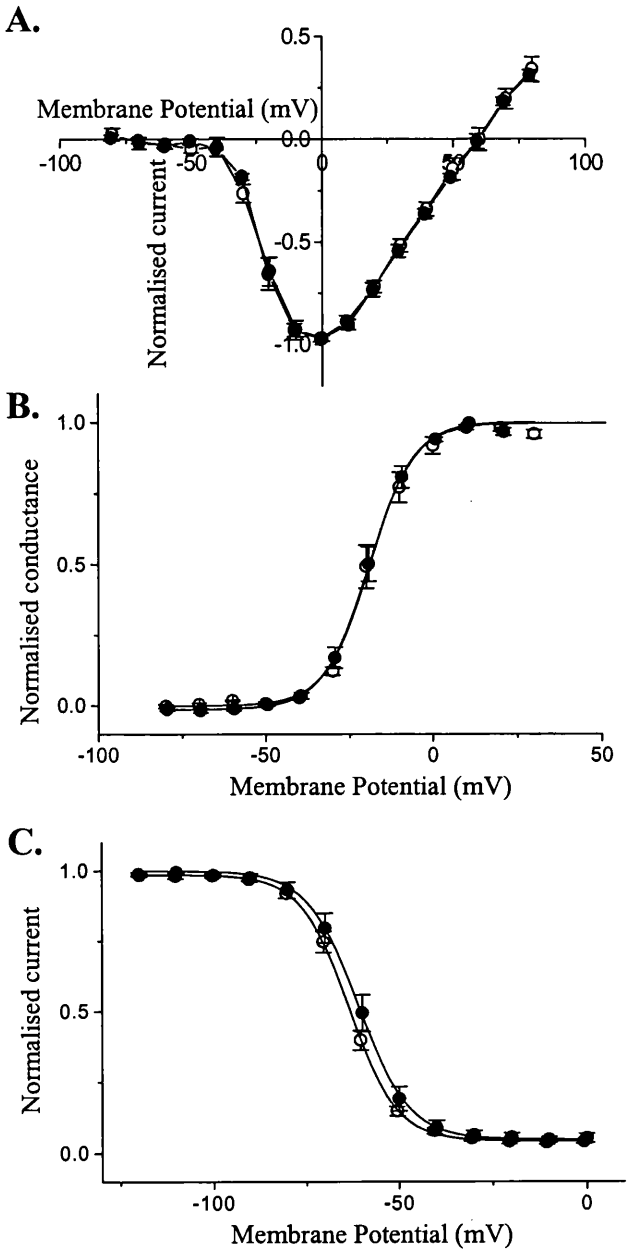

Figure 20: Effects of 500μM GTPγS on the $Na_v1.3$ Na^+ current in CHO cells.

A. Normalised current-voltage plot under control conditions (○) and after addition of GTPγS (●). Data shown as mean ± SEM (n = 7).

B. Activation curves in the absence (○) and presence of GTPγS (●) were obtained as described previously (*figure 18B*) and fitted with a Boltzmann function (*equation 2, Chapter 2*). The $V_{1/2}$ values were as follows: -18.4 ± 1.8mV (control, n=7) and -20.1 ± 1.5mV (GTPγS, n=7). Slopes were 5.4 ± 0.65mV (control, n=7) and 6.8 ± 0.4mV (GTPγS, n=7).

C. The effect of GTPγS on the Na^+ current inactivation curve. Normalised current values were plotted against test potential (as described for *figure 18C*) before (○) and after (●) addition of GTPγS. In control recordings the $V_{1/2}$ and slope values were -63.5 ± 1.1mV and 6.5 ± 0.3mV (n=7), respectively. These values are very similar after addition of GTPγS, with $V_{1/2}$ = -71.1 ± 0.2mV and slope = 6.8 ± 0.2mV (n=7).

3.8 DISCUSSION

The biophysical properties of the Na^+ channel in SCG neurones and of human $Na_v1.3$ brain Na^+ channels expressed in CHO cells were characterised using the whole cell recording technique. Both cells exhibit a TTX sensitive Na^+ current, which is reversibly blocked by 100nM TTX. In the CHO cell line, in addition to the transient current seen in SCG neurones, Na^+ channels displayed a persistent Na^+ current upon depolarisation. There was no persistent current component to the Na^+ current recorded in SCG neurones. Drugs known to alter protein kinase activity were investigated to see if they played a modulatory effect on these two types of channel.

3.8.1 Biophysical parameters of the sodium current in SCG neurones and of human $Na_v1.3$ brain sodium current in CHO cells

The sodium channel can occupy three functional states: closed, activated and inactivated. Typical gating behaviour of the macroscopic Na^+ current upon depolarising voltage steps reflects the successive transition of conformational states in the protein. Voltage sensitivity and time course of transitions may vary with the preparation, but typically both activation and inactivation are nearly complete within a few milliseconds. In some cases this inactivation is much more delayed, yielding a slow, persistent current.

The biophysical parameters of the sodium currents measured in the two models were similar except for that of inactivation. Human $Na_v1.3$ brain Na^+ channel was capable of exhibiting a persistent current in addition to the transient current. The neuronal Na^+ channel displayed a fully inactivating current only. The nature of the $Na_v1.3$ Na^+ channels contributing the persistent component remains unclear.

Recordings in SCG neurones were done under reduced extracellular sodium conditions (35mM). The reason for this was to improve the chances of obtaining a good clamp by decreasing the size of the currents. When using 140mM extracellular Na^+ during recordings in SCG neurones, the peak amplitude of the Na^+ current exceeded 10nA, which made it impossible to clamp the cell. With 35mM Na^+, chances of getting a good clamp were significantly higher. In CHO cells a high Na^+

concentration had to be used in order to see the persistent component. The high Na^+ concentration was not a problem in these cells, because of the absence of any processes. Recordings in SCG cells with high extracellular Na^+ did not show a persistent component and the current fully inactivated within 10ms. The amplitude of the persistent current in CHO cells was consistently around 10% of the total current recorded at the beginning of the depolarising step.

The current-voltage relationship of the Na^+ channel in SCG cells demonstrated the rapid Na^+ channel activation kinetics, whereby the onset, peak and decay of current occured in milliseconds. During depolarisation, the Na^+ current recorded in SCG neurones began to activate at ~ -40mV. The threshold for current activation in CHO cells was very similar (~ -45mV), for both the transient and persistent Na^+ currents. The membrane potential at which peak current amplitude was recorded varied slightly between the two models, with the currents in SCGs reaching a peak at ~ -10mV and in CHO cells ~ -0mV.

In CHO cells the transient current reached a peak within 10ms and the persistent current could be seen after 100ms. The I-V relationship for the transient current was constructed by using the peak current amplitude evoked by step depolarisations. However, for the persistent current the values given by a ramp protocol were used. The ramp was run from -90 to +80mV in 2s. At this speed the transient current was completely inactivated and the observed current was due to the persistent component. In CHO cells both the transient and the persistent currents showed very similar biophysical properties; both currents reached a peak at ~ 0mV and reversed at ~ +60mV, which is close to the theoretical value of +67mV.

The activation and inactivation characteristics of the transient human brain $Na_v1.3$ and the rat neuronal Na^+ currents were quite similar.

Activation

Activation of the sodium channel is thought to result from a voltage-driven conformational change from resting, closed conformation to an open conformation, accompanied by the translocation of positive charges in the S4 segment across the membrane. The voltage-dependence of sodium channel activation is sigmoidal, reflecting the change in the open probability of the channels. Since the principal polypeptide of the Na^+ channel has four homologous domains which are postulated to

form its transmembrane pore, it has been proposed that the multiple transitions leading to activation of the channel represent conformational changes in each of the four channel domains (Noda *et al.*, 1986).

In SCG neurones, the voltage at which half of the channels were activated ($V_{1/2}$) was ~ -21mV. In CHO cells, the $V_{1/2}$ value of the transient current was ~ -18mV. The slope of the curves, which indicates the voltage-dependence of activation had a value of ~ 5.5mV in both cells. The activation curve for the persistent component was constructed from ramp values and showed a $V_{1/2}$ value of ~ -14mV - a slightly more depolarised value when compared to the transient curve. The persistent component had a very similar slope value to the transient current (~ 6mV), suggesting similar voltage sensitivities.

Inactivation

The voltage-dependence of Na^+ current inactivation in SCG neurones was sigmoidal, with half inactivation potential of ~ -61mV and a slope factor of ~ 5mV. In CHO cells the transient Na^+ current has very similar steady state inactivation parameters to the native neuronal Na^+ current, with a $V_{1/2}$ value of ~ -64mV and a slope of ~ 6.5mV.

It is still controversial whether the transient and persistent currents are mediated by two different populations of Na^+ channels with different gating kinetics or whether individual channels of a uniform population can switch between gating modes. In fact, three general hypotheses about the origin of the persistent current have been presented: (1) the "*window*" current hypothesis based on Hodgkin-Huxley whole-cell current properties (Hodgkin & Huxley, 1952c); (2) the possibility that persistent currents are generated by an unusual subtype of sodium channels that do not inactivate (Stafstrom *et al.*, 1985; French *et al.*, 1990); and (3) that the Na^+ channel may adopt different gating modes, causing changes in inactivation properties.

The concept of a window current comes directly from the Hodgkin and Huxley model. Due to the partial superimposition of activation and steady state inactivation voltage-dependence curves, the persistent current can be derived from an incomplete steady inactivation of transient Na^+ channels over a narrow voltage window. Plots of h, the probability that a sodium channel is inactivated, and m, the probability that a

sodium channel is activated, *vs* membrane potential overlap over a small potential range, predicting a steady sodium conductance over this range. Using measurements of *h* and *m* from CA1 hippocampal pyramidal cells, French *et al* calculated the steady-state window conductance for the transient current (G_{Na}) and compared it with conductance of the persistent current (G_{NaP}), measured from the same neurone. In hippocampal neurones, the activation curve for G_{Na} increases following a Boltzmann curve with a $V_{1/2}$ of ~ –50mV and does not decrease. In contrast, the predicted window current peaks at around –50mV and rapidly falls to zero with further depolarisation. Similarly, Hamill *et al* (1986) looked at single Na^+ channel properties and found repetitive Na^+ channel openings only around threshold potentials, suggesting that the persistent Na^+ current is a "window" current present only in a narrow range of voltages where Na^+ channels were activated but where inactivation was too weak to shut the channels. These findings were challenged by Alzheimer *et al.* (1993), who could not confirm results by Hamill *et al.*, and have found persistent current to occur more frequently between –40 and –20mV.

Persistent currents could be mediated by a noninactivating subtype of sodium channels, which would allow a different spatial distribution in a neurone for transient and noninactivating sodium channels. Llinas, (1988) found the noninactivating current at or near the soma of Purkinje cells. Moreover, Westenbroek *et al* (1989) measured a high concentration of the immunologically distinct $Na_v1.1$ Na^+ channels in neuronal soma, whereas $Na_v1.2$ was located primarily in axons. Because persistent currents appeared to be predominantly generated at or near the soma, the differential spatial distribution of Na^+ channel subtypes led to the hypothesis that $Na_v1.2$ would primarily mediate action potentials, whereas the somatic $Na_v1.1$ channel would generate persistent currents. My data shows that the persistent and transient currents have similar thresholds for activation and half activation, $V_{1/2}$ values. This suggests that it is unlikely that persistent current flows through a different subset of channels than those underlying the transient current.

My recordings show that the transient and persistent currents share the same reversal potential and activation, which suggests that these currents are generated by the same sodium channel. The simplest explanation of the persistent current is that the persistent current is a result of a rare and atypical gating mode of the same transient Na^+ channel and there is a temporary blockade of the transition to an inactivated state.

Single channel data from cloned $Na_v1.3$ and $Na_v1.4$ Na^+ channels have indicated that these Na^+ channels occasionally failed to inactivate and entered a prolonged bursting mode (Moorman *et al.*, 1990; Zhou *et al.*, 1991; Ukomadu *et al.*, 1992). Alzheimer *et al* (1993) have also made similar observations with native persistent Na^+ currents recorded in cortical pyramidal neurones.

3.8.2 Characterisation of the sodium channel in SCG neurones

The fully inactivating Na^+ current recorded in SCG neurones has not yet been characterised. It was therefore important to identify which subtype yields the transient current in sympathetic neurones and if the $Na_v1.3$ subtype, which appears to have a persistent component when expressed in CHO cells, is also present in neurones.

The results of the RT-PCR on the rat brain show the presence of $Na_v1.1$, $Na_v1.2$, $Na_v1.3$ and $Na_v1.6$ Na^+ channel mRNAs. These results coincide with the work of Felts *et al*, who have shown the different expression patterns of these Na^+ channels in developing rat nervous system (Felts *et al.*, 1997). They have also shown that the level of $Na_v1.3$ sodium channel mRNA decreases slowly with development and in a 30-day old animal $Na_v1.3$ sodium channel is barely detectable. Therefore in a 17-day-old animal this subtype should be detectable. $Na_v1.7$ channel is predominantly expressed in PNS neurones, such as DRG neurones and it is not surprising not to find them in the brain.

The RT-PCR data from the whole SCG, which includes glial and neuronal cells, shows the presence of $Na_v1.7$ channel mRNA in addition to $Na_v1.1$, $Na_v1.2$, $Na_v1.3$ and $Na_v1.6$ sodium channels. The role of voltage-gated sodium channels in glial cells is not clear. There is some information about which isoforms are expressed in glia. A recent study utilising RT-PCR showed that $Na_v1.1$, $Na_v1.2$ and $Na_v1.3$ channels are expressed in the optic nerve (Oh *et al.*, 1994) and since there are no neurones in the optic nerve, they concluded that these isoforms are also expressed in glia.

I was interested in finding out which particular sodium channel isotype(s) are present in SCG neurones and not in glial cells. For this I tried single cell RT-PCR. It is known that SCG are abundant in G-proteins (Haley *et al.*, 1998). Therefore, in order

to establish optimal conditions for single cell RT-PCR reaction $G\alpha_o$ primers were used to amplify the G protein α_o subunit. The same conditions were used to amplify sodium channel isoforms, however I was unable to detect the isoforms present in a single neurone. One problem with this technique is that the amount of sodium channel protein does not come close to the abundance of G-proteins. This meant that mRNA may not necessarily be detected.

In order to confirm the results of the RT-PCR in SCG, and to check if the mRNA is actually translated into a sodium channel protein, immunocytochemistry was used. The results of this show the presence of $Na_v1.1$, $Na_v1.2$, $Na_v1.3$ and $Na_v1.7$ sodium channel proteins in SCG cells, therefore it is possible that a mixture of $Na_v1.1$, $Na_v1.2$, $Na_v1.3$ and $Na_v1.7$ sodium channels contribute to the native current. However, it is possible that although the channel proteins are present, they may not all be conducting current. Thus, due to the negative results of the single cell RT-PCR I was unable to show exactly which sodium channel subtypes are responsible for the current recorded in SCG neurones.

It was interesting to find the presence of $Na_v1.3$ sodium channel mRNA in SCG neurones, as well as the channel protein from immunocytochemical experiments. Since sodium currents recorded in SCG neurones do not show a persistent component, it is possible that either $Na_v1.3$ mRNA does not get translated into a functional protein, or that $Na_v1.3$ current in SCG neurones is under some physiological regulation (perhaps by protein kinases or G proteins), giving rise to fully inactivating currents. Therefore it was important to study the modulation of the native Na^+ current in SCG cells and $Na_v1.3$ channel expressed in CHO cells, as this would provide means to control the level of persistent Na^+ current and therefore cell excitability.

3.8.3 Modulation of the sodium current in SCG neurones and $Na_v1.3$ sodium channels expressed in CHO cells by protein kinases and G protein coupled pathways

Protein kinases are a whole family of enzymes. PKC is a member of this family and up to 11 different isoforms of PKC are known to exist (Mellor & Parker, 1998). Certain compounds are known to specifically stimulate or block PKC activity.

Phorbol esters, such as *PDBu* and *PMA*, known to activate PKC, were used in order to discover if PKC might be a modulator of the Na^+ current. The effect of PMA was examined on the peak Na^+ current in SCG neurones over a thirty-minute interval. A dramatic decrease in the current was observed in these neurones. This result indicates that PKC could play a modulatory role in these neurones. However, the kinetics of the current remained the same, with the current fully inactivating after PMA treatment. This is in contrast with a publication showing that activation of PKC with PMA actually induced persistent current in rat neocortical cells (Astman *et al.*, 1998).

The effect of PDBu was examined on the peak and persistent component of the $Na_v1.3$ Na^+ currents in CHO cells. No changes were observed neither on the peak transient nor the persistent current amplitudes on application of PDBu. There were also no significant changes in the activation and inactivation parameters of the channel, as illustrated by unchanged activation and inactivation curves. These results indicate that PKC does not play a role in modulating the transient and persistent components of $Na_v1.3$ Na^+ channels expressed in CHO cells. The lack of effect of PKC in CHO cell line may be due to biochemical differences found between neurones and transfected cell lines. It is quite probable that the CHO cell line does not have the full components of protein kinases and second messengers found in neurones or at least not at the same intracellular concentrations. However, it is also possible that such modulation by PKC may truly not exist in $Na_v1.3$ brain Na^+ channels. In order to answer this question the same experiments would have to be repeated in SCG neurones that have been transfected with the $Na_v1.3$ Na^+ channels.

In order to check if some other protein kinases may be involved in modulation of the $Na_v1.3$ Na^+ channel in CHO cells the effect of a non-selective inhibitor of protein kinases, namely staurosporine, was investigated. It was found that non-selective inhibition of protein kinases also did not have any effect on the peak and persistent currents. Again, this can be interpreted as either lack of modulation of the $Na_v1.3$ Na^+ channel expressed in CHO cells by protein kinases or lack of intermediary components and second messengers, necessary to evoke a regulatory response following protein kinase activation.

The results detailed above seem to indicate that direct activation of PKC has a significant effect on the peak Na^+ current in SCG neurones. It was interesting to see whether a more physiological activation of PKC via a G protein coupled membrane

receptor would give similar results. In SCG neurones application of both oxo-M and norepinephrine had no effect on the peak Na^+ current. This rules out the involvement of M_1 muscarinic acetylcholine receptors and α-adrenoceptors in modulation of the Na^+ current in these neurones.

The effect of direct and constant G-protein stimulation by GTPγS was also investigated in both SCG neurones and $Na_v1.3$ Na^+ current in CHO cell lines. There was no change in the peak Na^+ current in SCG neurones when GTPγS was included in the pipette solution. To test that GTPγS is able to produce an effect in SCG cells, my colleague, Jose Fernandez, recorded G-protein regulated inward rectifier K^+ (*GIRK*) currents in the presence and absence of this GTP analogue. As expected, GTPγS inhibited the K^+ current (Fernandez-Fernandez *et al.*, 2001). As in SCG neurones, GTPγS did not have any effect on the sodium current in CHO cells, with no changes observed in the transient and persistent Na^+ current amplitudes or kinetics. However, the question of whether or not the cell line has all of the mediators necessary to see the response needs to be answered. In fact, it is not very clear if cell lines have enough of the G-protein subunits to evoke a change. Therefore future experiments can include reproducing the work of Ma and overexpressing Gα and Gβγ subunits in CHO cells transfected with $Na_v1.3$ Na^+ channel.

The results presented in this chapter indicate that $Na_v1.3$ Na^+ channel expressed in CHO cells, which is capable of showing a persistent sodium current component, and the fully inactivating Na^+ current found in SCG neurones, possibly a mixture of $Na_v1.1$, $Na_v1.2$, $Na_v1.3$ and $Na_v1.7$ Na^+ channels, show very similar biophysical properties, except that of inactivation. Pharmacological studies show that they are TTX sensitive channels, however their modulation is slightly different. Activation of PKC by a phorbol ester in SCG neurones dramatically decreased the peak Na^+ current. However G-protein coupled membrane receptors did not show any modulation of the current. In a CHO cell line the $Na_v1.3$ Na^+ current was not modulated by PKC, or any other protein kinases. Activation of G-proteins also did not show any changes in the transient or persistent currents.

CHAPTER 4

EFFECTS OF THE NOVEL ANTICONVULSANT DRUG RETIGABINE ON EXPRESSED KCNQ POTASSIUM CURRENTS AND NATIVE NEURONAL M-TYPE POTASSIUM CURRENTS.

4.1 INTRODUCTION

M-type potassium (K^+) currents ($I_{K(M)}$) are a species of subthreshold voltage-gated K^+ current that serves to stabilise the membrane potential and control neuronal excitability (see Brown, 1988, and Marrion, 1997, for reviews).

Recent evidence suggests that native M channels in rat sympathetic neurones are composed of a heteromeric assembly of KCNQ2 and KCNQ3 K^+ channel subunits (Wang *et al.*, 1998; see also Hadley *et al.*, 2000; Selyanko *et al.*, 2000; Shapiro *et al.*, 2000). These are K^+ channel gene products that are widely distributed in the nervous system, mutations of which give rise to a form of congenital epilepsy termed Benign Familial Neonatal Convulsions (BFNC: Biervert *et al.*, 1998; Charlier *et al.*, 1998; Singh *et al.*, 1998; see Jentsch, 2000 and Rogawski, 2000 for reviews). This implies that M channels may assist in controlling seizure discharges, and drugs that enhance M channel activity might be effective anti-epileptic agents. Retigabine (D-23129; N-(2-amino-4-(4-fluorobenzylamino)-phenyl) carbamic acid ethyl ester) (Rostock *et al.*, 1996; Tober *et al.*, 1996) is a novel anticonvulsant compound that is now in clinical phase II development for the treatment of epilepsy. It has been reported to open K^+ channels in NG108-15 neuroblastoma-glioma hybrid cells (Rundfeldt, 1997). When I started my studies on retigabine, the molecular identity of the K^+ channels enhanced by retigabine was not yet reported. However, during the course of my studies, Main *et al.*, (2000), Rundfeldt *et al.*, (2000) and Wickenden *et al.*, (2000) published the observation that retigabine enhances currents generated by KCNQ2/3 K^+ channels when expressed in CHO cells, in part by shifting their voltage sensitivity to more hyperpolarised membrane potentials.

However, two questions arise concerning the effect of retigabine. First, KCNQ2 and KCNQ3 are members of a larger family of homologous K^+ channels comprising, in addition, a subunit (KCNQ1) of the cardiac delayed rectifier current (Barhanin *et al.*, 1996; Sanguinetti *et al.*, 1996), a subunit (KCNQ4) present in the auditory system (Kharkovets *et al.*, 2000; Kubisch *et al.*, 1999), and another recently-identified subunit (KCNQ5) widely distributed in the central and peripheral nervous system (Lerche *et al.*, 2000; Schroeder *et al*, 2000a). All of these subunits, when expressed as homomultimers, generate 'M-like' currents as defined kinetically and pharmacologically (Hadley *et al.*, 2000; Selyanko *et al.*, 2000; Schroeder *et al.*,

2000a). Because the KCNQ channels have similar pharmacological profiles, a potential problem in the development of drugs that target neuronal KCNQ channels is that the cardiac KCNQ1 channel may also be affected and lead to adverse side effects. And it is not yet known whether all KCNQ channels are equally sensitive to retigabine. Second, it has yet to be established whether retigabine affects native neuronal M currents in the same way that it affects expressed KCNQ2/3 channels. Accordingly, the aim of my studies was to compare the action of retigabine on heteromeric KCNQ2/3 currents expressed in mammalian CHO cells with its action on expressed homomeric KCNQ1, 2, 3 and 4 currents on the one hand, and on native M currents in rat sympathetic neurones on the other.

4.2 KCNQ2/3 SUBUNITS ARE THE MOLECULAR CORRELATES OF THE M CHANNEL

The M current was first described in bullfrog sympathetic ganglia (Brown & Adams, 1980), as a slowly activating and slowly deactivating K^+ current that showed no inactivation. The mammalian equivalent was soon described in rat superior cervical ganglion (SCG) cells (Constanti & Brown, 1981). Identification of the candidate genes responsible for generation of the M-current has been hampered due to a lack of selective pharmacological agents to block the channel. With the discovery of linopirdine (Nickolson *et al.*, 1990) and a related compound XE991, it was concluded that KCNQ2 and KCNQ3 heteromultimers could be the molecular correlates of the M current in rat SCG neurones (Wang *et al.*, 1998, Cooper *et al.*, 2000).

To compare the biophysical properties of the KCNQ2/3 currents and the native M-current in rat SCG neurones, KCNQ2 and KCNQ3 cDNAs were co-expressed in a 1:1 ratio in CHO hm1 cells (see *Chapter 2*) and recorded 1 day after transfection using the perforated patch clamp technique. As a marker for successfully transfected cells, all transfections included cDNA coding for the CD8 receptor. Prior to recordings CD8 beads were added to the dish and beaded CHO cells were chosen for recordings.

The native M-current and expressed KCNQ2/3 currents were recorded in response to the conventional M-current voltage protocol (Adams *et al.*, 1982). That is, the membrane was held at –20mV in order to activate the current and then the current

was deactivated by series of 1 sec hyperpolarising steps to –80mV in SCG neurones and –90mV in CHO cells, delivered in 10mV increments, *figure 21A*. Typical KCNQ2/3 current responses are shown on *figure 21B* and native M-current records are shown in *figure 21C*. Like the sympathetic M-current (*figure 21C*), KCNQ2/3 current is manifested as a standing current at –20mV, and shows characteristic M-like deactivation tails, with increasingly rapid relaxations on stepping to progressively more negative potentials.

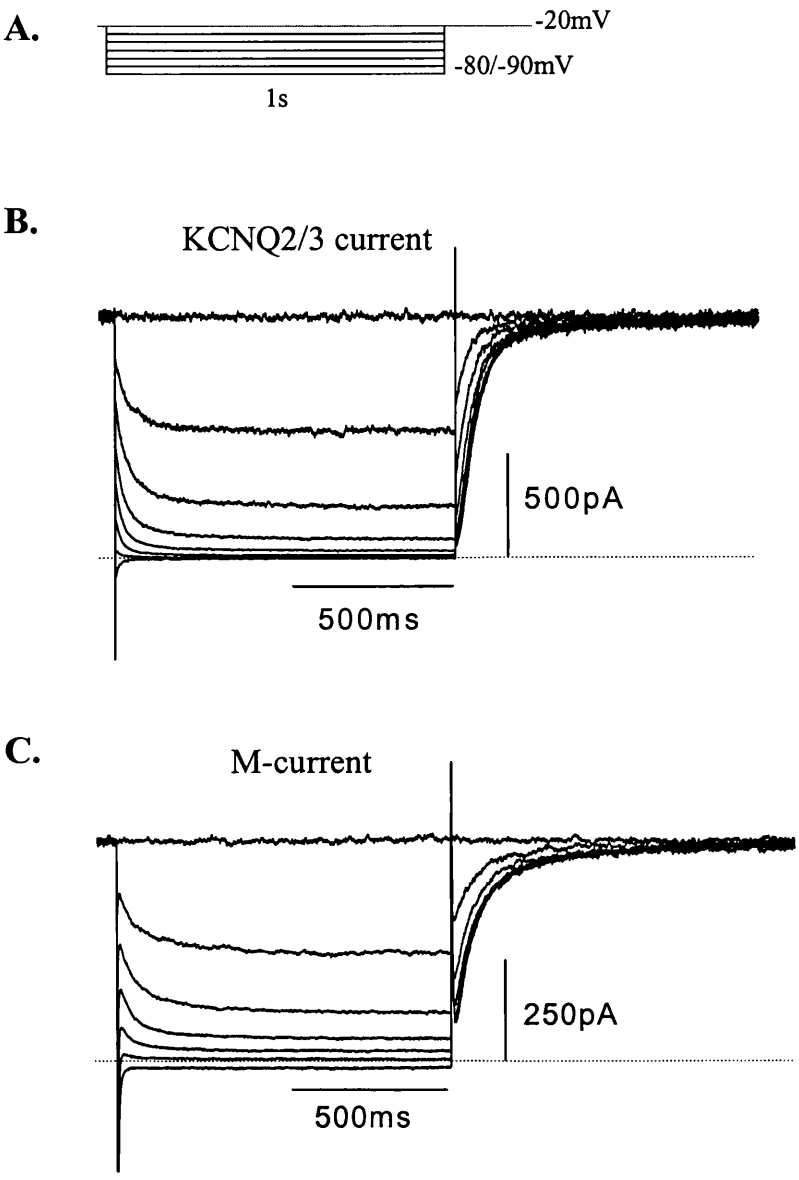

Figure 21: Comparison of currents through KCNQ2/3 channels expressed in CHO hm1 cells with the native M-current in SCG neurones.

A. Voltage command protocol: currents were activated by clamping the membrane at -20mV and then deactivated by 1sec hyperpolarisations to -80/-90mV in 10mV increments. Currents were reactivated by repolarising the membrane potential back to -20mV.

B. Currents in response to the voltage protocol in *(A)* through expressed KCNQ2/3 heteromultimeric channels, recorded in CHO hm1 cells.

C. For comparison, the M-current recorded in SCG neurones is shown, obtained with the same voltage command protocol. Dotted lines represent zero current level.

4.3 ACTIVATION OF HETEROMERIC KCNQ2/3 AND HOMOMERIC KCNQ1, KCNQ2, KCNQ3 AND KCNQ4 CURRENTS EXPRESSED IN CHO hm1 CELLS

The proposal that KCNQ2/3 heteromultimers are the only channels underlying the M-current may be an over simplification. Expression of other known KCNQ genes in either CHO (Hadley *et al.*, 2000; Selyanko *et al.*, 2000) or HEK 293 cells (Shapiro *et al.*, 2000) have shown that KCNQ1, KCNQ2, KCNQ3 and KCNQ4 homomultimers, as well as KCNQ2/3 heteromultimers, can produce functional currents that display M-like characteristics. Indeed, all combinations of current can be inhibited by M_1 muscarinic activation (Selyanko *et al.*, 2000) and blocked by linopirdine (Wang *et al.*, 1998). To compare the biophysical properties of homomeric KCNQ1, KCNQ2, KCNQ3 and KCNQ4 channels with heteromeric KCNQ2/3 channel activation, cDNAs encoding these KCNQ channels were transfected in CHO hm1 cells, as described in *Chapter 2*, and currents recorded using series of 1 sec depolarising voltage steps to +50mV in 10mV increments from a holding potential of –70mV, *figure 22*.

There was a striking difference in the sizes of currents produced by the KCNQ subunits. When looking at the current amplitude following step depolarisations to +50mV, KCNQ2 + KCNQ3 heteromeric channels expressed most rapidly and current amplitudes of about 2-5nA were recorded only one day after transfection. Two and three days after transfection, currents were even larger and recording stability was compromised. KCNQ2 and KCNQ4 channels expressed alone gave much smaller currents one day after transfection (< 1nA) and were usually recorded two days after transfection. Homomeric KCNQ1 and KCNQ3 channels gave very low expression levels one day after transfection (< 0.2nA) and were usually recorded two or three days after transfection (*figure 22*).

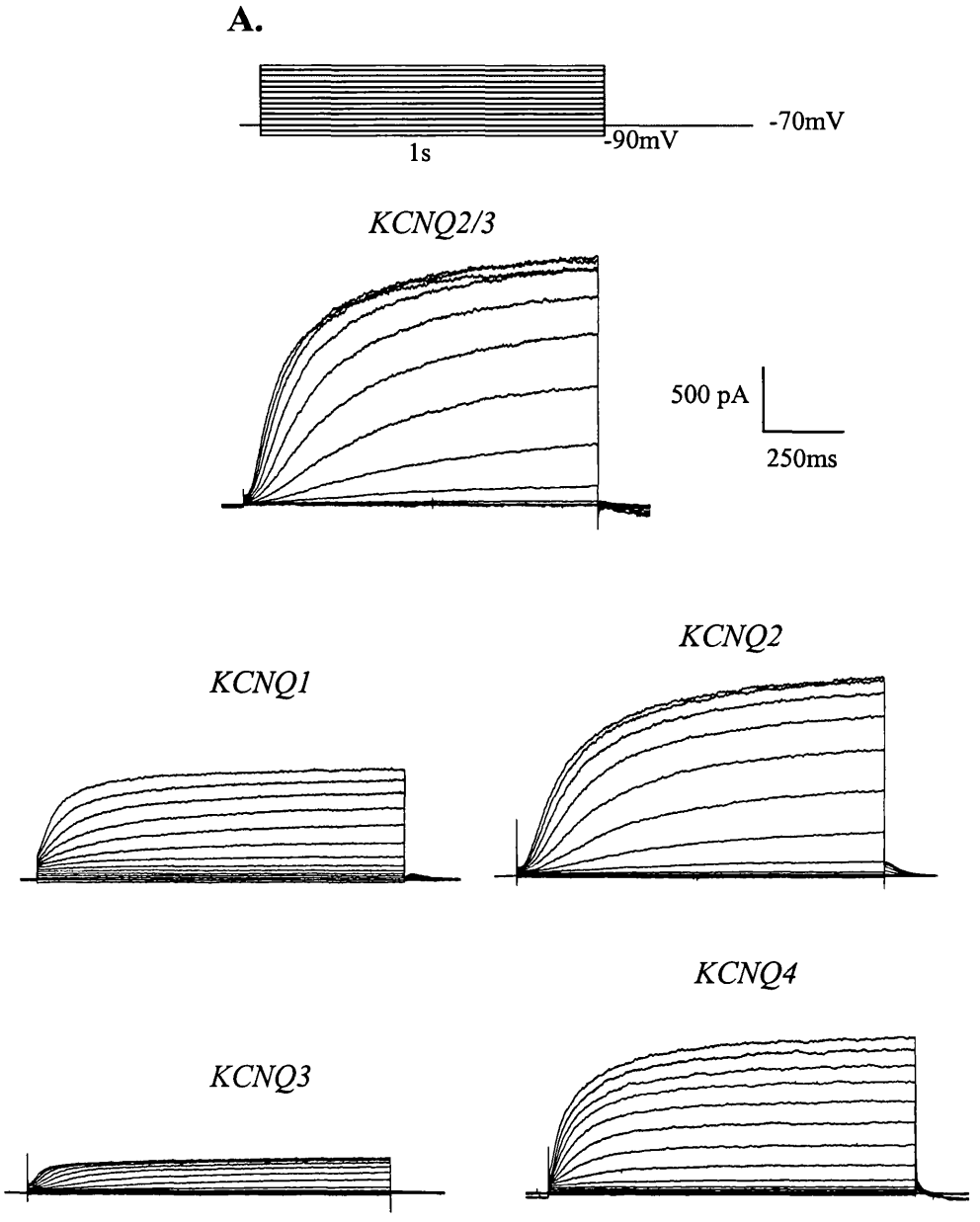

Figure 22: Activation of heteromeric KCNQ2/3 and homomeric KCNQ2-4 channels expressed in CHO cells.
Currents were activated by 1sec depolarising pulses in 10mV increments to +50mV from a holding potential of -70mV. Note that KCNQ2/3 currents were recorded 24 hours after transfection and KCNQ1-4 homomultimers were recorded 48 hours after transfection. Also note the differences in maximum current amplitude.

To further compare the activation of heteromeric KCNQ2/3 and homomeric KCNQ1-4 currents, activation curves were constructed and plotted in *figure 23*. This was done by recording each of the mentioned KCNQ currents in response to the voltage protocol shown in *figure 23A*. The membrane was held at –70mV and KCNQ currents were fully activated by 0.5 sec depolarisations to +50mV, before sequentially deactivating them by series of 1 sec hyperpolarisations to –110mV in 10 mV increments, and recording the tail current at –120mV. The relative amount of conductance at the end of each 1 sec hyperpolarising step is related to the amplitude of the tail current recorded at –120mV following that particular hyperpolarising step (see *figure 23A*). The amplitude of the tail current was determined as described in *Chapter 2*. The values were normalised to the maximum conductance value (at +50mV) and plotted against corresponding hyperpolarising step potential, *figure 23B*. Points were fitted with Boltzmann equation (*equation 4, Chapter 2*), with $V_{1/2}$ (membrane potential at which half of the channels are open) and slope values indicated in the legend. KCNQ2/3, KCNQ1, KCNQ2 and KCNQ4 channels had quite similar $V_{1/2}$ values, ranging from ~ -12.5mV to ~ -17mV. KCNQ3 had a more hyperpolarised $V_{1/2}$ value (~ -29mV). Slopes on the other hand, which give an indication of the voltage sensitivity of channel activation, were very similar for all the KCNQ channels tested (between ~ 10-12mV).

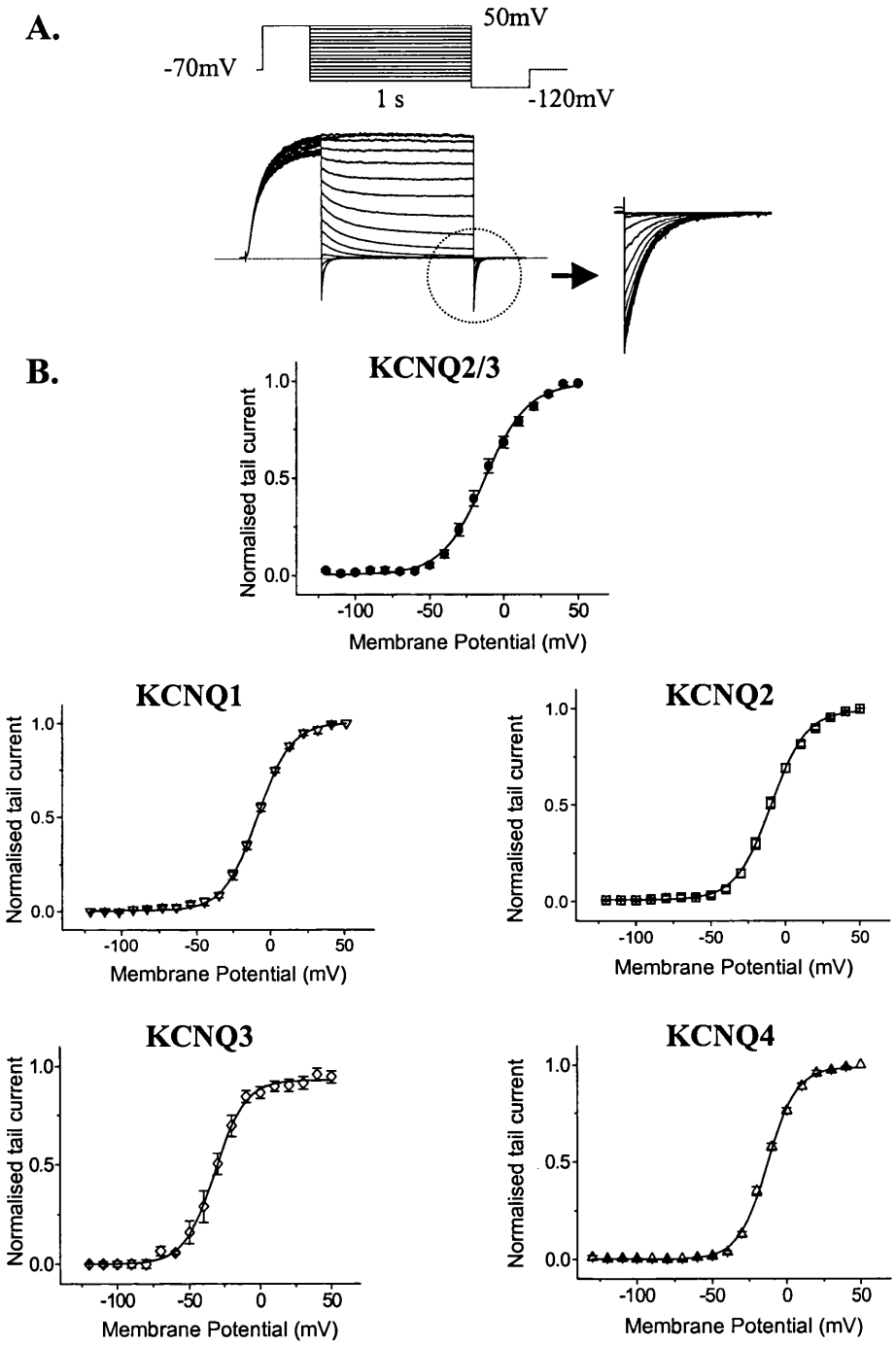

Figure 23: Activation curves for KCNQ2/3 and KCNQ1-4 channels expressed in CHO hm1 cells.

A. Currents were activated by depolarising pulses to +50mV from a holding potential of -70mV and deactivated by 1s hyperpolarising pulses to various potentials between +50 and -120mV, followed by a step to -120mV. The inset shows, as an example, KCNQ2/3 tail currents recorded at -120mV, which were used to construct activation curves (KCNQ2/3 current is shown as an example).

B. Activation curves were obtained from tail currents as described in *Chapter 2, Materials and Methods* and fitted with Boltzmann equation 4. The $V_{1/2}$ and slope values were as follows: KCNQ2/3 (●), -17.3 ± 2.2 mV and 12.9 ± 1.2 mV (n=9); KCNQ1 (▽), -12.5 ± 1.1 mV and 12.4 ± 0.9 mV (n=11); KCNQ2 (□), -11.5 ± 1.5 mV and 10.9 ± 0.6 mV (n=16); KCNQ3 (◇), -28.7 ± 2.5 mV and 11.4 ± 0.9 mV (n=7); KCNQ4 (△), -12.6 ± 0.7 mV and 10.1 ± 0.3 mV respectively. Data shown as mean ± SEM, n = 6-13.

4.4 *ACTION OF RETIGABINE ON KCNQ1, KCNQ2, KCNQ3, KCNQ2/3 AND KCNQ4 CURRENTS EXPRESSED IN CHO hm1 CELLS*

4.4.1 Retigabine enhances KCNQ2-4 currents in CHO cells.

Figure 24 illustrates recordings in CHO cells transfected with cDNAs for KCNQ2/3, KCNQ2, KCNQ3 and KCNQ4. Currents were recorded using a classic 'M current protocol' (Constanti & Brown, 1981) – that is, the cell was pre-depolarised to –20 mV to activate the current, then hyperpolarised to -80 or –90 mV in steps of 10 mV to deactivate the current. Deactivation is registered by the slow tail currents, and re-activation on stepping back to –20 mV by the slow outward current. In these experiments, currents through heteromeric KCNQ2/3 and homomeric KCNQ2, KCNQ3 and KCNQ4 channels were recorded under control conditions (*left panel*), in the presence of 10μM retigabine (*middle panel*) and 10 min after washout of the drug (*right panel*). The following points emerge from this comparison. (1) No appreciable current could be recorded from control (untransfected) cells, and retigabine had no significant effect on these cells (*figure 24B*). (2) As predicted from the previous experiments of Main *et al.* (2000), Wickenden *et al.* (2000) and Rundfeldt & Netzer (2000), retigabine increased the outward current recorded at –20 mV in cells transfected with KCNQ2 + KCNQ3 cDNAs. However, it also increased the holding current at –20 mV in cells transfected solely with KCNQ2, KCNQ3 or KCNQ4 cDNAs to comparable (or greater) extents. (3) The additional current at –20 mV induced by retigabine in KCNQ2 and KCNQ2/3-transfected cells was removed by hyperpolarising the membrane to –90 mV. However, an additional component of inward current was recorded at –90 mV in KCNQ3 and KCNQ4-transfected cells. This implies that a component of KCNQ3 or KCNQ4 current persisted in the presence of retigabine negative to resting potentials (-60 mV: Selyanko *et al.*, 2000) where these channels would normally be fully deactivated. (4) Retigabine slowed the deactivation of the currents during step-hyperpolarisations and accelerated the reactivation on repolarisation. This effect was most pronounced with KCNQ3, for which the time-dependence of current deactivation was lost except at very negative potentials, and least pronounced for KCNQ4. Thus, these tests indicate that the previously reported

enhancing effect of retigabine on KCNQ2/3 channels also extends to homomeric KCNQ2, 3 and 4 channels, albeit with quantitative differences.

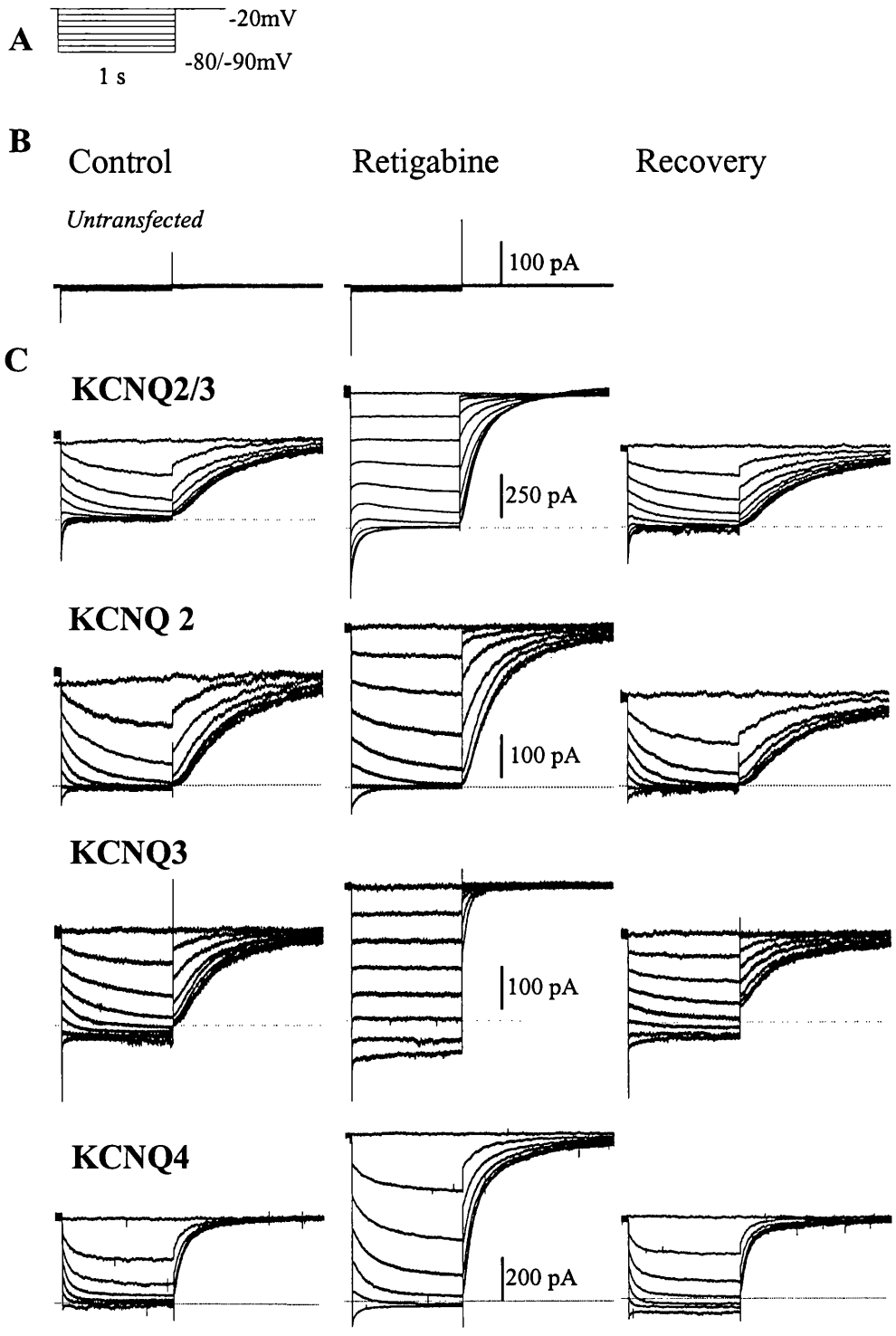

Figure 24: Enhancement of heteromeric KCNQ2/3 and homomeric KCNQ2-4 currents in CHO hm1 cells by retigabine.

A. Voltage protocol: currents were activated by clamping the membrane at -20mV and then deactivated by 1s hyperpolarisations to -80 or -90mV in 10mV increments.

B. Retigabine (10μM) did not activate any endogenous currents in untransfected CHO cells.

C. KCNQ currents generated by the voltage protocol in *(A)* recorded in the absence *(left)*, presence *(centre)* and 10 min after washout *(right)* of 10 μM retigabine. Dotted lines denote zero current.

Augmentation of KCNQ2-4 currents by retigabine was confirmed following current activation from –70 mV to +50 mV in 10 mV steps (*figures 25 and 26*). *Figure 25* illustrates currents recorded in response to step depolarisations from –90mV to +50mV in 10 mV increments (*figure 25A*). Untransfected cells did not show significant current in response to the voltage protocol shown in *(A)* and 10 μM retigabine did not change the current in these cells. In KCNQ2/3, KCNQ2, KCNQ3 and KCNQ4 transfected CHO cells retigabine clearly accelerated the onset of all currents at all voltages (*figure 25C*). This effect was most prominent for KCNQ3. From *figure 25*, the effect of retigabine on individual currents at each voltage was not very clear. Therefore, in *figure 26*, current responses to –40, -20, 0 and +20mV are shown for clarity, under control conditions (*left panel*) and in the presence of 10 μM retigabine (*right panel*). Retigabine clearly augments KCNQ2/3, KCNQ3 and KCNQ4 currents at -40, -20, 0 and +20mV. However, KCNQ2 currents at more positive potentials (+20mV and above) are unaffected by retigabine. This voltage dependent action of retigabine is further demonstrated in *figure 27*, where current-voltage curves were plotted for KCNQ2/3, KCNQ2, KCNQ3 and KCNQ4 under control conditions and in the presence of 10 μM retigabine. This was done by measuring current amplitudes following depolarising pulses from –90 to +50mV in 10mV increments, under control conditions and in the presence of retigabine, as shown in *figure 25A*. These values were normalised against the maximum current at +50mV in control recordings and plotted against depolarising membrane potential. Two important points emerge from these graphs. Firstly, the uniform effect of retigabine was to produce a leftward shift in the current-voltage relationship of the KCNQ channels, which is an important point in explaining the enhancement of current seen in *figures 24, 25*. For KCNQ2/3, 2 and 4 this corresponded to a ~20-30 mV negative shift in threshold for current activation. For KCNQ3 the shift was much greater since the current was still active at the holding potential (-70 mV): in effect, retigabine converted the KCNQ3 current from a time- and voltage-dependent current with a threshold of –50 mV to a substantially time- and voltage-independent 'leak' current from –90 mV upwards. Secondly, retigabine clearly increased current generated by KCNQ3 and KCNQ4 channels (and, to varying extents, by KCNQ2/3 channels) across a range of potentials, including the maximum current at +50mV. For KCNQ2, however, current enhancement was seen at voltages between -50mV to +30mV only. Variation in the

amount by which retigabine increased the maximum current amplitude through different KCNQ channels may reflect a variable component of secondary blocking action at positive potentials (see KCNQ1, *section 4.4.6*).

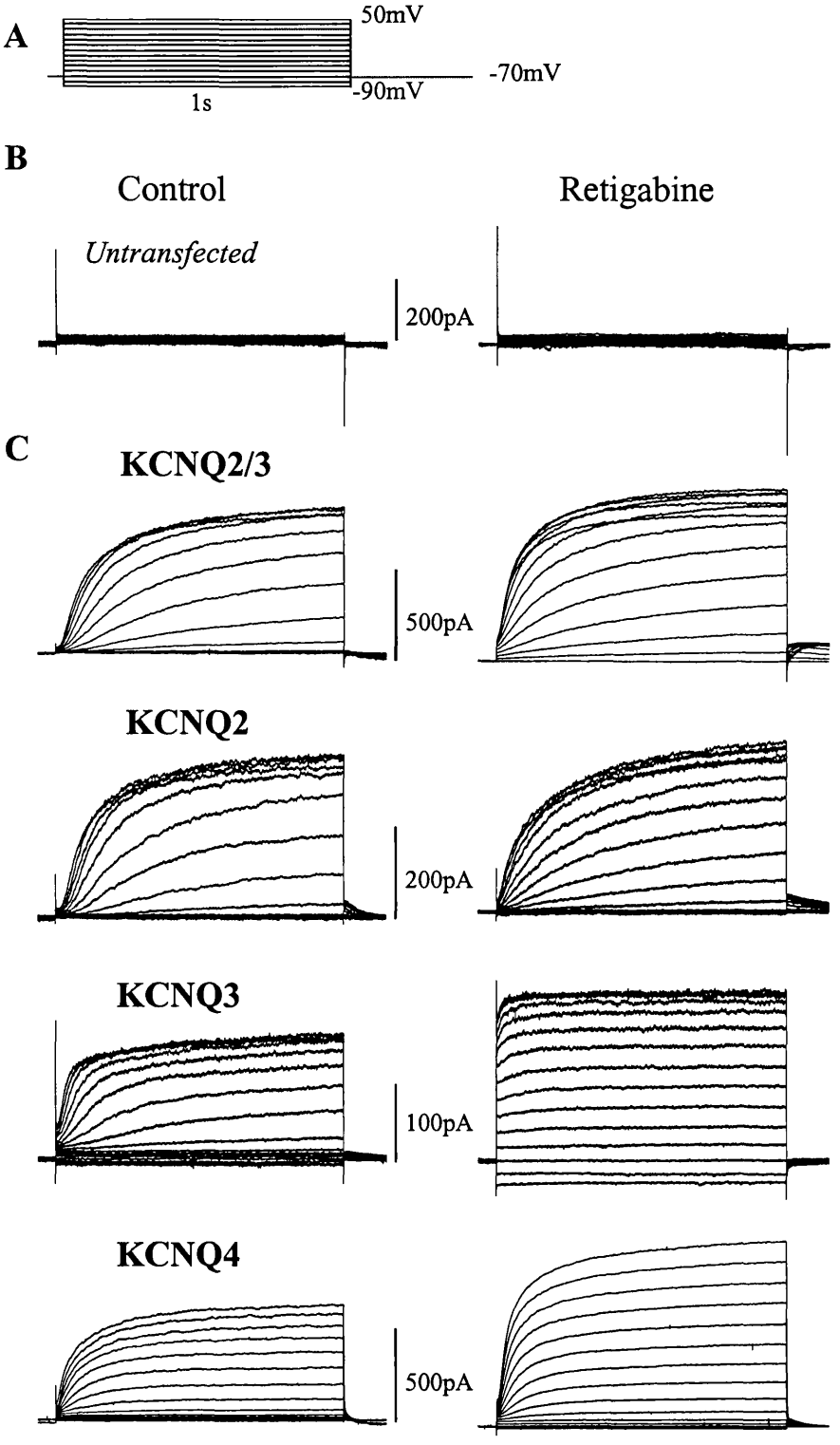

Figure 25: Activation of heteromeric KCNQ2/3 and homomeric KCNQ2-4 channels expressed in CHO hm1 cells in the absence and presence of retigabine.

A. Voltage protocol: currents were activated by 1 sec depolarising pulses in 10mV increments to +50mV from a holding potential of -70mV.

B. Retigabine (10μM) did not activate any endogenous currents in untrasfected CHO cells.

C. KCNQ currents generated by the voltage protocol in *(A)* recorded in the absence *(left)* and presence *(right)* of retigabine.

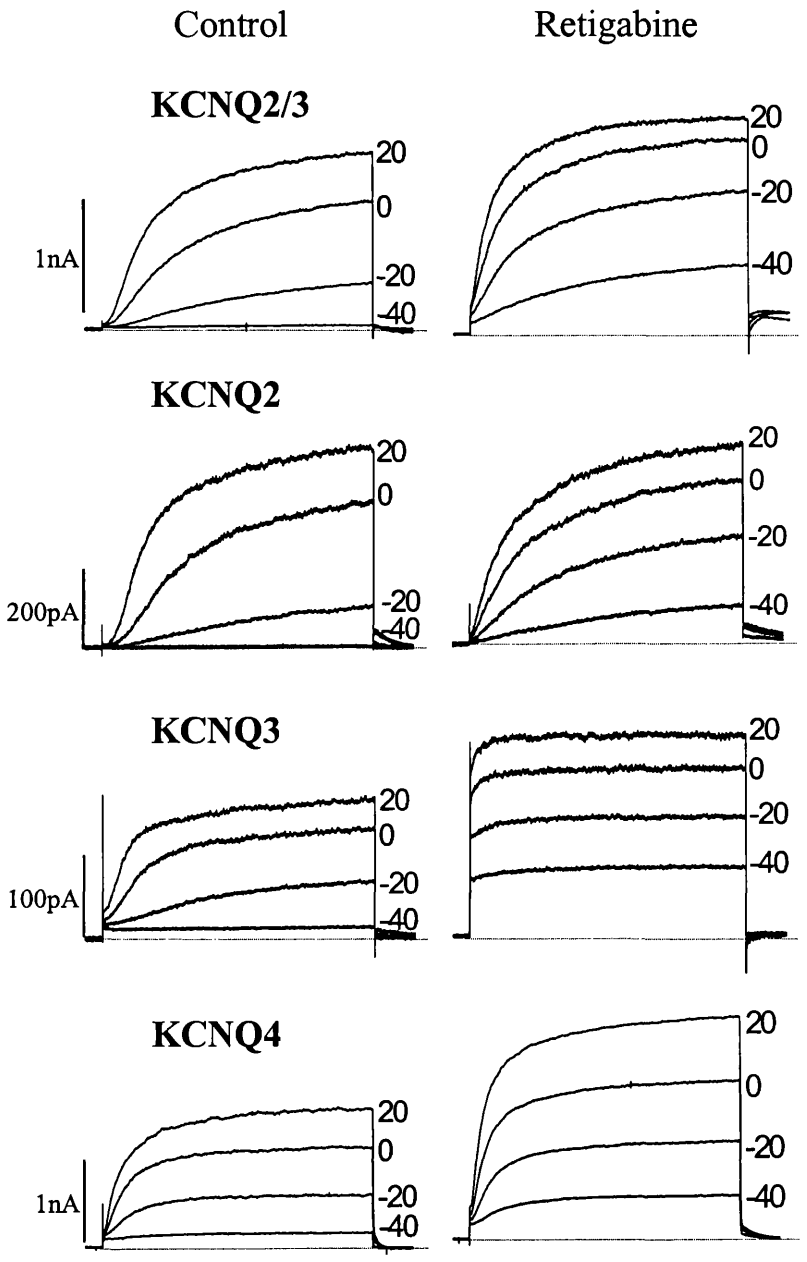

Figure 26: Effect of retigabine on heteromeric KCNQ2/3 and homomeric KCNQ2-4 current activation at selective voltages.

Currents were activated by 1 sec depolarising pulses in 10mV increments to +50mV from a holding potential of -70mV, as in *figure 25A*. Currents were recorded in the absence *(left)* and presence *(right)* of retigabine (10μM). Records show currents recorded at -40, -20, 0, and +20mV. Note that KCNQ3 and KCNQ4, but not KCNQ2/3 and KCNQ2 currents are increased at all voltages by retigabine.

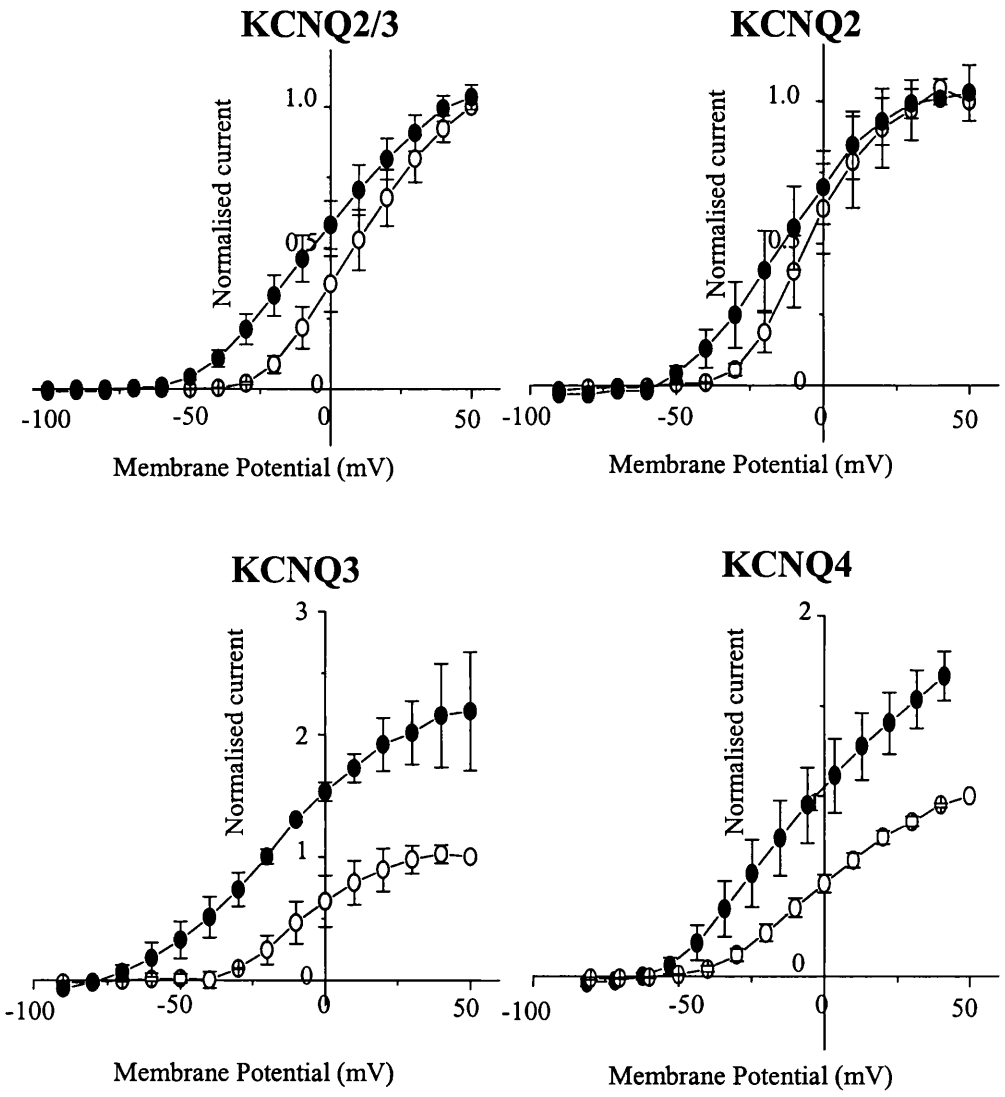

Figure 27: Effects of retigabine on KCNQ2-4 current-voltage relationships.
Normalised current values were plotted against command potential before (○) and after addition of 10μM retigabine (●). Data shown as mean ± SEM (n = 7-11). To obtain normalised values, peak current amplitudes in response to depolarising pulses from a holding potential of -70mV to +50mV in 10 mV increments (protocol shown in *figure 25A*) were normalised against the maximum current amplitude at +50mV in control recordings. Retigabine shifts the threshold for channel activation and augments KCNQ current amplitude across a range of membrane potentials.

4.4.2 Retigabine shifts KCNQ2-4 activation curves.

The current-voltage curves in *figure 27* suggest that one effect of retigabine was to produce a negative shift in the KCNQ current activation curve. This was further tested using the protocol shown in *figure 23A*, in which the current was first fully activated by stepping to +50 mV, then stepped for 1 s to various potentials between +50 and –110 mV, followed by a final step to –120 mV. The relative amount of conductance at each test potential, following a 1 s step at +50mV, could then be determined directly from the residual tail-current at –120 mV. Activation curves were constructed in this way for KCNQ2/3, KCNQ2, KCNQ3 and KCNQ4 under control conditions and in the presence of retigabine. Boltzmann plots, *figure 28*, confirmed that 10 μM retigabine produced a significant left-shift of the activation curves and half activation potentials, $V_{1/2}$, in the order KCNQ3 (-43 mV) > KCNQ2/3 (-30 mV) > KCNQ2 (-24 mV) >KCNQ4 (-14 mV). (Values in brackets give mean shift in half-activation potential $V_{1/2}$). In contrast, the slopes of the activation curves were not significantly changed by retigabine. The legend in *figure 28* shows $V_{1/2}$ and slope values for KCNQ2/3, KCNQ2, KCNQ3 and KCNQ4 activation curves under control conditions and in the presence of retigabine.

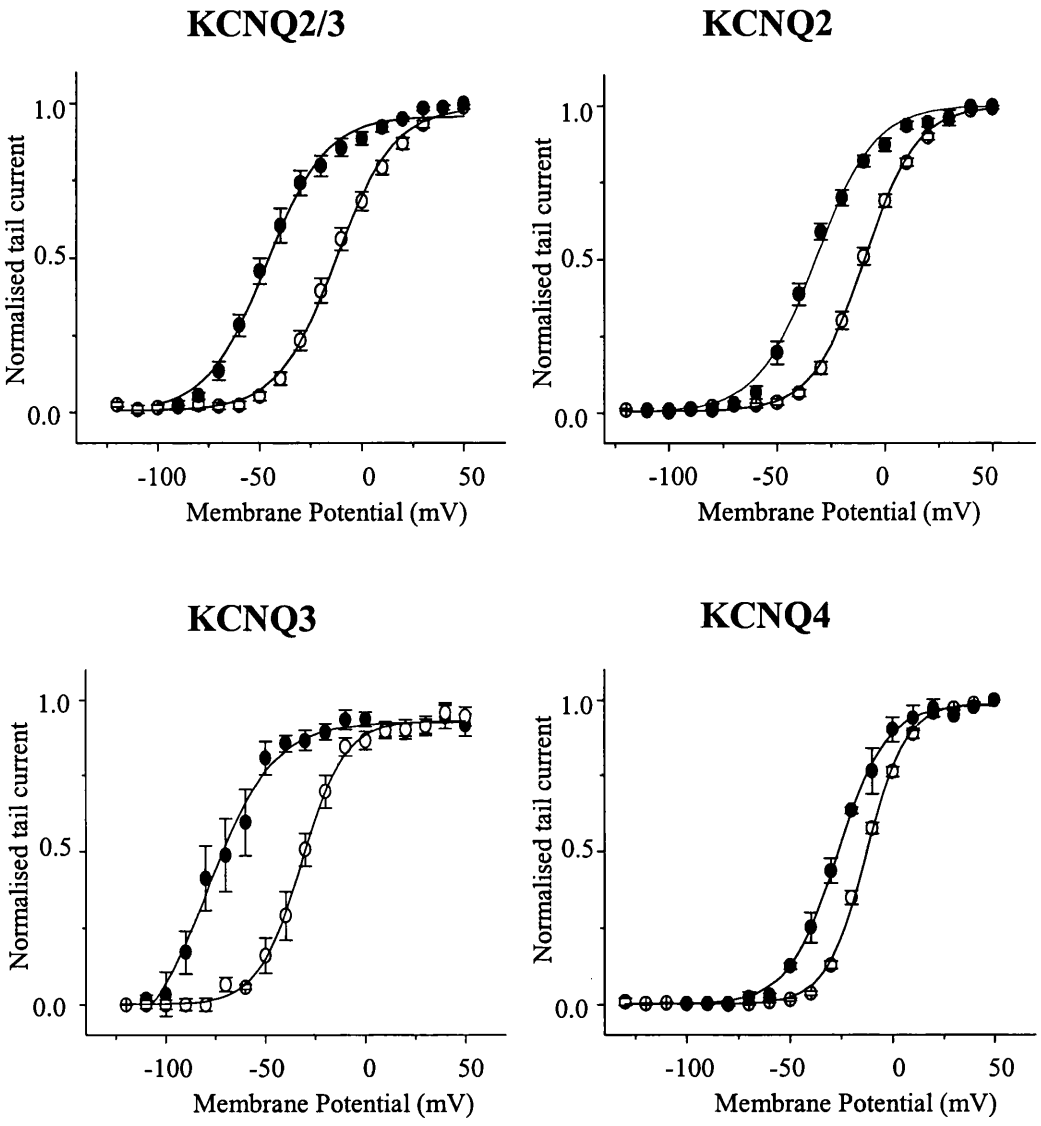

Figure 28: Effects of retigabine on KCNQ2-4 activation curves.
Activation curves in the absence (○) and presence (●) of 10 μM retigabine were obtained from tail currents recorded at -120mV as described for *figure 23*, and fitted with the Boltzmann equation 4. The $V_{1/2}$ values were as follows: KCNQ2/3, -17.3 ± 2.2 mV for control (n=9) and -47.7 ± 2.7 mV for retigabine-treated cells (n=9); KCNQ2, -11.5 ± 1.5 mV for control (n=16) and -35.7 ± 2.1 mV for retigabine-treated cells (n=6); KCNQ3, -28.7 ± 2.5 mV for control (n=7) and -71.5 ± 3.1 mV for retigabine-treated cells (n=7); and KCNQ4, -12.6 ± 0.7 mV for control (n=4) and -26.2 ± 0.6 mV for retigabine-treated cells (n=4). Slopes were as follows: KCNQ2/3, 12.9 ± 1.2 mV (control, n=9) and 11.4 ± 1.3 mV (retigabine, n=5); KCNQ2, 10.9 ± 0.6 mV (control, n=16) and 11.2 ± 0.9 mV (retigabine, n=6); KCNQ3 11.4 ± 0.9 mV (control, n=7) and 10.9 ± 0.9 mV (retigabine, n=7); and KCNQ4, 10.1 ± 0.3 mV (control, n=4) and 12.1 ± 1.6 mV (retigabine, n=4). Data shown as mean ± SEM.

The $V_{1/2}$ and slope values for KCNQ2/3, KCNQ2, KCNQ3 and KCNQ4 activation curves under control conditions and in the presence of retigabine are summarised in *table 3*. The uniform effect of retigabine was to produce a leftward shift in $V_{1/2}$ values, to varying extents.

	Control ($V_{1/2}$; slope) (mV)	***Retigabine ($V_{1/2}$; slope) (mV)***
KCNQ2/3	-17.3 ± 2.2; 12.9 ± 1.2	-47.7 ± 2.7; 11.4 ± 1.3
KCNQ2	-11.5 ± 1.5; 10.9 ± 0.6	-35.7 ± 2.1; 11.2 ± 0.9
KCNQ3	-28.7 ± 2.5; 11.4 ± 0.9	-71.5 ± 3.1; 10.9 ± 0.9
KCNQ4	-12.6 ± 0.7; 10.1 ± 0.3	-26.2 ± 0.6; -12.1 ± 1.6

Table 3: Summary of activation parameters for KCNQ2-4 channels under control conditions and in the presence of retigabine.

Columns show $V_{1/2}$ and slope values obtained from the activation curves shown in figure 28 for KCNQ2/3, KCNQ2, KCNQ3 and KCNQ4 under control conditions and in the presence of retigabine. Data are shown as mean ± SEM, n = 4-13.

4.4.3 Concentration-response of retigabine for KCNQ2/3, KCNQ2, KCNQ3 and KCNQ4.

The differential effects shown in *figure 28* were obtained using a fixed (10 μM) concentration of retigabine. In order to measure the potency of retigabine, the shift in the activation curves produced by incremental concentrations of retigabine were determined, as illustrated in *figure 29,* for KCNQ2/3 and KCNQ4. Currents were recorded using the voltage protocol shown on *figure 29A*. The membrane was depolarised to +50mV to open all channels, before progressively deactivating them by series of 1sec hyperpolarising steps to –110mV in 10mV increments. To amplify the inward tail currents at –120 mV (and hence improve the accuracy of the deduced activation curves), the external K^+ concentration was raised to 25 mM for these experiments. This did not itself affect the action of retigabine since the shift of the KCNQ2/3 activation curve produced by 10 μM retigabine in 25 mM [K^+], shown in *figure 29B* was indistinguishable from that observed in 2.5 mM [K^+], illustrated in *figure 28*. Activation curves were plotted under control conditions and in the presence of 1, 3, 10, 30, 100 and 300 μM retigabine for KCNQ2/3, KCNQ2 and KCNQ3. For KCNQ4, 1mM retigabine was also applied in order to achieve maximum effect of the drug. The magnitude of the shift in the activation curves was clearly dependent on the concentration of retigabine (*figure 29B*). The shift in $V_{1/2}$ value obtained with each concentration of retigabine was normalised against the maximum shift in $V_{1/2}$ (obtained with 10 μM retigabine for KCNQ2/3, KCNQ2, KCNQ3 and 1mM with KCNQ4) and plotted against corresponding retigabine concentration. The relation between the concentration of retigabine and the shift in the half-activation potential $V_{1/2}$ for KCNQ2/3, KCNQ2, KCNQ3 and KCNQ4 channels, deduced from these experiments, is shown in *figure 30*. Data points could be fitted with a Hill equation (*equation 5, Chapter 2*), with slope ~1, but EC_{50} values varying from 0.6 μM for KCNQ3 and 5.2 μM for KCNQ4 (see legend to *figure 30*).

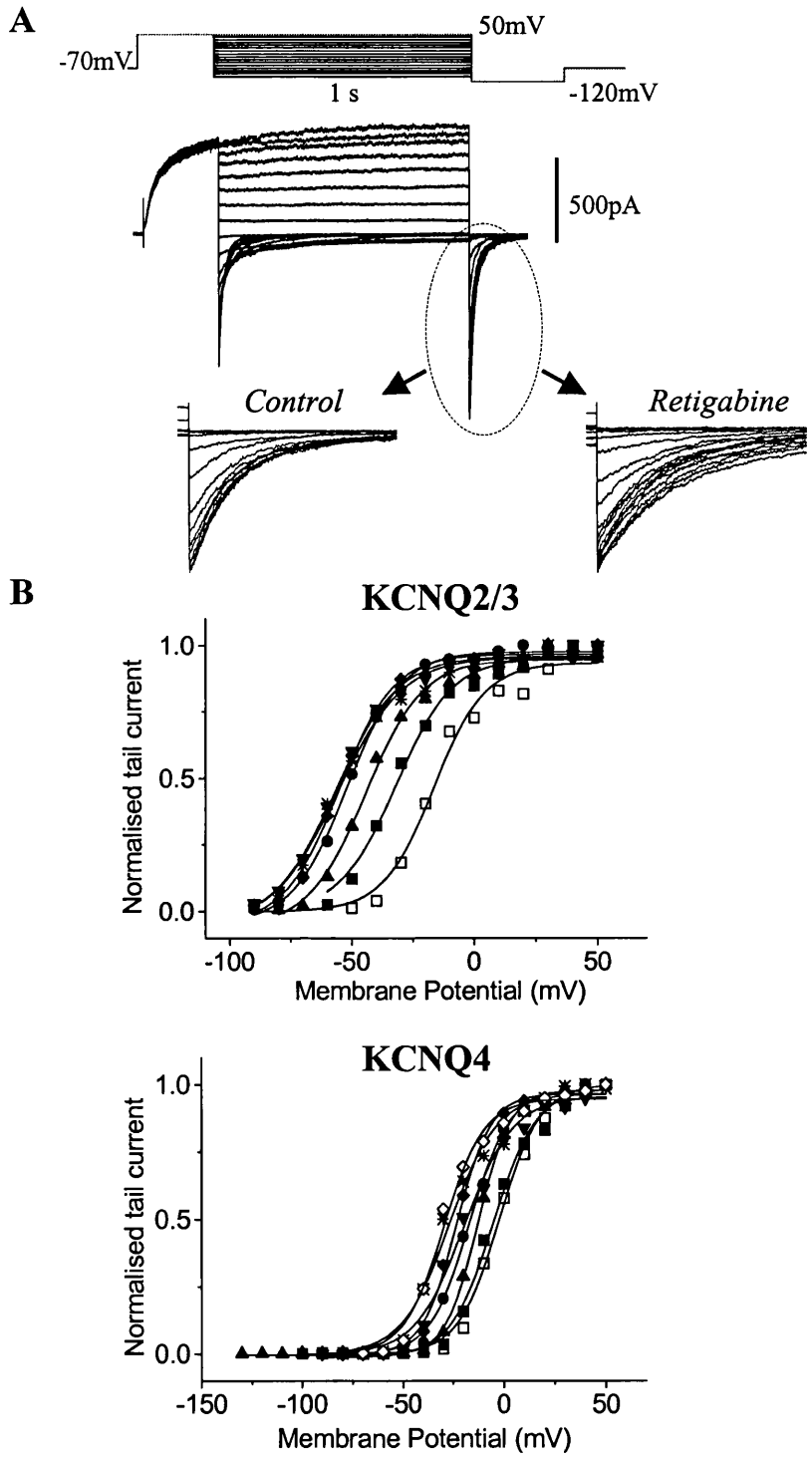

Figure 29: Effects of retigabine on KCNQ currents are concentration dependent.
A. Experiments were performed in high extracellular K^+ (25 mM) solution to enhance the tail currents. A family of currents for KCNQ2/3 and the voltage protocol under these conditions is shown. Application of retigabine led to a slowing in the rate of decline of the KCNQ tail current (inset).
B. Representative activation curves for KCNQ2/3 and KCNQ4 generated in the absence (□) and presence of 1 μM (■), 3 μM (▲), 10 μM (●), 30 μM (▼), 100 μM (◆) and 300 μM (✳) retigabine. For KCNQ4 1000 μM retigabine (◇) was also applied.

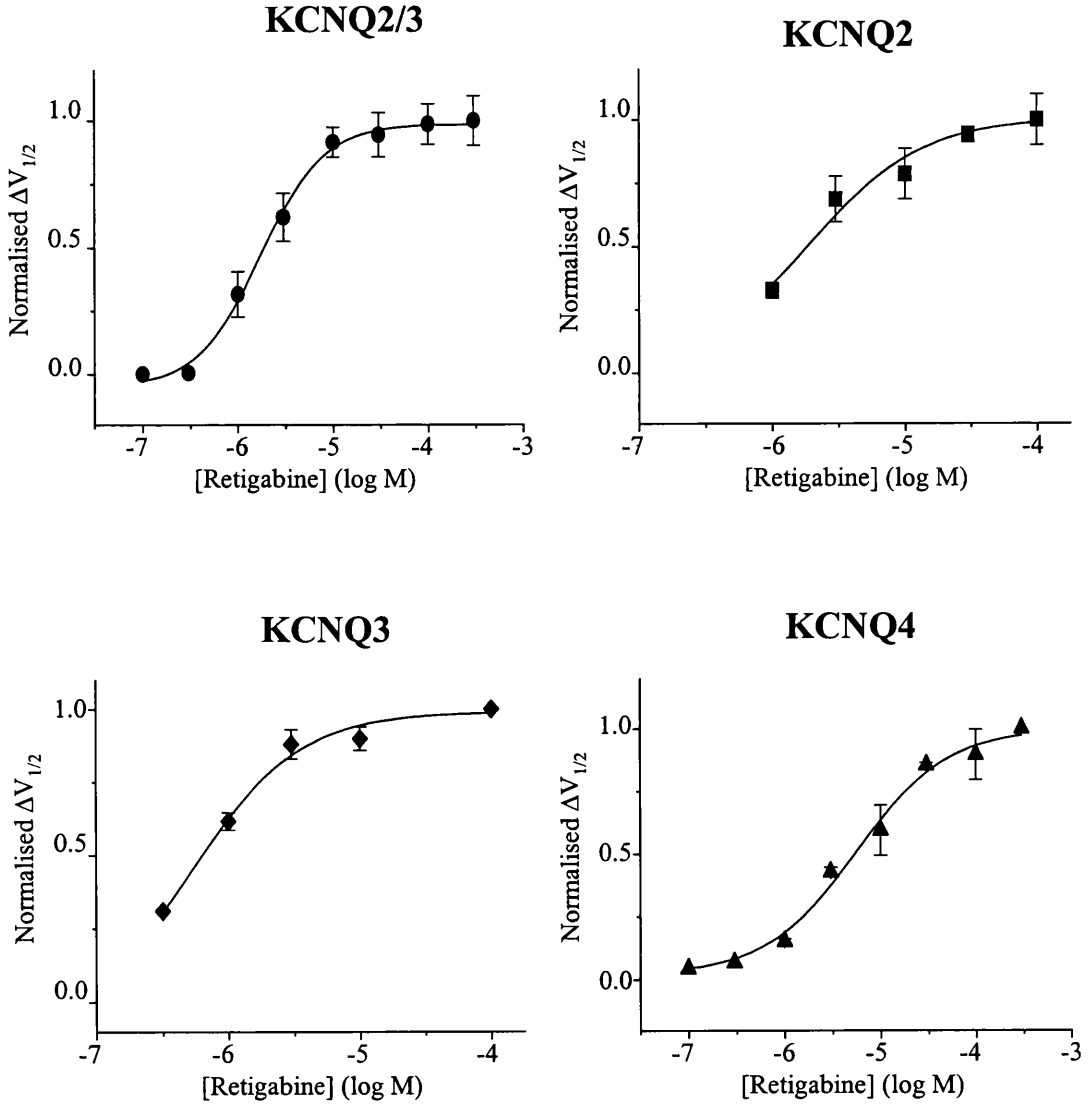

Figure 30: Concentration-response curves for KCNQ2/3, KCNQ2, KCNQ3 and KCNQ4.
The leftward shift in the half activation potential ($V_{1/2}$) at different concentrations of retigabine, determined from experiments like those illustrated in *figure 29*, was normalised to the average maximum shift (ordinates) and plotted against log M retigabine concentration (abscissae). The maximum shift in the activation curve was obtained with 10 μM retigabine for KCNQ2/3 KCNQ2, KCNQ3 and 1mM for KCNQ4. Each point shows mean ± SEM of the measured normalised shift. Data were fitted with *equation 5, Chapter 2*. Mean values for EC_{50} and slope (p) ± SEM (n = number of experiments) were: EC_{50} = 1.9 ± 0.2 μM and slope = 1.3 ± 0.2 for KCNQ2/3 (n=5); EC_{50} = 2.5 ± 0.6 μM and slope = 1.1 ± 0.5 for KCNQ2 (n=5); EC_{50} = 5.2 ± 0.9 μM and slope = 0.9 ± 0.2 for KCNQ4 (n=3); and EC_{50} = 0.6 ± 0.3 μM and 1.2 ± 0.4 for KCNQ3 (n=3).

As well as having different EC_{50} values for retigabine (*figure 30*), the maximum shift of $V_{1/2}$ also varied with different KCNQ channels. The order of potency as determined from EC_{50} values (KCNQ3 > KCNQ2/3 > KCNQ2 > KCNQ4) accords with the apparent 'efficacy', as measured by the maximum shift in $V_{1/2}$, and the values are summarised in *table 4* below.

	Maximum shift in $V_{1/2}$ (mV)	***Retigabine EC_{50} (μM)***	***slope***
KCNQ2/3	-30.4	1.9 ± 0.2	1.3 ± 0.2
KCNQ2	-24.2	2.5 ± 0.6	1.1 ± 0.5
KCNQ3	-42.8	0.6 ± 0.3	1.2 ± 0.4
KCNQ4	-24.6	5.2 ± 0.9	0.9 ± 0.2

Table 4: Potency of retigabine against KCNQ2/3, KCNQ2, KCNQ3 and KCNQ4.

Columns show the maximum leftward shift in $V_{1/2}$ (see figure 28) induced by retigabine and the corresponding EC_{50} and slope values for the shift for KCNQ2-4 (see figure 30), calculated as the mean ± SEM of the shifts produced in the individual experiments. Note that 10 μM retigabine was sufficient to produce maximum shift for KCNQ2/3, KCNQ2 and KCNQ3; for KCNQ4, 1 mM retigabine was required.

4.4.4 Effect of retigabine on KCNQ current deactivation

It is clear from current records in *figure 24* that retigabine slows the deactivation kinetics of KCNQ channels, which is the transition from open to closed state. This was further examined by looking at the deactivation time constants, τ, for KCNQ2/3 channel under control conditions and in the presence of retigabine. In these experiments currents were recorded in response to the usual M-current protocol, where the membrane was held at –20mV in order to activate the current, before progressively deactivating it by a series of 1 sec hyperpolarising steps from –20mV to –110mV in 10mV steps, before and after addition of 10μM retigabine. As an example, current response to a single step hyperpolarisation from –20mV to –50mV is shown in *figure 31A* under control conditions (*top*) and in the presence of the drug (*bottom*). Current deactivations at each potential were fitted with a double exponential function (superimposed image of KCNQ current and double exponential function curve in red is shown as inset in *figure 31B*) and the resulting time constants, τ_{slow} and τ_{fast} deactivation were plotted against membrane potential, *figure 31B*. Under control conditions, channel deactivation gets faster at more negative membrane potentials. In the presence of retigabine, the same trend is observed, however, deactivation is much slower at all potentials. It appears that retigabine slows down both slow and fast deactivation time constants at potentials more negative to -60mV, with little or no change in the time constants at membrane potentials more positive to -60mV.

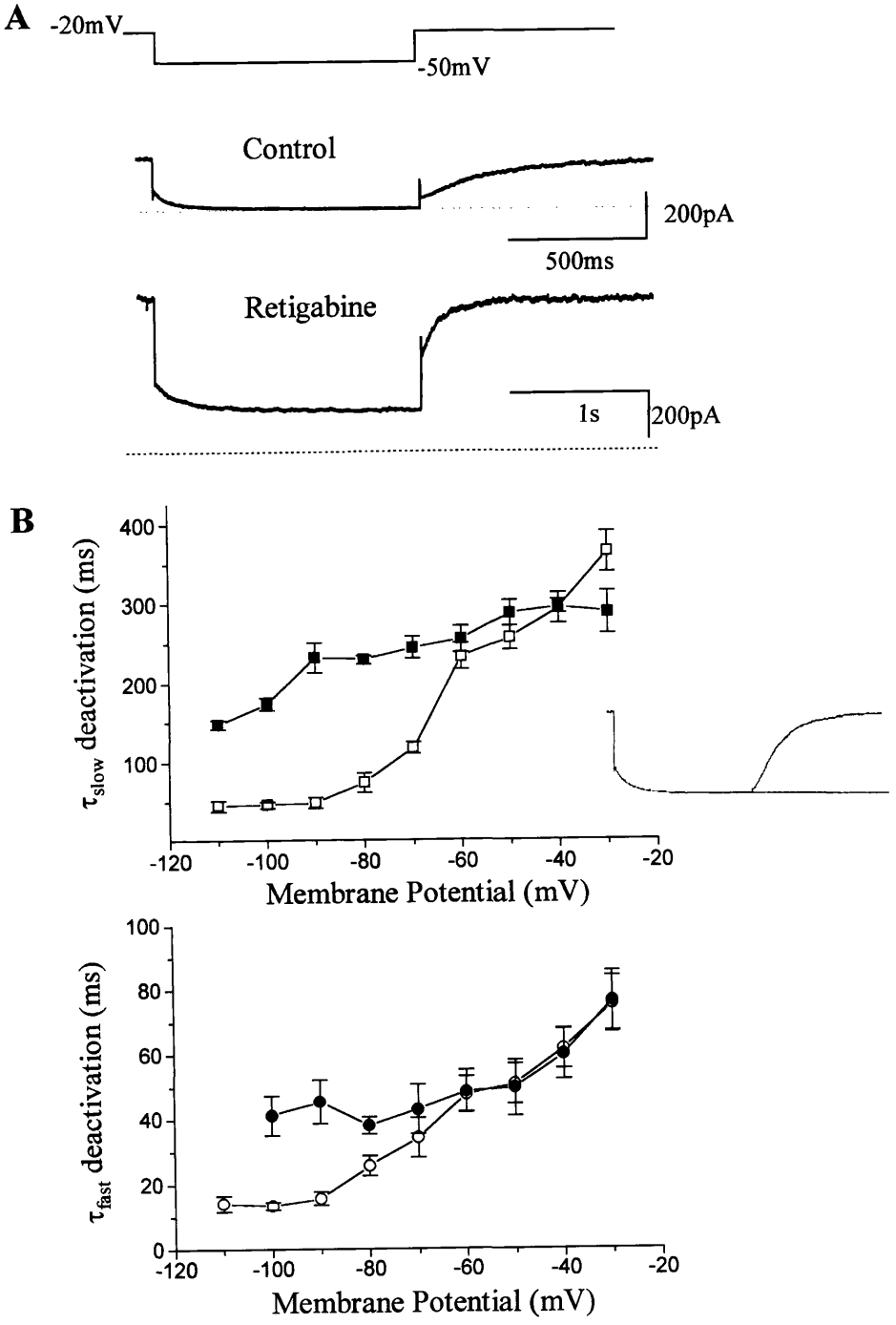

Figure 31: Retigabine slows down the rate of KCNQ current deactivation.

A. Deactivating KCNQ2/3 tail currents were elicited by hyperpolarisations to -110mV in 10 mV increments from a holding potential of -20mV, as described in *figure 24*. Current records in response to hyperpolarisations from -20mV to -50mV only are shown, in the absence *(top)* and presence of 10 μM retigabine *(bottom)*. In control recordings hyperpolarisations were 1s in duration, in the presence of retigabine hyperpolarising steps were 2s in duration in order to allow the current to reach baseline and allow more accurate exponential fits. Dotted lines denote zero current.

B. Deactivating tail currents were fitted with a double exponential function (shown in red in inset) and the slow and fast deactivation time constants, τ_{slow} and τ_{fast}, were plotted against the hyperpolarising step for control (□,○) recordings and in the presence of retigabine (■,●). Data are shown as mean ± SEM (n=7).

4.4.5 Interaction of retigabine and linopirdine on KCNQ2/3 currents

M channels have been reported to be blocked by the M-channel blocker, linopirdine (Aiken *et al.*, 1995; Lamas *et al.*, 1997). The blocking action of the M-channel antagonist linopirdine on KCNQ2/3 currents was quantified in the absence and presence of retigabine. Current was recorded in response to 1sec step hyperpolarisations from –20mV to –50mV under control conditions and upon addition of 0.1, 1, 3, 10, 30 and 100 μM linopirdine, *figure 32A*. The percentage of relaxation current (shown by arrows in inset of *figure 32B*) blocked by each concentration of linopirdine was then plotted against linopirdine concentration. Points were fitted with a Hill equation (*equation 5, Chapter 2*). The same experiment was repeated in the presence of 10 μM retigabine in the bath solution. *Figure 32B* illustrates dose-response curves for linopirdine in the absence and presence of retigabine. The concentration of linopirdine required to produce one half of maximum effect, i.e. the IC_{50} value obtained from Hill plots of the data was unaffected by the presence of retigabine. IC_{50} values were 7.3 ± 1.7 μM (n = 3) in the absence of retigabine and 11.1 ± 2.3 μM (n = 4) in the presence of 10 μM retigabine. These values were not significantly different (P=0.27, *t-test*). The IC_{50} in the absence of retigabine is not dissimilar from that (4.0 ± 0.5 μM) previously reported by Wang *et al.* (1998) against KCNQ2/3 currents expressed in frog oocytes.

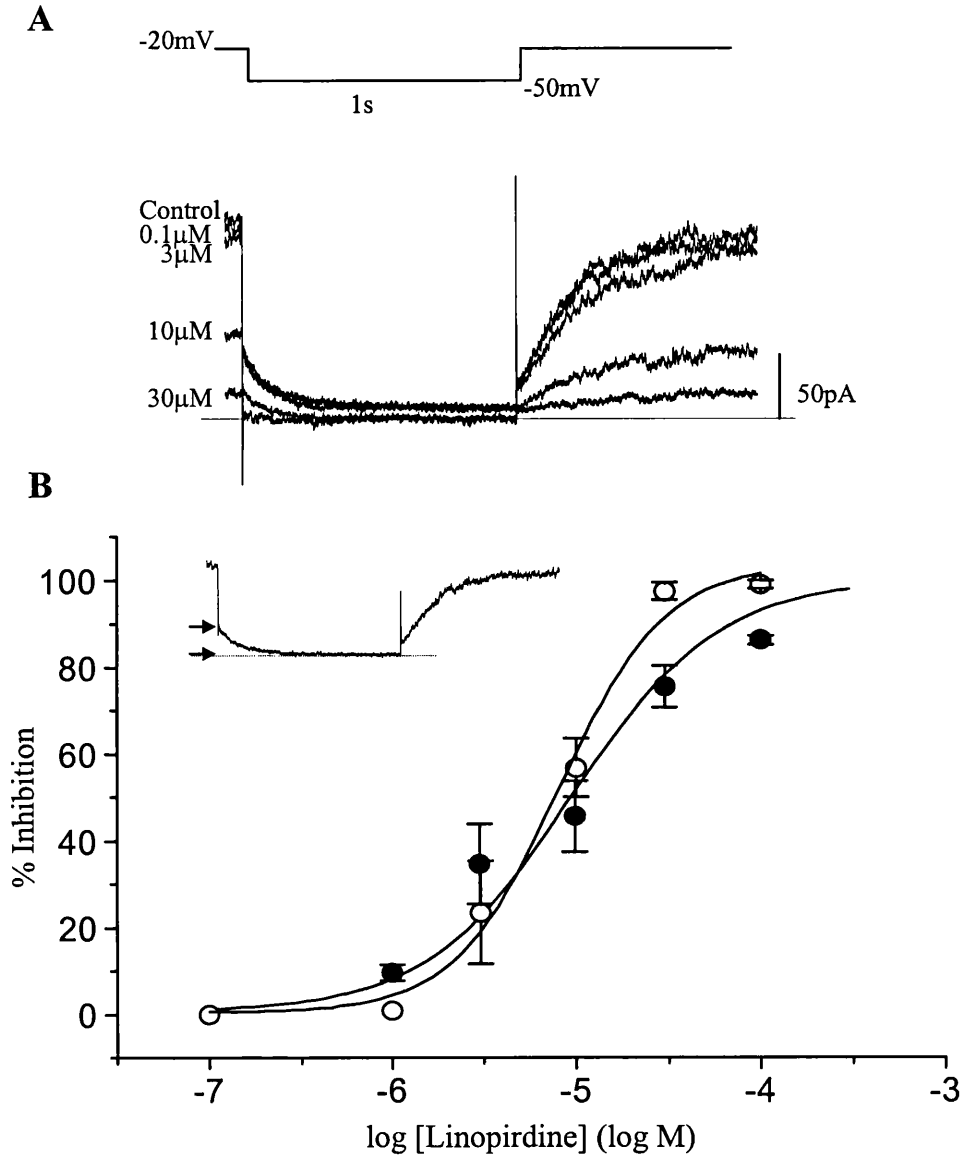

Figure 32: Concentration-response curves for linopirdine on KCNQ2/3 currents in the absence and presence of retigabine.

A. KCNQ2/3 currents were recorded in response to 1sec hyperpolarising steps from a holding potential of -20mV to -50mV. Increasing concentrations of linopirdine were added and the percentage of current inhibited was used to construct dose-response curves. The same experiment was repeated in the presence of 10 μM retigabine in the bath solution. Dotted lines denote zero current.

B. Current inhibition with linopirdine was monitored by measuring the KCNQ relaxation current amplitude *(marked with arrows in inset)* under control conditions and in the presence of 0.1, 1, 3, 10, 30 and 100 μM linopirdine. The percentage of current inhibited was plotted against the corresponding linopirdine concentration and points fitted with *equation 4* (see *Chapter 2*). Under normal conditions, i.e. no retigabine, (○), the IC_{50} for the inhibition was 7.3 ± 1.7 μM (n=3) and in the presence of retigabine (●), IC_{50} = 11.1 ± 2.3 μM (n=4) . These IC_{50} values were not significantly different (p=0.27; *t test*).

4.4.6 KCNQ1 currents are resistant to enhancement by retigabine.

As mentioned in *section 4.1*, a potential problem with development of drugs that target neuronal KCNQ channels is that the cardiac KCNQ1 channel, which together with the KCNE1 accessory subunit underlies the cardiac delayed rectifier current, may also be affected, which can lead to adverse side effects. It was therefore important to test whether or not retigabine affected cardiac KCNQ1 channels.

CHO hm1 cells transfected with KCNQ1 cDNAs were recorded two or three days after transfection. Currents were initially recorded using the standard M-current protocol, shown in *figure 33A*, where the current is activated by holding the membrane potential at –20mV and then progressively deactivated by series of 1s hyperpolarising steps to –90mV in 10mV increments. Current records are shown in *figure 33A*, under control conditions *(left)* and in the presence of 10 μM retigabine *(right)*. In contrast to its effects on neuronal KCNQ2-4 currents, retigabine (10 μM) did not enhance currents generated by homomeric KCNQ1 channels in CHO cells. This was confirmed by plotting KCNQ1 current activation curves under control conditions and in the presence of retigabine in *figure 33B*. (Activation curves were constructed as described previously for *figure 28*). Retigabine did not change the KCNQ1 activation curve. The half activation potential, $V_{1/2}$, for KCNQ1 under control conditions was -12.5 ± 1.1 mV and the slope = 12.4 ± 0.9mV (n=11); in the presence of retigabine (10 μM) the $V_{1/2}$ was -13.2 ± 1.2 mV and the slope was 12.4 ± 0.9mV (n=5). The slope values are clearly indistinguishable and the $V_{1/2}$ values are not significantly different (P=0.7; *t-test*).

When KCNQ1 currents were activated by series of step depolarisations from –70mV to +50mV, application of higher concentrations of retigabine (100 μM) led to a decrease in the KCNQ1 current amplitude. Retigabine reduced the KCNQ1 current amplitude in an apparently voltage-dependent manner, the fractional reduction increasing with increasing positivity. This is demonstrated in *figure 33C*, where normalised current-voltage relationships are plotted for KCNQ1 current under control conditions and in the presence of 100 μM retigabine. Currents were activated by 1 sec depolarising voltage steps from a holding potential of –70mV to +50mV in 10mV increments. Current amplitudes recorded at the end of each depolarising voltage step were normalised against the maximum current recorded at +50mV and plotted against

corresponding membrane potential, as described for *figure 27*. Application of 100 μM retigabine did not affect the current recorded at more negative potentials, i.e. from –110 to –25mV. However, the current amplitude recorded at potentials more positive to about –20mV was reduced on application of 100 μM retigabine (*figure 33C*). This effect was even more pronounced on application of 1 mM retigabine. The voltage-dependent inhibition of KCNQ1 current by retigabine is also illustrated in *figure 33D*, where the fraction of current inhibited at each potential tested was plotted against the corresponding membrane potential. No current was inhibited at potentials between –110mV to -25mV. Only current recorded from about –20mV to +50mV was susceptible to the blocking action of retigabine. This blocking action of retigabine on KCNQ1 current was quantified by applying 3, 10, 30, 100, 300 and 1000 μM retigabine and measuring the reduction of current at +50mV. Fractional inhibition of the current was then plotted against retigabine concentration in *figure 33E*, and points fitted with a Hill equation (*equation 5, Chapter 2*), with a slope of 1.26 ± 0.16 and IC_{50} of 100.1 ± 6.5 μM (n=4). Note that only ~ 65% of the KCNQ1 current was inhibited with 1mM retigabine. Retigabine had similar effects (no activation shift and partial current block at positive potentials) on currents generated by co-expressed KCNQ1 + KCNE1 channels (n=4). It is important to highlight the finding that the IC_{50} value for inhibition of the KCNQ1 current is about 50 – 100 times greater than the EC_{50} values required for the KCNQ2-4 current enhancing action. Thus this blocking action of retigabine on KCNQ1 current is unlikely to provide a major constraint against the therapeutic applications of retigabine.

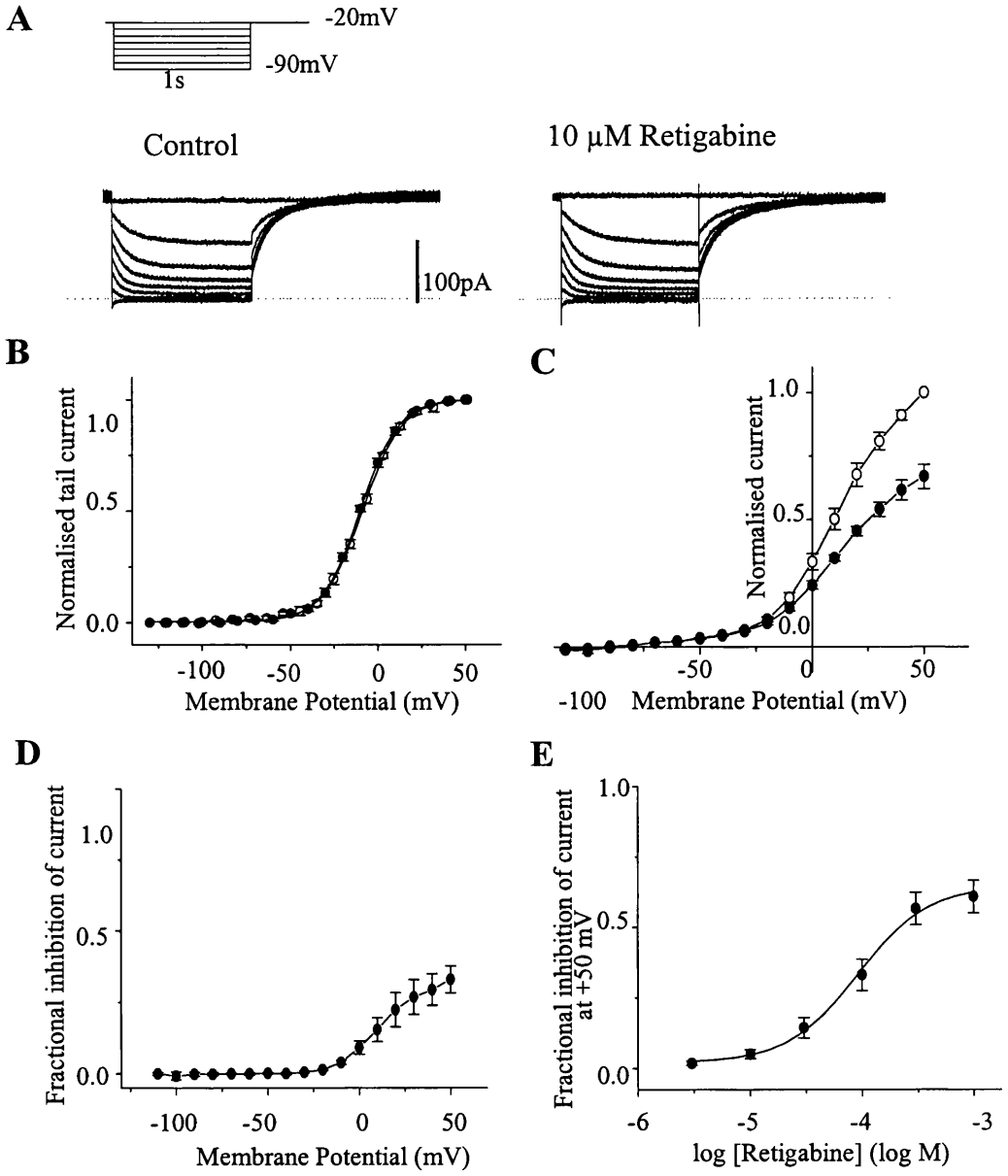

Figure 33: Retigabine does not enhance KCNQ1 current in CHO cells.

A. KCNQ1 currents were recorded using the protocol shown in inset in the absence *(left)* and presence *(right)* of 10 μM retigabine.

B. Activation curves were constructed for KCNQ1 in the absence (○, n=11) and presence (●, n=5) of 10 μM retigabine as described in *figure 28*. Lines are Boltzmann fits to the data, giving $V_{1/2}$ of -12.5 ± 1.1 mV and slope of 12.4 ± 0.9 mV for control and $V_{1/2}$ = -13.2 ± 1.2 mV and slope of 12.4 ± 0.9 mV in the presence of retigabine. These values are not significantly different (p=0.7; *t-test)*.

C. Normalised current-voltage curve for KCNQ1 in the absence (○) and presence (●) of 100 μM retigabine. Voltage protocol as in *figure 25*. Note the reduction of peak current in the presence of retigabine.

D. The current-voltage relation in *(C)* was replotted as fraction of current blocked by 100 μM retigabine at each voltage.

E. The inhibition of KCNQ1 current observed at +50 mV was measured with increasing concentrations of retigabine. The fractional inhibition (ordinate) was plotted against log M retigabine concentration (abscissa). Data were fitted with equation 5 (see *Chapter 2*). Mean value for IC_{50} was 100.1 ± 6.5 μM and for the slope, 1.26 ± 0.16. Data shown as mean ± SEM, with n=4.

4.5 THE S4 SEGMENT IN KCNQ CHANNEL STRUCTURE AS A CANDIDATE FOR RETRIGABINE BINDING SITE

KCNQ proteins have six transmembrane domains and are structurally related to Kv potassium channels. Like other Kv channels, KCNQ channels have a single P-loop that forms the selectivity filter of the pore, a positively charged fourth transmembrane domain (S4) that acts as a voltage sensor, and intracellular amino and carboxy termini, *figure 34A*. KCNQ channel proteins share between 30 and 65% amino acid homology (*table 5*), with particularly high homology throughout the membrane spanning regions and the conserved pore region between transmembrane segments S5 and S6.

KCNQ	*1*	*2*	*3*	*4*
1	100	-	-	-
2	60	100	-	-
3	31	41	100	-
4	38	44	37	100
5	40	50	50	65

Table 5: Percentage of KCNQ amino acid homology – taken from Robbins, 2000.

The S4 transmembrane domain, as in other shaker-like K^+ channels, has been suggested to form the voltage sensor. The role of the voltage sensor is to detect the voltage change and transfer its energy to the pore to control the gate. Since retigabine affects the voltage dependence of channel activation, it is possible that retigabine binds and somehow modifies the action of the S4 segment, making the channels more readily open. Thus the S4 segment is a possible candidate for the binding site for retigabine. There is about 70% homology between the S4 segments of KCNQ1-4. Retigabine clearly does not enhance KCNQ1 channels, and enhances KCNQ2-4. Therefore, retigabine might bind to a residue on the S4 segment that is conserved among KCNQ2, KCNQ3 and KCNQ4 but differs in KCNQ1. The following paragraph shows the

amino acid sequence of the S3 to S4 loops and the S4 segments for KCNQ1-4, where the sites conserved among KCNQ2-4 are in blue and the corresponding residue in KCNQ1 is in red:

S4

KCNQ1: (217) SKG QVFATSAIRGIRFLQILRMLHVDRQ

KCNQ2: (187) SQG NVFATSALRSLRFLQILRMIRMDRR

KCNQ3: (216) NQG NVLATS-LRSLRFLQILRMLRMDRR

KCNQ4: (193) TQG NIFATSALRSMRFLQILRMVRMDRR

Thus, there is one possible binding site on the S3 to S4 linker and six on the S4 segment itself. I investigated four of these differences; namely *Q* (Glutamine) in KCNQ2-4 and the corresponding residue in KCNQ1- *K* (Lysine); *S* (Serine) in KCNQ2-4 and *G* (Glycine) in KCNQ1; *R* (Arginine) in KCNQ2-4 and *H* (Histidine) in KCNQ1; and *R* (Arginine) in KCNQ2-4 and *Q* (Glutamine) in KCNQ1. In the next part (*section 4.5.1*), each of these four residues in KCNQ2 were mutated to substitute them with the corresponding residue found in KCNQ1, in an attempt to make KCNQ2 insensitive or less sensitive to the current enhancing effects of retigabine. In the following part (*section 4.5.2*) the reverse mutations were carried out, i.e. the residues in KCNQ1 were mutated and substituted with the corresponding residue in KCNQ2 in an attempt to make KCNQ1 sensitive to retigabine's current enhancing effect.

4.5.1 Expression of KCNQ2 point mutated channels in CHO hm1 cells

KCNQ2/KCNQ1 point mutants were constructed as described in *Chapter 2*. The positions of the mutations are marked with a red symbol in *figure 34A*. Wildtype (WT) KCNQ2, KCNQ2 (Q188K), KCNQ2 (S199G), KCNQ2 (R210H) and KCNQ2 (R214Q) cDNAs were transfected in CHO hm1 cells as described previously using the Lipofectamine Plus reagent. Currents were recorded 48 hours after transfection using the perforated patch clamp technique.

Wildtype and mutated KCNQ2 currents were activated by series of 1 sec step depolarisations from a holding potential of –70mV up to +50mV in 10 mV increments, as described for wildtype KCNQ2-4 recordings in *figure 25*. The maximum current recorded at the end of the step to +50mV was measured and divided by the cell capacitance (as read from the amplifier) to obtain the current density for each KCNQ2 channel. The results of this are summarised in a bar graph in *figure 34B*. Clearly, in comparison to wiltdype KCNQ2 channels, the mutated KCNQ2 channels failed to generate any appreciable current. Application of retigabine (10 μM) did not change the current density for any of the mutated KCNQ2 channels. Lack of current through mutated KCNQ2 channels suggests that these point mutations in the S3 to S4 loop and the S4 segment somehow interfere with the formation or transportation to the membrane of functional KCNQ channels.

KCNQ2 point mutated channels were tagged with a Myc sequence at the N-terminus. This enabled me to check the expression levels of KCNQ2 point mutated channels by immunolabelling CHO cells with the anti-Myc antibody and thus localising mutated channels. The dominant negative mutant of KCNQ2, KCNQ2 (G298S), was also Myc tagged, and has previously been shown to reach the cell membrane, by its clear membrane bound staining (Tatulian *et al.*, 2000). Therefore, this was a good positive control. CHO cells were transfected with KCNQ2 (G298S) – positive control, and KCNQ2 (Q188K), KCNQ2 (S100G), KCNQ2 (R210H) and KCNQ2 (R214Q) cDNAs. As before, the cells were left for 48 hours for sufficient levels of channels to be expressed. CHO cells were labelled with the anti-myc primary antibody, and then immunolabelled using TRITC conjugated anti-mouse secondary antibody, as described in *section 2.5.2, Chapter 2*. The labelled KCNQ2 proteins were visualised under a confocal microscope. The results are shown in *figure 35*. As expected, KCNQ2 (G298S) showed membrane bound staining, *figure 35A*. The right panel in *figure 35A* shows a photograph of the CHO cell, and superimposed on it is the staining for KCNQ2 (G298S). Clearly, the protein is localised near or at the cell membrane.

Immunolabelling of KCNQ2 (Q188K), KCNQ2 (S299G), KCNQ2 (R210H) and KCNQ2 (R214Q) proteins revealed some membrane bound staining, but most of the staining was cytoplasmic (*figure 35B*). Combined with the observation that no

appreciable current could be recorded from cells transfected with these cDNAs (*figure 34B*), it is possible that mutating these residues somehow interferes with either formation and assembly of functional channels or their transport to the cell membrane. Thus I was unable to get any information about the site of action of retigabine from these experiments.

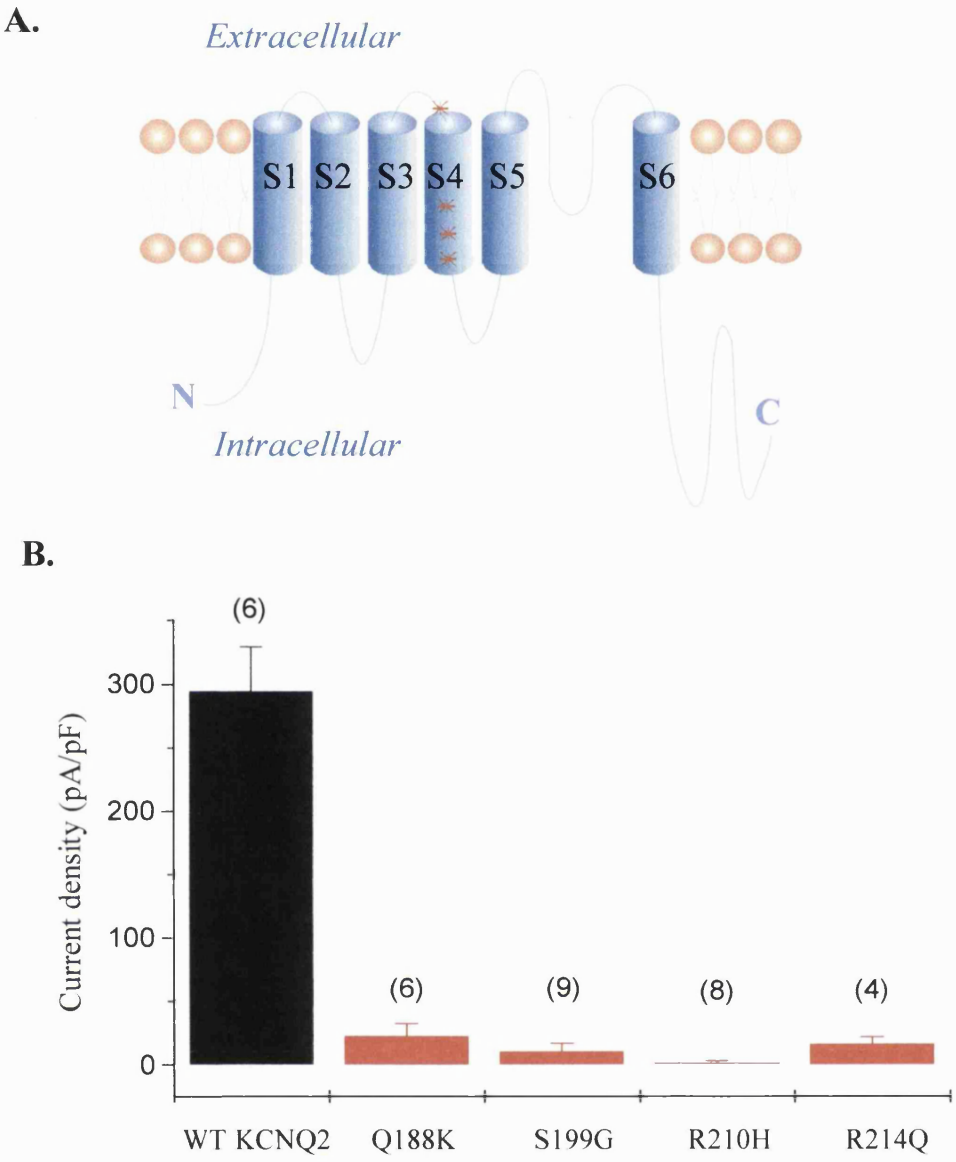

Figure 34: Expression of KCNQ2 point mutated channels in CHO cells.

A. Subunit structure of KCNQ channels, showing the intracellular *N* and *C* termini, and six transmembrane segments, marked *S1 - S6*. The approximate position of KCNQ2 point mutations; KCNQ2 (Q188K) - on *S3-S4 linker*, KCNQ2 (S199G) - on *S4 segment*, KCNQ2 (R210H) - on *S4 segment* and KCNQ2 (R214Q) - on *S4 segment*, are marked in red. Point mutants were constructed as described in *secion 2.4.2, Chapter 2.*

B. Comparison of the wildtype (WT) KCNQ2 current density with the current density of KCNQ2 point mutant channels expressed in CHO cells. Currents were activated by series of step depolarisations to +50mV in 10mV increments from a holding potential of -70mV (as described in *figure 25*). The maximum current amplitude at +50mV was divided by the cell capacitance to obtain current density. KCNQ2 point mutated channels, KCNQ2 (Q188K), KCNQ2 (S199G), KCNQ2 (R210H) and KCNQ2 (R214Q) expressed in CHO cells did not conduct any appreciable current. Data are shown as mean $\pm$ SEM with the number of experiments indicated in brackets above each bar.

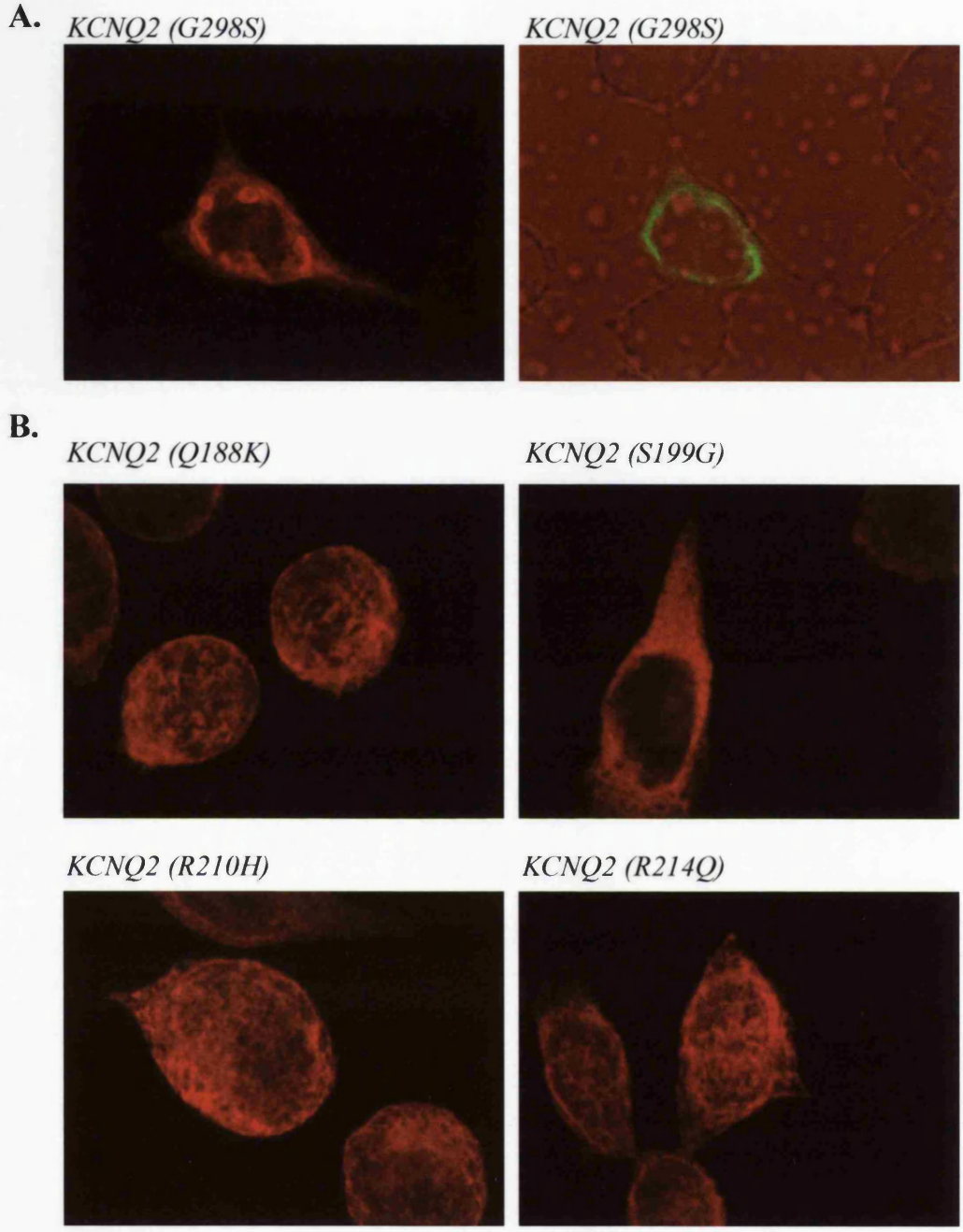

Figure 35: Immunolocalisation of KCNQ2 point mutated channels expressed in CHO cells.
KCNQ2 point mutants were labelled with an *anti-myc* mouse primary antibody following transfection in CHO cells, in order to check expression levels of the proteins. The primary antibody was immunolabelled using TRITC conjugated anti-mouse secondary antibody (see *section 2.5.2, Chapter 2* for details) and visualised using a confocal microscope.
A. Myc-tagged KCNQ2 (G298S) (dominant negative) was used as a positive control. The staining is restricted to the cell membrane only *(left panel)*. The *right panel* shows superimposed image of the membrane bound antibody staining (green) and the CHO cells photographed under transmitted light.
B. Immunolabelling of KCNQ1 (Q188K), KCNQ1 (S199G), KCNQ1 (R210H) and KCNQ1 (R214Q) expressed in CHO cells show some membrane bound staining, but labelling is mainly cytosolic, suggesting unsuccessful translocation of the proteins to the cell membrane.

4.5.2 Expression of KCNQ1 point mutated channels in CHO hm1 cells

In the next step, the reverse mutations were created, i.e. KCNQ1 channels were mutated in an attempt to make them sensitive to the current enhancing effects of retigabine. KCNQ1 (K218Q), KCNQ1 (G229S), KCNQ1 (H240R) and KCNQ1 (Q244R) point mutated channels were constructed as described in *section 2.4.2, Chapter 2.* CHO hm1 cells were then transfected with cDNAs encoding wildtype (WT) KCNQ1, KCNQ1 (K218Q), KCNQ1 (G229S), KCNQ1 (H240R) and KCNQ1 (Q244R) channels. Currents were recorded 48 hours after transfection, using the voltage protocol shown in *figure 36A.* That is, the membrane was held at –70mV and currents were gradually activated by 1 sec step depolarisations from –80mV to +50mV in 10 mV increments. *Figure 36A* shows current responses recorded from WT KCNQ1 transfected cells (*left*), KCNQ1 (H240R) (*middle*) and KCNQ1 (Q244R) (*right*). Again, KCNQ1 point mutated channels, namely KCNQ1 (K218Q), KCNQ1 (G229S) and KCNQ1 (H240R), were unable to generate any appreciable current. As an example, recording for KCNQ1 (H240R) only is shown. KCNQ1 (Q244R) mutated channels were able to generate 'normal' looking KCNQ currents. The results of these experiments are summarised in *figure 36B*, where the maximum current amplitude recorded at +50mV was divided by the cell capacitance (read from the amplifier) and plotted as a bar graph for WT KCNQ1, KCNQ1 (K218Q), KCNQ1 (G229S), KCNQ1 (H240R) and KCNQ1 (Q244R) cells. Although current recorded through KCNQ1 (Q244R) channels was very similar in form to current through WT KCNQ1 channels, KCNQ1 (Q244R) current density was just over half of that recorded for WT KCNQ1. Application of 10 μM retigabine did not change the current amplitude for KCNQ1 (Q244R), not did it induce currents through KCNQ1 (K218Q), KCNQ1 (G229S) and KCNQ1 (H240R). The reasons for lack of current through KCNQ1 (K218Q), KCNQ1 (G229S) and KCNQ1 (H240R) channels could be the same reasons mentioned for the KCNQ2 mutants, that is, either functional channels are not formed, or the channels are not transported to the cell membrane. I can, however conclude that the *R* (Arginine) residue in KCNQ2-4 *by itself* does not account for the sensitivity of the channels to retigabine, as application of retigabine did not enhance the current through KCNQ1 (Q244R) channels. Although it is possible that this residue forms *part* of the binding

site for retigabine, therefore it would be wrong to rule out the involvement of this residue from these sets of experiments.

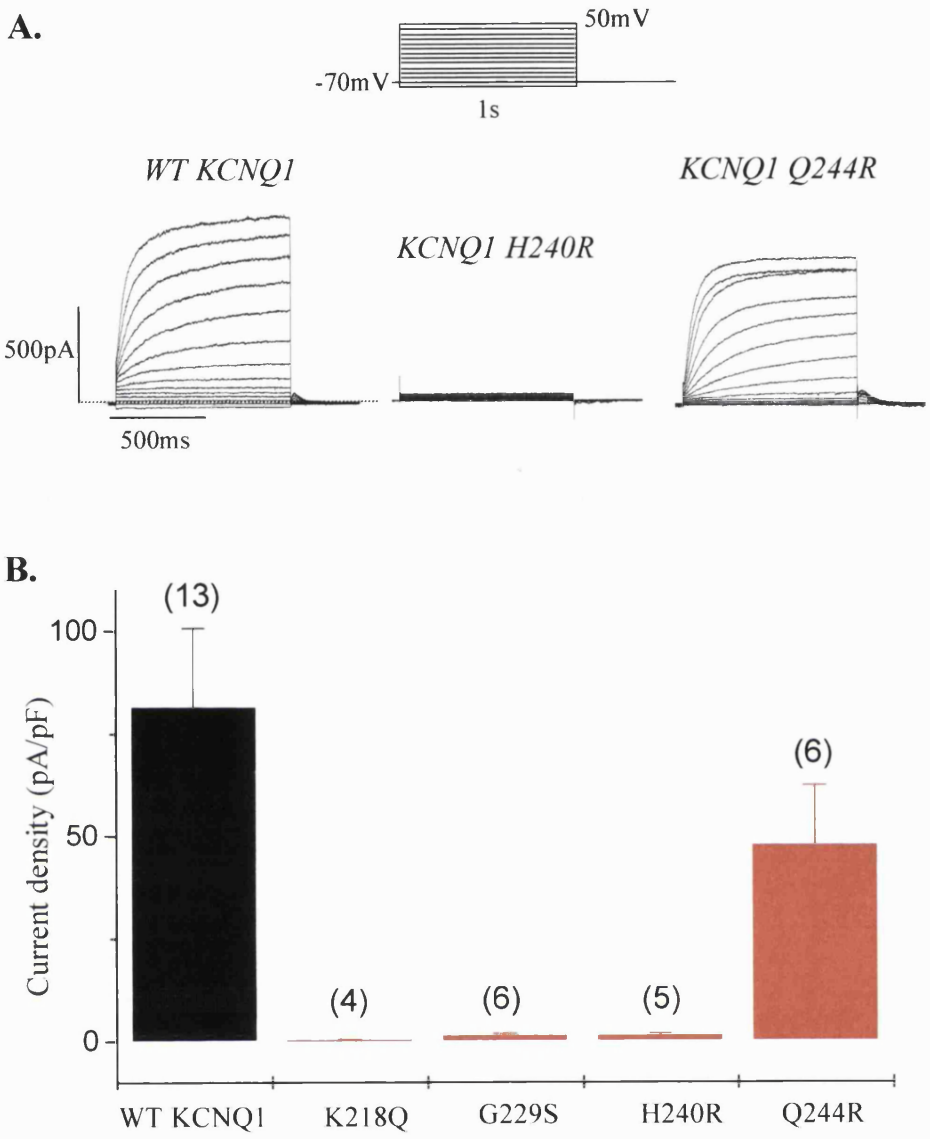

Figure 36: Expression of KCNQ1 point mutated channels in CHO cells.

A. KCNQ1 point mutants, KCNQ1 (K218Q), KCNQ1 (G229S), KCNQ1 (H240R) and KCNQ1 (Q244R) were constructed as described in *secion 2.4.2, Chapter 2* and expressed in CHO cells. Currents were activated by 1sec depolarising steps to +50mV in 10mV increments from a holding potential of -70mV. Wildtype (WT) KCNQ1 currents were also recorded for comparison. KCNQ1 (K218Q), KCNQ1 (G229S) and KCNQ1 (H240R) channels did not produce any appreciable currents (KCNQ1 (H240R) only is illustrated). In contrast, KCNQ1 (Q244R) channels produced currents similar in form to WT KCNQ1 currents, but with only about half of the amplitude of the currents through WT channels. Application of retigabine did not change the current amplitude through any of the mutated KCNQ1 channels.

B. Summary of current density produced by WT KCNQ1 and KCNQ1 point mutated channels. The maximum current amplitude at +50mV, recorded following the protocol in *(A)*, was divided by the cell capacitance to obtain current density. Data are shown as mean $\pm$ SEM with the number of experiments indicated in brackets above each bar.

4.6 *ACTION OF RETIGABINE ON NATIVE M CURRENTS IN RAT SYMPATHETIC NEURONES*

The native M current in rat superior cervical sympathetic (SCG) neurones has been attributed to currents carried through heteromeric KCNQ2/3 channels (Wang *et al.*, 1998). Hence, retigabine might be expected to affect these native M currents in a manner resembling its effect on KCNQ2/3 channels. In the following experiments, the effect of retigabine was studied on the native M currents in dissociated rat SCG neurones.

4.6.1 Retigabine enhances native M currents in sympathetic neurones

M current recordings in SCG neurones were performed using the perforated patch clamp technique, as described for KCNQ current recordings in CHO cells, using solutions described in *Chapter 2*. The native M current in SCG neurones was recorded using the standard 'M current protocol', in which M current was recorded in isolation from inactivating currents by pre-depolarising to –20 mV in order to activate the M current, and then progressively deactivating the current by 1sec step-hyperpolarisations down to –80 mV in 10mV increments (*figure 37A*; *cf.* figure 21). *Figure 37A* illustrates M currents recorded in this way under control conditions (*left*) and in the presence of 10 μM retigabine (*right*). Retigabine clearly enhances the outward holding current at –20mV, as seen for KCNQ currents in CHO cells (in *figure 24*). Retigabine also slows the deactivation kinetics of the current and accelerates the reactivation kinetics. The slowing of the deactivation kinetics was quantified by fitting currents at each hyperpolarising membrane potential with an exponential function, under control conditions and in the presence of 10 μM retigabine. M current deactivation appeared to have two components; fast and slow, and could be fitted accurately with a double exponential function – an example of the double exponential fit to the M current deactivation is shown in *figure 37A*. *Figure 37B* illustrates the effect of retigabine on the slow component (*top graph*) and on the fast component (*bottom graph*). Retigabine does not appear to change the time constant of the slow component (τ_{slow}) of M-current deactivation. However, it does significantly slow down the time constant

for the fast component (τ_{fast}), in a similar way to that seen previously for the KCNQ2/3 current deactivation (in *figure 31B*).

4.6.2 Concentration dependent modulation of the M current by retigabine

To study the dose-response relationship for retigabine on the M current, the M current was recorded in response to 1 sec step-hyperpolarisations from –20mV to –50mV. Incremental addition of increasing concentrations of retigabine; i.e. 0.1, 0.3, 1, 3, 10 and 30 μM retigabine produced a progressive increase in the steady outward current at –20 mV, *figure 38A*. There was also an increase in the residual SCG M-current at –50 mV in the presence of retigabine, implying that the hyperpolarising step no longer fully deactivated the M current (as expected from the negative shift of the activation curve).

The dose-response curve in *figure 38B* was constructed by measuring the amplitude of the relaxation current (as marked by arrows in the inset) at each concentration of retigabine applied, and plotting this value against the corresponding retigabine concentration. Points were fitted with a Hill equation (*equation 5, Chapter 2*), with an EC_{50} of ~ 0.8 μM (*figure 38B*; mean 0.84 ± 0.03 μM; $n = 5$).

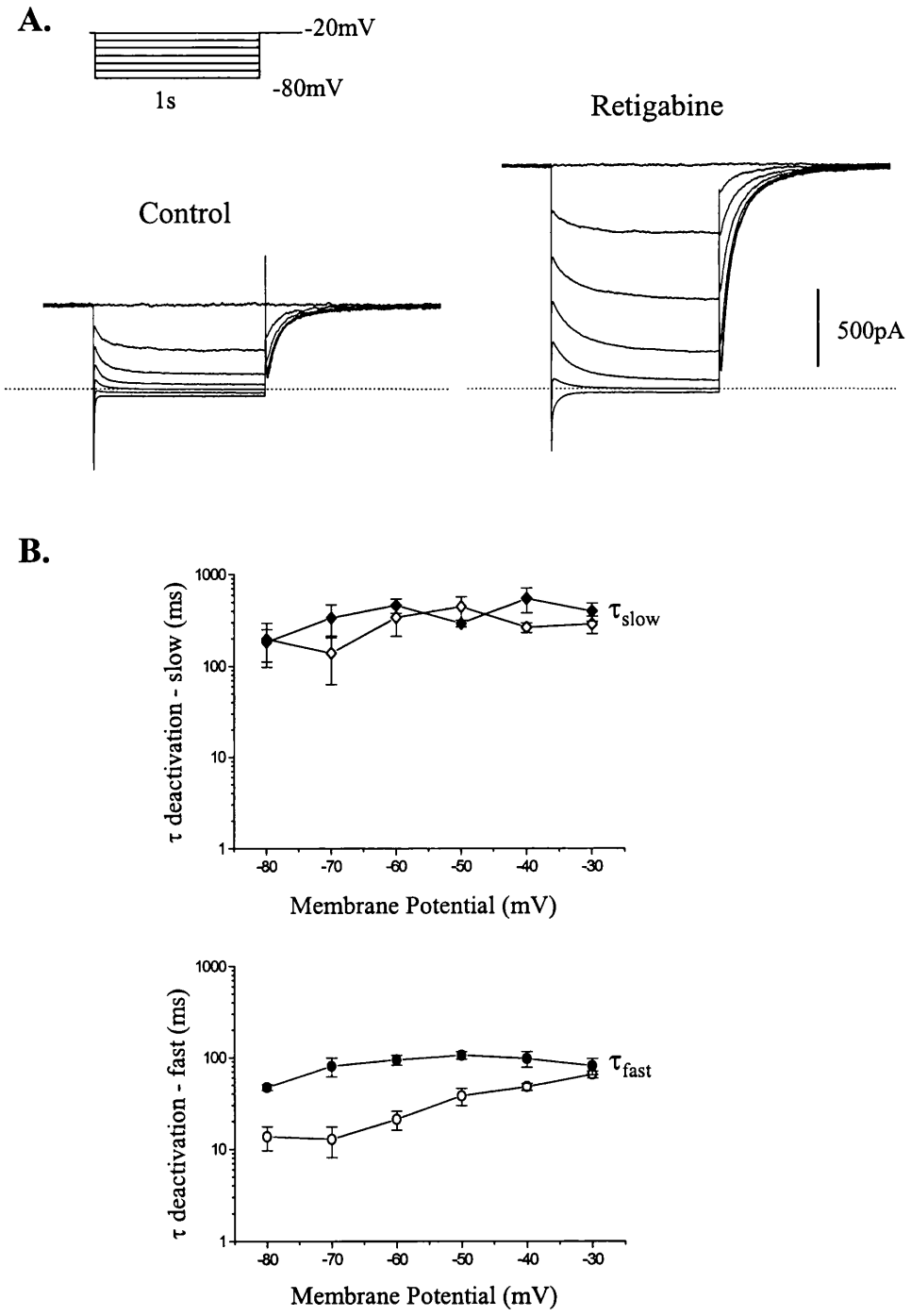

Figure 37: Retigabine enhances M current amplitude and slows channel deactivation in SCG neurones.

A. Currents were produced by holding the membrane potential at -20mV and applying 1 sec hyperpolarising pulses to -80mV in 10 mV increments. Families of M-current deactivations were obtained before (*left panel*) and after addition of 10μM retigabine *(right panel)*.

B. Tail current decay, produced by using the protocol in *(A)*, was fitted with a double exponential function. The relative contribution of the slow component (τ_{slow}) in the absence (◇) and presence of retigabine (◆) was plotted against each voltage. Similarly, the fast component (τ_{fast}) at each voltage was plotted in the absence(○) and presence of 10μM retigabine (●). Symbols represent the mean ± SEM (n=5).

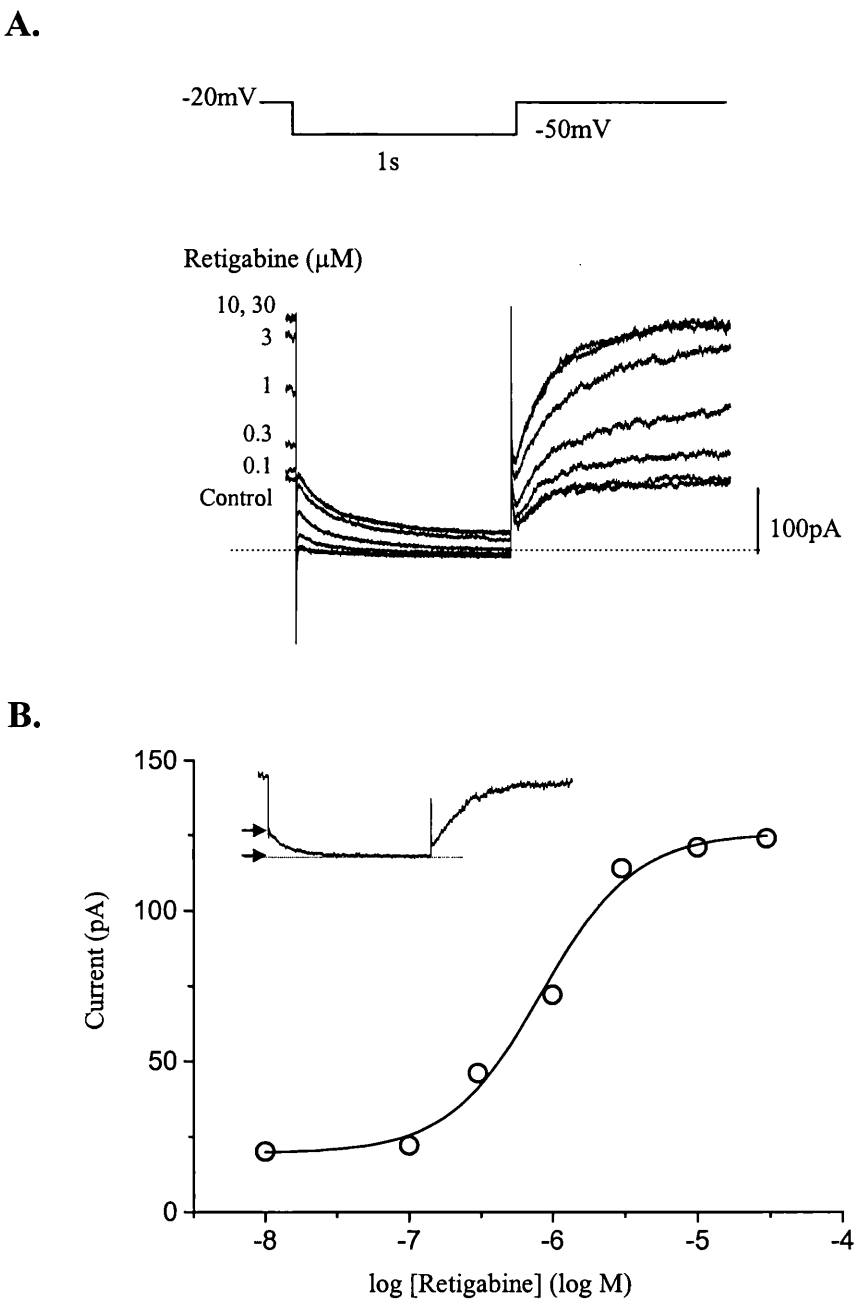

Figure 38: Modulation of the M current by retigabine is concentration dependent.

A. Superimposed M-current traces before and after cumulative addition of retigabine (0.1 - 30 μM). The M current was recorded in response to 1 sec hyperpolarising steps from a holding potential of -20mV to -50mV.

B. The amplitude of M-current deactivation relaxation (*highlighted by arrows in inset*) was plotted against retigabine concentrations for the cell illustrated in *(A)*. Solid lines represent best fits to the Hill equation (*equation 5, Chapter 2*), with an EC_{50} value of 0.84 μM and a Hill coefficient (slope) of 1.33. Mean values are given in the text.

4.6.3 Effect of retigabine on M current activation

The enhancement of the M-current by retigabine was confirmed by studying the activation of the M-current. *Figure 39A* illustrates the effect of 10 μM retigabine on the outward currents evoked in a dissociated rat SCG neurone by 1 s depolarising steps from –80 mV up to –10mV in 10mV increments. In the absence of retigabine, activation of M current is manifest by the appearance of a slow time-dependent component of outward current at command potentials of –40 mV and upwards, subsequent to the transient (~50-100 ms duration) 'A-current' (*figure 39A*). In the presence of retigabine, two differences are seen: the time-dependent component appears at a more negative command potential (-60 mV); and the total outward current is increased at all command potentials. The extra current induced by retigabine is indicated by the subtracted currents in *figure 39B*: this current is clearly 'M-like' in appearance, with slow activation and deactivation, and saturates at –20 mV. Note that, unlike the raw currents, the subtracted current is devoid of an initial transient A-current component, implying that the A-current was not enhanced by retigabine.

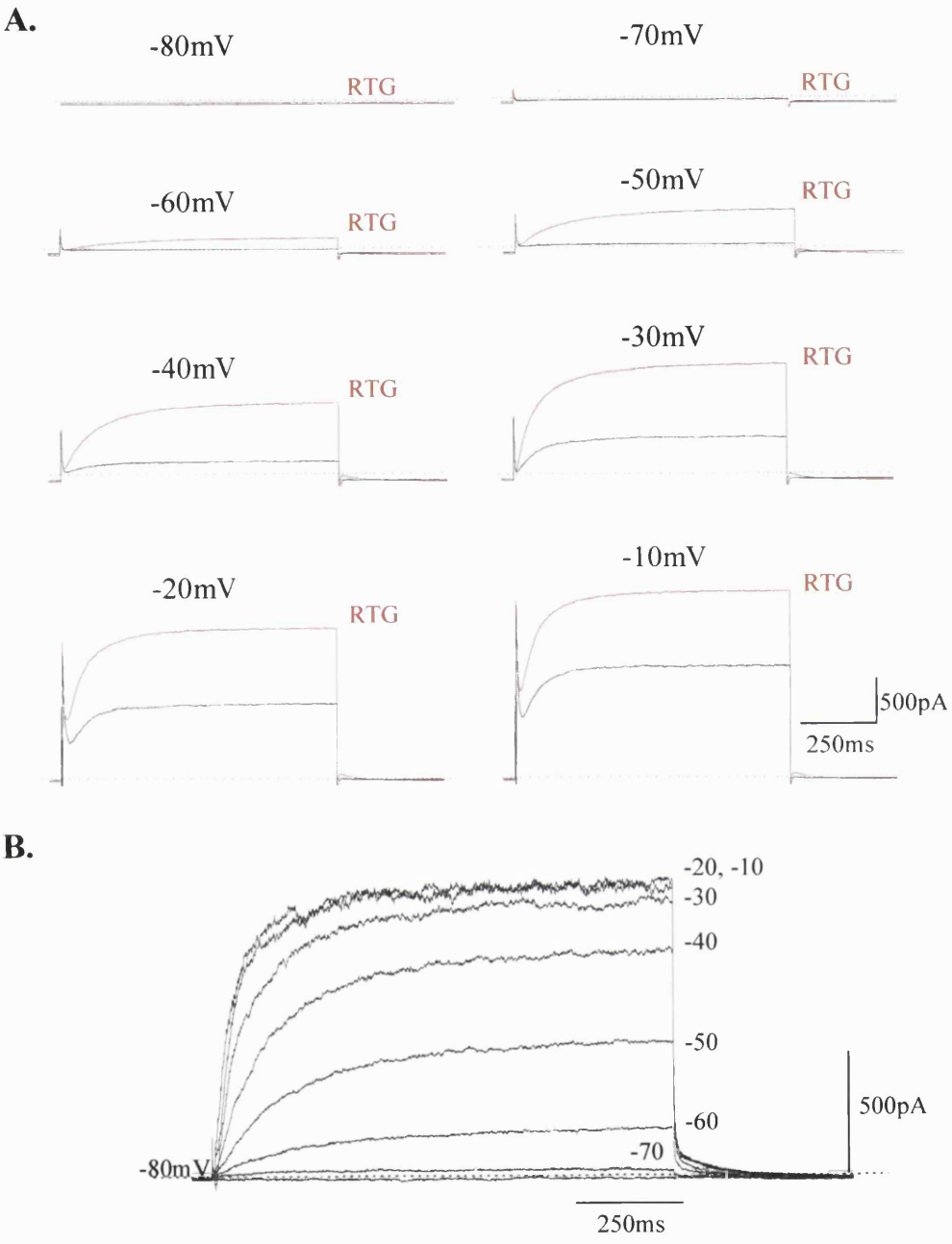

Figure 39: Retigabine enhances outward currents in SCG neurones.

A. Families of currents recorded from a rat SCG neurone elicited by 1 sec depolarising voltage steps from a holding potential of -80mV to test potential from -70 to -10mV (as indicated). Retigabine (RTG) was applied via bath perfusion at 10 μM.

B. Retigabine-induced outward currents obtained by subtracting control currents from currents in the presence of retigabine. Note the saturation of currents at potentials positive to -20mV.

4.6.4 Effect of retigabine on the M current-voltage relationship in SCG neurones

The effect of retigabine on the current-voltage curves for the native M current was further examined by applying slow voltage-ramps (-100mV to 0mV at 5mV/s) in the presence and absence of the M current blocker linopirdine (10 μM). *Figure 40A* illustrates current records in response to this slow ramp, where the horizontal time scale has been converted to membrane potential, calculated from the ramp speed. Current recorded in the presence of linopirdine was then digitally subtracted from current recorded under control conditions and in this way, the component of outward rectification in the current-voltage curves attributable to M current could be identified as that component of current blocked by linopirdine (*figure 40B*). In the presence of retigabine, this component of rectification was shifted ~20 mV in the negative direction (mean, -21 $\pm$ 2 mV; n = 5). As a result, the threshold for the outwardly-rectifying M-current was shifted from between –50 and –60 mV to around –80 mV. However, a small component of linopirdine-sensitive outward current, which appeared insensitive to voltage, could also be detected at potentials negative to –80 mV in the presence of retigabine. This was confirmed in the form of a persistent inward current on raising external [K^+] to 20 mM (*figure 40C*). As with expressed KCNQ2/3 and KCNQ2 channels (see *figure 27*), retigabine did not increase the maximum amplitude of the linopirdine-sensitive component of current. Thus, the effects of retigabine on the linopirdine-sensitive (presumed M) component of current – a negative shift in the current-voltage curve without increased maximum – were in qualitative agreement with its effects on expressed KCNQ2/3 channels. (Although the concentration of linopirdine used in these experiments was unlikely to have completely blocked the M current, the fraction blocked was presumably the same in the absence and presence of retigabine, since retigabine did not affect the action of linopirdine on expressed KNCQ2/3 currents - see *section 4.4.5* and *figure 32*).

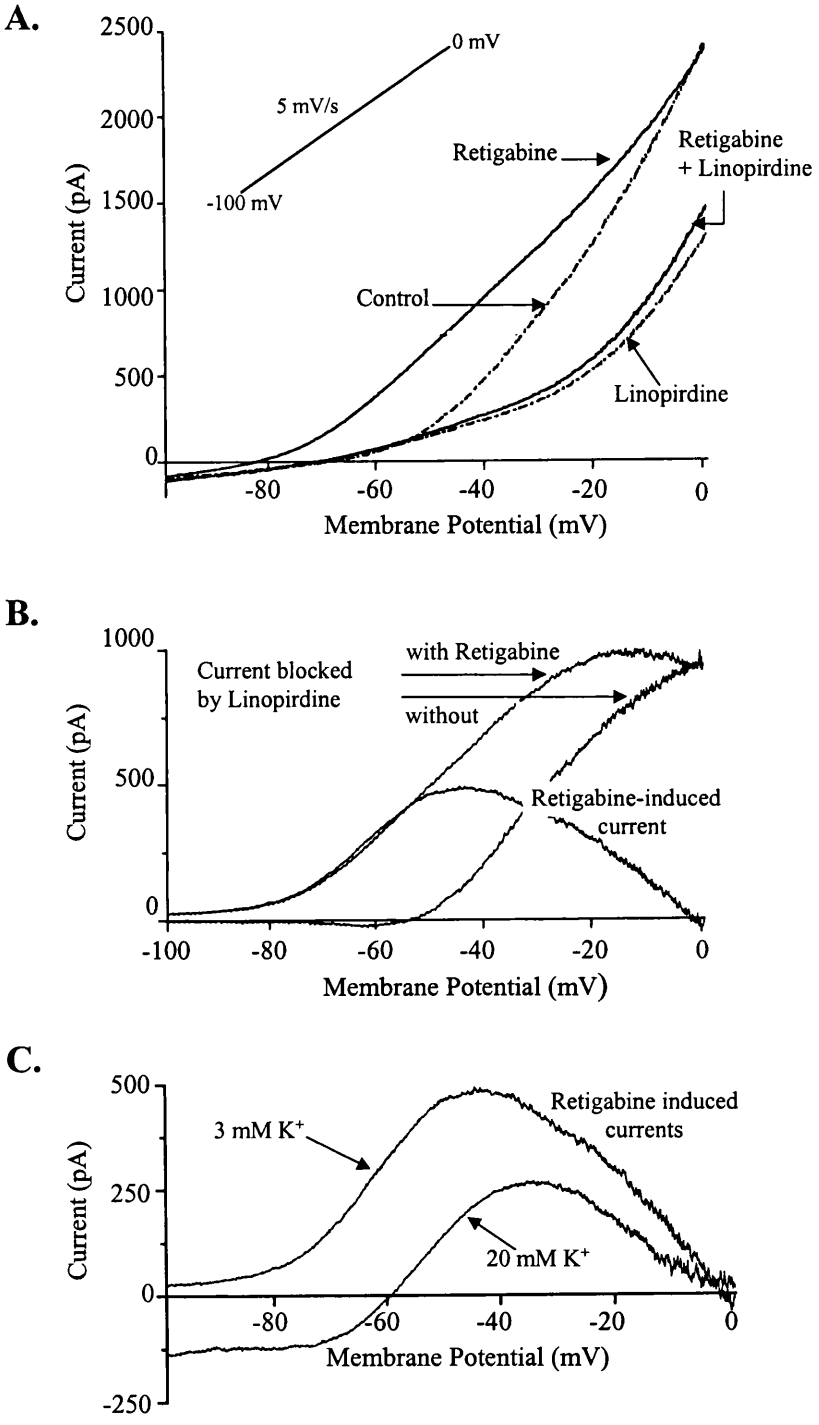

Figure 40: Retigabine shifts the voltage dependence of activation of the M current.

A. Superimposed steady-state *I-V* relationships (determined using a voltage ramp from -100 to 0mV at 5mV/sec) from a single cell in control conditions and after addition of linopirdine (10 μM), and retigabine (10 μM, after washout of linopirdine), and retigabine + linopirdine.

B. Difference currents obtained by digitally subtracting the *I-V* relationships shown in *A*. Note the leftward shift in the activation of the M current (linopirdine-sensitive current) induced by retigabine and the bell shape of the retigabine induced current.

C. Retigabine-induced current in the presence of 3 and 20 mM external K^+. Calculated E_K values were -102 and -56mV, respectively.

4.6.5 Physiological consequences of retigabine action.

Because the M-current acts as a braking current on action potential discharges (Brown, 1988) retigabine might be expected to reduce spike activity. *Figure 41* illustrates a test for this on an SCG neurone. In *figure 41A*, the neurone was challenged with 1s-depolarising or hyperpolarising current injections from a resting membrane potential of ~ -60 mV. The depolarising pulses typically evoked a phasic discharge of 1 or 2 spikes. The application of retigabine (10 μM) hyperpolarised the cells by about -8 ± 2 mV (n = 4). When the membrane potential was brought back to -60 mV, the original depolarising current injections no longer induced spikes (*figure 41B*). This occurs because the increase of M current conductance exerts a more effective and rapid brake on firing, as evidenced by the appearance of hyperpolarising sags upon depolarisation (*figure 41B*). In the presence of retigabine, larger depolarising current injections are required to reach action potential threshold and to generate an action potential spike (*figure 41C*). Thus, in the presence of retigabine and enhanced M-current conductance, neurones are clearly less excitable.

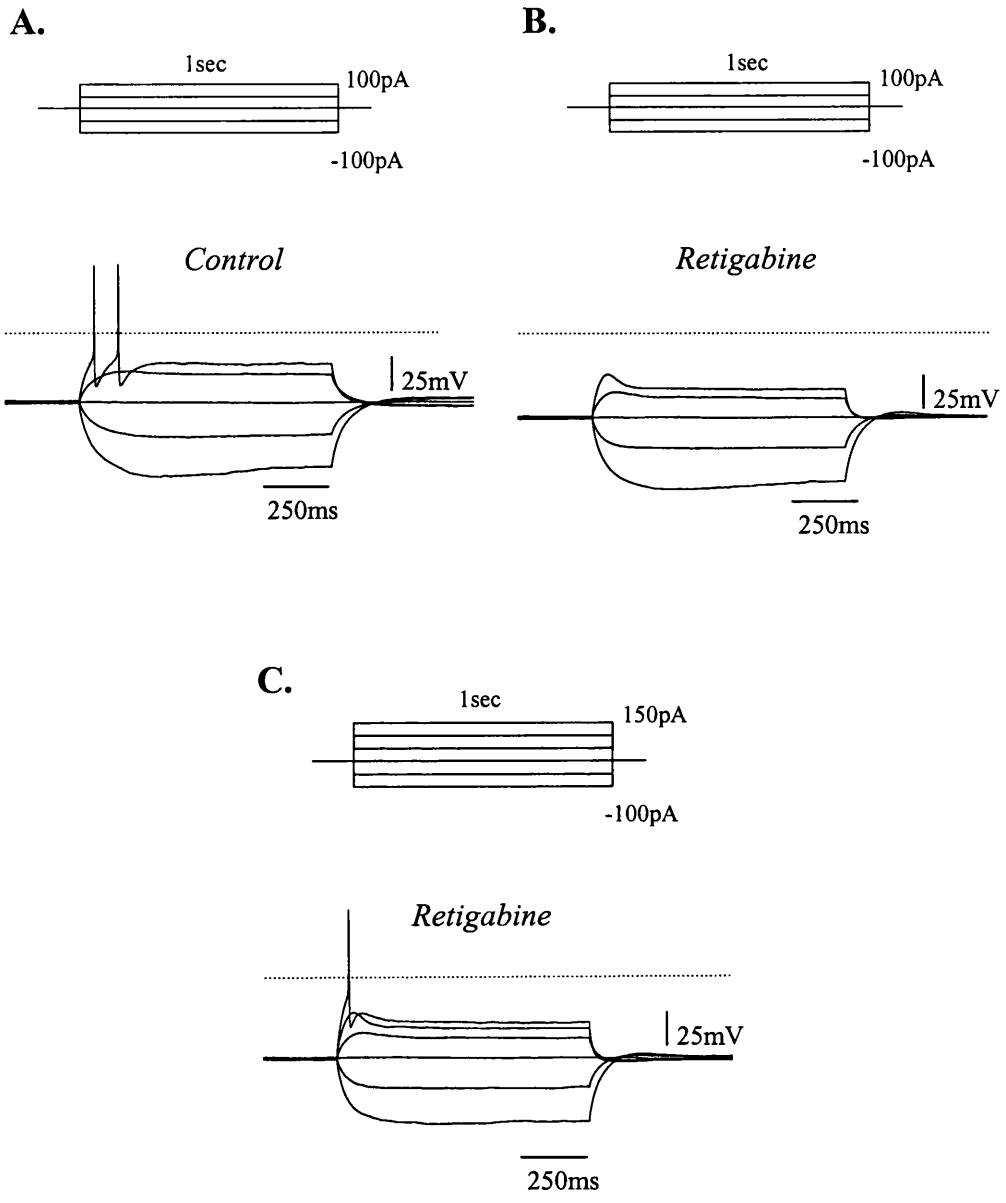

Figure 41: Retigabine abolishes firing in SCG neurones.
Voltage responses to depolarising and hyperpolarising current pulses recorded from an SCG neurone before *(A)* and after application of retigabine (10 μM) *(B, C)*. Note in *(C)* that larger depolarising current pulses are required to evoke an action potential in the presence of retigabine.

4.7 DISCUSSION

The present experiments show that the previously described property of retigabine to enhance K^+ currents through heteromeric KCNQ2/3 channels (Main *et al.*, 2000; Rundfeldt & Netzer, 2000; Wickenden *et al.*, 2000) also extends to currents through homomeric KCNQ2 and KCNQ3 channels, and through the homologous KCNQ4 channels. Available information suggests that the recently cloned KCNQ5 channels (Lerche *et al.*, 2000; Schroeder *et al.*, 2000a) are also sensitive to retigabine (B. Jensen, personal communication). In contrast, the cardiac KCNQ1 channels, expressed homomerically or as heteromeric assemblies with their natural cardiac subunit KCNE1, appear to be insensitive to the current-enhancing action of retigabine. Hence, sensitivity to retigabine is confined to neurally-expressed KCNQ channels – an important requirement for a potential anti-epileptic drug.

In agreement with Wickenden *et al.* (2000), I found that the principal action of retigabine is to produce a shift in the KCNQ activation curve to more hyperpolarised potentials. The maximum shift varied with different KCNQ channels in the order KCNQ3 > KCNQ2/3 > KCNQ2 > KCNQ4; the potency of retigabine, as measured by the concentration required to produce a half-maximal shift, also followed the same order. This shift is accompanied by a slowing of current deactivation and acceleration of current activation. Slowing of the deactivation kinetics by retigabine is one of the consequences of the shift in the activation curves of the KCNQ channels shown in *figure 28*, so in theory, the channels are sensing a more hyperpolarised potential when comparing to control. However, it is an oversimplification to assume that the slowing of current deactivation is purely due to a shift in the voltage dependence of activation. In order to check whether or not retigabine slows current deactivation by simply shifting the voltage-dependence of current activation, I looked at the deactivation time constants for the KCNQ2/3 current under control conditions and in the presence of retigabine (*figure 31*). I then attempted to relate these experimentally derived values with mathematically calculated predictions for the time constants under control conditions and by taking into account a –30mV shift (caused by the shift in KCNQ2/3 activation curve in the presence of retigabine) and comparing these with the time constant measured in the presence of the drug. The reasoning behind this is to see whether the time constants in the presence of retigabine coincide with the predicted

time constant values derived from shifting the control values by –30mV. The only limitation in this is that I have used mathematical equations that describe the M current kinetics in bullfrog sympathetic neurones (Adams *et al.*, 1982). The M current deactivation in these neurones can be fitted with a single exponential function. However, KCNQ2/3 deactivations are fitted best with a double exponential function. I have treated each deactivation component (fast and slow) as two different channels and used the same set of equations to predict what would happen to the fast time constant and separately what would happen to the slow time constant. Therefore the following calculations are very general approximations.

Similarly to the M current in bullfrog sympathetic neurones, KCNQ2/3 current shows sigmoidal activation, with a half-activation voltage of ~ -17mV and a slope of ~ 13mV. In the presence of retigabine the half-activation potential is shifted by ~ -30mV to ~ -47mV, with the slope remaining unchanged (*figure 42A*). If we assume that KCNQ2/3 channel conductance and the voltage dependence of the on and off time constants follows a simplified form of Hodgkin-Huxley kinetics, in which the channel may be either in open or shut states, we can suppose that the probability of a channel being in the open configuration is governed by a Boltzmann distribution so that:

$$y = \left\{1 + \exp\frac{ze}{kT}(V_0 - V)\right\}^{-1}$$

where y = normalised tail current, ze/kT = slope factor (kT/e = RT/F = 25mV at 22°C), V_0 is the half activation potential – see *figure 42A*.

The voltage sensitivity of the time constant, τ may be expressed as:

$$\frac{1}{\tau} = \alpha + \beta$$

where α and β are the opening and closing rate constants, varying with voltage as follows:

$$\alpha = \alpha(0)\exp\frac{+ze}{2kT}(V - V_0),\ \beta = \beta(0)\exp\frac{-ze}{2kT}(V - V_0)$$

where $\alpha(0)$ and $\beta(0)$ are the rate constants at half activation potential, V_0.

The dashed blue lines in *figure 42B (left panel)* show how α and β change with voltage under control conditions for the fast component, assuming $\alpha(0)=\beta(0) = 6.25s^{-1}$, predicted from *figure 31B*. The solid line in *figure 42B (left panel)* is the mathematical calculation of $1/\tau$, with the experimental $1/\tau$ (fast) indicated as blue open circles. The experimental points appear to fit the mathematically calculated line reasonably well, suggesting that although the equations used are not specific for this model, they are a reasonable approximation. The *right panel* in *figure 42B* shows the mathematically calculated τ value as a solid blue line and the experimental τ (fast) under control conditions shown as open blue circles, with the time constant for deactivation getting slower as the membrane approaches half activation potential. If the effect of retigabine was only a shift in the voltage dependence of activation by -30mV, then the curves for $1/\tau$ and τ would simply be shifted to more hyperpolarised potentials by -30mV, as shown by solid red lines in *figure 42B*. In this case, for example at -50mV, the time constant for deactivation is ~ 0.08s, compared to ~ 0.05s prior to the shift, so deactivation is much slower. Following the leftward shift, current reactivation at –20mV is much faster with a time constant of ~ 0.045s, compared to ~ 0.075s prior to the shift. Thus, slowing of deactivation and acceleration of reactivation could indeed be explained by a shift in the hyperpolarising direction of the voltage dependence of the time constant. However, when the experimental τ (fast) values in the presence of retigabine were fitted (shown by filled red circles in *figure 42B (right panel)* and $1/\tau$ (fast) in *figure 42B (left panel)* against membrane potential, the experimental values clearly did not fully correspond to the mathematical values, as predicted by shifting the curves by -30mV. In fact, in the presence of the drug, the time constants remained unchanged at potentials more positive to -60mV. If the effect of the drug was a straightforward shift in the voltage dependence then the experimental τ values in the presence of the drug would be expected to be closer to the predicted values, shown by the solid red line in *figure 42B*.

Using the same equations, the mathematically calculated rate constants for the slow component were plotted against membrane potential in *figure 42C (left panel)* under control conditions (shown as blue dashed lines) and following a -30mV shift

(shown in red dashed lines). In this case, $\alpha(0) = \beta(0) = 1.25s^{-1}$, as predicted from *figure 31B*. The solid blue line in *figure 42C (right panel)* shows how the τ (slow) value would change as a function of membrane potential calculated mathematically, with open blue squares experimental τ (slow) values. Similarly to the fast τ values, the experimental values match quite closely with the mathematical values. Again, the time constant gets slower as membrane potential approaches the half activation potential. The α and β values were re-plotted following a -30mV shift in *figure 42C* (*left panel;* red dashed lines), with $1/\tau$ as a solid red line. Experimental $1/\tau$ (slow) values are plotted as filled red squares. The right panel in *figure 42C* shows the mathematical curve for τ values following a -30mV shift, with the experimental values for τ (slow) shown as red filled squares. Once again, the mathematically predicted τ values, following a -30mV shift do not match experimental τ (slow) values, measured in the presence of retigabine. This suggests that the slowing of deactivation is not solely due to the fact that the channels are sensing a more hyperpolarised potential, since the change in kinetics does not quantitatively match that predicted from the original kinetic scheme for a given shift in steady-state activation. Indeed, the shift in the voltage-dependence of activation does play a part in slowing deactivation and accelerating reactivation, however, there is also a secondary action of the gating which cannot be explained by this shift.

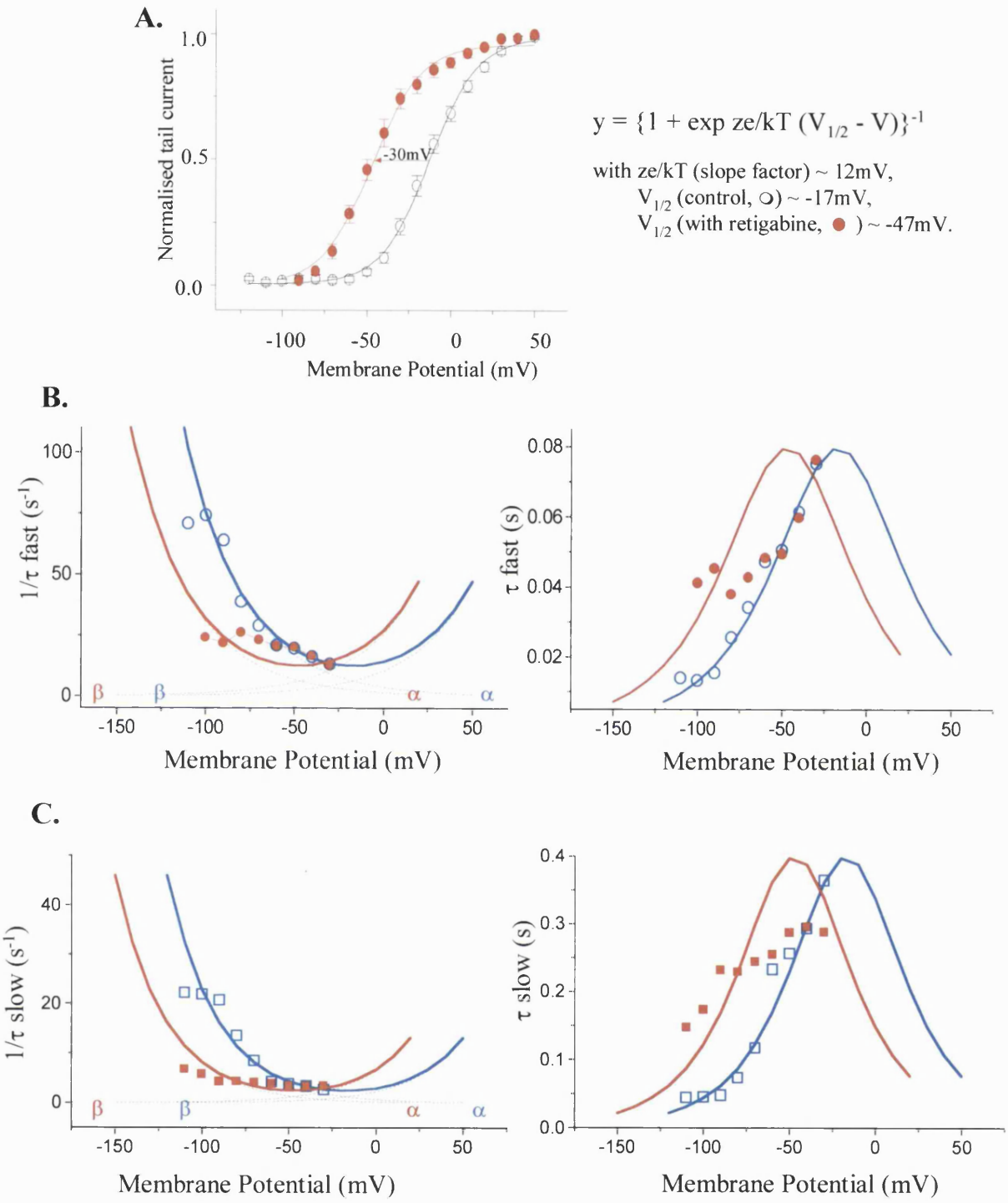

Figure 42: Approximate model of KCNQ2/3 current deactivation kinetics.

A. Retigabine shifts KCNQ2/3 activation curve towards hyperpolarised potentials by ~ 30mV ($V_{1/2}$ under control (○) conditions ~ -17mV and in the presence of 10 μM retigabine (●), ~ -47mV.

B. Mathematically derived rate constants, α and β for the fast component of deactivation were plotted under control conditions (blue dotted lines) and following a -30mV shift (red dotted lines), representing the predicted shift in the fast deactivation time constant, *τ fast*. See text for equations. Experimental values for τ fast are shown as open blue circles (○) for control and filled red circles in the presence of retigabine (●).

C. Similarly the same equations were used to predict the shift in the slow time constant for deactivation, *τ slow*, with open blue squares (□) showing τ slow under control conditions and filled red squares (■) showing τ slow in the presence of 10 μM retigabine.

It is important to note that M channel kinetics are clearly more complex than the equations above describe (see Marrion, 1997; Selyanko & Brown, 1999), and the kinetics of KCNQ channels *per se* have not yet been analysed in sufficient detail to suggest a more precise interpretation of the action of retigabine. For example, kinetic analysis of M-channel activity by Selyanko and Brown (1999), has revealed that the activity can be described by a five-state sequential model, with three closed states – short (C_S), medium (C_M), long (C_L) and two open states – short (O_S) and long (O_L): C_L-O_S-C_M-O_L-C_S. The longest closed state, C_L, was suggested to becoming dominant near threshold potentials for M-channel activation and is probably the state that the channel dwells when it is deactivated at potentials more negative than -60mV. Consistent with this, retigabine seems to affect deactivation at potentials more negative than -60mV. One possible explanation for the increased activity of M/KCNQ channels could be the loss of this C_L state. Loss of C_L has also been suggested to describe increased M-channel activity and ~20mV negative shift in the activation curve for the M-channel as a result of patch excision into a Ca^{2+} free solution (Selyanko and Brown, 1999). The reasons for its loss after the patch excision are not clear.

The most reliable method for understanding the mode of action of retigabine would be to carry out single channel recordings of KCNQ currents under control conditions and in the presence of retigabine. Clearly one of the effects of retigabine is increased KCNQ current amplitude. Since the amplitude of the whole cell current is equal to $N \bullet i \bullet Po$ (where N is the number of expressed channels, i is the mean single channel current and Po is the mean open probability of a single channel), then an increase in the whole cell current can be attributed to three factors. 1) An increase in the number of expressed channels, 2) An increase in the single channel current/conductance or 3) An increase in the open probability of single channels. In order to establish whether the increase in current is related to the number of expressed channels or the difference in their abilities to generate currents, the integral current ($i \bullet Po$) through a single KCNQ channel can be measured under control conditions and in the presence of retigabine. If this integral current is greater in the presence of retigabine than under control conditions, then the possibility of an increased number of channels causing an increase in measured macroscopic current caused by the presence of retigabine can be ruled out. Single channel analysis of KCNQ2/3, KCNQ2 and KCNQ3 currents (Selyanko *et al.*, 2001) have revealed that mean *Po* was highest for

KCNQ3 channels (0.58) and lowest for KCNQ2 channels (0.25), with KCNQ2/3 channels having an intermediate mean *Po* (0.36). In some cases, *Po* for KCNQ3 was very close to 1 (0.91 - i.e. 100%) with *Po* for KCNQ2 being as low as 0.06 and KCNQ2/3 having an intermediate *Po* of 0.1. Therefore, if retigabine increased the macroscopic current amplitude by simply increasing the *Po*, then its effect on KCNQ3 current would be expected to be minimal, since it has a very high *Po* anyway. And the effect would be most prominent for KCNQ2, which has a very low *Po* under control conditions. However, I observed the opposite – retigabine has the greatest current enhancing effect on KCNQ3. Therefore it is unlikely that retigabine only increases the open probability of single channels.

Kinetic analysis of KCNQ currents at the single channel level would provide us with valuable information regarding the amount of time that each channel spends in the open or shut states. By comparing these times with those calculated in the presence of retigabine it should be possible to understand kinetic changes associated with the enhanced current. It can be predicted that the open times for single channels will be greater in the presence of the drug, and the longer period of time that the channels spend in open state will lead to an enhanced macroscopic current.

Physiologically, these effects of retigabine are highly significant, because a hyperpolarising shift in the voltage dependence of KCNQ channel activation and channel deactivation provides a mechanism whereby sustained KCNQ currents will contribute to cellular excitability over a range of membrane potentials.

One of the most important observations of my studies was the fact that retigabine does not enhance currents through cardiac KCNQ1 channels and appears to be selective for neuronal KCNQ channels. This is very important because this means administration of retigabine to treat epilepsy will not have adverse side effects on the heart. However, more detailed experiments on KCNQ1 revealed that in fact higher concentrations of retigabine (~100 μM) actually blocked the channel in a voltage dependent manner, with the degree of block increasing with more positive potentials. This is unlikely to be a potential problem for the therapeutic administration of retigabine since the IC_{50} for the inhibition of KCNQ1 channel is about 50-100 times greater than the EC_{50} values for KCNQ2-4 current enhancement.

The voltage dependent inhibition of KCNQ1 current by retigabine suggests that at strongly positive potentials, the action of retigabine on KCNQ channels appears to

be complicated by a secondary blocking action. This is seen most clearly with KCNQ1 channels, in which there is no voltage-shift and hence no current enhancement, but probably extends to KCNQ2 and KCNQ2/3 channels, so accounting for the limited increase in maximal current through these channels, illustrated in *figure 27.* (The maximum P_{open} through KCNQ2 and KCNQ2/3 channels expressed in CHO cells is well below unity when recorded in the absence of retigabine: Selyanko *et al.*, 2001 and unpublished, and hence does not preclude an increase in maximum current through these channels in the presence of retigabine). This blocking action may not be uniform among different KCNQ channels and appears less pronounced for KCNQ4 channels. The differential effect of retigabine on the KCNQ1 current could imply that retigabine affects KCNQ channels in two ways, perhaps as a result of binding to two different sites. Firstly, it enhances KCNQ currents (as seen with KCNQ2-4) and secondly, higher concentrations block the current (as seen with KCNQ1 channels, where the absence of the current enhancing effect makes the secondary blocking action possible to detect).

Although there is still no direct evidence, it is likely that retigabine binds to a site on the KCNQ channel and induces a direct effect, simply because of its rapid action, rather than involving a secondary messenger system. However the binding site for retigabine is unknown. Linopirdine also binds KCNQ and M channels and is believed to directly block these channels from the outside. Thus, the fact that there is no significant change in the IC_{50} value of linopirdine in the absence and presence of retigabine, suggests that there is no interaction between the site of action of linopirdine and the site of action of retigabine on the KCNQ channel. This is consistent with the observation that KCNQ1 channels are susceptible to blocking effects of linopirdine, but lack the binding site for retigabine responsible for the current enhancing effect.

Judging from the observation that retigabine affects the gating of KCNQ channels and somehow stabilises the channels in an open configuration, one of the candidates as a binding site for retigabine could be the voltage sensor – the S4 segment. By aligning the sequences of S4 segments in KCNQ1 and KCNQ2, four possible residues were identified which were conserved among KCNQ2-4 but differed in KCNQ1. If one of these four residues was responsible for the retigabine binding site, then substitution of this residue found in KCNQ2 for the corresponding residue in KCNQ1 and vice versa would have been a way of making KCNQ2 insensitive or less

sensitive to retigabine, and KCNQ1 sensitive to the current enhancing effect of retigabine. Unfortunately transfection of these point mutated KCNQ2 and KCNQ1 channels in CHO cells did not yield functional channels (with the exception of KCNQ1 (Q244R) channel, which did yield a current although it was unaffected by retigabine). Thus, I was unable to identify a site of action for retigabine from these experiments. However, creating point mutants and/or chimeras between KCNQ1 and KCNQ2 might be an effective way of identifying the site of action.

A second important point established in the present experiments is that retigabine also enhances currents through the native M channels in rat sympathetic neurones. The action of retigabine in SCG neurones is specific for the M type potassium channel. As pointed out in connection with *figure 39*, retigabine (10 μM) had no significant effect on the transient 'A-type' current recorded in rat SCG neurones (n = 12), which is probably mediated by Kv4.2 K^+ channels (Malin & Nerbonne, 2000). Experiments carried out by my colleague, Patrick Delmas have demonstrated that 10 μM retigabine did not affect the hyperpolarisation-activated cation current I_h (n = 4; see Lamas, 1998) or the N-type Ca^{2+} current (n = 6). However, it did exert a small (20 ± 2%; n = 4) inhibitory effect on the Ca^{2+}-activated K^+ current driving the post-spike after-hyperpolarisation (Tatulian *et al.*, 2001).

As with KCNQ channels, enhanced currents through the native M channels in rat SCG neurones are due primarily to a hyperpolarising shift in the voltage-dependence of M current activation. This provides additional support for the view that these native M currents are carried by KCNQ channels (Wang *et al.*, 1998). The calculated shift of -21 mV at 10 μM retigabine was less than that (-34 mV) for the shift of the KCNQ2/3 activation curve. However, the full activation curve of the native M current in SCG neurones could not be determined because of interference by other currents at positive potentials, so the shift was estimated from that component of voltage-dependent current blocked by 10 μM linopirdine. Retigabine also appeared to have a lower potency on native M currents (0.74 μM, measured from the enhancement of outward current at –20 mV; *figure 29*) than that predicted (~ 0.1 μM) from the shift of the KCNQ2/3 activation curves, or previously reported for the enhancement of KCNQ2/3 outward currents (0.34 μM: Wickenden *et al.*, 2000). One possible explanation for these differences (apart from differences in recording methods) might

be that the contribution of heteromeric KCNQ2/3 to the native ganglionic M current may be supplemented by an additional contribution of homomeric KCNQ2 channels, or of KCNQ4 (or 5) channels.

From a functional viewpoint, the shift in voltage-dependence of the M current has the consequence that, in the presence of 10 μM retigabine, a substantial fraction (30-40%) of the M current became activated at the normal resting potential (around -60 mV under perforated-patch recording conditions: see Selyanko *et al.*, 1992). Hence, retigabine induced a substantial outward current, leading to membrane hyperpolarisation. In addition, the enhanced M current further dampened the neurone's ability to generate action potentials during an imposed depolarisation, and abbreviated the discharge train. If replicated in central neurones, this would provide a satisfactory mechanistic explanation for retigabine's reported anti-epileptic action.

CHAPTER 5

GENERAL DISCUSSION AND CONCLUSION

5.1 GENERAL DISCUSSION

Characterisation of the native sodium channel in rat sympathetic neurones (fully inactivating) and comparison with $Na_v1.3$ sodium channel is CHO cells (persistent)

The results presented in this thesis have shown for the first time which sodium channel isoforms are present in rat sympathetic cells, along with their detailed biophysical and kinetic behaviour. Results of RT-PCR and immunolabelling have revealed that $Na_v1.1$, $Na_v1.2$, $Na_v1.3$, and $Na_v1.7$ sodium channel isoforms are found in the rat SCG. Because these isoforms are all TTX sensitive, it is possible that currents through $Na_v1.1$, $Na_v1.2$, $Na_v1.3$, and $Na_v1.7$ channels all contribute to the native TTX sensitive current recorded in these cells. However, it is also possible that not all of these sodium channel mRNAs get translated into a functional protein. Although the specificity of the antibodies used in this study has been tested (Whittaker *et al.*, 2001) it is possible that not all channel proteins are functional and able to conduct current. Therefore, from these experiments it is not clear exactly which subtype of sodium channel gives rise to the current recorded in SCG neurones. The single cell PCR would have provided the answer, as after recording from each neurone the cell could be subjected to single cell PCR and the subtype of channel giving rise to the current could be established.

The sodium current activation curve in SCG neurones was fit with a single Boltzmann function with a mean $V_{1/2}$ of ~ -21mV and a slope of 5.6 mV. The $V_{1/2}$ and slope values for currents through individual Na^+ channels, namely through $Na_v1.1$, $Na_v1.2$, $Na_v1.3$ and $Na_v1.7$ channels are very similar to the values seen in SCG neurones. Currents recorded through $Na_v1.1$ Na^+ channels expressed in CHO cells had a $V_{1/2}$ value of ~ -30mV with a slope of ~ 6mV (earlier experiments carried out by myself). I have shown in *section 3.6, Chapter 3* that $V_{1/2}$ and slope values for currents through $Na_v1.3$ Na^+ channels expressed in CHO cells are ~ -18mV and ~ 6mV, respectively. Xie *et al* (2001) have shown that when $Na_v1.2$ Na^+ channels are expressed in CHO cells, currents activate with a $V_{1/2}$ potential of ~ -24mV and a slope

of ~ 5mV. Finally, currents recorded through $Na_v1.7$ channels in DRG neurones have a $V_{1/2}$ value of ~ -20mV and a slope of ~ 6.5mV (Sangameswaran *et al.*, 1997).

Clearly $Na_v1.1$, $Na_v1.2$, $Na_v1.3$ and $Na_v1.7$ sodium channels have similar slope values, which could explain why the activation curve for the current through native sodium channels (possibly a mixture of $Na_v1.1$, $Na_v1.2$, $Na_v1.3$ and $Na_v1.7$ channels) in SCG cells can be fit with a single Boltzmann equation. Similarly, the $V_{1/2}$ value for the sodium current in SCG neurones is very similar to the individual $V_{1/2}$ values for $Na_v1.1$, $Na_v1.2$, $Na_v1.3$ and $Na_v1.7$ channels, which suggests that the native Na^+ current in SCG neurones could be mediated by a mixture of $Na_v1.1$, $Na_v1.2$, $Na_v1.3$ and $Na_v1.7$ Na^+ channels. However, these are only possibilities and further experiments would need to be carried out before being sure about the exact sodium channel subtypes involved in generating the current in SCG neurones.

Whole cells patch clamp recordings have shown that the native Na^+ current in SCG neurones activates, reaches a peak and fully inactivates within 10ms, and appears to follow the Hodgkin & Huxley model for sodium current activation. The Na^+ current in SCG neurones appears to be modulated by PKC activation, since application of PMA lead to a decrease in current amplitude. However, more physiological activation of PKC via G-protein coupled membrane receptors (oxo-M and norepinephrine) did not affect the Na^+ current.

Although SCG neurones express $Na_v1.3$ Na^+ channels, the current recorded in these cells fully inactivated. This is interesting, since expression of human $Na_v1.3$ brain sodium channel in CHO cells produced a persistent sodium current, which in amplitude, made up 10% of the total current recorded. There are a number of reasons for this. Firstly, it is possible that natively found $Na_v1.3$ channels are in association with an auxiliary subunit, which controls the gating and inactivation kinetics, and which is clearly absent when $Na_v1.3$ α subunit alone is expressed in CHO cells. The second possibility is that in native cells the persistent component of native $Na_v1.3$ Na^+ current is under control by regulators and mediators such as protein kinases and G-proteins. When the $Na_v1.3$ channel is expressed in a cell line, such as CHO, this regulation is disrupted and the persistent component is detected. To investigate this second possibility I looked at the regulation of persistent and transient components of

the $Na_v1.3$ sodium current in CHO cells, following activation and inhibition of protein kinases and activation of G-proteins. This study is also important from a therapeutic point of few, since active sodium channels are associated with increased hyperexcitability of cells, leading to disease states such as epilepsy. In CHO cells, human $Na_v1.3$ channels did not appear to be modulated by PKC activation or inhibition, since application of PDBu - leading to activation of PKC, and staurosporine - leading to inhibition of not only PKC but also other protein kinases, did not modify the transient or persistent currents. Similarly, constant G-protein stimulation by GTPγS did not appear to regulate the persistent or transient components of the current through human $Na_v1.3$ sodium channel expressed in CHO cells.

Although the results of the first part of my study did not provide any answers as to how persistent Na^+ currents are regulated, it is possible that the same channel is able to generate a fully inactivating current and, as a result of some modulation, can change its gating and also exhibit a persistent component. It would be interesting to express the human $Na_v1.3$ Na^+ channel in a SCG neurone and see if the biophysical and pharmacological properties of the channel would change. One way to distinguish between the expressed current from the endogenous one would be to mutate the $Na_v1.3$ Na^+ channel to make it TTX resistant before the transfection. The endogenous current in SCG neurones can be blocked by including 100nM TTX in the extracellular solution and the expressed $Na_v1.3$ channel can thus be isolated and studied in a neurone rather than a cell line.

Activation of KCNQ and M type potassium currents by the novel anticonvulsant retigabine

In the second part of my thesis I have shown that the new anticonvulsant drug retigabine, which has been shown to be effective in a number of epilepsy models, exerts its antiepileptic effects by enhancing currents through expressed neuronal KCNQ channels and through native M type potassium channels. The enhanced M current has the effect of reducing cell excitability and making the cell fire action potentials less readily.

Enhancement of current is accompanied by a shift in voltage dependence of channel activation in the hyperpolarising direction, along with slowing of current deactivation kinetics and acceleration of reactivation kinetics. The shift in the activation curve does explain the changes in kinetics to a certain extent. However, there is another change in the gating mode of the channel, in which the channel seems to be stabilised in an open configuration. Currently, the mode of action of the drug is not known. However, I propose that the drug increases the open probability of the channel as a result of removal of one of the closed states (long closed, C_L) believed to be involved in M channel gating, so that the channel spends longer time in the open states than closed. Removal of a closed state in KCNQ/M channel gating can also explain the acceleration of current activation observed on membrane depolarisation in *figures 25* and *26*. Under control conditions KCNQ currents activate after a short delay. However, in the presence of retigabine this delay is no longer visible. This hypothesis, that retigabine removes C_L state, can be studied further by looking at the activity of single KCNQ2/3 or M-channels in the presence and absence of retigabine. Preliminary results of single channel recordings in CHO cells transfected with KCNQ2, KCNQ3 and KCNQ2/3 channels have indicated that in the presence of retigabine, the channel open probability is increased (unpublished observations by Selyanko).

Voltage dependent ion channels are extremely sensitive to membrane potential, so much so that a depolarisation of only 10mV can cause a 100-fold increase of open probability (Schoppa *et al.*, 1992; Hirschberg *et al.*, 1995). The main component of the voltage sensor in the ion channel is the S4 segment. Therefore, it is possible that retigabine, which clearly changes the voltage sensitivity of the channel, binds to and somehow changes the normal function of the S4 segment. *Arginine* residues are well-known to be involved in the binding of carboxylate groups and analogues of these. For example, they have been shown to participate in the agonist binding of ionotropic glutamate receptors, as well as the γ-aminobutyric acid receptor type A, $GABA_A$ and metabotropic glutamate receptors, $mGlu_1$ (Laube *et al.*, 1997; Armstrong *et al.*, 1998; Lampinen *et al.*, 1998; Jensen *et al.*, 2000). Point mutations in KCNQ2 channels, including R210H and R214Q residues resulted in channels, which on expression in CHO cells, did not yield much current above background level. Therefore, the idea that if a particular residue in the S4 segment was responsible for binding retigabine,

then mutating it would result in retigabine-insensitive (or less sensitive) KCNQ2 channels, could not be tested in the experiments carried out for this thesis. The corresponding point mutations in the KCNQ1 channel were also unsuccessful. Therefore, the question of where on the KCNQ channel structure retigabine interacts with, still remains unanswered. The S4 segment is not the only candidate. In response to a membrane depolarisation, voltage-gated K^+ channels, such as KCNQ channels, open an activation gate at the cytoplasmic entrance of the pore. It has been suggested that part of the S6 transmembrane segment lines the cavity between the gate and the ion selectivity filter. The recently solved structure of a bacterial K^+ channel shows that the S6 homologues cross in a bundle, leaving an aperture at the bundle crossing, and that gating occurs at the bundle crossing, possibly through a conformational change in the bundle itself. Furthermore, substituting *cysteine* at a particular position in the last transmembrane region (S6) of the homomeric *Shaker* K^+ channel, creates metal binding sites at which Cd^{2+} ions can bind with high affinity. The bound Cd^{2+} ions form a bridge between the introduced *cysteine* in one channel subunit and a native *histidine* in another subunit, and the bridge traps the gate in the open state (Holmgren *et al.*, 1998). Perhaps retigabine binds a site on the S6 segment, thus forming an intersubunit bridge that stabilises the open configuration of the channel. This bridge may trap the channel in the open state either by disrupting the interaction between the S6 and a neighbouring voltage sensor or gate, or by "freezing" the S6 bundle in the open conformation. Therefore, future experiments could involve creating point mutations between KCNQ2 and KCNQ1 channels in the S6 segments (much like the work on S4 segments) in order to check if the S6 segment is involved in retigabine binding. Perhaps it would be quicker to create chimeras between KCNQ2 and KCNQ1. By cutting both plasmids at the beginning of the S4 segment and putting together chimeras with residues upstream of S4 belonging to KCNQ2 and residues downstream of S4 belonging to KCNQ1, and vice versa, it would be possible to identify which part of the channel is involved in retigabine binding.

The findings that retigabine activated KCNQ2-4 and M currents at low concentrations but blocked KCNQ1 currents at high concentrations may suggest that there may be multiple binding sites for retigabine on the KCNQ channel, with the KCNQ1 lacking the site responsible for the current enhancing effect. Multiple binding sites have been proposed to explain the dual action of a benzodiazepine, R-L3 on

KCNQ1 channel (Salata *et al.*, 1998) and dihydropyridines such as Bay K 8644 on the L-type Ca^{2+} channel (Brown *et al.*, 1986; Kokubun *et al.*, 1986). The higher concentrations needed to see the blocking action described for R-L3 on KCNQ1 channel was 3-10 times greater than the concentrations required to see current enhancement. On the other hand, the concentration required to see the blocking action of retigabine on KCNQ1 was 20-100 times greater than the concentrations required for the enhancing effect of retigabine on KCNQ2-4 currents, and at such high drug concentrations non specific effects on channels cannot be ruled out.

5.2 CONCLUSION

In this thesis, the involvement of Na^+ and M type K^+ channels in the control of epilepsy were studied. Drugs that will selectively block persistent Na^+ channels and those that will activate M channels will result in membrane hyperpolarisation and thus control epileptic seizures. Although I was unable to identify the mode of control of persistent Na^+ channels, I have carried out a detailed study of the action of a new drug, retigabine, undergoing phase II clinical trials for epilepsy, on expressed KCNQ1-4 channels and native M currents. The current enhancing effect of retigabine on KCNQ and M current appear to be due to three factors; (1) a shift in the activation curve to more hyperpolarised potentials, (2) slowing of current deactivation kinetics and (3) acceleration of current reactivation kinetics. An important requirement for an effective anticonvulsant is specificity, and retigabine's specificity is highlighted by the fact that cardiac KCNQ1 currents are resistant to the current enhancing effect of retigabine. The native M current, which is thought to be generated by KCNQ2/3 channel subunits, and also possibly KCNQ4 and KCNQ5 (not studied for the purpose of this thesis), undergo similar changes in the presence of retigabine. This not only provides further evidence that M current is generated by neuronal KCNQ subunits, but also identifies a novel mode of action for anticonvulsant drug therapy.

The mode of action of retigabine is still not known. It could be a direct effect on the channel, where the drug binds and somehow stabilises the channel in an open configuration. The questions regarding the site of binding and the mode of action of the drug remain unanswered. Future experiments are already underway and include further mutational studies in order to identify the site of action of retigabine and single channel studies in order to identify the mode of action of retigabine.

CHAPTER 6

REFERENCE LIST

Adams, P. R. & Brown, D. A. (1982). Synaptic inhibition of the M-current: slow excitatory post-synaptic potential mechanism in bullfrog sympathetic neurones. *J.Physiol* **332**. 263-72.

Adams, P. R., Brown, D. A., & Constanti, A. (1982). M-currents and other potassium currents in bullfrog sympathetic neurone. *J.Physiol* **330**. 537-572.

Agnew, W. S., Levinson, S. R., Brabson, J. S., & Raftery, M. A. (1978). Purification of the tetrodotoxin-binding component associated with the voltage-sensitive sodium channel from Electrophorus electricus electroplax membranes. *Proc.Natl.Acad.Sci.U.S.A* **75**, 2606-2610.

Aiken, S. P., Lampe, B. J., Murphy, P. A., & Brown, B. S. (1995). Reduction of spike frequency adaptation and blockade of M-current in rat CA1 pyramidal neurones by linopirdine (DuP 996), a neurotransmitter release enhancer. *Br.J.Pharmacol.* **115**, 1163-1168.

Akopian, A. N., Sivilotti, L., & Wood, J. N. (1996). A tetrodotoxin-resistant voltage-gated sodium channel expressed by sensory neurons. *Nature* **379**, 257-262.

Akopian, A. N., Souslova, V., Sivilotti, L., & Wood, J. N. (1997). Structure and distribution of a broadly expressed atypical sodium channel. *FEBS Lett.* **400**, 183-187.

Alonso, A. & Llinas, R. R. (1989). Subthreshold Na^+-dependent theta-like rhythmicity in stellate cells of entorhinal cortex layer II. *Nature* **342**, 175-177.

Alroy, G., Su, H., & Yaari, Y. (1999). Protein kinase C mediates muscarinic block of intrinsic bursting in rat hippocampal neurons. *J.Physiol* **518**, -9.

Alzheimer, C., Schwindt, P. C., & Crill, W. E. (1993). Modal gating of Na^+ channels as a mechanism of persistent Na^+ current in pyramidal neurons from rat and cat sensorimotor cortex. *J.Neurosci.* **13**, 660-673.

Amitai, Y. (1994). Membrane potential oscillations underlying firing patterns in neocortical neurons. *Neuroscience* **63**, 151-161.

Arena, J. P. & Kass, R. S. (1988). Block of heart potassium channels by clofilium and its tertiary analogs: relationship between drug structure and type of channel blocked. *Mol.Pharmacol.* **34**, 60-66.

Armand, V., Rundfeldt, C., & Heinemann, U. (2000). Effects of retigabine (D-23129) on different patterns of epileptiform activity induced by low magnesium in rat entorhinal cortex hippocampal slices. *Epilepsia* **41**, 28-33.

Armstrong, C. M. & Bezanilla, F. (1977). Inactivation of the sodium channel. II. Gating current experiments. *J.Gen.Physiol* **70**, 567-590.

Armstrong, C. M. (1981). Sodium channels and gating currents. *Physiol Rev.* **61**, 644-683.

Armstrong, N., Sun, Y., Chen, G. Q., & Gouaux, E. (1998). Structure of a glutamate-receptor ligand-binding core in complex with kainate. *Nature* **395**, 913-917.

Aronson, J. K. (1992). Potassium channels in nervous tissue. *Biochem.Pharmacol.* **43**, 11-14.

Astman, N., Gutnick, M. J., & Fleidervish, I. A. (1998). Activation of protein kinase C increases neuronal excitability by regulating persistent Na^+ current in mouse neocortical slices. *J.Neurophysiol.* **80**, 1547-1551.

Attwell, D., Cohen, I., Eisner, D., Ohba, M., & Ojeda, C. (1979). The steady state TTX-sensitive ("window") sodium current in cardiac Purkinje fibres. *Pflugers Arch.* **379**, 137-142.

Auld, V. J., Goldin, A. L., Krafte, D. S., Marshall, J., Dunn, J. M., Catterall, W. A., Lester, H. A., Davidson, N., & Dunn, R. J. (1988). A rat brain Na^+ channel alpha subunit with novel gating properties. *Neuron* **1**, 449-461.

Barchi, R. L., Cohen, S. A., & Murphy, L. E. (1980). Purification from rat sarcolemma of the saxitoxin-binding component of the excitable membrane sodium channel. *Proc.Natl.Acad.Sci.U.S.A* **77**, 1306-1310.

Barhanin, J., Lesage, F., Guillemare, E., Fink, M., Lazdunski, M., & Romey, G. (1996). KvLQT1 and lsK (minK) proteins associate to form the I(Ks) cardiac potassium current. *Nature* **384**, 78-80.

Barres, B. A. (1999). A new role for glia: generation of neurons! *Cell* **97**, 667-670.

Barry, P. H. & Lynch, J. W. (1991). Liquid junction potentials and small cell effects in patch-clamp analysis. *J.Membr.Biol.* **121**, 101-117.

Bean, B. P. (1989). Multiple types of calcium channels in heart muscle and neurons. Modulation by drugs and neurotransmitters. *Ann.N.Y.Acad.Sci.* **560**. 334-45.

Beckh, S., Noda, M., Lubbert, H., & Numa, S. (1989). Differential regulation of three sodium channel messenger RNAs in the rat central nervous system during development. *EMBO J.* **8**, 3611-3616.

Beckh, S. (1990). Differential expression of sodium channel mRNAs in rat peripheral nervous system and innervated tissues. *FEBS Lett.* **262**, 317-322.

Belluzzi, O., Sacchi, O. & Wanke, E. (1985). Identification of delayed potassium and calcium current in the rat sympathetic neurone under voltage clamp. *J.Physiol.* ***358***, 109-129.

Belluzzi, O. & Sacchi, O. (1986). A quantitative description of the sodium current in the rat sympathetic neurone. *J.Physiol.* **380**, 275-291.

Bernheim, L., Mathie, A., & Hille, B. (1992). Characterization of muscarinic receptor subtypes inhibiting Ca^{2+} current and M current in rat sympathetic neurons. *Proc.Natl.Acad.Sci.U.S.A* **89**, 9544-9548.

Bezanilla, F. (2000). The voltage sensor in voltage-dependent ion channels. *Physiol.Rev.* **80(3)**, 555-592.

Biervert, C., Schroeder, B. C., Kubisch, C., Berkovic, S. F., Propping, P., Jentsch, T. J., & Steinlein, O. K. (1998). A potassium channel mutation in neonatal human epilepsy. *Science* **279**, 403-406.

Black, J. A., Yokoyama, S., Higashida, H., Ransom, B. R., & Waxman, S. G. (1994). Sodium channel mRNAs I, II and III in the CNS: cell-specific expression. *Brain Res.Mol.Brain Res.* **22**, 275-289.

Bosma, M. M., Bernheim, L., Leibowitz, M. D., Pfaffinger, P. J. & Hille, B. (1990). Modulation of M current in frog sympathetic ganglion cells. In: G proteins and signal transduction. Rockefeller University press, New York, 43-59.

Breitwieser, G. E. (1991). G protein-mediated ion channel activation. *Hypertension* **17**, 684-692.

Brown, D. A. & Adams, P. R. (1980). Muscarinic suppression of a novel voltage-sensitive K^+ current in a vertebrate neurone. *Nature* **283**, 673-676.

Brown, A. M., Kunze, D. L. & Yatani, A. (1986). Dual effects of dihydropyridines on whole cell and unitary calcium currents in single ventricular cells of guinea-pig. *J.Physiol.* **379**. 495-514.

Brown, D. (1988). M-currents: an update. *Trends Neurosci.* **11**, 294-299.

Brown, D. A. & Higashida, H. (1988). Voltage- and calcium-activated potassium currents in mouse neuroblastoma x glioma hybrid cells. *J.Physiol* **397**. 149-165.

Brown, D. A., Marrion, N. V., & Smart, T. G. (1989). On the transduction mechanism for muscarine-induced inhibition of M-current in cultured rat sympathetic neurones. *J.Physiol* **413**. 469-88.

Brysch, W., Creutzfeldt, O. D., Luno, K., Schlingensiepen, R., & Schlingensiepen, K. H. (1991). Regional and temporal expression of sodium channel messenger RNAs in the rat brain during development. *Exp.Brain Res.* **86**, 562-567.

Buckley, N. J., ffrench-Mullen, J., & Caulfield, M. (1995). Use of antisense oligodeoxynucleotides and monospecific antisera to inhibit G-protein gene expression in cultured neurons. *Biochem.Soc.Trans.* **23**, 137-141.

Burgess, D. L., Kohrman, D. C., Galt, J., Plummer, N. W., Jones, J. M., Spear, B., & Meisler, M. H. (1995). Mutation of a new sodium channel gene, Scn8a, in the mouse mutant 'motor endplate disease'. *Nat.Genet.* **10**, 461-465.

Cantrell, A. R., Ma, J. Y., Scheuer, T., & Catterall, W. A. (1996). Muscarinic modulation of sodium current by activation of protein kinase C in rat hippocampal neurons. *Neuron* **16**, 1019-1026.

Cantrell, A. R., Smith, R. D., Goldin, A. L., Scheuer, T., & Catterall, W. A. (1997). Dopaminergic modulation of sodium current in hippocampal neurons via cAMP-dependent phosphorylation of specific sites in the sodium channel alpha subunit. *J.Neurosci.* **17**, 7330-7338.

Catterall, W. A. (1986). Voltage-dependent gating of sodium channels: correlating structure and function. *Trends Neurosci.* **9**, 7-10.

Catterall, W. A. (1992). Cellular and molecular biology of voltage-gated sodium channels. *Physiol Rev.* **72**, S15-S48.

Catterall, W. A. (1995). Structure and function of voltage-gated channels. *Annu Rev Biochem.* **64**, 493-531.

Cha, A., Snyder, G. E., Selvin, P. R. & Bezanilla, F. (1999). Atomic scale movement of the voltage-sensing region in a potassium channel measured via spectroscopy. *Nature.* **402**, 809-813.

Charlier, C., Singh, N. A., Ryan, S. G., Lewis, T. B., Reus, B. E., Leach, R. J., & Leppert, M. (1998). A pore mutation in a novel KQT-like potassium channel gene in an idiopathic epilepsy family. *Nat.Genet.* **18**, 53-55.

Chen, T. C., Law, B., Kondratyuk, T., & Rossie, S. (1995). Identification of soluble protein phosphatases that dephosphorylate voltage-sensitive sodium channels in rat brain. *J.Biol.Chem.* **270**, 7750-7756.

Chen, L. Q., Santarelli, V., Horn, R., & Kallen, R. G. (1996). A unique role for the S4 segment of domain 4 in the inactivation of sodium channels. *J.Gen.Physiol.* **108**, 549-556.

Chomczynski, P. & Sacchi, N. (1987). Single-step method of RNA isolation by acid guanidinium thiocyanate-phenol-chloroform extraction. *Anal.Biochem.* **162**, 156-159.

Clare, J. J., Dale, T. J., Xie, X., Peakman, T. C. & Chen, Y. (1999). Cloning and functional analysis of the type III Na^+ channel from human brain. *Ann.N.Y.Acad.Sci.* **868**, 80-83.

Codina, J., Yatani, A., Grenet, D., Brown, A. M., & Birnbaumer, L. (1987). The alpha subunit of the GTP binding protein Gk opens atrial potassium channels. *Science* **236**, 442-445.

Cohen, S. A. & Levitt, L. K. (1993). Partial characterization of the rH1 sodium channel protein from rat heart using subtype-specific antibodies. *Circ.Res.* **73**, 735-742.

Colquhoun, D. & Ritchie, J. M. (1972). The kinetics of the interaction between tetrodotoxin and mammalian nonmyelinated nerve fibers. *Mol.Pharmacol.* **8**, 285-292.

Constanti, A. & Brown, D. A. (1981). M-currents in voltage-clamped mammalian sympathetic neurones. *Neurosci.Lett.* **24**, 289-294.

Constanti, A. & Sim, J. A. (1987). Muscarinic receptors mediating suppression of the M-current in guinea-pig olfactory cortex neurones may be of the M_2-subtype. *Br.J.Pharmacol.* **90**, 3-5.

Cooper, E. C., Aldape, K. D., Abosch, A., Barbaro, N. M., Berger, M. S., Peacock, W. S., Jan, Y. N., & Jan, L. Y. (2000). Colocalization and coassembly of two human brain M-type potassium channel subunits that are mutated in epilepsy. *Proc.Natl.Acad.Sci.U.S.A* **97**, 4914-4919.

Costa, M. R., Casnellie, J. E., & Catterall, W. A. (1982). Selective phosphorylation of the alpha subunit of the sodium channel by cAMP-dependent protein kinase. *J.Biol.Chem.* **257** , 7918-7921.

Costa, M. R. & Catterall, W. A. (1984). Phosphorylation of the alpha subunit of the sodium channel by protein kinase C. *Cell Mol.Neurobiol.* **4**, 291-297.

Costa, A. M. & Brown, B. S. (1997). Inhibition of M-current in cultured rat superior cervical ganglia by linopirdine: mechanism of action studies. *Neuropharmacology* **36**, 1747-1753.

Coward, K., Aitken, A., Powell, A., Plumpton, C., Birch, R., Tate, S., Bountra, C. and Anand, P. (2001). Plasticity of TTX-sensitive sodium channels PN1 and Brain III in injured human nerves. *NeuroReport.* **12(3)**, 495-500.

Crill, W. E. (1996). Persistent sodium current in mammalian central neurons. *Annu.Rev.Physiol* **583**. 49-62.

Cuervo, L. A. & Adelman, W. J. (1970). Equilibrium and kinetic properties of the interaction between tetrodotoxin and the excitable membrane of the squid giant axon. *J.Gen.Physiol* **55**, 309-335.

Dascal, N. & Lotan, I. (1991). Activation of protein kinase C alters voltage dependence of a Na^+ channel. *Neuron* **6**, 165-175.

De Biasi, M., Hartmann, H. A., Drewe, J. A., Taglialatela, M., Brown, A. M., & Kirsch, G. E. (1993). Inactivation determined by a single site in K^+ pores. *Pflugers Arch.* **422**, 354-363.

Delmas, P., Brown, D. A., Dayrell, M., Abogadie, F. C., Caulfield, M. P., & Buckley, N. J. (1998). On the role of endogenous G-protein beta gamma subunits in N-type Ca^{2+} current inhibition by neurotransmitters in rat sympathetic neurones. *J.Physiol* **506**, 319-29.

Dib-Hajj, S. D., Tyrrell, L., Black, J. A., & Waxman, S. G. (1998). NaN, a novel voltage-gated Na channel, is expressed preferentially in peripheral sensory neurons and down-regulated after axotomy. *Proc.Natl.Acad.Sci.U.S.A* **95**, 8963-8968.

Dietrich, P. S., McGivern, J. G., Delgado, S. G., Koch, B. D., Eglen, R. M., Hunter, J. C., & Sangameswaran, L. (1998). Functional analysis of a voltage-gated sodium channel and its splice variant from rat dorsal root ganglia. *J.Neurochem.* **70**, 2262-2272.

Doyle, D. A., Cabral, J. M., Pfuetzner, R. A., Kuo, A., Gulbis, J. M., Cohen, S. L., Chait, B. T. & MacKinnon, R. (1998). The structure of the potassium channel: molecular basis of K^+ conduction and selectivity. *Science* **280**, 69-77.

Eaholtz, G., Zagotta, W. N., & Catterall, W. A. (1998). Kinetic analysis of block of open sodium channels by a peptide containing the isoleucine, phenylalanine, and methionine (IFM) motif from the inactivation gate. *J.Gen.Physiol* **111**, 75-82.

Eaholtz, G., Colvin, A., Leonard, D., Taylor, C., & Catterall, W. A. (1999). Block of brain sodium channels by peptide mimetics of the isoleucine, phenylalanine, and methionine (IFM) motif from the inactivation gate. *J.Gen.Physiol* **113**, 279-294.

Felipe, A., Knittle, T. J., Doyle, K. L., & Tamkun, M. M. (1994). Primary structure and differential expression during development and pregnancy of a novel voltage-gated sodium channel in the mouse. *J.Biol.Chem.* **269**, 30125-30131.

Felts, P. A., Yokoyama, S., Dib-Hajj, S., Black, J. A., & Waxman, S. G. (1997). Sodium channel alpha-subunit mRNAs I, II, III, NaG, Na6 and hNE (PN1): different expression patterns in developing rat nervous system. *Brain Res.Mol.Brain Res.* **45**, 71-82.

Fernandez-Fernandez, J. M., Abogadie, F. C., Milligan, G., Delmas, P. & Brown, D. A. (2001). Multiple pertussis toxin-sensitive G-proteins can couple receptors to GIRK channels in rat sympathetic neurons when expressed heterologously, but only native G_i -proteins do so in situ. *Eur.J.Neurosci.* **14(2)**, 283-292.

French, C. R., Sah, P., Buckett, K. J., & Gage, P. W. (1990). A voltage-dependent persistent sodium current in mammalian hippocampal neurons. *J.Gen.Physiol* **95**, 1139-1157.

Freschi, J. E. (1983). Membrane currents of cultured rat sympathetic neurons under voltage clamp. *J.Neurophysiol.* **50 (6)**, 1460-1478.

Frohnwieser, B., Weigl, L., & Schreibmayer, W. (1995). Modulation of cardiac sodium channel isoform by cyclic AMP dependent protein kinase does not depend on phosphorylation of serine 1504 in the cytosolic loop interconnecting transmembrane domains III and IV. *Pflugers Arch.* **430**, 751-753.

Frohnwieser, B., Chen, L. Q., Schreibmayer, W., & Kallen, R. G. (1997). Modulation of the human cardiac sodium channel alpha-subunit by cAMP-dependent protein kinase and the responsible sequence domain. *J.Physiol* **498**, -18.

Gautron, S., Dos-Santos, G., Pinto-Henrique, D., Koulakoff, A., Gros, F., & Berwald-Netter, Y. (1992). The glial voltage-gated sodium channel: cell- and tissue-specific mRNA expression. *Proc.Natl.Acad.Sci.U.S.A* **89**, 7272-7276.

George, A. L., Knittle, T. J., & Tamkun, M. M. (1992). Molecular cloning of an atypical voltage-gated sodium channel expressed in human heart and uterus: evidence for a distinct gene family. *Proc.Natl.Acad.Sci.U.S.A* **89**, 4893-4897.

Gershon, E., Weigl, L., Lotan, I., Schreibmayer, W., & Dascal, N. (1992). Protein kinase A reduces voltage-dependent Na^+ current in Xenopus oocytes. *J.Neurosci.* **12**, 3743-3752.

Godoy, C. M. & Cukierman, S. (1994a). Multiple effects of protein kinase C activators on Na^+ currents in mouse neuroblastoma cells. *J.Membr.Biol.* **140**, 101-110.

Godoy, C. M. & Cukierman, S. (1994b). Diacylglycerol-induced activation of protein kinase C attenuates Na^+ currents by enhancing inactivation from the closed state. *Pflugers Arch.* **429(2)**, 245-252.

Goh, J. W., Kelly, M. E., Pennefather, P. S., Chicchi, G. G., Cascieri, M. A., Garcia, M. L., & Kaczorowski, G. J. (1992). Effect of charybdotoxin and leiurotoxin I on potassium currents in bullfrog sympathetic ganglion and hippocampal neurons. *Brain Res.* **591**, 165-170.

Goldin, A. L., Barchi, R. L., Caldwell, J. H., Hofmann, F., Howe, J. R., Hunter, J. C., Kallen, R. G., Mandel, G., Meisler, M. H., Netter, Y. B., Noda, M., Tamkun, M. M., Waxman, S. G., Wood, J. N., & Catterall, W. A. (2000). Nomenclature of voltage-gated sodium channels. *Neuron* **28**, 365-368.

Gordon, D., Merrick, D., Auld, V., Dunn, R., Goldin, A. L., Davidson, N., & Catterall, W. A. (1987). Tissue-specific expression of the RI and RII sodium channel subtypes. *Proc.Natl.Acad.Sci.U.S.A* **84**, 8682-8686.

Guy, H. R. & Seetharamulu, P. (1986). Molecular model of the action potential sodium channel. *Proc.Natl.Acad.Sci.U.S.A* **83**, 508-512.

Hadley, J. K., Noda, M., Selyanko, A. A., Wood, I. C., Abogadie, F. C., & Brown, D. A. (2000). Differential tetraethylammonium sensitivity of KCNQ1-4 potassium channels. *Br.J.Pharmacol.* **129**, 413-415.

Haley, J. E., Abogadie, F. C., Delmas, P., Dayrell, M., Vallis, Y., Milligan, G., Caulfield, M. P., Brown, D. A., & Buckley, N. J. (1998). The alpha subunit of Gq contributes to muscarinic inhibition of the M-type potassium current in sympathetic neurons. *J.Neurosci.* **18**, 4521-4531.

Halliwell, J. V. & Adams, P. R. (1982). Voltage-clamp analysis of muscarinic excitation in hippocampal neurones. *Brain Res.* **250(1)**, 71-97.

Hamill, O. P., Marty, A., Neher, E., Sakmann, B., & Sigworth, F. J. (1981). Improved patch-clamp techniques for high-resolution current recording from cells and cell-free membrane patches. *Pflugers Arch.* **391**, 85-100.

Hamill, O. P., Huguenard, J. R., Enayati, E. F. & Prince, D. A. (1986). Single channel currents underlying slow threshold Na^+ conductances in rat neocortical neurones. *Soc.Neurosci.Abstr.* **12**, 950.

Hamilton, S. E., Loose, M. D., Qi, M., Levey, A. I., Hille, B., McKnight, G. S., Idzerda, R. L., & Nathanson, N. M. (1997). Disruption of the m_1 receptor gene ablates muscarinic receptor-dependent M current regulation and seizure activity in mice. *Proc.Natl.Acad.Sci.U.S.A* **94**, 13311-13316.

Hartshorne, R. P. & Catterall, W. A. (1981). Purification of the saxitoxin receptor of the sodium channel from rat brain. *Proc.Natl.Acad.Sci.U.S.A* **78**, 4620-4624.

Hartshorne, R. P. & Catterall, W. A. (1984). The sodium channel from rat brain. Purification and subunit composition. *J.Biol.Chem.* **259**, 1667-1675.

Hartshorne, R. P., Messner, D. J., Coppersmith, J. C., & Catterall, W. A. (1982). The saxitoxin receptor of the sodium channel from rat brain. Evidence for two nonidentical beta subunits. *J.Biol.Chem.* **257**, 13888-13891.

Hille, B (1992a). Ionic channels of excitable membranes, 2nd edition. Sunderland, Massachusetts: Sinauer Associates Inc.

Hille, B. (1992b). G protein-coupled mechanisms and nervous signaling. *Neuron* **9**, 187-195.

Hille, B. (1994). Modulation of ion-channel function by G-protein-coupled receptors. *Trends Neurosci.* **17**, 531-536.

Hirschberg, B., Rovner, A., Lieberman, M., & Patlak, J. (1995). Transfer of twelve charges is needed to open skeletal muscle Na^+ channels. *J.Gen.Physiol* **106**, 1053-1068.

Ho, K., Nichols, C. G., Lederer, W. J., Lytton, J., Vassilev, P. M., Kanazirska, M. V., & Hebert, S. C. (1993). Cloning and expression of an inwardly rectifying ATP-regulated potassium channel. *Nature* **362**, 31-38.

Hodgkin, A. L. & Huxley, A. F. (1952a). The components of membrane conductance in the giant axon of *Loligo. J. Physiol.***116**, 473-496.

Hodgkin, A. L. & Huxley, A. F. (1952b). The dual effect of membrane potential on sodium conductance in the giant axon of *Loligo. J. Physiol.***116**, 497-506.

Hodgkin, A. L. & Huxley, A. F. (1952c). A quantitative description of membrane current and its application to conduction and excitation in nerve. *J. Physiol.***117**, 500-544.

Holmgren, M., Shin, K. S. & Yellen, G. (1998). The activation gate of a voltage-gated K^+ channel can be trapped in the open state by an intersubunit metal bridge. *Neuron* **21 (3)**, 617-621.

Hoshi, T., Zagotta, W. N., & Aldrich, R. W. (1990). Biophysical and molecular mechanisms of Shaker potassium channel inactivation. *Science* **250**, 533-538.

Ikeda, S. R. (1996). Voltage-dependent modulation of N-type calcium channels by G-protein beta gamma subunits. *Nature* **380**, 255-258.

Isacoff, E. Y., Jan, Y. N., & Jan, L. Y. (1991). Putative receptor for the cytoplasmic inactivation gate in the Shaker K^+ channel. *Nature* **353**, 86-90.

Ismailov, I. I., Jovov, B., Fuller, C. M., Berdiev, B. K., Keeton, D. A., & Benos, D. J. (1996). G-protein regulation of outwardly rectified epithelial chloride channels incorporated into planar bilayer membranes. *J.Biol.Chem.* **271**, 4776-4780.

Isom, L. L., De Jongh, K. S., Patton, D. E., Reber, B. F., Offord, J., Charbonneau, H., Walsh, K., Goldin, A. L., & Catterall, W. A. (1992). Primary structure and functional expression of the beta 1 subunit of the rat brain sodium channel. *Science* **256**, 839-842.

Isom, L. L., De Jongh, K. S., & Catterall, W. A. (1994). Auxiliary subunits of voltage-gated ion channels. *Neuron* **12**, 1183-1194.

Isom, L. L., Ragsdale, D. S., De Jongh, K. S., Westenbroek, R. E., Reber, B. F., Scheuer, T., & Catterall, W. A. (1995). Structure and function of the beta 2 subunit of brain sodium channels, a transmembrane glycoprotein with a CAM motif. *Cell* **83**, 433-442.

Jahnsen, H. & Llinas, R. (1984). Voltage-dependent burst-to-tonic switching of thalamic cell activity: an in vitro study. *Arch.Ital.Biol.* **122**, 73-82.

Jan, L. Y. & Jan, Y. N. (1997). Cloned potassium channels from eukaryotes and prokaryotes. *Annu.Rev.Neurosci.* **2091-123**, -123.

Jensen, A. A., Sheppard, P. O., O'Hara, P. J., Frogsgaard-Larsen, P. & Brauner-Osborne, H. (2000). The role of Arg^{78} in the metabotropic glutamate receptor $mGlu_1$ for agonist binding and selectivity. *Eur.J.Pharmacol.* **397**. 247-253.

Jentsch, T. J. (2000). Neuronal KCNQ potassium channels: physiology and role in disease. *Nat.Rev.Neurosci.* **1**, 21-30.

Kaczmarek, L. K. & Blumenthal, E. M. (1997). Properties and regulation of the minK potassium channel protein. *Physiol Rev.* **77**, 627-641.

Kallen, R. G., Cohen, S. A., & Barchi, R. L. (1993). Structure, function and expression of voltage-dependent sodium channels. *Mol.Neurobiol.* **7**, 383-428.

Kayano, T., Noda, M., Flockerzi, V., Takahashi, H., & Numa, S. (1988). Primary structure of rat brain sodium channel III deduced from the cDNA sequence. *FEBS Lett.* **228**, 187-194.

Ketchum, K. A., Joiner, W. J., Sellers, A. J., Kaczmarek, L. K., & Goldstein, S. A. (1995). A new family of outwardly rectifying potassium channel proteins with two pore domains in tandem. *Nature* **376**, 690-695.

Kharkovets, T., Hardelin, J. P., Safieddine, S., Schweizer, M., El Amraoui, A., Petit, C., & Jentsch, T. J. (2000). KCNQ4, a K^+ channel mutated in a form of dominant deafness, is expressed in the inner ear and the central auditory pathway. *Proc.Natl.Acad.Sci.U.S.A* **97**, 4333-4338.

Kikkawa, U., Kishimoto, A., & Nishizuka, Y. (1989). The protein kinase C family: heterogeneity and its implications. *Annu.Rev.Biochem.* **58**, 31-44.

Klink, R. & Alonso, A. (1993). Ionic mechanisms for the subthreshold oscillations and differential electroresponsiveness of medial entorhinal cortex layer II neurons. *J.Neurophysiol.* **70**, 144-157.

Kokubun, S., Prod'hom, B., Becker, C., Porzig, H., & Reuter, H. (1986). Studies on Ca^{2+} channels in intact cardiac cells: voltage-dependent effects and cooperative interactions of dihydropyridine enantiomers. *Mol.Pharmacol.* **30**, 571-584.

Kraner, S. D., Tanaka, J. C., & Barchi, R. L. (1985). Purification and functional reconstitution of the voltage-sensitive sodium channel from rabbit T-tubular membranes. *J.Biol.Chem.* **260**, 6341-6347.

Kubisch, C., Schroeder, B. C., Friedrich, T., Lutjohann, B., El Amraoui, A., Marlin, S., Petit, C., & Jentsch, T. J. (1999). KCNQ4, a novel potassium channel expressed in sensory outer hair cells, is mutated in dominant deafness. *Cell* **96**, 437-446.

Kubo, Y., Baldwin, T. J., Jan, Y. N., & Jan, L. Y. (1993). Primary structure and functional expression of a mouse inward rectifier potassium channel. *Nature* **362**, 127-133.

Kurachi, Y. (1995). G protein regulation of cardiac muscarinic potassium channel. *Am.J.Physiol* **269** , C821-C830.

Lamas, J. A. (1998). A hyperpolarisation activated cation current (Ih) contributes to resting potential in rat superior cervical sympathetic neurones. *Pflugers Arch.* **436**, 429-435.

Lamas, J. A., Selyanko, A. A., & Brown, D. A. (1997). Effects of a cognition-enhancer, linopirdine (DuP 996), on M-type potassium currents (I_{KM}) and some other voltage- and ligand-gated membrane currents in rat sympathetic neurons. *Eur.J.Neurosci.* **9**, 605-616.

Lambolez, B., Audinat, E., Bochet, P., Crepel, F., & Rossier, J. (1992). AMPA receptor subunits expressed by single Purkinje cells. *Neuron* **9**, 247-258.

Lampinen, M., Pentikainen, O., Johnson, M. S., & Keinanen, K. (1998). AMPA receptors and bacterial periplasmic amino acid-binding proteins share the ionic mechanism of ligand recognition. *EMBO J.* **17**, 4704-4711.

Larsson, H. P., Baker, O. S., Dhillon, D. S., & Isacoff, E. Y. (1996). Transmembrane movement of the shaker K^+ channel S4. *Neuron* **16**, 387-397.

Laube, B., Hirai, H., Sturgess, M., Betz, H., & Kuhse, J. (1997). Molecular determinants of agonist discrimination by NMDA receptor subunits: analysis of the glutamate binding site on the NR2B subunit. *Neuron* **18**, 493-503.

Lehmann-Horn, F. & Jurkat-Rott, K. (1999). Voltage-gated ion channels and hereditary disease. *Physiol Rev.* **79**, 1317-1372.

Lerche, C., Scherer, C. R., Seebohm, G., Derst, C., Wei, A. D., Busch, A. E., & Steinmeyer, K. (2000). Molecular cloning and functional expression of KCNQ5, a potassium channel subunit that may contribute to neuronal M-current diversity. *J.Biol.Chem.* **275**, 22395-22400.

Lesage, F., Guillemare, E., Fink, M., Duprat, F., Lazdunski, M., Romey, G., & Barhanin, J. (1996). TWIK-1, a ubiquitous human weakly inward rectifying K^+ channel with a novel structure. *EMBO J.* **15**, 1004-1011.

Li, M., West, J. W., Lai, Y., Scheuer, T., & Catterall, W. A. (1992). Functional modulation of brain sodium channels by cAMP-dependent phosphorylation. *Neuron* **8**, 1151-1159.

Li, M., West, J. W., Numann, R., Murphy, B. J., Scheuer, T., & Catterall, W. A. (1993). Convergent regulation of sodium channels by protein kinase C and cAMP-dependent protein kinase. *Science* **261**, 1439-1442.

Lipowsky, R., Gillessen, T., & Alzheimer, C. (1996). Dendritic Na^+ channels amplify EPSPs in hippocampal CA1 pyramidal cells. *J.Neurophysiol.* **76**, 2181-2191.

Liu, Y., Jurman, M. E., & Yellen, G. (1996). Dynamic rearrangement of the outer mouth of a K^+ channel during gating. *Neuron.* **16**, 859-867.

Llinas, R. & Sugimori, M. (1980). Electrophysiological properties of in vitro Purkinje cell dendrites in mammalian cerebellar slices. *J.Physiol* **305**. 197-213.

Llinas, R. (1988). The intrinsic electrophysiological properties of mammalian neurones: insights into central nervous system function. *Science* **242**, 1654-1664.

Lombet, A. & Lazdunski, M. (1984). Characterization, solubilization, affinity labeling and purification of the cardiac Na^+ channel using Tityus toxin gamma. *Eur.J.Biochem.* **141**, 651-660.

Loscher, W. (1998). New visions in the pharmacology of anticonvulsion. *Eur.J.Pharmacol.* **342**, 1-13.

Lotan, I., Dascal, N., Naor, Z., & Boton, R. (1990). Modulation of vertebrate brain Na^+ and K^+ channels by subtypes of protein kinase C. *FEBS Lett.* **267**, 25-28.

Lu, Z. & MacKinnon, R. (1994). Electrostatic tuning of Mg^{2+} affinity in an inward-rectifier K^+ channel. *Nature* **371**, 243-246.

Ma, J. Y., Catterall, W. A., & Scheuer, T. (1997). Persistent sodium currents through brain sodium channels induced by G protein betagamma subunits. *Neuron* **19**, 443-452.

Ma, J. Y., Li, M., Catterall, W. A., & Scheuer, T. (1994). Modulation of brain Na^+ channels by a G-protein-coupled pathway. *Proc.Natl.Acad.Sci.U.S.A* **91**, 12351-12355.

Macdonald, R. L. & Kelly, K. M. (1995). Antiepileptic drug mechanisms of action. *Epilepsia* **36 (suppl 2)**. S2-12.

MacKinnon, R. (1991). Determination of the subunit stoichiometry of a voltage-activated potassium channel. *Nature* **350**, 232-235.

MacKinnon, R. (1995). Pore loops: an emerging theme in ion channel structure. *Neuron* **14**, 889-892.

Main, M. J., Cryan, J. E., Dupere, J. R., Cox, B., Clare, J. J. & Burbidge, S. A. (2000). Modulation of KCNQ2/3 potassium channels by the novel anticonvulsant retigabine. *Mol.Pharmacol.* **58 (2)**, 253-262.

Makita, N., Bennett, P. B., & George, A. L. (1994). Voltage-gated Na^+ channel beta 1 subunit mRNA expressed in adult human skeletal muscle, heart, and brain is encoded by a single gene. *J.Biol.Chem.* **269**, 7571-7578.

Malin, S. A. & Nerbonne, J. M. (2000). Elimination of the fast transient in superior cervical ganglion neurones with expression of Kv4.2(W362F): molecular dissection if I_A. *J.Neurosci.* **20**. 5191-5199.

Malo, D., Schurr, E., Dorfman, J., Canfield, V., Levenson, R., & Gros, P. (1991). Three brain sodium channel alpha-subunit genes are clustered on the proximal segment of mouse chromosome 2. *Genomics* **10**, 666-672.

Manavalan, P., Dearborn, D. G., McPherson, J. M., & Smith, A. E. (1995). Sequence homologies between nucleotide binding regions of CFTR and G-proteins suggest structural and functional similarities. *FEBS Lett.* **366**, 87-91.

Marrion, N. V., Smart, T. G., Marsh, S. J., & Brown, D. A. (1989). Muscarinic suppression of the M-current in the rat sympathetic ganglion is mediated by receptors of the M1-subtype. *Br.J.Pharmacol.* **98**, 557-573.

Marrion, N. V. & Adams, P. R. (1992). Release of intracellular calcium and modulation of membrane currents by caffeine in bull-frog sympathetic neurones. *J.Physiol.* **445**, 515-35.

Marrion, N. V. (1997). Control of M-current. *Annu.Rev.Physiol.* **59**, 483-504.

Mathie, A. & Watkins, C. S. (1997). Is EAG the answer to the M-current? *Trends Neurosci.* **20**, 14.

Matsuda, J. J., Lee, H., & Shibata, E. F. (1992). Enhancement of rabbit cardiac sodium channels by beta-adrenergic stimulation. *Circ.Res.* **70**, 199-207.

Meldrum, B. (1996). Action of established and novel anticonvulsant drugs on the basic mechanisms of epilepsy. *Epilepsy Res.Suppl* **1167-77**, -77.

Mellor, H. & Parker, P. J. (1998). The extended protein kinase C superfamily. *Biochem.J.* **332**, -92.

Mittmann, T. & Alzheimer, C. (1998). Muscarinic inhibition of persistent Na^+ current in rat neocortical pyramidal neurons. *J.Neurophysiol.* **79**, 1579-1582.

Moore, S. D., Madamba, S. G., Joels, M., & Siggins, G. R. (1988). Somatostatin augments the M-current in hippocampal neurons. *Science* **239**, 278-280.

Moore, S. D., Madamba, S. G., & Siggins, G. R. (1990). Ethanol diminishes a voltage-dependent K^+ current, the M-current, in CA1 hippocampal pyramidal neurons in vitro. *Brain Res.* **516**, 222-228.

Moorman, J. R., Kirsch, G. E., VanDongen, A. M., Joho, R. H., & Brown, A. M. (1990). Fast and slow gating of sodium channels encoded by a single mRNA. *Neuron* **4**, 243-252.

Morgan, K., Stevens, E. B., Shah, B., Cox, P. J., Dixon, A. K., Lee, K., Pinnock, R. D., Hughes, J., Richardson, P. J., Mizuguchi, K., & Jackson, A. P. (2000). Beta 3: an additional auxiliary subunit of the voltage-sensitive sodium channel that modulates channel gating with distinct kinetics. *Proc.Natl.Acad.Sci.U.S.A* **97**, 2308-2313.

Mullaney, I., Dodd, M. W., Buckley, N., & Milligan, G. (1993). Agonist activation of transfected human M_1 muscarinic acetylcholine receptors in CHO cells results in down-regulation of both the receptor and the alpha subunit of the G-protein Gq. *Biochem.J.* **289**, 125-131.

Murphy, B. J., Rossie, S., De Jongh, K. S., & Catterall, W. A. (1993). Identification of the sites of selective phosphorylation and dephosphorylation of the rat brain Na^+ channel alpha subunit by cAMP-dependent protein kinase and phosphoprotein phosphatases. *J.Biol.Chem.* **268**, 27355-27362.

Murray, K. T., Hu, N. N., Daw, J. R., Shin, H. G., Watson, M. T., Mashburn, A. B., & George, A. L. (1997). Functional effects of protein kinase C activation on the human cardiac Na^+ channel. *Circ.Res.* **80**, 370-376.

Nathanson, N. M. (1987). Molecular properties of the muscarinic acetylcholine receptor. *Annu.Rev.Neurosci.* **10**, 195-236.

Neer, E. J. & Smith, T. F. (1996). G protein heterodimers: new structures propel new questions. *Cell* **84**, 175-178.

Neher, E. (1992). Correction for liquid junction potentials in patch clamp experiments. *Methods Enzymol.* **207**, 123-31.

Nickolson, V. J., Tam, S. W., Myers, M. J. & Cook, L. (1990). DuP 996 (3,3-bis(4-pyridinylmethyl)-1-phenylindolin-2-one) enhances the stimulus-induced release of acetylcholine from rat brain in vitro and in vivo. *Drug Dev.Res.* **19**, 285-300.

Noda, M., Shimizu, S., Tanabe, T., Takai, T., Kayano, T., Ikeda, T., Takahashi, H., Nakayama, H., Kanaoka, Y., Minamino, N., & et, a. (1984). Primary structure of Electrophorus electricus sodium channel deduced from cDNA sequence. *Nature* **312**, 121-127.

Noda, M., Ikeda, T., Suzuki, H., Takeshima, H., Takahashi, T., Kuno, M., & Numa, S. (1986). Expression of functional sodium channels from cloned cDNA. *Nature* **322**, 826-828.

Numann, R., Catterall, W. A., & Scheuer, T. (1991). Functional modulation of brain sodium channels by protein kinase C phosphorylation. *Science* **254**, 115-118.

Oh, Y., Black, J. A., & Waxman, S. G. (1994). The expression of rat brain voltage-sensitive Na^+ channel mRNAs in astrocytes. *Brain Res.Mol.Brain Res.* **23**, 57-65.

Papazian, D. M., Schwarz, T. L., Tempel, B. L., Jan, Y. N., & Jan, L. Y. (1987). Cloning of genomic and complementary DNA from Shaker, a putative potassium channel gene from Drosophila. *Science* **237**, 749-753.

Papazian, D. M., Timpe, L. C., Jan, Y. N., & Jan, L. Y. (1991). Alteration of voltage-dependence of Shaker potassium channel by mutations in the S4 sequence. *Nature* **349**, 305-310.

Papazian, D. M. (1999). Potassium channels: some assembly required. *Neuron* **23**, 7-10.

Pape, H. C. & Driesang, R. B. (1998). Ionic mechanisms of intrinsic oscillations in neurons of the basolateral amygdaloid complex. *J.Neurophysiol.* **79**, 217-226.

Parri, H. R. & Crunelli, V. (1998). Sodium current in rat and cat thalamocortical neurons: role of a non-inactivating component in tonic and burst firing. *J.Neurosci.* **18**, 854-867.

Patlak, J. B. & Ortiz, M. (1985). Slow currents through single sodium channels of the adult rat heart. *J.Gen.Physiol* **86**, 89-104.

Patton, D. E., Isom, L. L., Catterall, W. A., & Goldin, A. L. (1994). The adult rat brain beta 1 subunit modifies activation and inactivation gating of multiple sodium channel alpha subunits. *J.Biol.Chem.* **269**, 17649-17655.

Pennartz, C. M., Bierlaagh, M. A., & Geurtsen, A. M. (1997). Cellular mechanisms underlying spontaneous firing in rat suprachiasmatic nucleus: involvement of a slowly inactivating component of sodium current. *J.Neurophysiol.* **78**, 1811-1825.

Perozo, E., Santacruz-Toloza, L., Stefani, E., Bezanilla, F., & Papazian, D. M. (1994). S4 mutations alter gating currents of Shaker K channels. *Biophys.J.* **66**, 345-354.

Perozo, E., Cortes, D. M. & Cuello, L. G. (1998). Three-dimensional architecture and gating mechanism of a K^+ channel studied by EPR spectroscopy. *Nature Struct. Biol.* **5**, 459-469.

Perozo, E. Cortes, D. M. & Cuello, L. G. (1999). Structural rearangements underlying K^+ channel activation gating. *Science* **285**, 73-78.

Pfaffinger, P. (1988). Muscarine and t-LHRH suppress M-current by activating an IAP-insensitive G-protein. *J.Neurosci.* **8**, 3343-3353.

Pongs, O., Kecskemethy, N., Muller, R., Krah-Jentgens, I., Baumann, A., Kiltz, H. H., Canal, I., Llamazares, S., & Ferrus, A. (1988). Shaker encodes a family of putative potassium channel proteins in the nervous system of Drosophila. *EMBO J.* **7**, 1087-1096.

Rae, J., Cooper, K., Gates, P., & Watsky, M. (1991). Low access resistance perforated patch recordings using amphotericin B. *J.Neurosci.Methods* **37**, 15-26.

Ragsdale, D. S., Scheuer, T., & Catterall, W. A. (1991). Frequency and voltage-dependent inhibition of type IIA Na^+ channels, expressed in a mammalian cell line, by local anesthetic, antiarrhythmic, and anticonvulsant drugs. *Mol.Pharmacol.* **40**, 756-765.

Ragsdale, D. S. & Avoli, M. (1998). Sodium channels as molecular targets for antiepileptic drugs. *Brain Res.Brain Res.Rev.* **26**, 16-28.

Robbins, J., Caulfield, M. P., Higashida, H., & Brown, D. A. (1991). Genomic m_3-muscarinic receptros preferentially inhibit M-currents in DNA-transfected NG108-15 neuroblastoma x glioma hybrid cells. *Eur.J.Neurosci.* **3**, 820-824.

Robbins, J., Trouslard, J., Marsh, S. J., & Brown, D. A. (1992). Kinetic and pharmacological properties of the M-current in rodent neuroblastoma x glioma hybrid cells. *J.Physiol.* **451**, 159-85.

Robbins, J., Marsh, S. J., & Brown, D. A. (1993). On the mechanism of M-current inhibition by muscarinic m1 receptors in DNA-transfected rodent neuroblastoma x glioma cells. *J.Physiol* **469**, 153-78.

Robbins, J. (2000). KCNQ potassium channels: physiology, pathophysiology and pharmacology. *Pharmacol.Ther.* **90(1)**, 1-19.

Rogart, R. B., Cribbs, L. L., Muglia, L. K., Kephart, D. D., & Kaiser, M. W. (1989). Molecular cloning of a putative tetrodotoxin-resistant rat heart Na^+ channel isoform. *Proc.Natl.Acad.Sci.U.S.A* **86**, 8170-8174.

Rogawski, M. A. & Porter, R. J. (1990). Antiepileptic drugs: pharmacological mechanisms and clinical efficacy with consideration of promising developmental stage compounds. *Pharmacol.Rev.* **42**, 223-286.

Rogawski, M. A. (2000). KCNQ2/KCNQ3 K^+ channels and the molecular pathogenesis of epilepsy: implications for therapy. *Trends Neurosci.* **23(9)**, 393-398.

Rostock, A., Tober, C., Rundfeldt, C., Bartsch, R., Engel, J., Polymeropoulos, E. E., Kutscher, B., Loscher, W., Honack, D., White, H. S., & Wolf, H. H. (1996). D-23129: a new anticonvulsant with a broad spectrum activity in animal models of epileptic seizures. *Epilepsy Res.* **23**, 211-223.

Rundfeldt, C., Rohlfs, A. & Netzer, R. (1995). Multiple actions of the new anticonvulsant D-23129 on voltage-gated and GABA-induced currents in cultured neuronal cells. *Naunyn Schmiedeberg's Arch.Pharmacol.* **351 (suppl)**: R160.

Rundfeldt, C. (1997). The new anticonvulsant retigabine (D-23129) acts as an opener of K^+ channels in neuronal cells. *Eur.J.Pharmacol.* **336**, 243-249.

Rundfeldt, C. & Netzer, R. (2000). The novel anticonvulsant retigabine activates M-currents in Chinese hamster ovary cells transfected with human KCNQ2/3 subunits. *Neurosci.Lett.* **282(12)**, 73-76.

Salata, J. J., Jurkiewicz, N. K., Wang, J., Evans, B. E., Orme, H. T., & Sanguinetti, M. C. (1998). A novel benzodiazepine that activates cardiac slow delayed rectifier K^+ currents. *Mol.Pharmacol.* **54**, 220-230.

Sangameswaran, L., Delgado, S. G., Fish, L. M., Koch, B. D., Jakeman, L. B., Stewart, G. R., Sze, P., Hunter, J. C., Eglen, R. M., & Herman, R. C. (1996). Structure and function of a novel voltage-gated, tetrodotoxin-resistant sodium channel specific to sensory neurons. *J.Biol.Chem.* **271**, 5953-5956.

Sangameswaran, L., Fish, L. M., Koch, B. D., Rabert, D. K., Delgado, S. G., Ilnicka, M., Jakeman, L. B., Novakovic, S., Wong, K., Sze, P., Tzoumaka, E., Stewart, G. R., Herman, R. C., Chan, H., Eglen, R. M., & Hunter, J. C. (1997). A novel tetrodotoxin-

sensitive, voltage-gated sodium channel expressed in rat and human dorsal root ganglia. *J.Biol.Chem.* **272**, 14805-14809.

Sanguinetti, M. C., Curran, M. E., Zou, A., Shen, J., Spector, P. S., Atkinson, D. L., & Keating, M. T. (1996). Coassembly of KvLQT1 and minK (IsK) proteins to form cardiac I(Ks) potassium channel. *Nature* **384**, 80-83.

Schaller, K. L., Krzemien, D. M., McKenna, N. M., & Caldwell, J. H. (1992). Alternatively spliced sodium channel transcripts in brain and muscle. *J.Neurosci.* **12**, 1370-1381.

Schaller, K. L., Krzemien, D. M., Yarowsky, P. J., Krueger, B. K., & Caldwell, J. H. (1995). A novel, abundant sodium channel expressed in neurons and glia. *J.Neurosci.* **15**, 3231-3242.

Schmidt, J., Rossie, S., & Catterall, W. A. (1985). A large intracellular pool of inactive Na^+ channel alpha subunits in developing rat brain. *Proc.Natl.Acad.Sci.U.S.A* **82**, 4847-4851.

Schmidt, J. W. & Catterall, W. A. (1986). Biosynthesis and processing of the alpha subunit of the voltage-sensitive sodium channel in rat brain neurons. *Cell* **46**, 437-444.

Schmitt, N., Schwarz, M., Peretz, A., Abitbol, I., Attali, B., & Pongs, O. (2000). A recessive C-terminal Jervell and Lange-Nielsen mutation of the KCNQ1 channel impairs subunit assembly. *EMBO J.* **19**, 332-340.

Schnee, M. E. & Brown, B. S. (1998). Comparison of XE991 and linopirdine on M-currents in hippocampal CA1 neurones and PC12 cells. *Soc. Neurosci.Abstr.* **24**, 1083.

Schofield, G. G. & Ikeda, S. R. (1988). Sodium and calcium currents of acutely isolated adult rat superior cervical ganglion neurons. *Pflugers Arch.* **411**, 481-490.

Schoppa, N. E., McCormack, K., Tanouye, M. A., & Sigworth, F. J. (1992). The size of gating charge in wild-type and mutant Shaker potassium channels. *Science* **255**, 1712-1715.

Schreibmayer, W., Dascal, N., Lotan, I., Wallner, M., & Weigl, L. (1991). Molecular mechanism of protein kinase C modulation of sodium channel alpha-subunits expressed in Xenopus oocytes. *FEBS Lett.* **291**, 341-344.

Schreibmayer, W., Frohnwieser, B., Dascal, N., Platzer, D., Spreitzer, B., Zechner, R., Kallen, R. G., & Lester, H. A. (1994). Beta-adrenergic modulation of currents produced by rat cardiac Na^+ channels expressed in Xenopus laevis oocytes. *Receptors.Channels* **2**, 339-350.

Schreibmayer, W., Dessauer, C. W., Vorobiov, D., Gilman, A. G., Lester, H. A., Davidson, N., & Dascal, N. (1996). Inhibition of an inwardly rectifying K^+ channel by G-protein alpha-subunits. *Nature* **380**, 624-627.

Schreibmayer, W. (1999). Isoform diversity and modulation of sodium channels by protein kinases. *Cell Physiol Biochem.* **9**, 187-200.

Schroeder, B. C., Kubisch, C., Stein, V., & Jentsch, T. J. (1998). Moderate loss of function of cyclic-AMP-modulated KCNQ2/KCNQ3 K^+ channels causes epilepsy. *Nature* **396**, 687-690

Schroeder, B. C., Hechenberger, M., Weinreich, F., Kubisch, C., & Jentsch, T. J. (2000a). KCNQ5, a novel potassium channel broadly expressed in brain, mediates M-type currents. *J.Biol.Chem.* **275**, 24089-24095.

Schroeder, B. C., Waldegger, S., Fehr, S., Bleich, M., Warth, R., Greger, R., & Jentsch, T. J. (2000b). A constitutively open potassium channel formed by KCNQ1 and KCNE3. *Nature* **403**, 196-199.

Schwake, M., Pusch, M., Kharkovets, T., & Jentsch, T. J. (2000). Surface expression and single channel properties of KCNQ2/KCNQ3, M-type K^+ channels involved in epilepsy. *J.Biol.Chem.* **275**, 13343-13348.

Schwiebert, E. M., Gruenert, D. C., Guggino, W. B., & Stanton, B. A. (1995). G protein $G\alpha i_2$ inhibits outwardly rectifying chloride channels in human airway epithelial cells. *Am.J.Physiol* **269**, C451-C456.

Schwindt, P. C. & Crill, W. E. (1995). Amplification of synaptic current by persistent sodium conductance in apical dendrite of neocortical neurons. *J.Neurophysiol.* **74**, 2220-2224.

Scott, R. H. & Dolphin, A. C. (1987). Activation of a G protein promotes agonist responses to calcium channel ligands. *Nature* **330**, 760-762.

Segal, M. M. (1994). Endogenous bursts underlie seizurelike activity in solitary excitatory hippocampal neurons in microcultures. *J.Neurophysiol.* **72**, 1874-1884.

Segal, M. M. & Douglas, A. F. (1997). Late sodium channel openings underlying epileptiform activity are preferentially diminished by the anticonvulsant phenytoin. *J.Neurophysiol.* **77**, 3021-3034.

Selyanko, A. A., Stansfeld, C. E., & Brown, D. A. (1992). Closure of potassium M-channels by muscarinic acetylcholine-receptor stimulants requires a diffusible messenger. *Proc.R.Soc.Lond B Biol.Sci.* **250**, 119-125.

Selyanko, A. A. & Brown, D. A. (1996). Intracellular calcium directly inhibits potassium M channels in excised membrane patches from rat sympathetic neurons. *Neuron* **16**, 151-162.

Selyanko, A. A. & Brown, D. A. (1999). M-channel gating and simulation. *Biophys.J.* **77**, 701-713.

Selyanko, A. A., Hadley, J. K., Wood, I. C., Abogadie, F. C., Jentsch, T. J., & Brown, D. A. (2000). Inhibition of KCNQ1-4 potassium channels expressed in mammalian cells via M1 muscarinic acetylcholine receptors. *J.Physiol* **522 (3)**, 349-355.

Selyanko, A. A., Hadley, J. K. & Brown, D. A. (2001). Properties of single M-type KCNQ2/KCNQ3 potassium channels expressed in mammalian cells. *J.Physiol.* **534(1)**. 15-24.

Shapiro, M. S., Roche, J. P., Kaftan, E. J., Cruzblanca, H., Mackie, K., & Hille, B. (2000). Reconstitution of muscarinic modulation of the KCNQ2/KCNQ3 K^+ channels that underlie the neuronal M current. *J.Neurosci.* **20**, 1710-1721.

Shieh, C. C., Coghlan, M., Sullivan, J. P., & Gopalakrishnan, M. (2000). Potassium channels: molecular defects, diseases, and therapeutic opportunities. *Pharmacol.Rev.* **52**, 557-594.

Shin, H. G. & Murray, K. T. (2001). Conventional protein kinase C isoforms and cross-activation of protein kinase A regulate cardiac Na^+ current. *FEBS Lett.* **495**, 154-158.

Sigel, E. & Baur, R. (1988). Activation of protein kinase C differentially modulates neuronal Na^+, Ca^{2+}, and gamma-aminobutyrate type A channels. *Proc.Natl.Acad.Sci.U.S.A* **85**, 6192-6196.

Singh, N. A., Charlier, C., Stauffer, D., DuPont, B. R., Leach, R. J., Melis, R., Ronen, G. M., Bjerre, I., Quattlebaum, T., Murphy, J. V., McHarg, M. L., Gagnon, D., Rosales, T. O., Peiffer, A., Anderson, V. E., & Leppert, M. (1998). A novel potassium channel gene, KCNQ2, is mutated in an inherited epilepsy of newborns. *Nat.Genet.* **18**, 25-29.

Smith, P. A., Chen, H., Kurenny, D. E., Selyanko, A. A. & Zidichouski, J. A. (1992). Regulation of the M current: transduction mechanism and role in ganglionic transmission. *Can.J.Physiol.Pharmacol.* **70**, S12-S18.

Smith, R. D. & Goldin, A. L. (1992). Protein kinase A phosphorylation enhances sodium channel currents in Xenopus oocytes. *Am.J.Physiol* **263**, C660-C666.

Smith, R. D. & Goldin, A. L. (1996). Phosphorylation of brain sodium channels in the I-II linker modulates channel function in Xenopus oocytes. *J.Neurosci.* **16**, 1965-1974.

Smith, R. D. & Goldin, A. L. (1998). Functional analysis of the rat I sodium channel in xenopus oocytes. *J.Neurosci.* **18**, 811-820.

Sontheimer, H., Black, J. A., & Waxman, S. G. (1996). Voltage-gated Na^+ channels in glia: properties and possible functions. *Trends Neurosci.* **19**, 325-331.

Spencer, F., Ketner, G., Connely, C. & Hieter, P. (1993). Targeted recombination-based cloning and manipulation of large DNA segments in yeast. *Methods: A companion to methods in enzymology.* **5(2)**, 161-175.

Stafstrom, C. E., Schwindt, P. C., Chubb, M. C., & Crill, W. E. (1985). Properties of persistent sodium conductance and calcium conductance of layer V neurons from cat sensorimotor cortex in vitro. *J.Neurophysiol.* **53**, 153-170.

Stansfeld, C., Ludwig, J., Roeper, J., Weseloh, R., Brown, D., & Pongs, O. (1997). A physiological role for ether-a-go-go K^+ channels? *Trends Neurosci.* **20**, 13-14.

Starace, D. M., Stefani, E., & Bezanilla, F. (1997). Voltage-dependent proton transport by the voltage sensor of the Shaker K^+ channel. *Neuron* **19**, 1319-1327.

Steel, M. C. & Buckley, N. J. (1993). Differential regulation of muscarinic receptor mRNA levels in neuroblastoma cells by chronic agonist exposure: a comparative polymerase chain reaction study. *Mol.Pharmacol.* **43**, 694-701.

Stimers, J. R., Bezanilla, F. & Taylor, R. E. (1985). Sodium channel activation in the squid giant axon. Steady state properties. *J.Gen.Physiol.* **85**, 65-82.

Storm, J. F. (1989). An after-hyperpolarization of medium duration in rat hippocampal pyramidal cells. *J.Physiol* **409**, 171-190.

Stuart, G. & Sakmann, B. (1995). Amplification of EPSPs by axosomatic sodium channels in neocortical pyramidal neurons. *Neuron* **15**, 1065-1076.

Stuhmer, W., Conti, F., Suzuki, H., Wang, X. D., Noda, M., Yahagi, N., Kubo, H., & Numa, S. (1989). Structural parts involved in activation and inactivation of the sodium channel. *Nature* **339**, 597-603.

Tate, S., Benn, S., Hick, C., Trezise, D., John, V., Mannion, R. J., Costigan, M., Plumpton, C., Grose, D., Gladwell, Z., Kendall, G., Dale, K., Bountra, C., & Woolf, C. J. (1998). Two sodium channels contribute to the TTX-R sodium current in primary sensory neurons. *Nat.Neurosci.* **1**, 653-655.

Tatulian, L., Selyanko, A. A., Wood, I., Abogadie, F., Buckley, N. J., Delmas, P. & Brown, D. A. (2000). Dominant negative KCNQ4 blocks M-current in sympathetic neurones. *Eur.J.Neurosci.Abstr.* **12 (suppl. 11)**. 453.

Tatulian, L., Delmas, P. Abogadie, F. C. & Brown, D. A. (2001). Activation of expressed KCNQ potassium currents and native neuronal M-type potassium currents by the anti-convulsant drug retigabine. *J.Neurosci* **21(15)**, 5535-5545.

Taylor, S. S. (1989). CAMP dependent protein kinase. Model for enzyme family. *J.Biol.Chem.* **264 (15)**, 8443-8446.

Taylor, C. P. (1993). Na^+ currents that fail to inactivate. *Trends Neurosci.* **16**, 455-460.

Taylor, C. P. & Narasimhan, L. S. (1997). Sodium channels and therapy of central nervous system diseases. *Adv.Pharmacol.* **39**, 47-98.

Thompson, S. H. (1977). Three pharmacologically distinct potassium channels in molluscan neurones. *J.Physiol* **265**, 465-488.

Tilly, B. C., Kansen, M., van Gageldonk, P. G., van den Berghe, N., Galjaard, H., Bijman, J., & de Jonge, H. R. (1991). G-proteins mediate intestinal chloride channel activation. *J.Biol.Chem.* **266**, 2036-2040.

Tinel, N., Lauritzen, I., Chouabe, C., Lazdunski, M., & Borsotto, M. (1998). The KCNQ2 potassium channel: splice variants, functional and developmental expression. Brain localization and comparison with KCNQ3. *FEBS Lett.* **438**, 171-176.

Tober, C., Rundfeldt, C., Rostock, A. & Bartsch, R. (1994). The phenylcarbamic acid ester D-23129 is highly effective in epilepsy models for generalised and focal seizures at non toxic doses. *Soc.Neurosci.Abstracts.* **20**. 1641.

Tober, C., Rostock, A., Rundfeldt, C., & Bartsch, R. (1996). D-23129: a potent anticonvulsant in the amygdala kindling model of complex partial seizures. *Eur.J.Pharmacol.* **303**, 163-169.

Tokimasa, T., Tsurusaki, M., Ishimatsu, M., & Akasu, T. (1993). Intracellular ATP changes the voltage-dependence of delayed rectifier potassium current in bullfrog primary afferent neurons. *Neurosci.Lett.* **163**, 138-140.

Tokimasa, T., Ito, M., Simmons, M. A., Schneider, C. R., Tanaka, T., Nakano, T., & Akasu, T. (1995). Inhibition by wortmannin of M-current in bullfrog sympathetic neurones. *Br.J.Pharmacol.* **114**, 489-495.

Toledo-Aral, J. J., Moss, B. L., He, Z. J., Koszowski, A. G., Whisenand, T., Levinson, S. R., Wolf, J. J., Silos-Santiago, I., Halegoua, S., & Mandel, G. (1997). Identification of NAV1.7, a predominant voltage-dependent sodium channel expressed principally in peripheral neurons. *Proc.Natl.Acad.Sci.U.S.A* **94**, 1527-1532.

Trimmer, J. S., Cooperman, S. S., Tomiko, S. A., Zhou, J. Y., Crean, S. M., Boyle, M. B., Kallen, R. G., Sheng, Z. H., Barchi, R. L., Sigworth, F. J., & et, a. (1989). Primary

structure and functional expression of a mammalian skeletal muscle sodium channel. *Neuron* **3**, 33-49.

Tsien, R. W. (1983). Calcium channels in excitable cell membranes. *Annu.Rev.Physiol* **453**, 41-58.

Turski, L., Ikonomidou, C., Turski, W. A., Bortolotto, Z. A., & Cavalheiro, E. A. (1989). Review: cholinergic mechanisms and epileptogenesis. The seizures induced by pilocarpine: a novel experimental model of intractable epilepsy. *Synapse* **3**, 154-171.

Ukomadu, C., Zhou, J., Sigworth, F. J., & Agnew, W. S. (1992). μI Na^+ channels expressed transiently in human embryonic kidney cells: biochemical and biophysical properties. *Neuron* **8**, 663-676.

Upton, N. (1994). Mechanisms of action of new antiepileptic drugs: rational design and serendipitous findings. *Trends Pharmacol.Sci.* **15**, 456-463.

Vaughn, D. E. & Bjorkman, P. J. (1996). The (Greek) key to structures of neural adhesion molecules. *Neuron* **16**, 261-273.

Veselovskii, N. S., Fedulova, S. A., & Shirokov, R. E. (1986). Elektroupravliaemye natrievye kanaly somaticheskoi membrany simpaticheskikh neironov. [Electroregulated sodium channels of the somatic membrane of sympathetic neurons]. *Neirofiziologiia.* **18**, 108-117.

Villarroel, A., Marrion, N. V., Lopez, H., & Adams, P. R. (1989). Bradykinin inhibits a potassium M-like current in rat pheochromocytoma PC12 cells. *FEBS Lett.* **255**, 42-46.

Wang, Q., Curran, M. E., Splawski, I., Burn, T. C., Millholland, J. M., VanRaay, T. J., Shen, J., Timothy, K. W., Vincent, G. M., de Jager, T., Schwartz, P. J., Toubin, J. A., Moss, A. J., Atkinson, D. L., Landes, G. M., Connors, T. D., & Keating, M. T. (1996). Positional cloning of a novel potassium channel gene: KvLQT1 mutations cause cardiac arrhythmias. *Nat.Genet.* **12**, 17-23.

Wang, H. S., Pan, Z., Shi, W., Brown, B. S., Wymore, R. S., Cohen, I. S., Dixon, J. E., & McKinnon, D. (1998). KCNQ2 and KCNQ3 potassium channel subunits: molecular correlates of the M-channel. *Science* **282**, 1890-1893.

Watkins, C. S. & Mathie, A. (1996). A non-inactivating K^+ current sensitive to muscarinic receptor activation in rat cultured cerebellar granule neurons. *J.Physiol* **491**, -12.

West, J. W., Numann, R., Murphy, B. J., Scheuer, T., & Catterall, W. A. (1991). A phosphorylation site in the Na^+ channel required for modulation by protein kinase C. *Science* **254**, 866-868.

West, J. W., Patton, D. E., Scheuer, T., Wang, Y., Goldin, A. L., & Catterall, W. A. (1992). A cluster of hydrophobic amino acid residues required for fast Na^+ channel inactivation. *Proc.Natl.Acad.Sci.U.S.A* **89**, 10910-10914.

Westenbroek, R. E., Merrick, D. K., & Catterall, W. A. (1989). Differential subcellular localization of the RI and RII Na^+ channel subtypes in central neurons. *Neuron* **3**, 695-704.

Whitaker, W. R. J, Faull, R. L. M., Waldvogel, H. J., Plumpton, C. J., Emson, P. C. & Clare, J. J. (2001). Comparative distribution of voltage-gated sodium channel proteins in human brain. *Mol. Brain Res.* **88**, 37-53.

Wickenden, A. D., Yu, W., Zou, A., Jegla, T. & Wagoner, P. K. (2000). Retigabine, a novel-anticonvulsant, enhances activation of KCNQ2/Q3 potassium channels. *Mol.Pharmacol.* **58 (3)**, 591-600.

Wickman, K. & Clapham, D. E. (1995). Ion channel regulation by G proteins. *Physiol Rev.* **75**, 865-885.

Xie, X., Dale, T. J., John, V. H., Cater, H. L., Peakman, T. C., & Clare, J. J. (2001). Electrophysiological and pharmacological properties of the human brain type IIA Na^+ channel expressed in a stable mammalian cell line. *Pflugers Arch.* **441**, 425-433.

Yang, N. & Horn, R. (1995). Evidence for voltage-dependent S4 movement in sodium channels. *Neuron* **15**, 213-218.

Yang, W. P., Levesque, P. C., Little, W. A., Conder, M. L., Shalaby, F. Y., & Blanar, M. A. (1997). KvLQT1, a voltage-gated potassium channel responsible for human cardiac arrhythmias. *Proc.Natl.Acad.Sci.U.S.A* **94**, 4017-4021.

Yang, W. P., Levesque, P. C., Little, W. A., Conder, M. L., Ramakrishnan, P., Neubauer, M. G., & Blanar, M. A. (1998). Functional expression of two KvLQT1-related potassium channels responsible for an inherited idiopathic epilepsy. *J.Biol.Chem.* **273**, 19419-19423.

Yellen, G., Sodickson, D., Chen, T. Y., & Jurman, M. E. (1994). An engineered cysteine in the external mouth of a K^+ channel allows inactivation to be modulated by metal binding. *Biophys.J.* **66**, 1068-1075.

Yellen, G. (1998). The moving parts of voltage-gated ion channels. *Q Rev Biophys.* **31 (3)**, 239-95.

Zaczek, R., Chorvat, R. J., Saye, J. A., Pierdomenico, M. E., Maciag, C. M., Logue, A. R., Fisher, B. N., Rominger, D. H., & Earl, R. A. (1998). Two new potent neurotransmitter release enhancers, 10,10-bis(4-pyridinylmethyl)-9(10H)-anthracenone

and 10,10-bis(2-fluoro-4-pyridinylmethyl)-9(10H)-anthracenone: comparison to linopirdine. *J.Pharmacol.Exp.Ther.* **285**, 724-730.

Zhou, J. Y., Potts, J. F., Trimmer, J. S., Agnew, W. S., & Sigworth, F. J. (1991). Multiple gating modes and the effect of modulating factors on the microI sodium channel. *Neuron* **7**, 775-785.

Zhou, Z., Gong, Q., Ye, B., Fan, Z., Makielski, J. C., Robertson, G. A., & January, C. T. (1998). Properties of HERG channels stably expressed in HEK 293 cells studied at physiological temperature. *Biophys.J.* **74**, 230-241.